Spring 1-1-2012

Low-Cost Building-Integrated Photovoltaic/Thermal Module Prototype Design and Analysis

Gregory Martin Estep
University of Colorado Boulder, greg.estep@colorado.edu

Low-Cost Building-Integrated Photovoltaic/Thermal Module Prototype Design and Analysis

by

GREGORY MARTIN ESTEP

B.A., UNIVERSITY OF COLORADO AT BOULDER, 2004

A thesis submitted to the
Faculty of the Graduate School of the
University of Colorado in partial fulfillment
of the requirement for the degree of
Master of Science
Department of Civil, Environmental and Architectural Engineering
2012

This thesis entitled:
Building-Integrated Photovoltaic/Thermal Module Prototype Design and Analysis
written by Gregory Martin Estep
has been approved for the Department of Civil, Environmental and Architectural Engineering

Michael J. Brandemuehl Ph.D.

Moncef Krarti Ph.D.

John Zhai Ph.D.

Date

The final copy of this thesis has been examined by the signatories, and we find that both the content and the form meet acceptable presentation standards of scholarly work in the above mentioned discipline.

Estep, Gregory Martin (Masters, Civil Engineering)
Low Cost Building-Integrated Photovoltaic/Thermal Module Prototype Design and Analysis
Thesis directed by Associate Professor Michael J. Brandemuehl

ABSTRACT

In order to maximize solar energy gains per square foot on a residential roof, the development of a new Building-Integrated Photovoltaic/Thermal (BIPV/T) module was designed, built and tested. The concept for the design was constrained by a provisional patent entitled, *Low-cost, modular mounting system for building-integrated photovoltaic/thermal collector*. The novel aspect of the patent required that the framing/mounting system include an integrated heat conducting fluid conduit. Photovoltaic/Thermal collectors are capable of simultaneously producing electricity and hot water. A heat conducting fluid is passed underneath the PV laminate picking up the waste heat from the PV panel. The waste heat rejected to the fluid is useful for two reason; 1) it cools the PV cells allowing for higher power conversion efficiencies and 2) it provides a source of heat for low-grade temperature applications. In addition to the solar performance, the building-integrated modules are to serve as façade elements, replacing traditional shingles or siding, which is accomplished by designing the frame with integrating flanges and gaskets that overlap one another providing a smooth, low-profile and aesthetic array. A prototype was fabricated by a local plastic shop and a physical experiment was built on the roof of the engineering center. Data collected from the experiment was used to calibrate a TRNSYS computer model which simulated the annual performance of a 5kW BIPV/T array on a typical American household for 20 non-freezing climate cities. The computer simulation found the BIPV/T modules were capable of meeting up to 80% of the domestic hot water load (the solar fraction), and an improved electrical power efficiency up to 2.6% in certain climates.

Dedication

To my parents, Jay and Janet Estep, who have always supported my academic pursuits with enthusiasm and encouragement.

Also, to all of the struggling inventors, fabricators, product developers, and tradesmen of the world, thank-you for being the ones who truly get the job done.

Acknowledgements

I would like to acknowledge the University of Colorado's Technology Transfer Office (TTO) for providing me with the funding required to design, build, and test the prototype, as well as providing a means for me to eat and survive during the year of 2011.

I would also like to thank Professor Brandemuehl for always having a solution and a calm rationale to any problem that I was experiencing.

A great big thanks goes out to my roommate Tim Cureton. Who, without his extensive collection of tools and general construction knowledge, this project would have never been completed. I greatly appreciated that fact that I could come to you with a rookie construction questions and get a great answer without feeling embarrassed, thank you!

Additional thanks goes out to my fellow Building Systems colleagues, who would lend an ear when things were going poorly and a hand when I needed help carrying heavy expensive equipment. I couldn't have done it without you!

Thanks to Wayne Morrison, the departmental accountant, who finally realized that I needed a procurement card, and was never annoyed when I would show up with 50 late receipts. Thank you!

Contents

LIST OF TABLES

LIST OF FIGURES

CHAPTER 1 INTRODUCTION AND MOTIVATION

MOTIVATION FOR A MODULAR BIPV/T

The motivation for this project is to maximize solar energy at the lowest possible cost. Several variables come into play when considering this optimization and a great place to start is with the money trail. When looking at ones monthly energy bill there are two energy sources that are metered; electricity and combustible fuel (typically natural gas or fuel oil). The cost of generation, infrastructure, and delivery are passed on to the consumer. A typical residence can offset the cost of electrical energy and combustible fuel with the installation of photovoltaic and solar thermal modules, respectively. Photovoltaic energy conversion efficiencies are in the range of 3-15% and solar thermal energy conversion efficiencies range 20-40%. The traditional approach for achieving the maximum solar energy benefit has been to use both systems side-by-side. Due to issues of shading, building orientation and roof geometry, there is rarely enough room for both technologies to be utilized. Additional issues in using both systems side-by-side include additional installation costs and multiple mounting systems. One solution to all of the above issues would be to combine the technologies into a single module, a Photovoltaic/Thermal (PV/T).

Photovoltaic/Thermal (PV/T) systems have been studied for more than thirty years yet there are only a few commercially produced products available. Many past studies have been custom, one-of-a-kind designs, not intended for mass production (see RA-CELL). Additionally, many previous designs have decreased electrical efficiencies and have not identified a clear cost advantage. Of the existing PV/T designs on the market, there has been little emphasis on designing a modular Building-Integrated PV/T (BIPV/T) product.

OBJECTIVES

Funding for this project has come from the Technology Transfer Office (TTO), with the hope that this technology becomes patentable. As mentioned above, the invention is a solar module frame that serves as a low-profile façade mounting system and conduit through which a heat conducting fluid can be passed. The novel aspect of this invention is the use of the module frame as a pipe and integrated mounting system. Please see **APPENDIX A PROVISIONAL PATENT** for a copy of the provisional patent.

The purpose of this research is to design and build a patentable, modular BIPV/T prototype to assess the following:

- Performance
- Economics
- Constructability
- Operation and Maintenance

The performance and economics were assessed by building a physical experiment in which all parameters required to quantify both the electrical and thermal performance were measured. The data collected by the physical experiment was used to validate/calibrate a PV/T component in TRNSYS. Once the TRNSYS component had been calibrated to reflect the measured performance of the physical experiment, the component was used in a TRNSYS simulation that modeled the performance of the PV/T connected to a hot water tank in multiple U.S. cities. Simulations were run for an entire year and all engineering and economic parameters were calculated based on the simulation results. A plan for constructability is outlined in CHAPTER 2 MODULE DESIGN along with a discussion on operation and maintenance in Chapter 6.

PV/T MARKET PARTICIPANT REVIEW

Previous work by fellow University of Colorado Architectural Engineering students (Lilliestierna & Zdrowski, 2010) provides a comprehensive literature review of PV/T, BIPV, and BIPV/T technology. This paper is primarily concerned with possible competition with the designed prototype and will investigate PV/T products that are already on the market.

SOLARDUCT PV/T

SolarDuct PV/T is a modular rooftop application of PV/T technology that also acts as a PV racking system. This system mounts the PV modules to the top of the SolarDuct units, and the heat is drawn off the back of the PV modules and then ducted to the nearest rooftop air handler, as seen in Figure 1. The excess heat is then channeled into the building's HVAC system where it is used to offset the heating load. The SolarDuct system claims that the heat removal from behind the PV modules increases the electrical conversion efficiency by up to 10%. Since the SolarWall air heating panels serve as the racking system needed to mount the PV modules, the cost-effectiveness of the cogeneration system is increased by the elimination of the PV mounting rack system. (SolarWall, 2012)

Figure 1. This is a rendering of the SolarDuct modular system. The PV modules are mounted on top of the SolarWall and air is drawn in behind the PV and into the building air handler. (SolarWall, 2012)

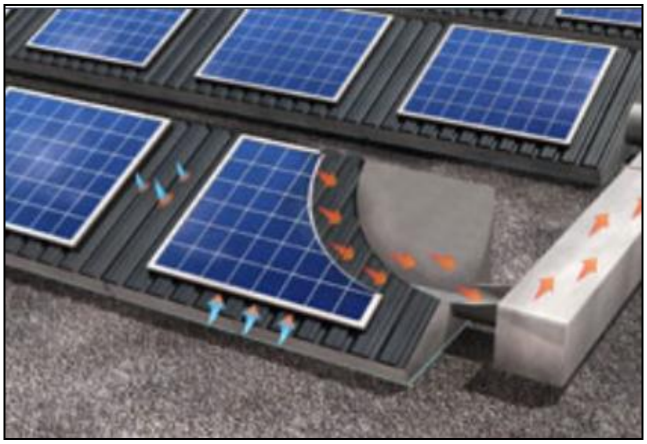

Figure 2. Heat flow in the SolarDuct system. (SolarWall, 2012)

The SolarDuct is indeed a PV/T, however it lacks the Building-Integrated component and is primarily targeting commercial buildings with large flat roofs so that the ducting and construction can be easily integrated into the nearest air handler. A couple of questions come to mind when considering this system. One, how does the waste heat get used during the cooling season, and two, there is no thermal storage for air systems. (SolarWall, 2012)

ECHO SOLAR SYSTEM (FORMALLY KNOWN AS PVT SOLAR)

The Echo Solar system is an air-based system designed for residential use. It includes a thermal module that is integrated into the residences' roof and ducted into an "energy transfer module", a little air handling unit, which is located in the home's attic. The energy transfer module contains an air filter, a heat exchanger and a fan. The fan inside the energy transfer module draws outside air through the plenum and heat is transferred from the solar panels to the air. The heated air then moves through ducts to the energy transfer module, where the air is filtered and drawn across a copper tube/aluminum fin coil heat exchanger. Cold water from the home's water tank is fed into the heat exchanger, extracting heat from the air and transferring it back to the tank via a circulator. After passing across the heat exchanger, the air is guided to either the inside of the home through the ducts of the HVAC system (for space heating) or exhausted when heating is not required. Figure 3 is a schematic of the system. (Echo Solar Systems, 2011)

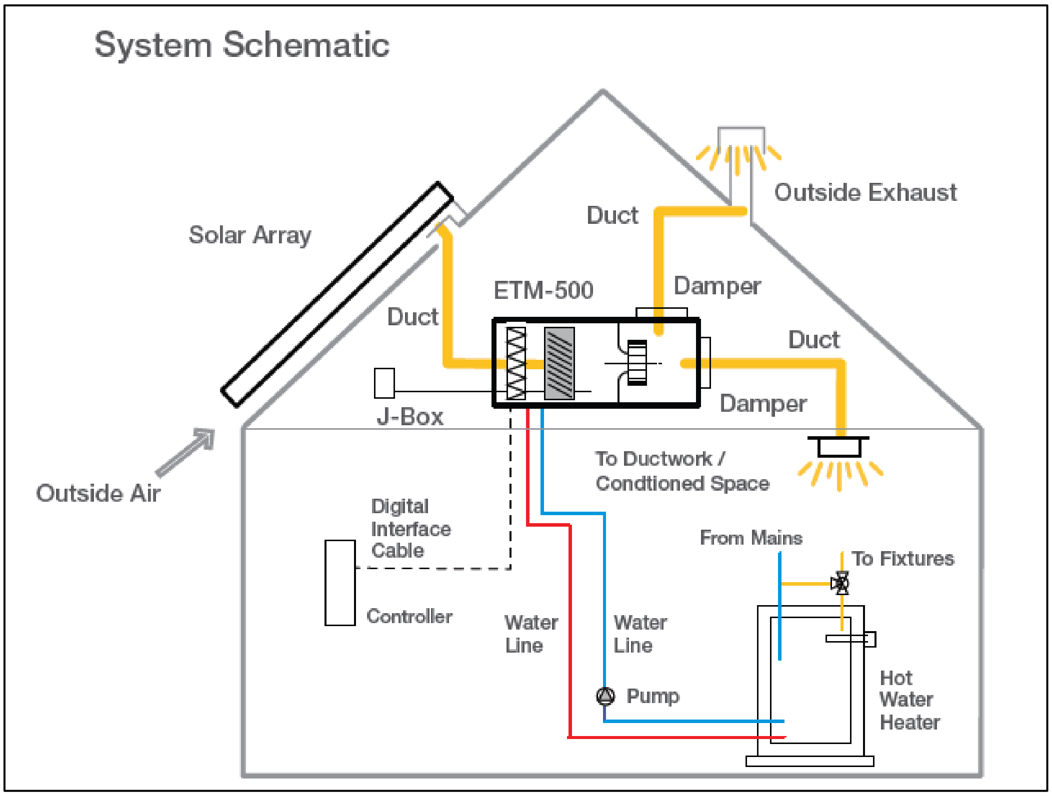

Figure 3. Schematic of the Echo Solar system. Air is heated underneath the PV modules by way of a special mounting module. The heated air is ducted into the energy transfer module, where the heat is transferred into the hot water tank via air-to-water heat exchanger. (Echo Solar Systems, 2011)

Echo solar is a very clever and versatile system that can be efficiently utilized in many different climate zones. Using air as the working fluid has its tradeoffs. One major benefit of the air system is the friendliness for sunny, freezing climates. There is no risk of freezing or water leaks, which is very reassuring for homeowners. On the other hand, the carrying capacity of air is four times less than that of water, and the energy required to move air is also significantly higher than that of water, due to the compressibility gas.

Echo Solar is targeting a different market than the proposed BIPV/T of this research. It is obvious that this system is not a low-cost option and by choosing to go with the air-based system there are significant energy losses by having to transfer the heat to the water via heat exchanger, and then having to dump the excess heat during the cooling season. The installed cost per kW will be significantly more than the modular water-based BIPV/T tested and simulated in this paper.

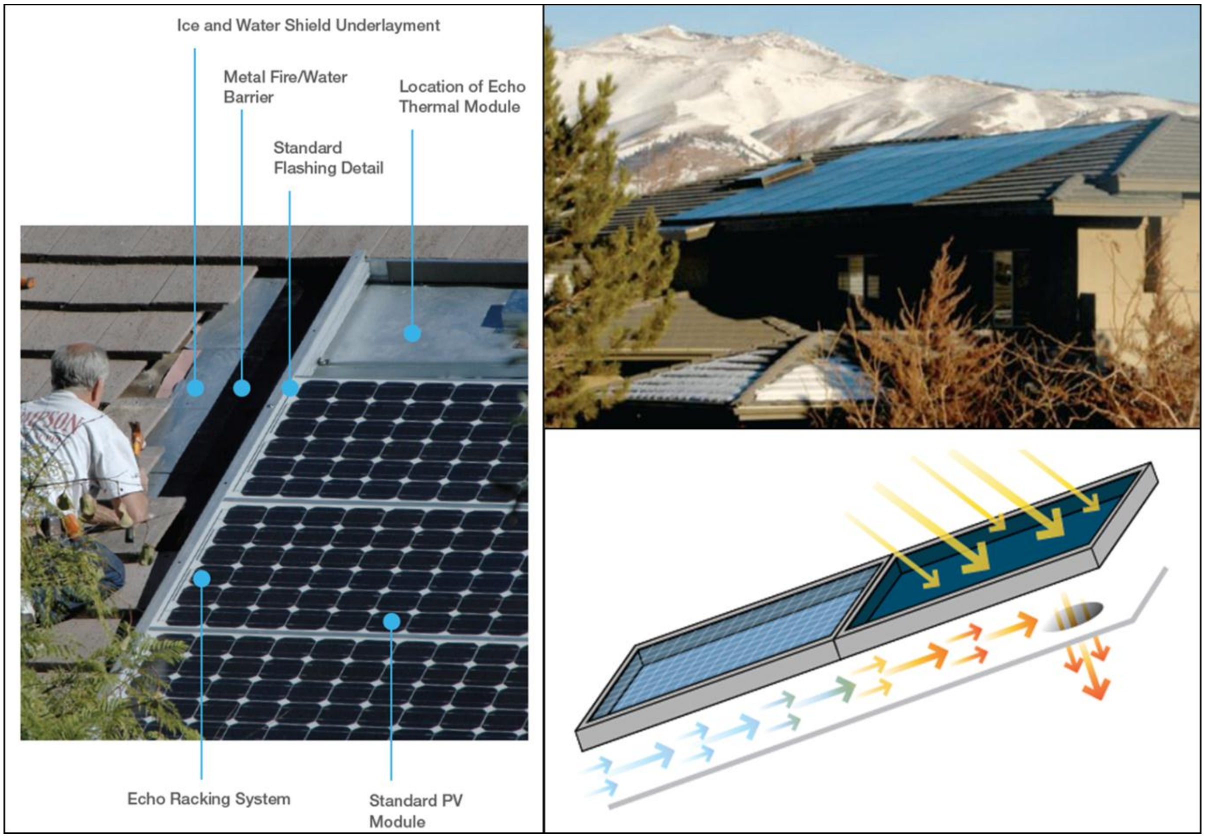

Figure 4. The figure on the left shows the building integration on the roof. The top right photo demonstrates a fairly low profile design. The bottom right image demonstrates the heat flow of outside air into the home via roof penetrations. (Echo Solar Systems, 2011)

It seems that the best season for combined electrical and thermal performance would be sunny, winter/fall days. Typical US markets for the Echo Solar would be the sunny climes of the Rocky Mountain region, including Colorado, Utah, New Mexico and Arizona, where intense winter sunshine combined with cool air and the need for space heating, make this a very desirable system.

MILLENNIUM SOLAR

The Multi Solar System (MSS) by Millennium Solar is a modular PV/T that generates electrical energy and thermal energy simultaneously. The MSS uses air and water pipes to cool the PV cells, increasing efficiency, and produces hot water and air which can be used for other low grade heating applications. The company has a patented technology for a Multi Solar PV/T/A (Solar PV/Thermal/Air) system, however the patent is certainly different than the patent that is being pursued in this research. They demonstrate little interest in the Building Integration aspect of the product and provide no mounting solution.

Figure 5. These photos demonstrate the concept of the PV/T designs by Millennium Solar. You can see the plumbing for the thermal component in the left-side photos. There is no building integration design or emphasis put on the aesthetics on a residence. (MillenniumSolar, 2011)

It appears that the products by Millennium Solar were designed to maximize efficiency and are most likely sold to commercial/power companies that can afford the technology. The residence is not a major target market for this company.

PVTWINS

PVTWINS is a spin-off company from the Energy Research Centre of The Netherlands (ECN) that produces PVT products and related system components. PVTWINS collectors are intended for residential use and can be applied in individual and collective domestic hot water systems.

Figure 6. PVTWINS PVT collector module. (PVTWINS, 2011)

This is a very similar concept to our BIPV/T, however, it is definitely missing the building-integration component, and is not attractive on a building façade.

RA-CELL

RA-cell is a research company specializing in electronic circuits and solar power, with a focus on processing and manufacturing semiconductor components. The company specializes in PV/T and PV modules for building integration, but does not have a specific product on the market. They work closely with architecture companies, and will custom design whatever the architectural firm has sold to its clients. Thus, the company is not a direct competitor to the product being developed in this research. (RA-cell, 2011)

SUMMARY OF MARKET PARTICIPANTS

Of all of the PV/T market participants, not one of them is doing what is being proposed in this paper. The SolarDuct is an air-based system that targets commercial flat rooftops with large air handling equipment. They are not targeting a residential market and would not be a competitor.

Echo solar would provide the greatest competition in the market of Building-Integrated Photovoltaic/Thermal systems. They produce a good looking, roof integrated system that has the flexibility to heat water and provide space heating via heated air. Echo solar is an air-based system, which has its tradeoffs. Benefits include the elimination of the risk of water leaks and freezing problems, opening them up to a market with locations in freezing climates. Disadvantages are a lack in thermal efficiency simply due to the larger carrying capacity of water versus air and the additional power required to pressurize air for transport, relative to water. Echo solar is most effective on cold sunny days where the air can be heated to high temperatures, and the heat can be transferred to the hot water tank, and the excess hot air downstream of the heat exchanger can be used for space heating. During the cooling season, the excess hot air must be exhausted and is wasted.

Millennium Solar offers up a high performing PV/T module, but provides no aesthetic integration into building facades, and is not a low cost option. They are primarily targeting power generation companies and/or commercial businesses that can afford the technology. Surely they're price can be beat.

PVTWINS's product is the most similar to the prototype of this paper, however it fails to compete on the building integration side of the market. Figure 6 is a photo of their module, and it is obvious that a racking system is required and that it simply looks awful.

RA-cell is a research company that is willing to custom fabricate any type of PV/T that is ordered from them by architectural firms, who have designed a building integrated PV or PV/T system for large-scale commercial projects. They are not selling a specific product.

Table 1 summarizes the above competitors and in bold is the BIPVT being developed in this research. A quick glance at the table demonstrates that the BIPVT module is different than all of the other competitors, and should have a good chance for success.

Table 1. Summary of PVT market participants and the BIPVT prototype in bold.

Summary of PVT Market Participants					
Competitor	**Headquarters**	**Working Fluid**	**Thermal Applications**	**Target Market**	**Ideal Environmental Conditions**
Echo	Berkeley, CA	Air	Hot water and space heating	Residential	Sunny and cool
Solar Wall	Toronto, ON	Air	Space Heating and Process drying	Commercial	Sunny and cool (space heating)
Millenium Solar	Israel	Air and Water	Power station, Co-generation power stations, Grid connected houses	Commercial and Residential	Hot and sunny
PVTWINS	Netherlands	Water	Hot water	Residential	Hot and Sunny
RA-Cell	Denmark	Water	Hot water	Commercial	Custom Product
BIPVT	**Boulder, CO**	**Water**	**Hot Water**	**Residential**	**Hot and sunny**

CHAPTER 2 MODULE DESIGN

The BIPV/T design had to meet the following criteria:

1. The fluid conduit must be integrated into the PV frame.
2. The modules are to be designed such that they create an aesthetically even façade on a roof.
3. Each module is to have weather resistant gaskets allowing the array of collectors to serve as façade elements, replacing shingles or siding.
4. The modules need to be able to be mounted directly on the roof.
5. The frame needs to be able to fit any PV manufacturer's laminates (they are not all the same shape).
6. The module needs to be Low cost.

A major constraint on the project was to use inexpensive materials, further separating this patentable design from existing PV/T designs that rely on relatively pricey metallic materials. It was important to design the prototype in anticipation of mass production. That being said, the most cost effective way to mass produce something would be to use multiple plastic extrusions that could be cut to the client's selected PV laminate dimensions and assembled around the PV in a shop/distribution warehouse. The desire for an extrudable absorber resulted in a simple design, best described by Figure 7

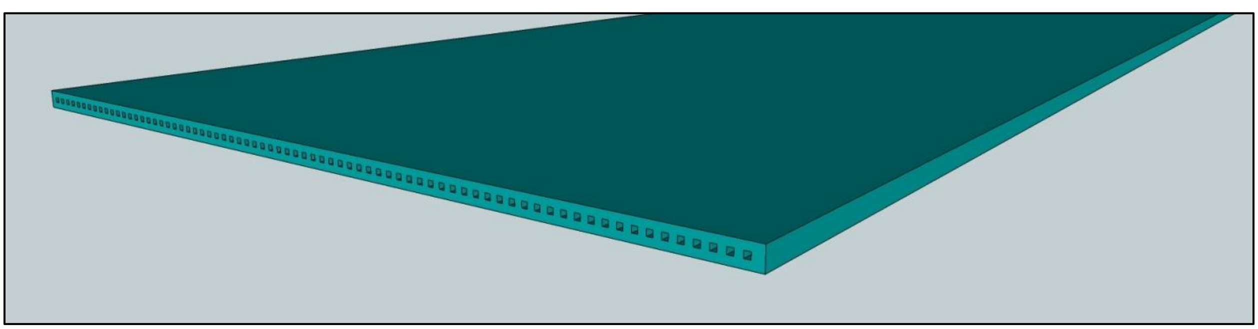

Figure 7 Concept for the extrudable absorber. Water is to flow through the square channels.

ABSORBER SIZING

ABSORBER ORIENTATION AND WIDTH

The first decision in designing the actual absorber prototype was to decide if the water was to flow along the portrait or landscape orientation of the PV. It was decided that the absorber was to flow water along the portrait view of the PV in order to maximize contact time for any given flow rate. The extrusion process will be able to provide any given length desired, most likely stocked in 10-15' long pieces, but the width will have to be a fixed dimension. The junction box on the back of all PV laminates is usually centered in portrait view, typically located a couple of inches from the top of the laminate and has dimension of (4-5")x(4-5")x1.25". The junction box forces each PV panel to have two absorbers on each side of the j-box. **APPENDIX C PV PANEL DIMENSION RANGES**, contains a table of the most popular PV manufacturers and all of their PV models. The table was used to get an idea of typical dimensions for sizing the absorber so that it would fit inside any PV laminate. Table 2 is a summary of the PV dimension compilation and an investigation of the width results shows that the average width of any given PV laminate is about 3 feet, with a standard deviation of about 4 inches. For two absorbers to fit on any given PV laminate the width was determined by the following equation.

$$Width_{absorber} \leq \frac{(Width_{PV,average} - Width_{j-box} - Width_{St.Dev})}{2} = 13.6" \qquad (2.1)$$

Table 2. Maximum, minimum, average and standard deviation for the lengths, widths and weights for the most common PV manufacturers and models.

	Length (in.)	Length (ft.)	Width (in)	Width (ft)	Depth (in.)(includes cover and/or frame)	Weight (lb)
Max	77.56	6.46	41.18	3.43	1.97	61.70
Min	51.57	4.30	26.30	2.19	1.40	27.50
Average	64.19	5.35	35.79	2.98	1.75	40.61
StDev	6.32	0.53	4.14	0.35	0.19	9.25

In accordance with equation 2.1, the width of the absorber for the prototype was set to be 12”.

FLOW CHANNEL SIZING

Adhering to design criteria number 6 (low cost), the design of the absorber was more focused on ease of extrusion and low cost tooling as opposed to optimized heat transfer. That being said, square flow channels were the geometry of choice. The rate of heat transfer by convection between a surface and a fluid can be calculated from the relation

$$q_c = \overline{h}_c A \Delta T \tag{2.2}$$

Where, q_c = rate of heat transfer by convection, W

A = heat transfer area, m^2

ΔT = difference between the surface temperature T_s and the fluid temperature T_{fluid}, K

$\overline{h}_c$ = average convection heat transfer coefficient over the area A, $W/m^2\ K$

When designing a heat exchanger the easiest way to increase the heat transfer rate is to increase the heat transfer area. In the case of flow channels, this is achieved by making the hydraulic diameter as small as possible, thus increasing the total surface area of fluid contact.

The other parameter of interest is the convective heat transfer coefficient, which is calculates as

$$\overline{h}_c = \frac{Nu * k}{D_H} \tag{2.3}$$

Where, Nu = the Nusselt number, dimensionless

k = the fluid thermal conductivity, W/m K

D_H = the hydraulic diameter, m

Increasing the convective heat transfer coefficient will naturally increase the rate of heat transfer, as seen in equation (2.2). The only parameter that is adjustable by design is the hydraulic diameter, which has an inverse relation to the coefficient. Thus, smaller absorber tubes increases the heat transfer coefficient, which increases the rate of heat transfer by convection. The fluid thermal conductivity is a thermodynamic property of the selected fluid and is, of course, a constant when determining the convective heat transfer coefficient.

The Nusselt number for forced convection in tubes is typically evaluated from empirical equations based on experimental results. A dimensional analysis of the experimental results of convection heat transfer reveal that the Nusselt number can be determined by an equation

$$Nu = \emptyset\ (Re)\varphi(\mathrm{Pr}) \tag{2.4}$$

For fully developed, laminar flow in tubes, the Nusselt number is determined by the above relation to be 3.7 for constant wall temperature and 4.4 for constant heat flux. In a solar collector the thermal condition is closely represented by a constant resistance between the flowing fluid and the constant temperature environment. If this resistance is large, then the thermal boundary condition approaches constant heat flux. If the resistance is small, then the boundary condition approaches constant temperature. Therefore, a solar collector will naturally have a Nusselt number in between the two values. For designing and modeling purposes a conservative value is preferred and it is assumed that the thermal boundary condition is constant wall temperature.

Therefore, in order to maximize the heat transfer rate from the absorber to the fluid:

- The heat transfer area should be maximized (achieved by increasing the number of flow channels)
- Minimize the hydraulic diameter in order to increase the convective heat transfer coefficient

- Increase the temperature gradient. The absorber temperature is a function of solar radiation, but the entering fluid temperature should be as cool as possible. Lower temperature water also increases the Prandtl number, increasing the convective heat transfer coefficient

The above analysis obviously suggests that the absorber should have as many flow channels as possible, where the limiting factors are the tradeoff of better heat transfer at the expense of increased pressure drop (increased pumping power) and the limitations of manufacturing.

When the design was taken to Colorado Plastics for quotation, the prototype fabricator, John Butler, recommended that the thickness of plastic separating the flow channels shouldn't be any smaller 3/32" (Butler, 2011). Using the channel wall thickness constraint, an algorithm that calculated the height of the flow channel such that the thickness of material above and below the channel was constrained to 3/32", and the ASHRAE/SRCC test flow rate metric of 0.1GPM/ft^2, the overall thickness of the absorber was varied until the calculated pressure drop along the flow path was comparable to that of other unglazed solar collectors, as reported in the directory of SRCC certified solar collector ratings. Table 3 shows the results for the parametric runs. Run 6 was chosen for the prototype because, the overall thickness was a convenient dimension (¼") and the pressure drop was a reasonable value.

Table 3. This table calculates the hydraulic diameter, the total number of flow channels, the Reynolds number, overall absorber weight, fluid velocity and pressure drop. The overall absorber thickness was varied to get an idea of the changing parameter

Parametric Table: Table 1

	T_{abs}	T_{ch}	$T_{ch,act}$	D_H	N	Re_D	Load	v_{fluid}	ΔP
	[in]	[in]	[in]	[in]			[lbf/in]	[in/min]	[in * WC]
Run 1	0.3	0.09375	0.09803	0.1125	57	274.2	53.48	164.1	1.095
Run 2	0.29	0.09375	0.0975	0.1025	60	285.9	53.45	187.8	1.509
Run 3	0.28	0.09375	0.09798	0.0925	63	301.7	53.43	219.6	2.167
Run 4	0.27	0.09375	0.0966	0.0825	67	318.1	53.41	259.6	3.22
Run 5	0.26	0.09375	0.09651	0.0725	71	341.6	53.39	317.2	5.095
Run 6	0.25	0.09375	0.09539	0.0625	76	370.2	53.37	398.8	8.619
Run 7	0.24	0.09375	0.09565	0.0525	81	413.5	53.34	530.3	16.24
Run 8	0.23	0.09375	0.09543	0.0425	87	475.5	53.32	753.4	35.21
Run 9	0.22	0.09375	0.09516	0.0325	94	575.6	53.3	1192	95.31
Run 10	0.21	0.09375	0.09515	0.0225	102	766.2	53.28	2293	382.4
Run 11	0.2	0.09375	0.09464	0.0125	112	1256	53.26	6765	3655
Run 12	0.19	0.09375	0.09506	0.0025	123	5718	53.23	154000	2.080E+06

Figure 8 through Figure 10 represent the details of the absorber.

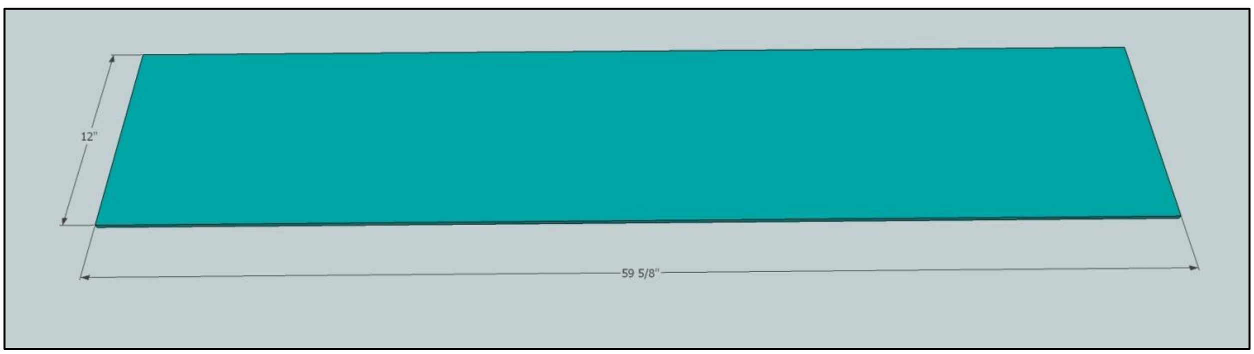

Figure 8. Overall absorber dimensions.

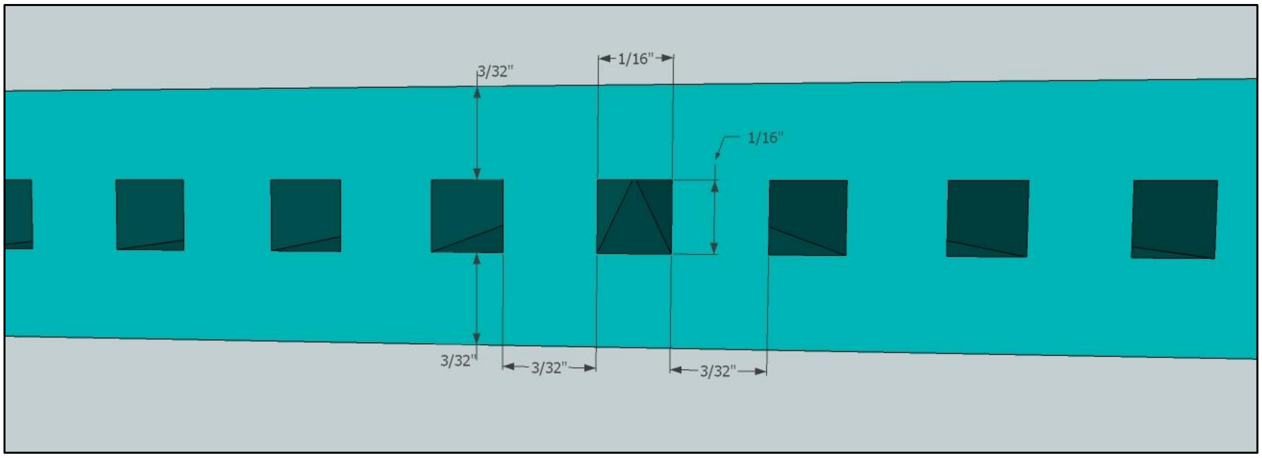

Figure 9. Absorber Flow channel detail.

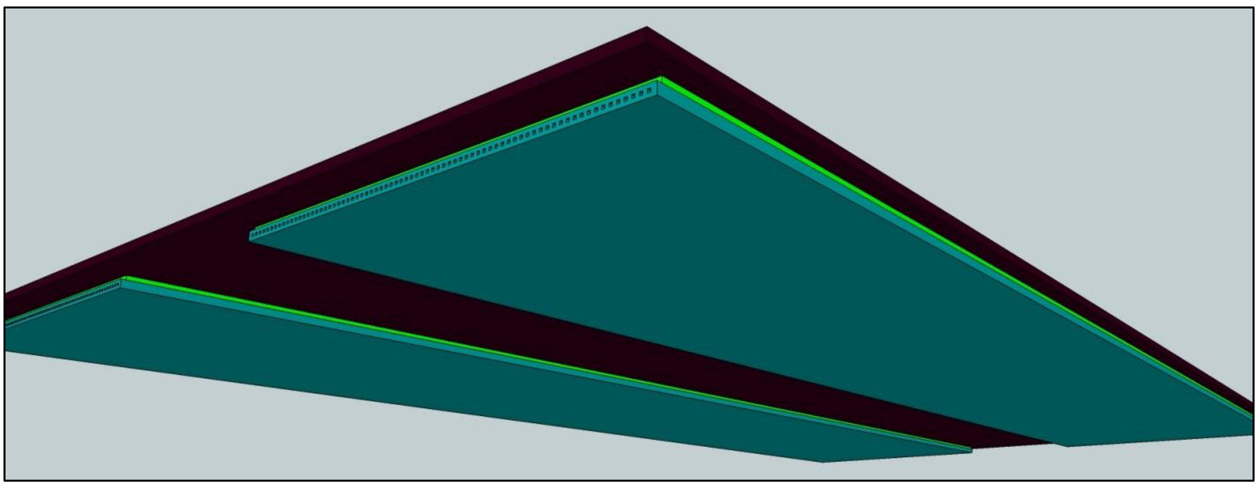

Figure 10. This image shows two spacers and two absorbers underneath one PV laminate.

FLUID HEADER DESIGN AND SIZING

HEADER SIZING

Sizing the fluid headers had to account for an estimated maximum number of modules that would be connected to each other. The sizing criteria followed the common recommendation that sets a velocity limit of 4 ft/sec for pipes 2" and smaller, and a head loss of 4 ft/100 ft of pipe for pipes larger than 2" (McQuiston, Parker, & Spitler, 2005).

Table 4. Header sizing criteria.

Flow rate per module (GPM)	Estimated maximum number of modules connected	Total GPM flowing in headers	Pipe Size accommodating the 4 ft./sec line and GPM line intersection
1	10	10	1"

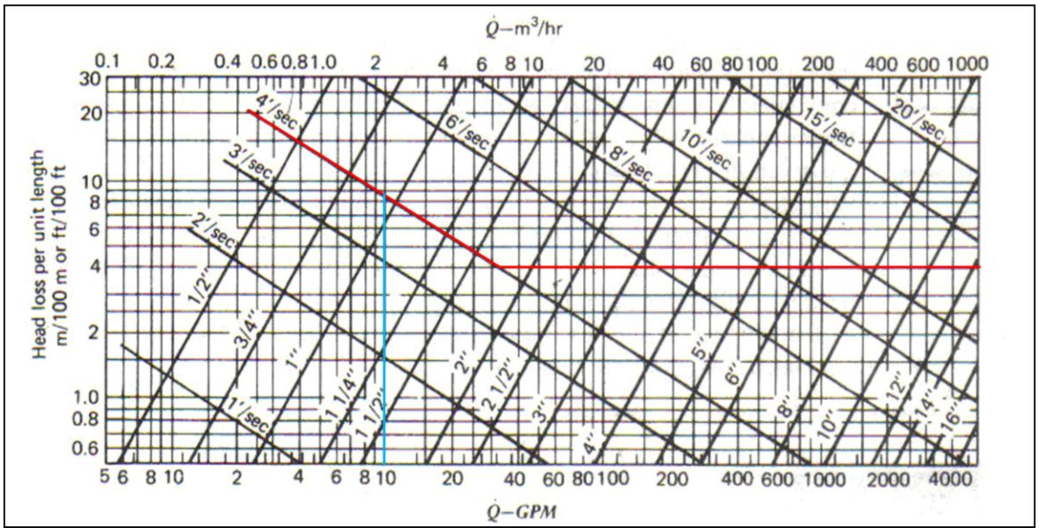

Figure 11. Friction loss due to flow of water in commercial steel pipe (schedule 40). From ASHRAE Handbook, Fundamentals Volume, 1989.

Applying the criteria of Table 4 and the recommendations of Figure 11 the module supply and return headers were sized to have a hydraulic diameter of 1". For a square conduit the lengths of the sides of the conduit were found by the relation

$$D_H = \frac{4\ Area_{cross-section}}{Perimeter} = \frac{4l^2}{4l} = l = 1" \tag{2.7}$$

HEADER DESIGN

The headers were designed such that their profiles could be easily extruded and cut to the size of any PV laminate. The upstream and downstream headers are not identical and differ in the way that the integrating flanges work. Adhering to design criteria 2 through 4, the headers need to integrate with each other such that an aesthetic façade is generated, the integrated array acts like roofing shingles, and the completed module can be mounted directly to the roof. Figure 12 show the details of the supply and return headers. The "integrating slip and flange" serve the purpose of generating the aesthetic and even façade to act like roofing shingles. During installation of an array, only two sides of the module will be accessible for fastening to the roof. In order to provide added support to the inaccessible sides, the "mounting integrating flanges", as seen in Figure 12, will provide the additional support (See Figure 13).

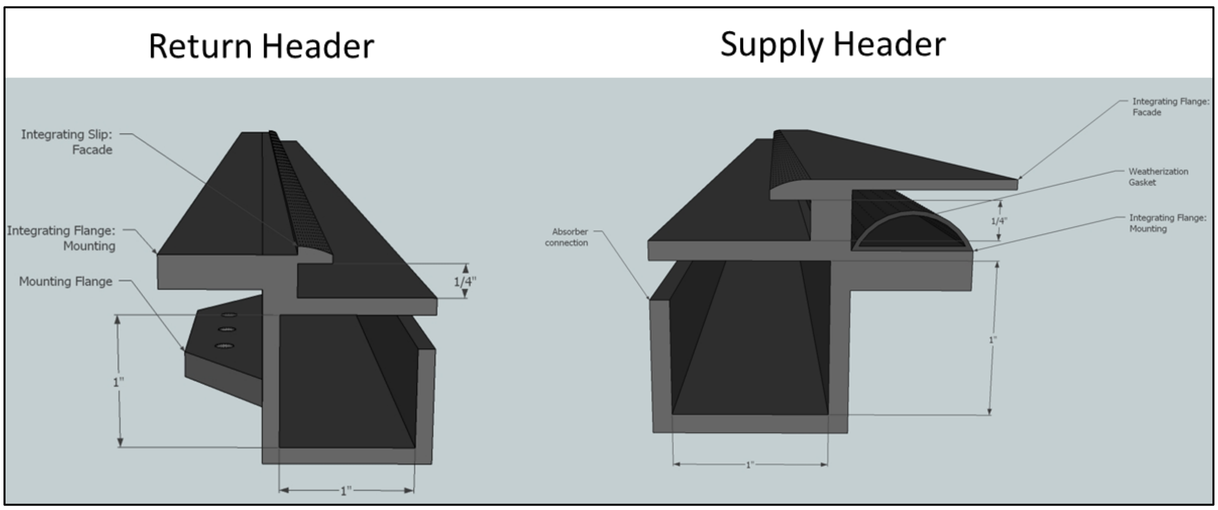

Figure 12. Supply and Return headers

The functionality of the integrating flanges is best demonstrated by Figure 13. The installation procedure for any given array is similar to the installation of roofing shingles. The array should be started in the lower left hand corner of the roof and work its way left-to-right, bottom-to-top.

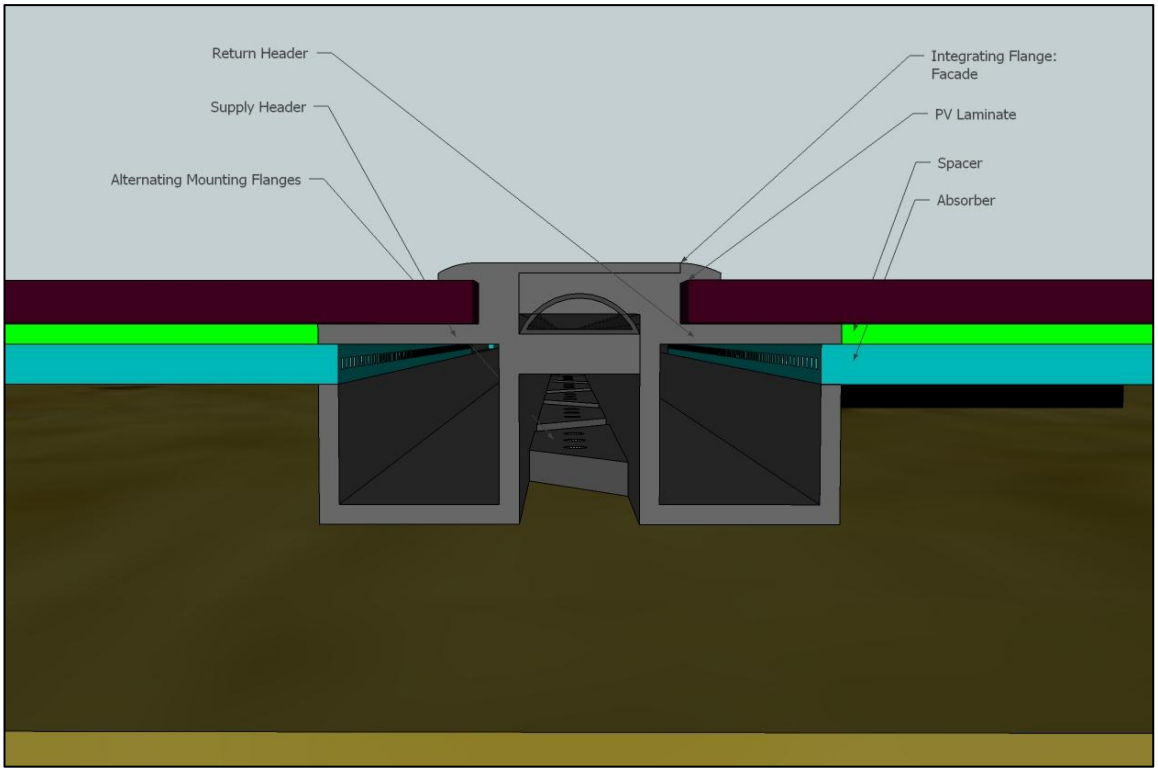

Figure 13. Detail of the Supply and Return Header Integration

SIDE-RAIL DESIGN

The side rails were designed with an extrudable profile in mind. Naturally, the height of the side-rails needs to match the height of the headers, and the width was chosen to be ½" primarily based on the convenient metric. The details of the side rails are shown in Figure 14. Similar to the header design, the "mounting integrating flanges" are for additional support when fastening to the roof when the mounting flanges are inaccessible.

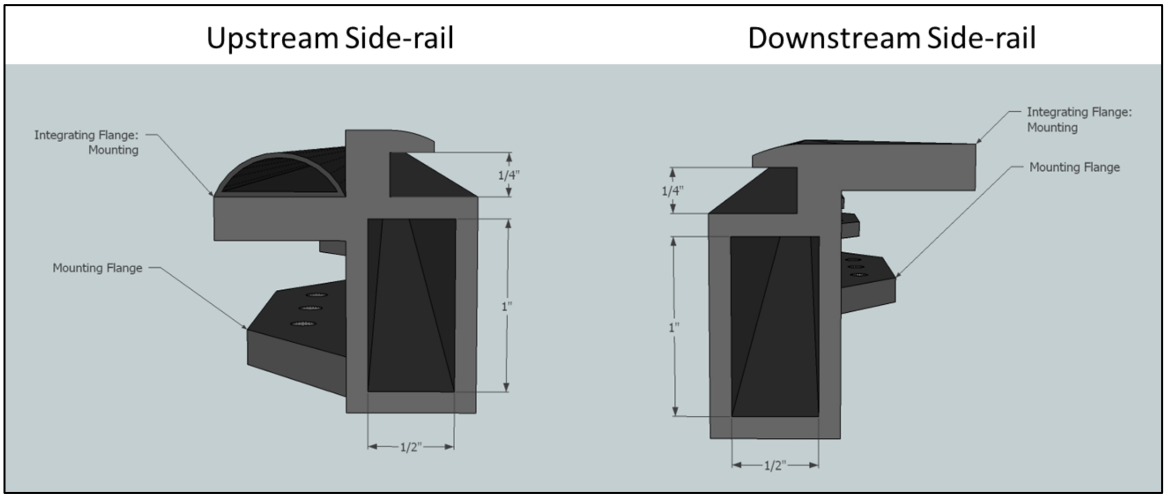

Figure 14. Side-Rail detail

Figure 15 is the detail of the side-rail integration. The gasket will be compressed into a full weatherproofing layer between the modules.

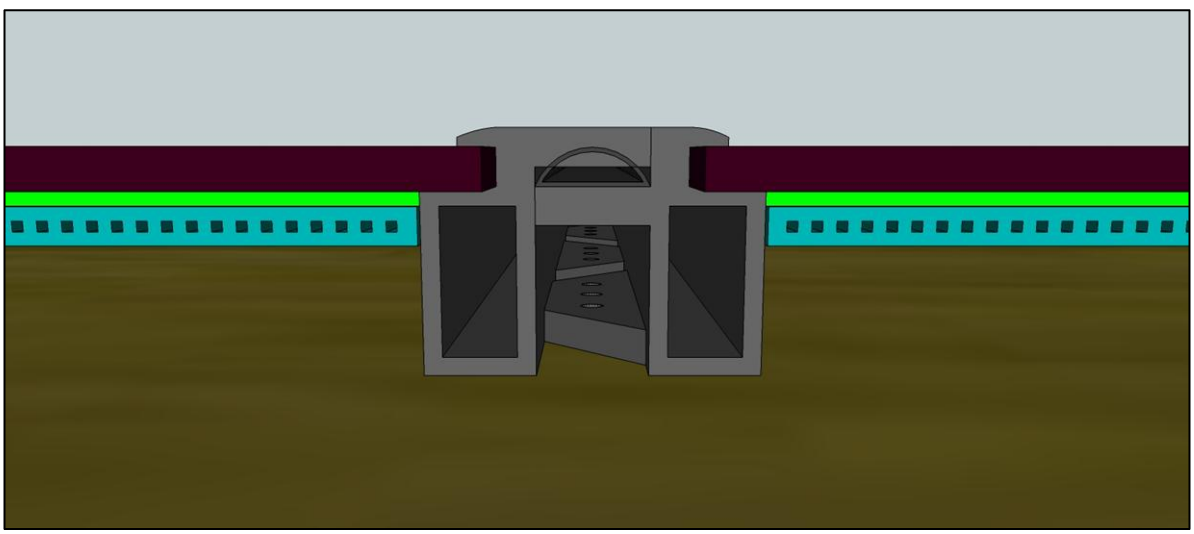

Figure 15. Side Rail integration detail

MOUNTING FLANGE SIZING AND DETAIL

The mounting flanges will be an extra extrusion that will have to be glued or welded onto each of the headers and side-rails. Figure 16 is the detail of the mounting flange. In mass production of the mounting flange, it is most likely that the screw holes will simply be punched out at 90° angles after the extrusion takes place. Due to the integration of the modules, there is no extra room for the mounting flange to stick out past the other integrating flanges, without occupying the same space as the neighboring module headers or side-rails. Thus, the wood screws will have to be inserted at an angle.

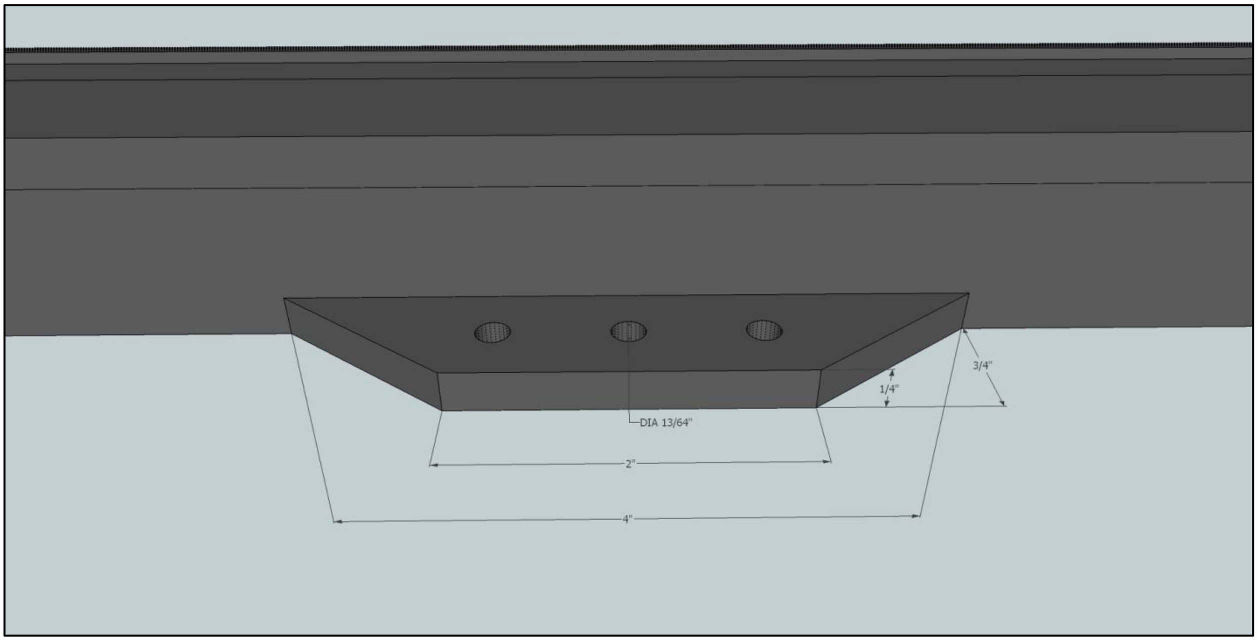

Figure 16. Mounting flange detail.

Figure 17 shows the angle of approach that the wood screw will have to be in order for fastening to the roof. The elevation angle is about 72° and the corresponding zenith angle is 18°. Assuming the installation will use a standard 10-gauge wood screw, with a shank diameter of 3/16", the effective shank diameter at an 18° zenith angle is 0.197". To account for the thickness of the mounting flange (1/4"), the diameter of the hole needs to be at least 0.28"

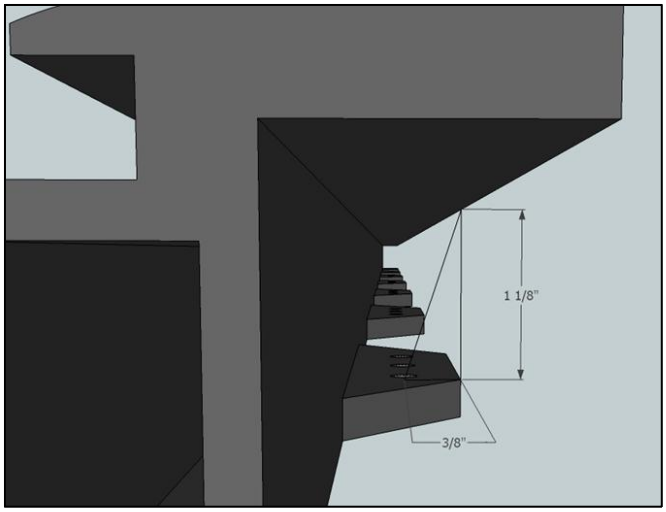

Figure 17. Roofing screw angle of approach.

JOINT DESIGN

The joint is the only piece of the module that can't be extruded. The joint is the critical piece that connects the headers to the side-rails. The connection is made by glued slip-fits.

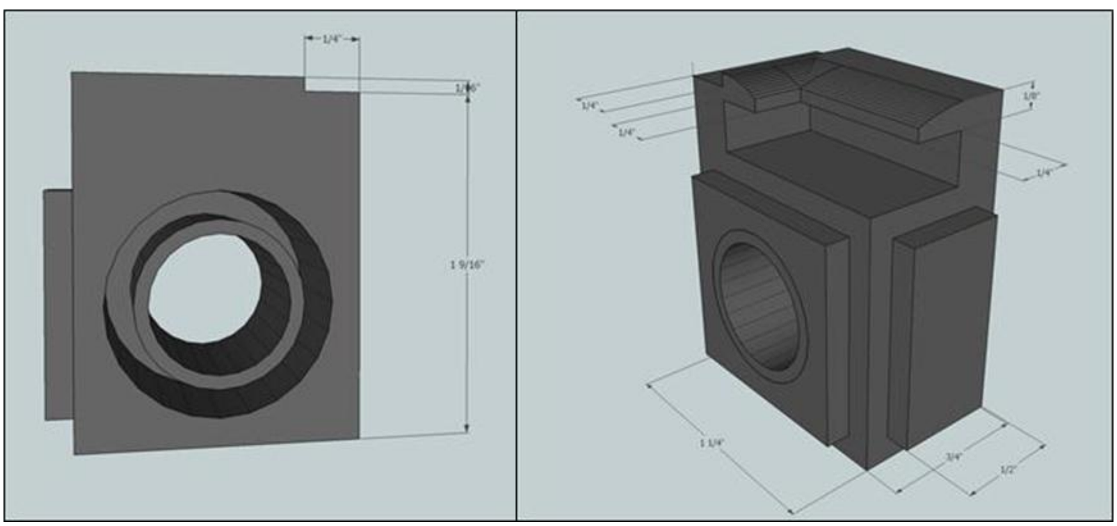

Figure 18. If flowing water from left-to-right, bottom-to-top, then these two images show the details of the downstream return joint (top right corner). One half of a 1/2" plastic union is to be countersunk into each joint, as seen in the image on the left.

Due to integration requirements, all four joints are slightly different. The mass production of these joints would be manufactured using an injection molded piece of tooling. All plastic thicknesses are 1/8" unless otherwise specified.

The top drawing of Figure 19 is an example of what an array would look like. The bottom drawing of Figure 19 is a zoomed in view of one of two 4-way junctions of the array in the top drawing. There is a gap between modules due to the union that connects the header of one module to the header of another module. A separate piece of plastic is to be manufactured to so that it closes the gap and attaches by a snap or push-fit mechanism.

For more detailed drawings and a recommended sequence of assembly, please see **APPENDIX B PROTOTYPE FABRICATION DRAWINGS**.

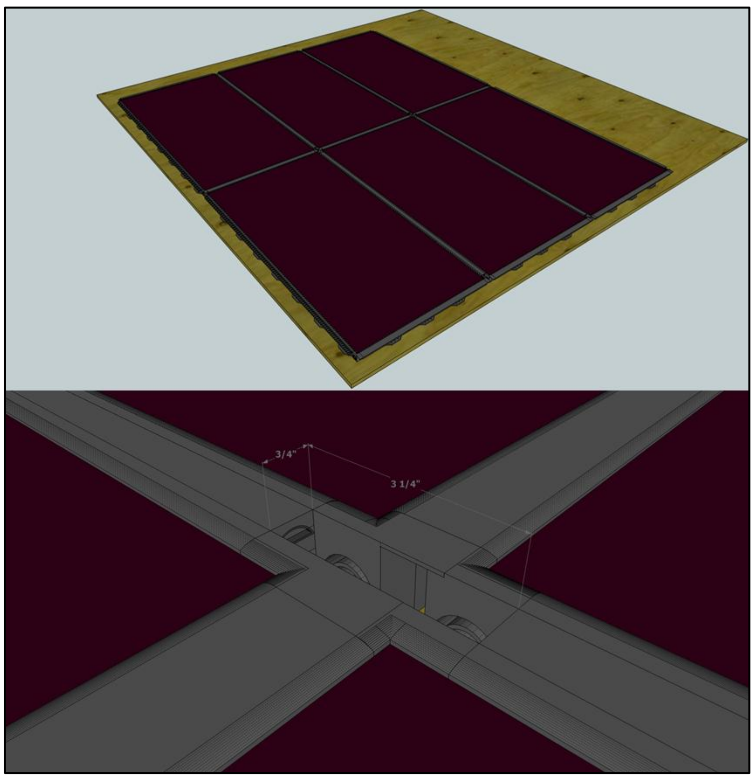

Figure 19. The drawing on top shows an example array fitted together. The bottom drawing is zoomed in at one of the junctions. An additional piece of plastic is to be push-fitted into all 4-way junctions.

MATERIAL SELECTION

When the original design was discussed with the master fabricator at Colorado Plastics it was decided that PVC would be an inexpensive, easily workable material for the job. Other materials that were discussed were polycarbonates. The polycarbonate would have been a nice option for the absorber because it comes as a sheet with rectangular channels already extruded. The problem with using the polycarbonate is that it doesn't bond with PVC, meaning that the entire module would have to be made from polycarbonate, which is an opaque color. Trusting the expertise of the fabricator PVC was selected and the fabrication began.

DESIGN MODIFICATIONS AND CONSTRUCTION PROBLEMS

The first issue with the designs that were sent to Colorado Plastics (see APPENDIX B PROTOTYPE FABRICATION DRAWINGS) was the lack of support the absorber. Being connected by an 1/8" at both ends of the 5' long run, caused the absorber to sag. John welded in some side rails on the inner sides of both absorber, and welded the absorber along the side rail.

The original design was sized around a particular union, but the unions that John picked up were slightly different. Thus, in order to get the profile height correct for the modules, a specific union needs to be selected to ensure that there is enough clearance in the profile height and to properly align the integrating flanges.

Construction issues with the absorber are discussed at length in CHAPTER 3 THE PHYSICAL EXPERIMENT. Basically, the technique used to machine and close the flow channels was unsuccessful, and water was not properly contained in the flow channels.

CHAPTER 3 THE PHYSICAL EXPERIMENT

As mentioned in Chapter 1, the purpose of this research is to design and build a patentable, modular BIPV/T prototype to assess the prototype's performance, economics, constructability and operation and maintenance. In order to accomplish these tasks, a physical experiment needed to be setup to test the modules. The first decision to be made was to decide where the experiment was to be built. The most practical place to test the modules was on campus. The Building Systems' Larson Laboratory is located on the second floor of the Civil Engineering wing, with direct access to the roof. Approval from the University's Facility Management was required before construction could begin. Having the BIPV/T experiment in the Larson Lab will be useful for many future solar thermal projects.

SHADING ANALYSIS

The location of choice is an 87 ft south facing wall along the south side of the Larson Lab. Of the 87 ft., about 30 ft. of the eastern most section of the wall is useful for solar testing. Before any construction began, a shading analysis was conducted. Google SketchUp was the tool for the job. The roof area needed to be drawn to scale such that the surrounding buildings' shadows could be modeled. Google SketchUp has several great features for performing the shading analysis. The first feature is the Match Photo tool. This tool allows you to import photos into the model space and generate 3D models to match the photo. Taken from Google SketchUp documentation (Google SketchUp Match Photo, 2011)

> **High-level steps for creating a model from photos**
>
> Creating a model from photos consists of 4 high-level steps:
>
> 1. Take digital pictures of a building or structure. Refer to Taking Digital Photos for Use When Matching for further information.
> 2. Start matching. Matching involves loading a digital picture and calibrating SketchUp's camera to the position and focal length of the camera used to take the actual photo (you are setting up the exact criteria used to take your picture so you can draw on the picture). You can also set the scale of the actual building or structure while matching, or just resize the entire model after it has been drawn. Refer to Creating a 3D Model to Match a Photo for further information.

3. Start sketching. Once you have duplicated the position and focal length of the camera used to take the picture, you can draw over the image in SketchUp. SketchUp moves into a 2D sketching mode from matching (it is 2D because you are drawing on a 2D photo that needs to be oriented at a specific camera angle to you). Refer to Creating a 3D Model to Match a Photo for further information.
4. Repeat Step 2 and 3 with any photos representing other views of the building or structure.

PHOTO MATCH

Following the above steps, the buildings were traced and pushed into 3D images. Figure 20 through Figure 23 show the similarities.

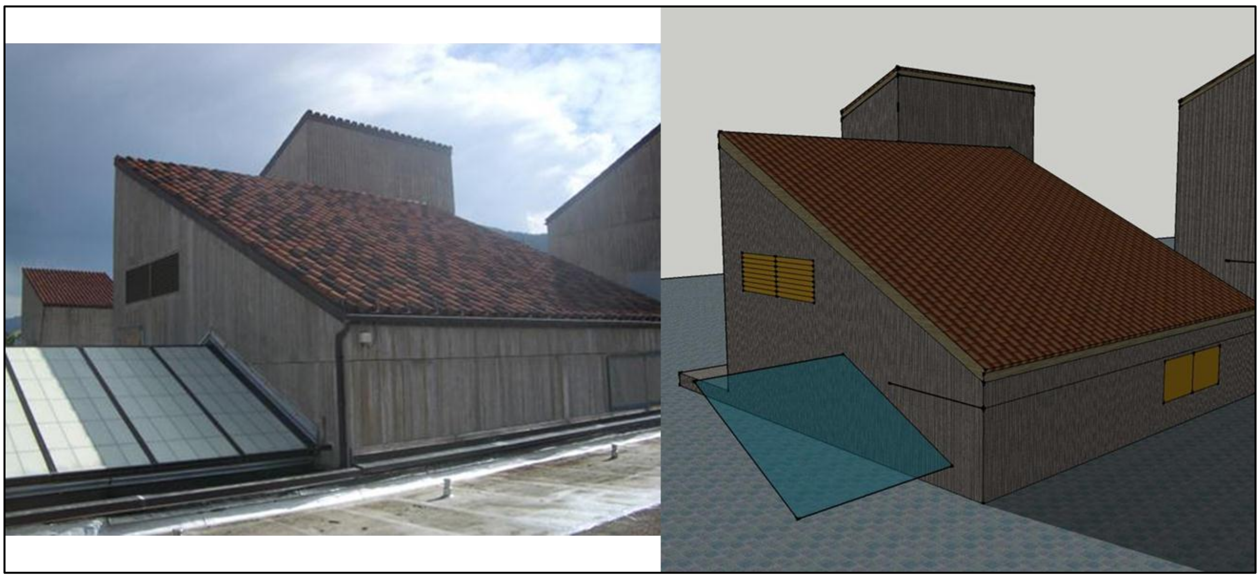

Figure 20. The building directly across from the array location.

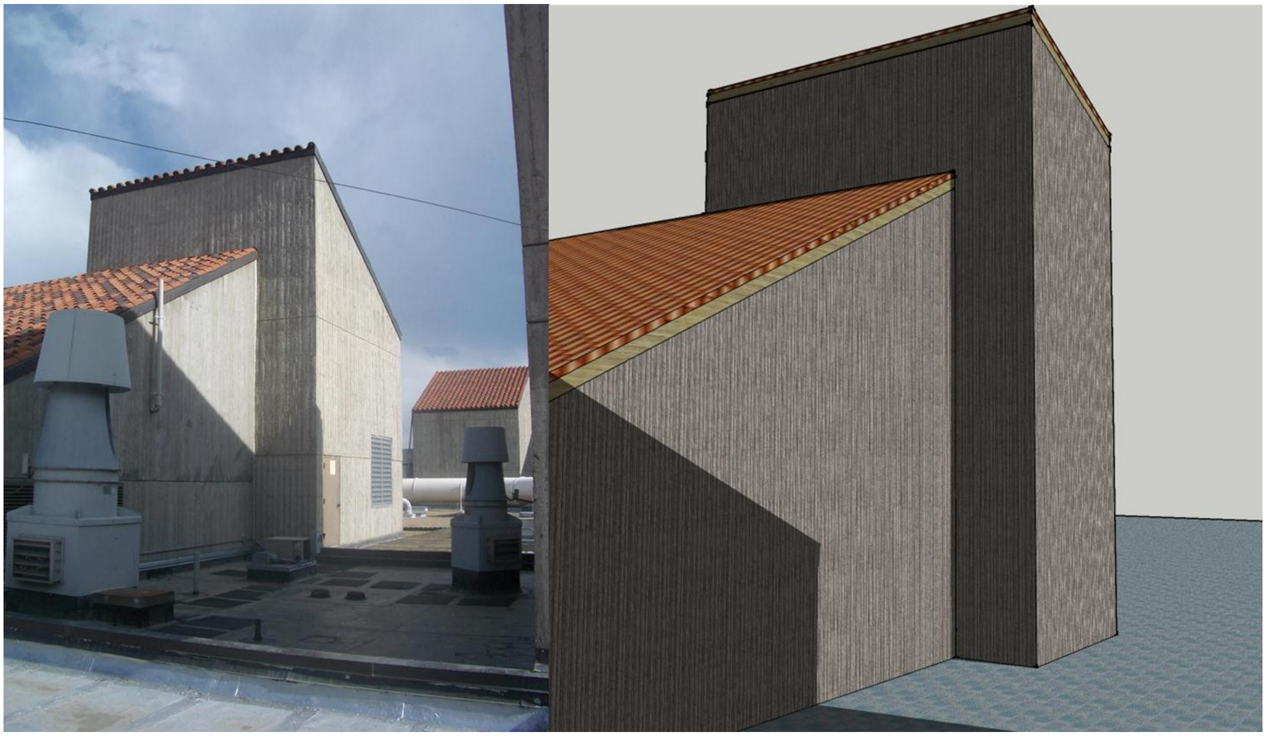

Figure 21. Same building as in the above figure, looking southeast.

Figure 22. Outside of the Larson Lab. This is the south facing wall to be used for testing.

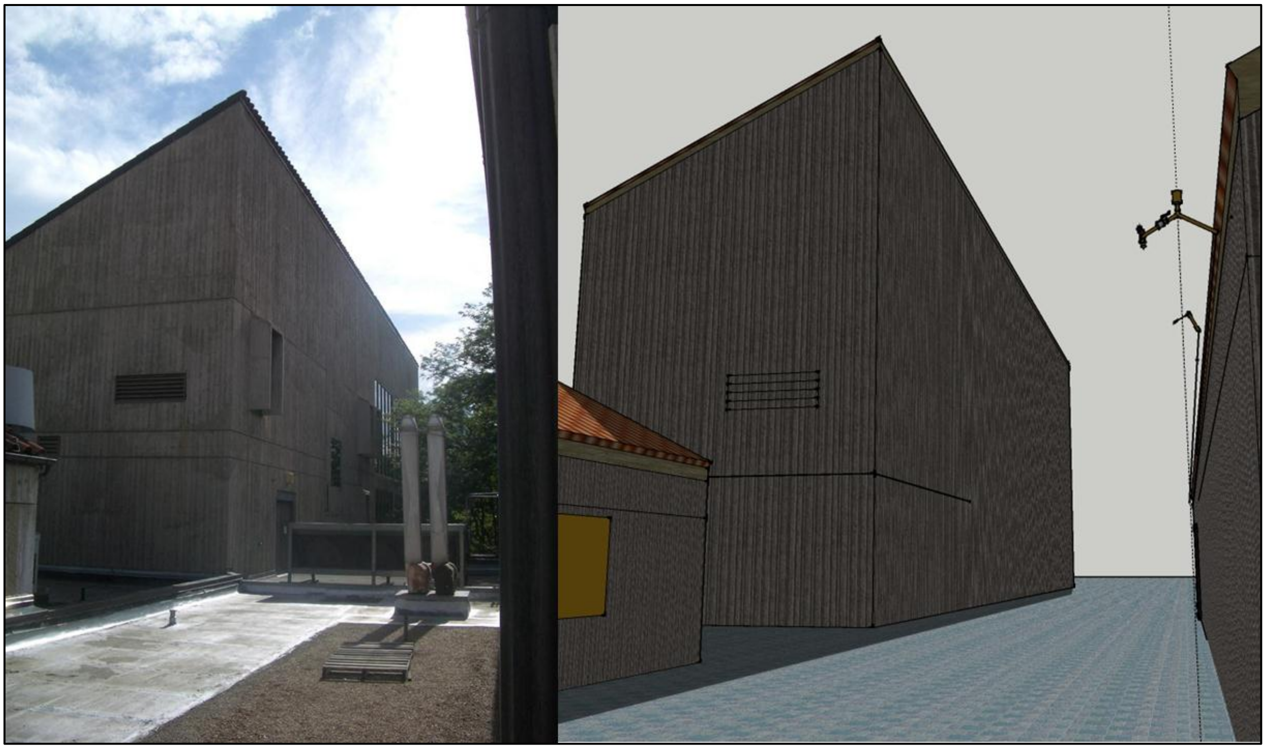

Figure 23. The tall building directly in front of the door from the Larson Lab onto the roof.

Using a tape measure, the layout and spacing of the three building was set.

GEO-LOCATION

The next step in using Google SketchUp as the shading modeling program is to properly set the latitude, longitude and orientation for the solar calculations. SketchUp has a couple very nice features for this. The Geo-location tool is extremely easy to use. Go to **Window>Model Info, and select Geo-location** from the left list of options. This launches Google Earth from within SketchUp. From here you can find the exact location of the model, select the region to the desired size, click "grab" and the image is automatically imported with a true north arrow centered in the zone. From here you can set your model exactly to the precise location and orientation. Figure 24 shows the roof top 3D model set against the Google Earth image. Note the latitude, longitude and the true north arrow. As can be seen from the figure, the wall faces dead south.

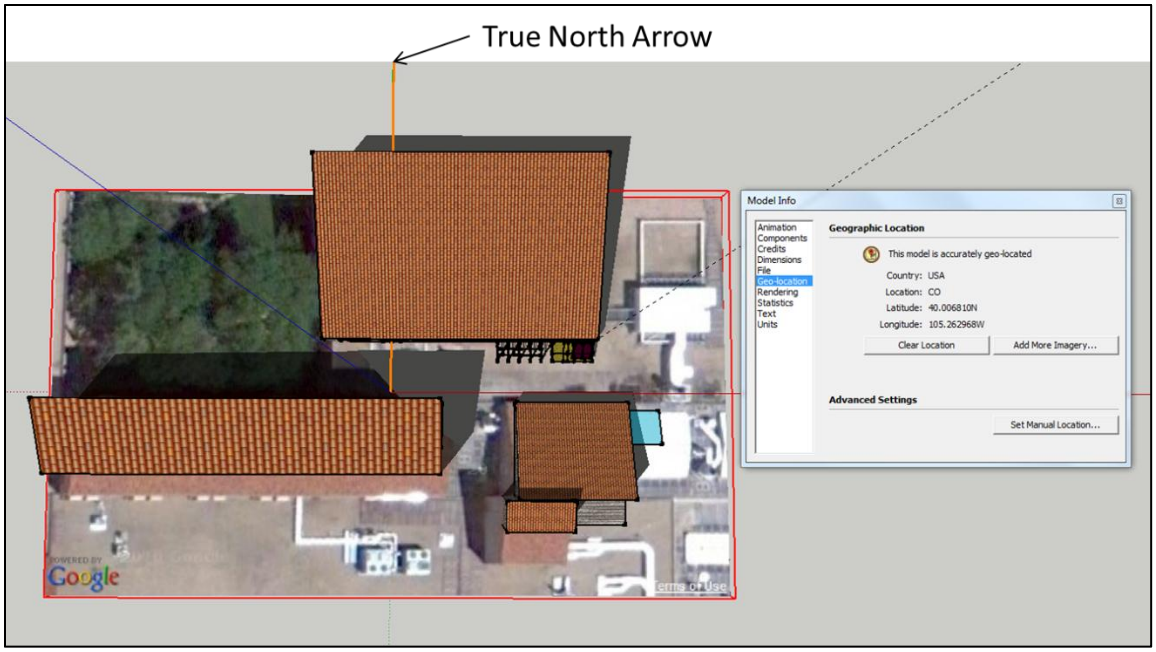

Figure 24. The roof top model set against the geo-location imported Google Earth image, with precise latitude and longitude and a true north arrow.

SHADING RESULTS

The shading results will be for two array scenarios:

1) The western most array of only two BIPV/T modules (of concern to this project) and
2) The entire array area for larger future project.

Figure 25 and Figure 26 show the shading results for January 23, at 2pm (the last time a shadow crosses the array between peak sun hours) and the shading results for January 24, from 10am-2pm, (the first time of the year that the array is not crossed by a shadow during peak sun hours) for the first scenario, respectively.

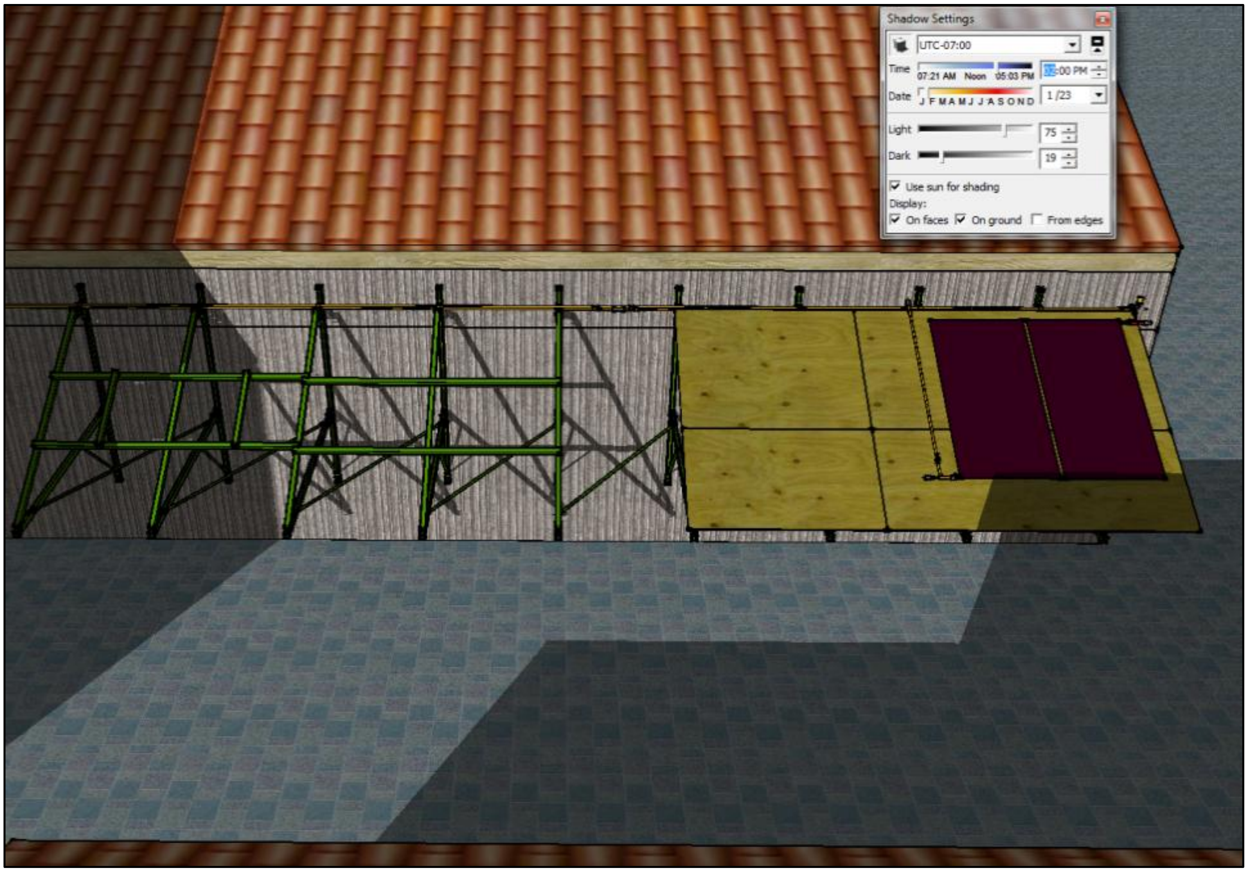

Figure 25. This is the last day and time between peak sun hours that a shadow crosses the BIPV/T array. [January 23 at 2:00pm]

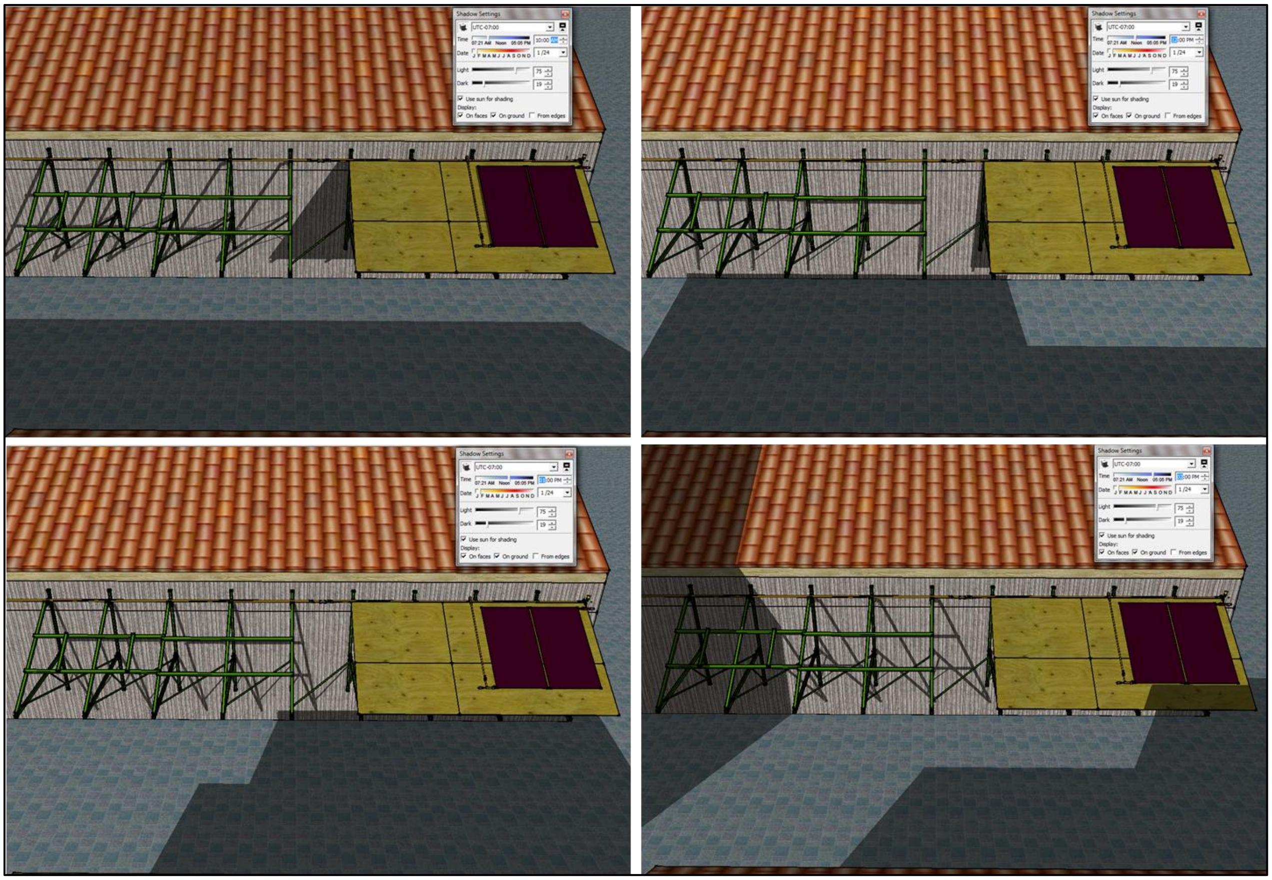

Figure 26. From left-to-right, top-to-bottom; Looking north, these are the shadows cast on the array at 10am, 12pm, 1pm, and 2pm. This is the first day of the year that the array is shadow-free during peak sun hours [January 24].

Array scenario 1, is shadow-free from 10am-2pm daily until November 19, as seen in Figure 27.

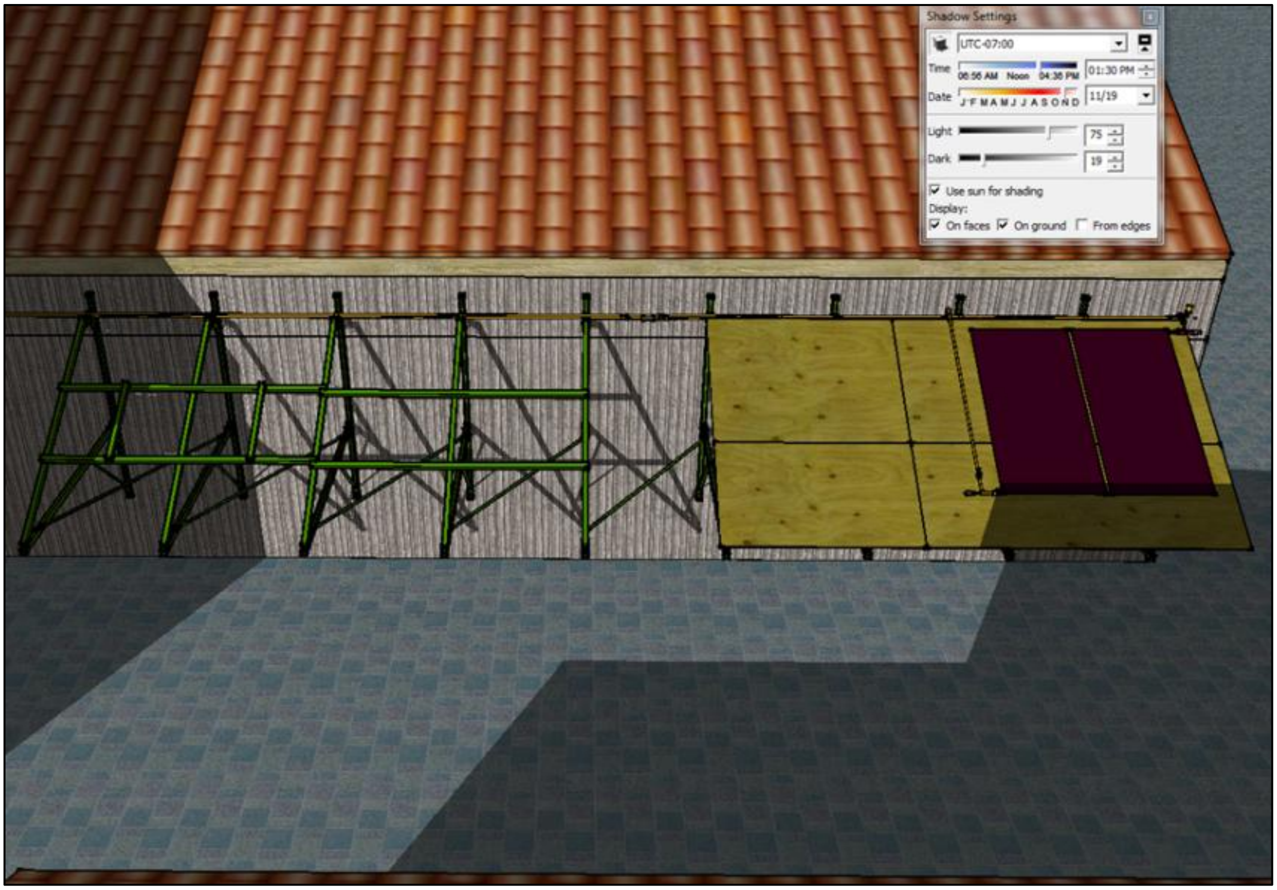

Figure 27. This is the shadow cast across the array on November 19 at 1:30pm. This is the first time that a shadow is cast across the array since January 23.

Figure 28 shows the shadow cast across array scenario 2, the entire array. The top image is on May 1 at 2pm, the first time of the year that no shadow is cast on the array between the hours of 10am-2pm. The bottom image is on August 10 at 2pm and is the last time of the year that no shadow is cast on the array between the hours of 10am-2pm.

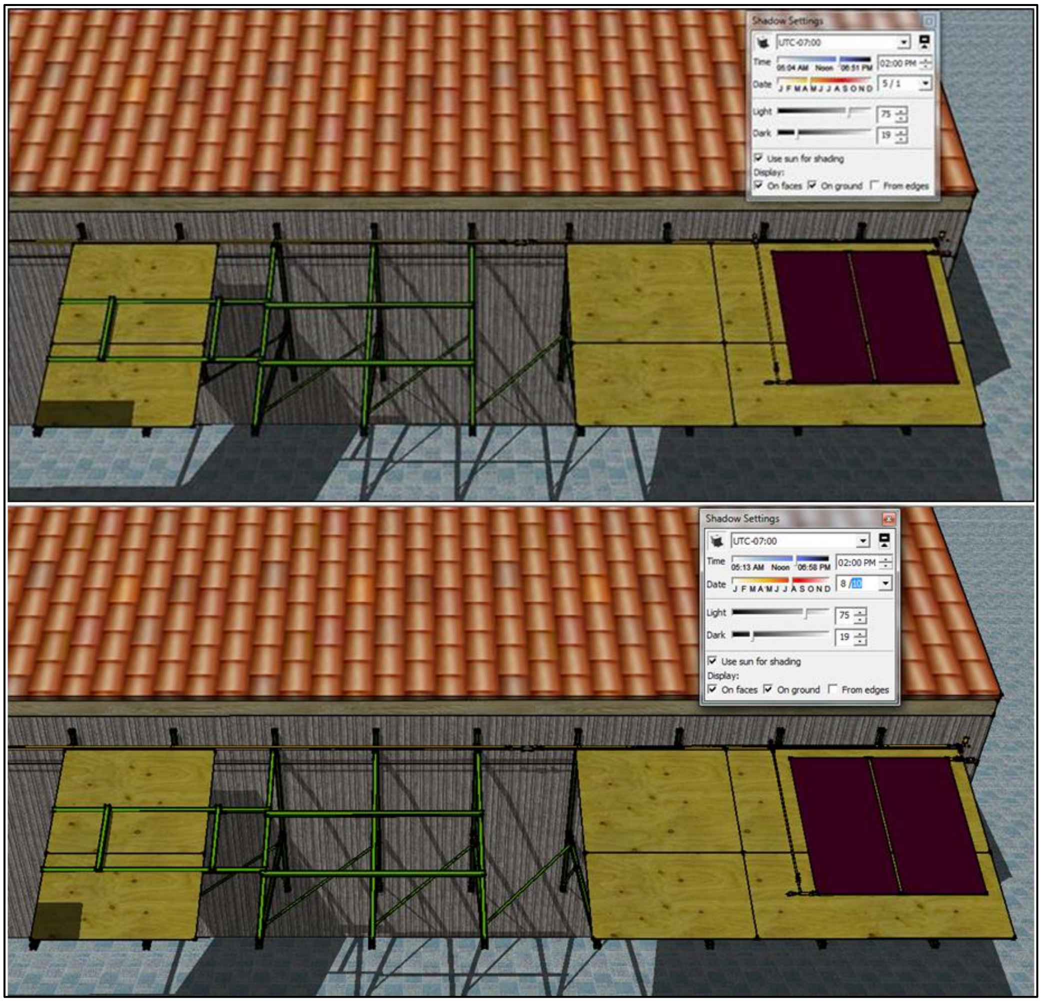

Figure 28. The top image is May 1 at 2pm. This day and time is the first day that the entire array is shadow free from 10am-2pm. This scenario lasts until August 10, as seen in the bottom image.

Table 5 is a summary of the shading results

Table 5. Summary of Shading Analysis.

Array Scenario	First Day of the year when the array is shadow-free	Last Day of the year when the array is shadow-free	Total consecutive Days of shadow-free exposure
1 – Western Side	January 24	November 19	299
2 – Entire Array	May 1	August 10	101

SIZING THE THERMAL STORAGE TANKS

The first step in sizing the thermal storage tanks was to decide on the highest temperature that was desired to be in the system. This value was selected to be 140°F, equal to the typical leaving water temperature of a DHW tank. The ΔT was then calculated assuming that the initial water temperature of the tanks would be at about room temperature, 75°F. NREL's *U.S. Solar Radiation Resource Maps* was used to find the average daily solar radiation per month, $\overline{H}_T$, from Figure 29 . September was chosen as the month in anticipation of running tests at that time.

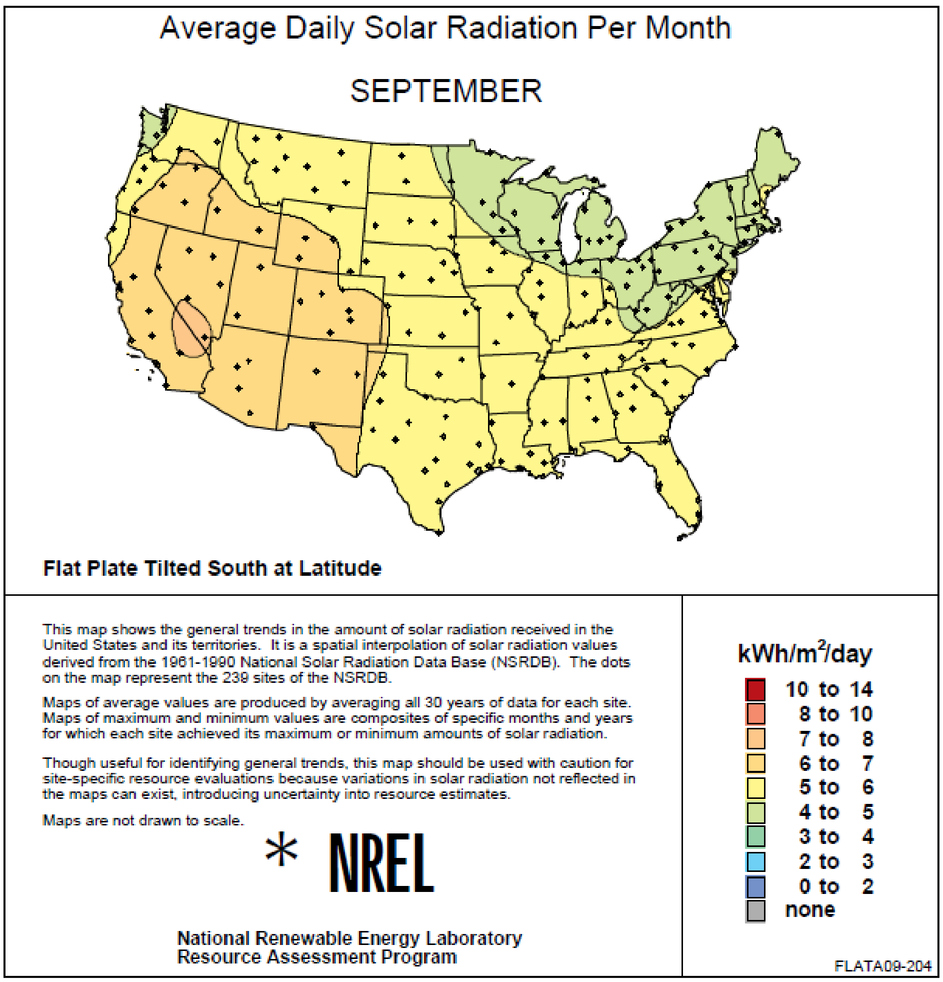

Figure 29. Average Daily Solar Radiation per Month. This map was used to size the water storage tanks.

$$\overline{H}_T = 7.5 \frac{kWh}{m^2 day} * 3600 \frac{s}{h} = \frac{mC_p\Delta T}{A_{collector} * \eta_{collector}} \tag{3.1}$$

Where, ΔT = 140°F - 75°F = 65°F or 18°C

$A_{collector}$ = 3 * 1.24m^2

$\eta_{collector}$ = .25

$C_p = 4.19 \frac{kJ}{Kg\ K}$

The tanks were sized in anticipation of having three BIPV/T prototypes and the efficiency of the collector was an approximate conservative value. Solving for the mass in equation (3.1) and converting to US gallons, the total thermal capacity of the system should be approximately 88 gallons. Thus two 55 gallon, plastic open top tanks were selected for the job.

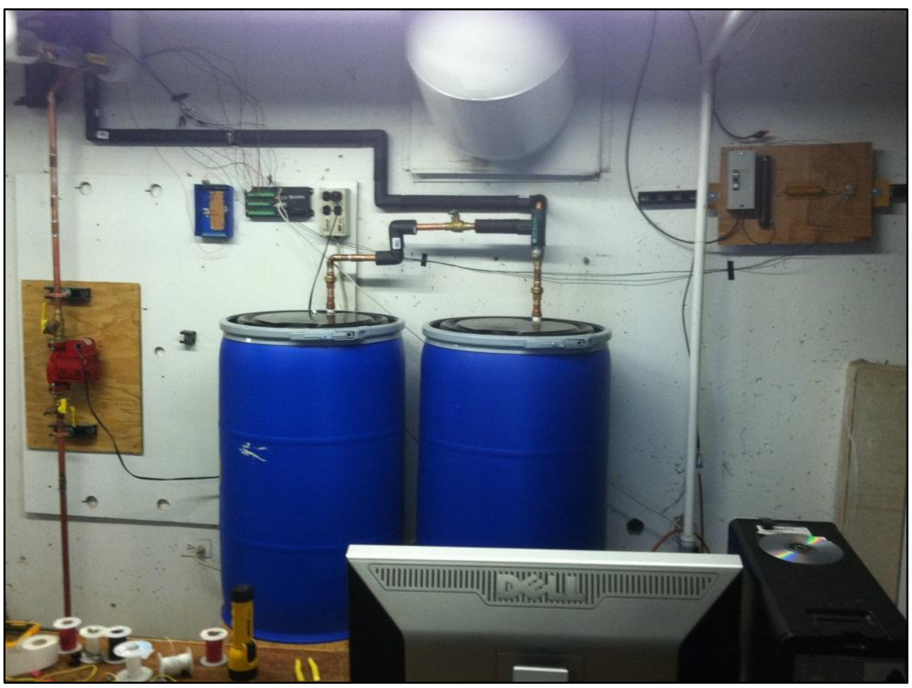

Figure 30. This is a photo of the experiment from inside of the Larson Lab. In the upper right hand corner is the electrical terminations and PV load dumping station. Centered in the photo are the two 55-gallon tanks, and the datalogger and thermistor enclosure. The 1/6 HP circulator pump is seen in the left hand side of the photo.

SIZING THE PUMP

Table 6 is used in conjunction with Table 7. The head loss calculations follow the methods outlined in (McQuiston, Parker, & Spitler, 2005). References to tables and figures in Table 6 are referring to the aforementioned text. 5 GPM was chosen as the highest test value to be flowed through two of the BIPV/T modules. Anticipated application flow rates will be less than 1 GPM/module.

Table 6. Criteria and constants to be used in calculating the system head loss for pump sizing.

Type L copper tubing			
Pipe size criteria			
maximum GPM:	5	GPM	
maximum head loss:	7	ft/100ft in main run	
3/4" copper pipe to be used			
Friction Factor (3/4") Fm table10-2	**0.025**		
	Fm Fig. 10-22a	**Fm Fig. 10-22b**	
Fittings	**K**	**L_eq**	
Tee's (branch flow, thermistor will be inserted along run flow)	1.5	4	
Ball Valves	0.075	0.33	
elbows	0.75	3	
flow meter	treating like ball valve		

Table 7 breaks up the piping system into 7 segments and calculates the fittings equivalent length and then calculates the head loss for each section. A safety factor of 15% was used to ensure extra capacity and to accommodate unforeseen plumbing issues.

Table 7. System head loss spreadsheet.

							Fittings					
Pipe Section No	Description	Flow Rate, gpm	Nominal Size, in	Fluid Velocity, ft/sec	Lost Head per 100 ft, ft/100ft	Pipe Length, ft	Type	Count	Fittings Equiv. Length, ft	Total Length, ft	Collector Lost Head, ft	Total Lost Head, ft
1	From Tanks	5	3/4"	3.272849	7	26	ball valves	2	0.66		-	
	to outside						elbows	5	15	41.66	-	2.9162
2		5	3/4"	3.272849	7	69	elbows	4	12		-	
							ball valves	4	1.32		-	
							flow meter	1	0.33		-	
	run to collector						Thermistor Tee	1	4	86.65	-	6.0655
3	thru collector	5	variable	variable	variable	-	-	-	-	-	-	10
4		5	3/4"	3.272849	7	1.5	elbows	2	6		-	
	collector to						Tee	1	4		-	
	straight run						ball valves	3	0.99	12.49	-	0.8743
5	run to inside	5	3/4"	3.272849	7	67.5	elbows	3	9	76.5	-	
6	building penetration	5	3/4"	3.272849	7	30.5	elbows	7	21			
	to tanks						ball valves	2	0.66	52.16	-	3.6512
7	tank 1 to tank 2	5	?	3.272849	7						-	-
Elevation											-	4
											total	27.5072
										Safety Factor (15%) total		31.63328

Having calculated the system head of 32 ft. at a flow rate of 5 GPM, the ARMSTRONG ARMflo E series circulator – model E8 was chosen see APPENDIX D PLUMBING COMPONENTS, for more pump information. Figure 31 is the selected pump performance curve. It is clear from the figure that the pump can handle 32 ft. of head at a flow rate of about 5 GPM. Figure 32 is a photo of the pump station.

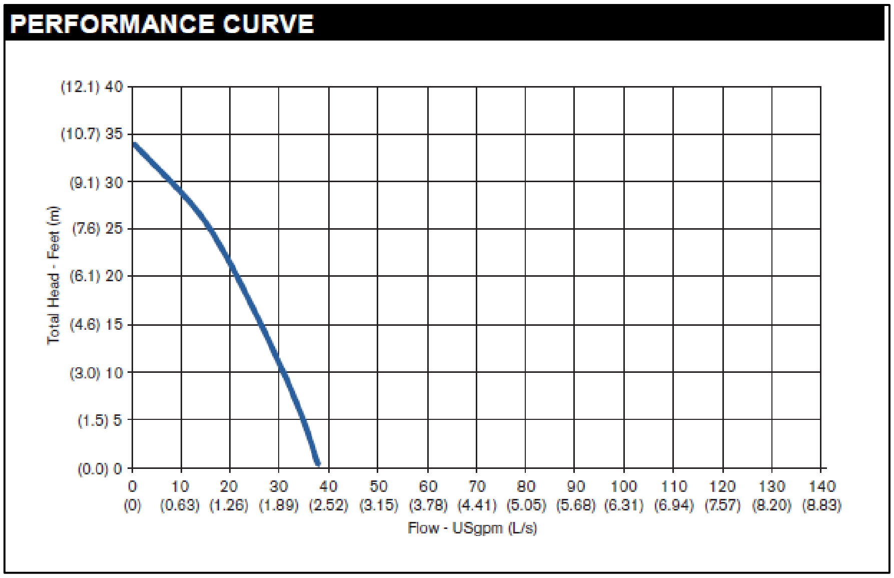

Figure 31. Armstrong E8 circulator pump performance curve.

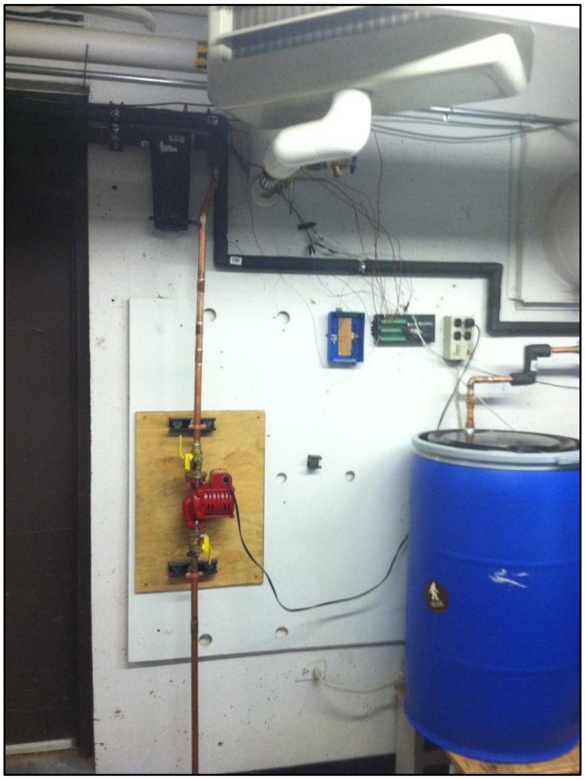

Figure 32. Photo of pump station and water filter.

CHARGING THE PUMP

The plumbing system that was installed is a closed-loop, open to atmosphere drain-back system. Unfortunately, starting the system was far more difficult than simply filling the tanks and turning on the pump, primarily due to air getting caught in the lines as a result of having to constantly drain the system to prevent freezing. The following list is a method that worked in charging the pump and starting water flow in the system:

1. *Fill system in collector bypass, closing valves along the way to the high point*
    a. *Close collector supply valve*
    b. *Close collector return valve*
    c. *Open bypass valve*
    d. *Open supply and return drain valves*
    e. *Open upper drain valve, next to air separator*
    f. *Fill from upper pump fill bib*
    g. *Close top pump valve*
    h. *Open bottom pump valve*
2. *Fill Tank 1 (closest to the pump) to the top*
    a. *As the city water starts to flow through the system, follow the water to all of the drain valves, and shut them down after the air has been pushed out*
    b. *Once all drain valves are closed, check the air separator for proper operation*
    c. *Confirm that the water is flowing into tank 1, and fill to the top*
3. *Open top pump valve (for a few seconds) to let the water column run back through the pump and push the air out of the pump back through the tank. Then close the valve*
4. *Turn on pump*
    a. *The pump will be deadheaded, but the pressure will rise allowing for system to start flowing*
    b. *Slowly open the top pump valve (allowing water to flow)*
5. *Open the valve to tank 2 and convince yourself that the water is circulating (not just falling from a higher head)*
6. *Slowly open collector fill valve until water flows out of the system through the upper drain hose bib (purging the collectors of air). Once water starts to flow through the system at a consistent rate, leave the valve in that position*
7. *Slowly start to close the bypass valve noting that the flow through the collectors will be increasing, thus increasing the pressure.*
    a. *As the flow through the collectors starts to increase, start throttling back the collector supply valve, as not to over pressurize the collectors and damage them. Completely close the bypass valve.*
8. *At this point water is still flow out the top drain valve and the collector is not pressurized.*

    a. *Open the collector return valve and close the drain hose bib*
9. *Read flow rate from data collector and adjust with the supply valve until the desired flow rate is achieved.*

WATER FILTRATION

Water filtration was required for this project in order to prevent the absorber flow channels from getting clogged with debris. The filter housing was selected to handle the highest of anticipated temperatures, while the filter cartridge only passed particles smaller than the diameter of the absorber flow channels. Please see APPENDIX D   PLUMBING COMPONENTS for the specification about the water filtration system.

SIZING THE POWER RESISTORS

It is imperative that the power generated by the PV panels be removed from the BIPV/T module, in order to appropriately account for the behavior of the system. Several power resistors were wired in series to dump the electrical energy. The power resistor bank was sized such that the equivalent resistance intersected the PV IV-curve at the maximum power point, as demonstrated in Figure 33.

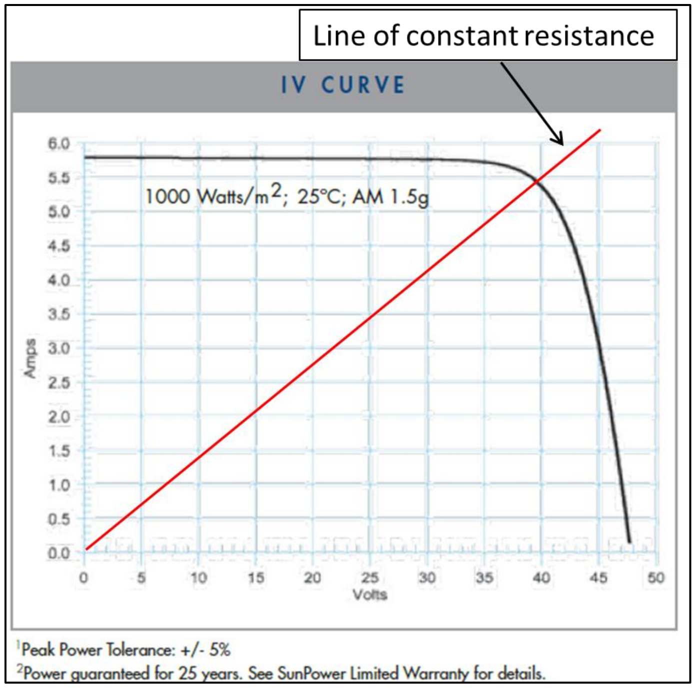

Figure 33. This figure demonstrates the PV operating point. The PV panel will operate at the intersection point of the IV-curve and the line of constant resistance (1/R).

For this project, there are two PV modules wired in series. When power generators are wired in series the power and voltage add, while the current remains the same (conservation of charge). Thus, for two SunPower SPR-215-BLK modules connected in series,

$$2P_{max} = \frac{(2V_{mp})^2}{R_{mp}} = 430W \tag{3.2}$$

Where, P_{max} = 215 W

V_{mp} = 40 V

R_{mp} = 14.9 Ω

When building the power resistor circuit, the total resistance should equal R_{mp}, thus forcing the PV to operate at the maximum power point. The total resistance of the power resistor circuit is shown in

Figure 34. The resistors used for this circuit are fairly uncommon, because it is rare to have low resistances and a how power ratings. These resistors were ordered from Mouser.com.

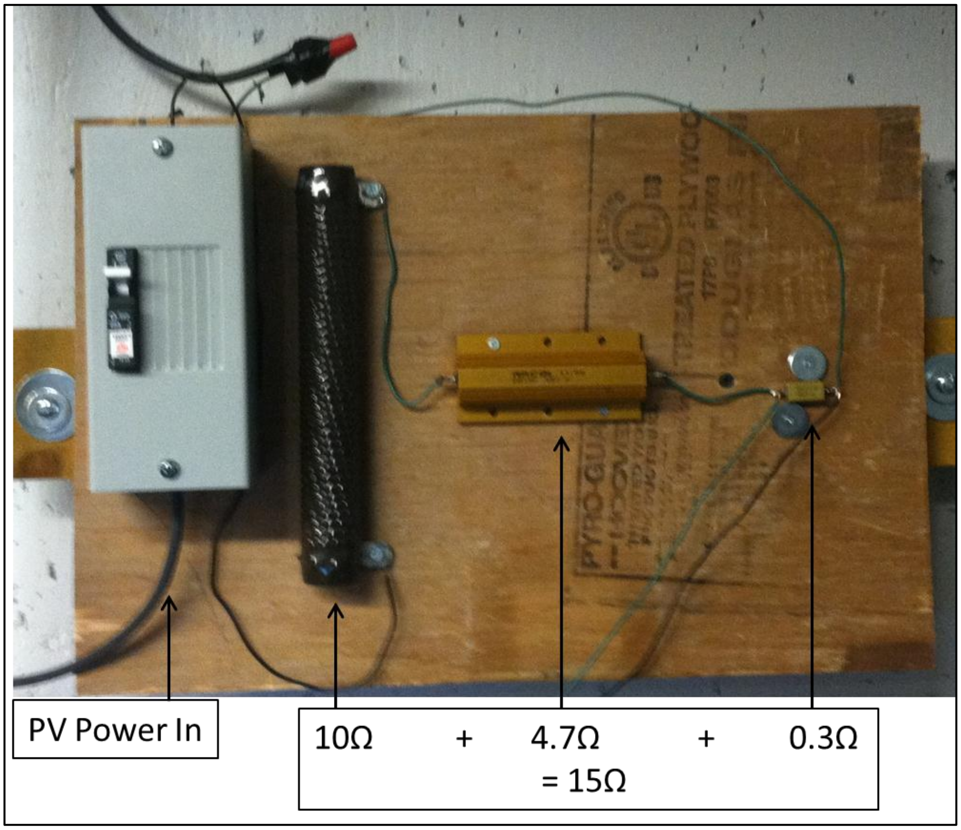

Figure 34. Power resistors for dumping the PV power as heat.

The reason for three resistors in series, as seen in Figure 34, was so that the voltage could be dropped to less than 2.5V in order to be within the detection range for the Campbell Scientific CR100 Datalogger.

FRAME DESIGN

The location for the experiment was on the roof of the Civil Wing of the Engineering Center. The frame was supposed to imitate a typical residential roof and was constructed of multiple triangular Unistrut trusses anchored to a vertical concrete wall, as seen in Figure 35. The depth of the mock roof was determined to be large enough such that, either two typical PV panels would fit in landscape orientation or one in portrait orientation. The slope of the roof was set at an angle of 30°, a typical residential roof angle.

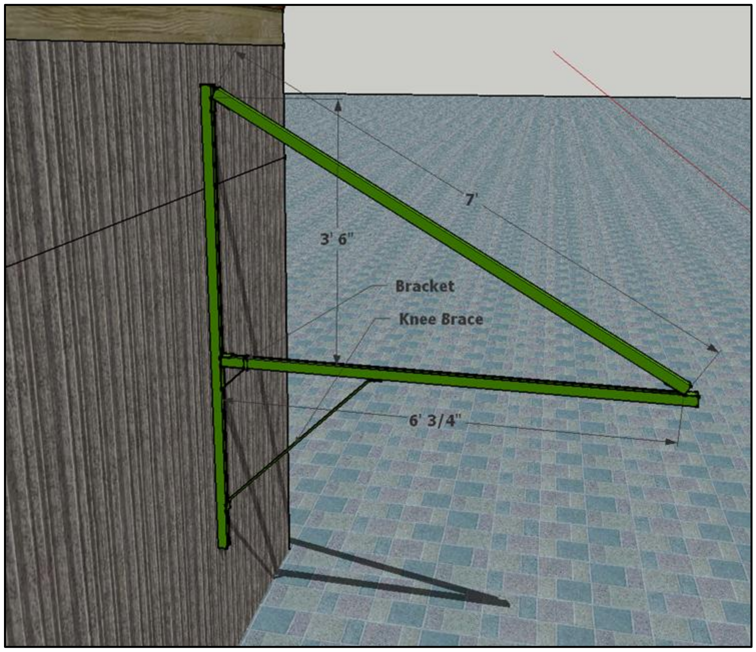

Figure 35. Detail of frame truss.

Each frame truss was spaced every four feet to develop the structural support for the solar modules. The original plan for construction was to build the full scale array as a permanent structure for the use of future student projects. Figure 36 shows the plans, where the right side has plywood to act like a roof and the left side is left flexible for other mounting options. Unistrut is an extremely convenient material to work with. It allows for lots of flexibility, which is an important factor for unknown future student projects. Please see APPENDIX G CONSTRUCTION MATERIAL SPECIFICATIONS, for information about all construction materials.

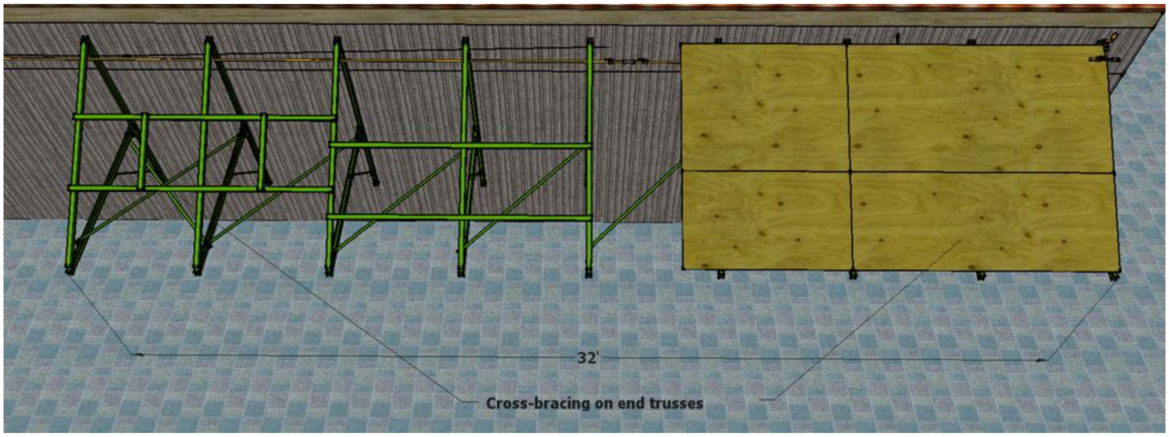

Figure 36. This shows the plan for the full scale array. Each truss is spaced 4 ft. on center. Cross-bracing at the end braces only is sufficient especially when other types of cross-bracing will be added for mounting solar panels, i.e. plywood, Unistrut channels, etc.

DATA ACQUISITION

Quantification of the BIPV/T modules performance required a full data acquisition system. Table 8 is a summary of all instrumentation. For all instrumentation specification sheets please see, APPENDIX H DATA ACQUISTION INSTRUMENTION.

Table 8. BIPV/T point list.

Point	Parameter	Instrument	Manufacturer	Point Name	Detection Method
1	Temperature	Thermocouple	Omega	T, in	Differential Voltage
2	Temperature	Thermocouple	Omega	T, out	Differential Voltage
3	Temperature	Thermocouples	Omega	PV cell Temp	Differential Voltage
3	Temperature	Thermistor	PreCon/Kele	T, ambient	Differential Voltage
4	Wind Speed	Cup Anemometer	InSpeed	Wind Speed	Pulse
5	Flow Rate	Flow Meter	Omega	Flow Rate	Pulse

6	Insolation	Pyranometer	Licor	Tilted Surface Solar Radiation	Differential Voltage
7	PV Power	Datalogger	Campbell Sci.	DC Voltage	Differential Voltage

DATALOGGER

A Campbell Scientific CR 1000 measurement and control datalogger was used for the data acquisition. This datalogger has capacity for eight channels of measured differential voltage levels, two pulse channel counters, and three outputs for precise excitation voltages for resistive bridge measurements (thermistors), among other unused features. Figure 37 shows the wiring panel for the datalogger. The CR1000 has 2 MB of flash memory for the operating system and 4 MB of battery-backed SRAM for CPU usage, program storage, and data storage. The data is conveniently stored in table format. Power is supplied to the datalogger via any 12 Vdc source.

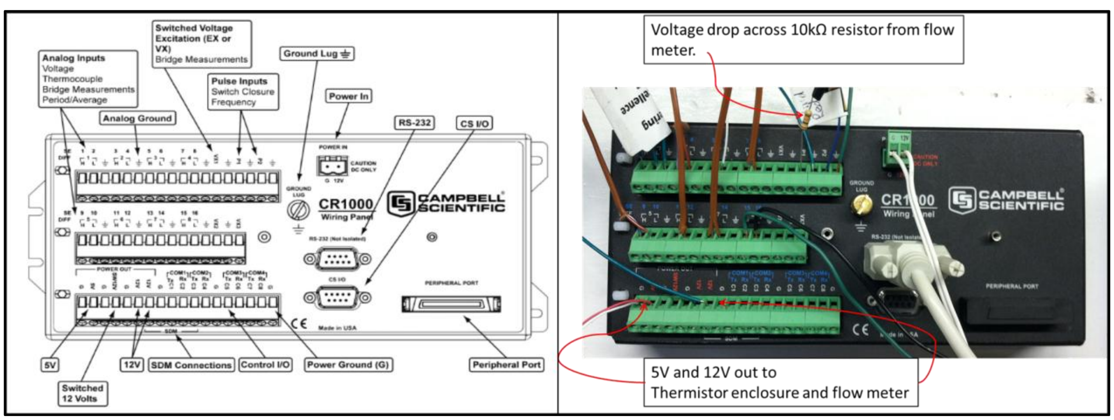

Figure 37. Campbell Scientific CR1000 datalogger wiring panel.

THERMOCOUPLES

Type T thermocouples, by Omega, were used to measure the temperature of the fluid entering and leaving the collectors. Thermocouples play very nicely with the Campbell Scientific datalogger and software, simply connect the thermocouple leads to the H and L differential voltage terminals and tell the software which thermocouple type is being used, and the temperature is reported.

THERMISTOR

Only one thermistor was used for this experiment, and that was to measure the ambient temperature. The Larson Lab had several thermistors lying around and one was grabbed and used for tests. A thermistor measurement is not as easy to read with the Campbell Scientific Datalogger as thermocouples are. A thermistor measurement is called a resistive bridge measurement, meaning that a precise excitation voltage is required to measure the resistance across the thermistor. It is also typical that the voltage is dropped across a 10kΩ resistor in series with the thermistor in order to minimize the self-heating effect. As with any current, the current flowing through the thermistor will generate heat which raises the temperature of the thermistor above its surroundings. If the temperature being measured is the ambient temperature, as in this experiment, then a correction factor must be applied to the measurement.

In order to solve for the temperature based on a differential voltage reading several steps must take place. The third-order Steinhart-Hart equation relates temperature to electrical resistance as follows

$$\frac{1}{T} = A + B * Ln(R) + C * Ln^3(R) \tag{3.3}$$

Where, $R = \frac{R_{ref} * V_{measured}}{V_{excitation} - V_{measured}}$ and,

R_{ref} = Reference Resistance = 10kΩ

$V_{measured}$ = Differential voltage measured

$V_{excitation}$ = Supplied excitation voltage = 5V (from the datalogger)

A, B, and C = The Steinhart-Hart parameters.

The Steinhart-hart parameters are determined by simultaneously solving three versions of equation (3.3) with three temperature and resistance points found from the thermistor manufacturer's resistance table (see APPENDIX H   DATA ACQUISTION INSTRUMENTION). The three points should be selected to represent the range of temperatures anticipated during the testing.

Figure 38 demonstrates the thermistor resistive bridge measurement technique. Although only one thermistor was used in this experiment, this custom enclosure is capable of handling 7 resistive bridge measurement devices. Currently three 10kΩ resistive bridge measurements are wired up, the remaining 4 instruments would have to be wired.

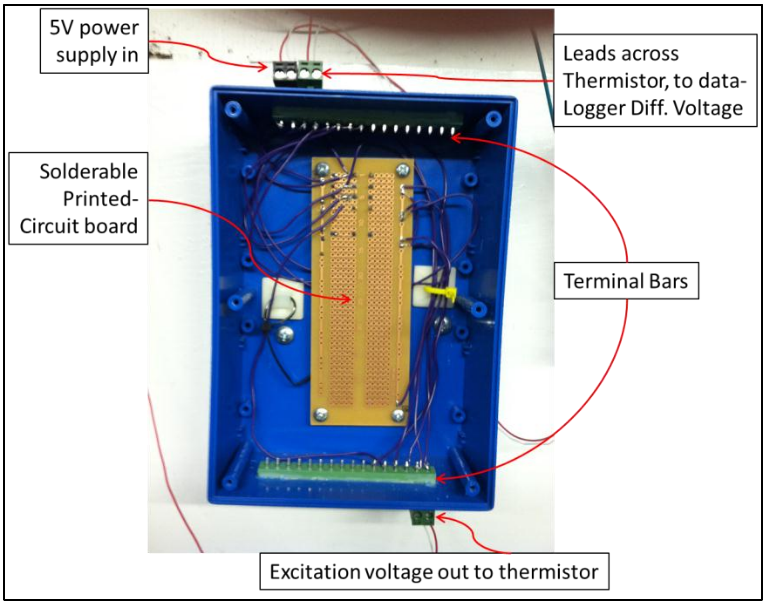

Figure 38. Custom made resistive bridge enclosure. A 5 volt power supply from the datalogger is fed into the solderable printed-circuit board. Soldered underneath the board are several 10k ohm resistors (one for each thermistor). Excitation voltage is sent to the thermistors after the voltage is dropped across the 10k ohm resistor. The measurement is taken across the thermistor leads and terminated in the datalogger's differential voltage terminals.

ANEMOMETER

Wind speed was measured using a cup anemometer. Wind speed is a critical parameter to monitor as it has a dramatic effect on the top loss heat transfer coefficient. The sensor consists of a 3-cup rotor connected to a reed switch/magnet, providing 1 pulse per rotation. No power is required for this instrument. The wind speed was calculated from the pulse counter by the following relation

$$MPH_{wind} = \frac{\#\ of\ Pulses}{2.5\ sec} \tag{3.5}$$

FLOW METER

In order to quantify the thermal performance of the collectors the flow rate must be measured. A ½" *Omega Super-jet Turbine Flowmeter*, with a pulse rate of 151.4 pulses/USGPM was used in this experiment. Care was taken to plumb the flowmeter with the standard 10 pipe diameters upstream and 5 pipe diameters downstream of uninterruptible flow. The flow meter, like the thermistor, requires an excitation voltage, so that when the turbine rotates it can send pulses to the datalogger. Figure 39 is the wiring schematic for the *Omega Super-jet Turbine Flowmeter*. In this experiment, (as called out in Figure 37) lead A is supplied 12VDC, and the resistance, R, is 10kΩ.

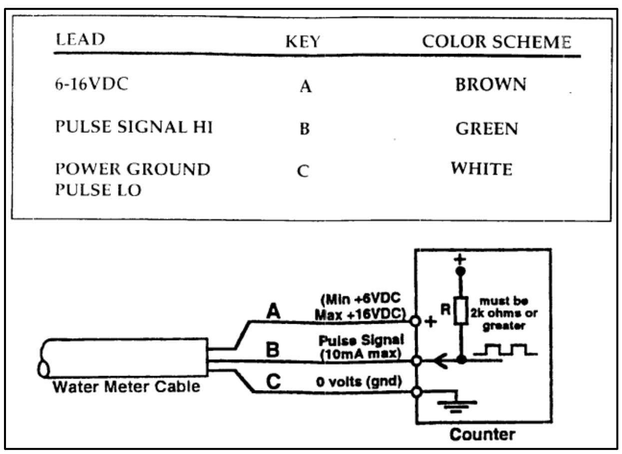

Figure 39. Wiring diagram for the Omega Flow meter.

PYRANOMETER

Total solar radiation was measured by a Licor pyranometer. This pyranometer features a silicon photovoltaic detector mounted in a fully cosine-corrected miniature head. The current output, which is directly proportional to solar radiation, was calibrated by NREL and the relationship for the differential voltage measurement is:

$$\frac{W_{solar\ energy}}{m^2} = 156.99 * mV_{measured} \tag{3.4}$$

During the calibration of the instrument at NREL, a resistor was wired in series such that the analog measurement would be in volts. There are three leads coming from the pyranometer, high voltage, low voltage and ground. The three leads are simply connected to the H, L and ground terminals in the differential voltage readings on the datalogger.

PV POWER

The power generated by the PV can be calculated from the voltage measured across the 0.3Ω power resistor as seen in Figure 34. Three resistors (instead of one) were used to dump the electrical energy so that the voltage could be dropped into the Datalogger's measurement range (+/- 2.5V). Applying ohm's law to the 0.3Ω resistor, the current can be calculated and since the three resistors are wired in series, the conservation of charge principle states that the current through all three resistors must be the same. Knowing the total circuit resistance and the circuit current, the power can be calculated.

$$V_{0.3\Omega} = IR_{0.3\Omega} \tag{3.5}$$

$$P_{generated} = I^2 R_{tot} \tag{3.6}$$

Where, $V_{0.3\Omega}$ = voltage measured across the 0.3Ω resistor

I = circuit current

R_{tot} = total circuit resistance

$P_{generated}$ = Power generated by the PV

It's important to know the instantaneous power generation along with the instantaneous solar radiation so that the PV instantaneous electrical efficiency can be calculated. One major attraction to the modular BIPV/T is that the temperature of the PV can be lowered by heat transfer into the fluid, therefore improving the electrical conversion efficiencies. Tests can be conducted with and without the fluid component engaged and the improvement of electrical conversion efficiencies can be quantified.

UNIVERSITY APPROVALS

STRUCTURAL APPROVAL

The University's structural engineer wanted to see some static and wind loading calculations to ensure stability and safety of the structure. Not being a professional structural engineer, a simplified approach was used for determining the pull-out strength of wind on the solar framing and the static loading on the structure and concrete anchors.

The fundamental equation for the wind calculation was determining the force of the wind on the plywood. It was assumed that the worst case scenario would be a gust that acts normal to the plywood from underneath. The following equation was used to find the force of the wind:

$$F_{wind} = \frac{\rho_{air} * V_{wind,design}{}^{2} * A_{plywood} * C_d}{2} \tag{3.6}$$

where, $V_{wind,design}$ = 110 mph

C_d = 1.17 (the drag coefficient for square flat plate at 90° angle, from reference table)

From this force the reaction force on the anchors was calculated.

The frame design that was chosen is statically indeterminate. However, by simplifying the frame, from bolted fixed supports to a simple triangle with a frictionless hinge at the top, frictionless hinge connecting the two members and a rough surface as the bottom support, then the problem can be statically determined. The reactions to be determined are at the hinges, which will define the required strength of the anchors to hold the plate on the hinge. The problem that was solved is simply a two-dimensional problem where the distributed load is simplified into a point load on one triangular frame with only one anchor providing the reaction. This was chosen because if one anchor can be proven to hold the load, then the additional two frames with 3 anchors each will certainly be sufficient. Please see APPENDIX I STRUCTURAL CALCULATIONS, for detailed explanation of the structural calculations.

Figure 40. Photo of the frame structure. Support for the plywood is 2x4's spaced every 24" on center. This photo is missing the cross bracing that is currently installed between the horizontal members.

ELECTRICAL APPROVAL

During talks with the Project Manager, it was determined that a professional electrician was to install all electrical connection. As time was of the essence, I side-stepped this requirement and installed the terminations myself. One, 200' MC3 extension cable was cut in half to make up the positive and negative leads. The positive lead terminated at a 20A breaker, and was connected to a power resistor array for load dissipation. The negative lead was connected to the other end of the power resistor, completing the circuit. The PV modules were left floating, ungrounded.

PLUMBING APPROVAL

During the meeting with Bobby Burke, it was mentioned that the university requires type L copper pipe. This specification was met by purchasing type L at the Home Depot. A vacuum breaker was required between the hose bib and the fill station (tanks).

FIRE RATING APPROVAL

The fire department required that the plywood be fire rated. Boulder Lumber Company was the distributor for the fire rated plywood, and they were able to provide a material specification sheet. Please see, APPENDIX G CONSTRUCTION MATERIAL SPECIFICATIONS, for documentation.

ARCHITECTURAL PLANNING APPROVAL

Approval for a permanent structure to be built on the University of Colorado's property needs approval from the architectural planning department. The major requirement for approval is a full blown 3D computer rendering of the structure and the surrounding buildings. Approval would be guaranteed if the computer rendering could prove that the structure is not visible from anywhere on campus. This rendering was not completed, and as of now, the structure is temporary. However, the structure is not visible from the ground. Since approval from the architectural planning department was not met the 32' structure to accommodate future work was not installed. Instead, only three trusses were mounted, enough to accommodate this project. Figure 40 is a photo of the finished frame. Hopefully, approval will be granted to leave the structure up indefinitely.

THE DATA

Data was finally collected on a clear day on November 30, 2011. Data was collected every minutes from 7:27am – 3:43pm. During this particular day, the morning sunlight was covered by a large lenticular cloud that finally burned off around 10am. The data collected from 10am – 12:15pm is the highest quality data to be used for the computer calibration because there were no obstructing clouds, and the surrounding buildings don't cast any shadow on the PV until after 12:15pm. Figure 41 shows the shading on November 30, 2011. In reality the shadow was cast on the bottom left corner of the PV at this point in time, and spreads across the PV until after 2pm.

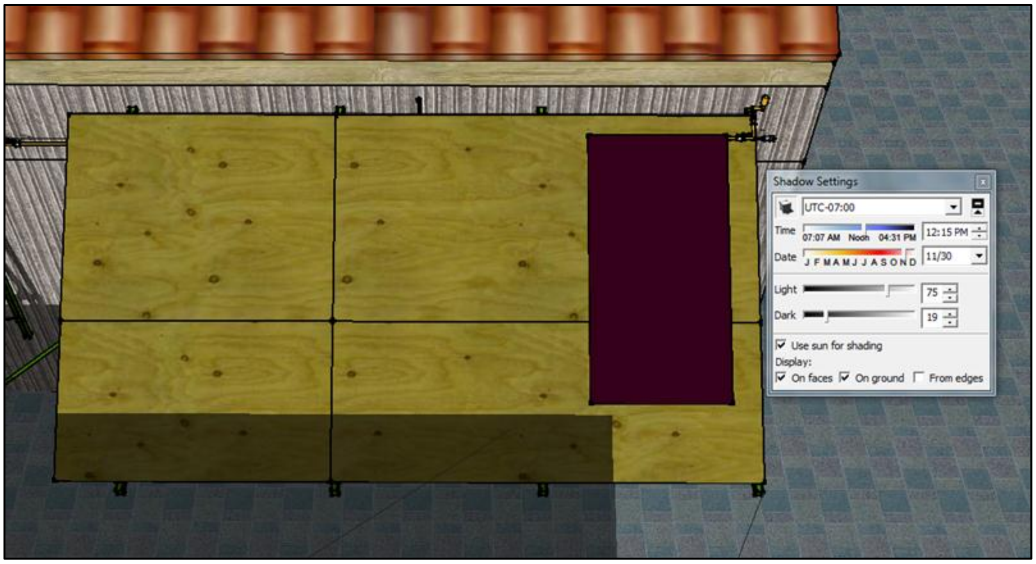

Figure 41. This is the shading image for November 30, 2011 at 12:15pm. The actual location of the PV may not be exactly the same as shown here, but this verifies that the shading results are quite accurate. In reality at this point in time the shadow is cast on the bottom left corner of the PV and spreads across until after 2pm.

The data recorded by the Campbell Scientific datalogger is stored as a *.dat file in a table format. The *.dat file was opened in MS Excel where further manipulations were conducted. Table 9 shows an example of the data headers and how the raw data was organized.

Table 9. This is how the raw data from the datalogger was imported into Excel.

Timestamp	Record	PYRA	T_{in}	T_{amb}	T_{out}	$T_{PV,top}$	$T_{PV,mid}$	$T_{PV,bot}$	PV_{volt}	Flowmeter	Anemometer
TS	RN	W/m^2	Deg C	Deg C	Deg C	Deg C	Deg C	Deg C	mV	GPM	m/s
.	.	.	.	.	.	.	.	.	.	.	.

Four parameters were used to calibrate the computer model from the collected data

1. Useful energy gain

$$Q_{useful} = \dot{m}C_p\Delta T \left[\frac{kJ}{hr}\right] \tag{3.7}$$

Where, $\dot{m}$ = mass flow rate, as read from the flow meter, converted to Kg/hr

ΔT = T_{out} - T_{in}

2. Leaving fluid temperature

    a. As measured by the thermocouple and recorded by the datalogger

3. Temperature of the PV

    a. Calculated the average of $T_{PV,top}$, $T_{PV,mid,}$ and $T_{PV,bot}$.

4. PV power generated

    a. Calculated as described in PV Power on page 50.

Figure 42 shows the results of the four parameters over the time frame of 10am to 12:15pm. As will be described in the next chapter (see pg. 62), completely clear skies were desired for data collection.

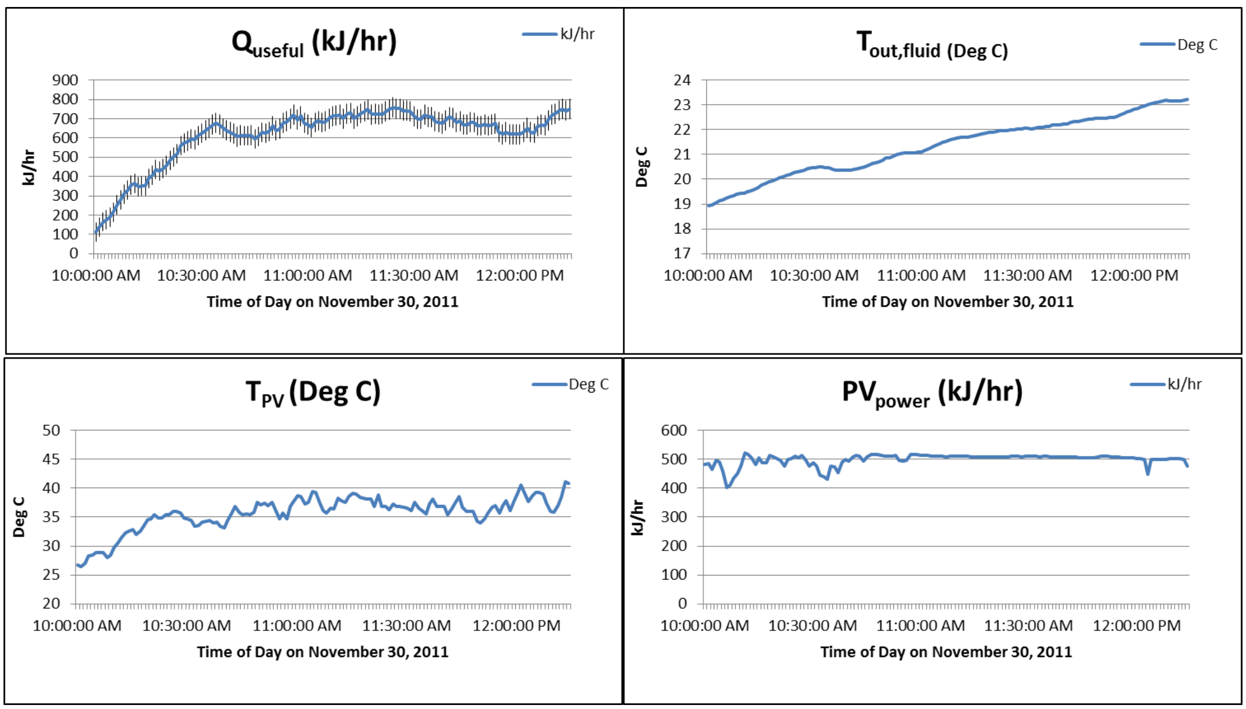

Figure 42. These plots are the four tuning parameters used to calibrate the computer model and to analyze the performance of the collector.

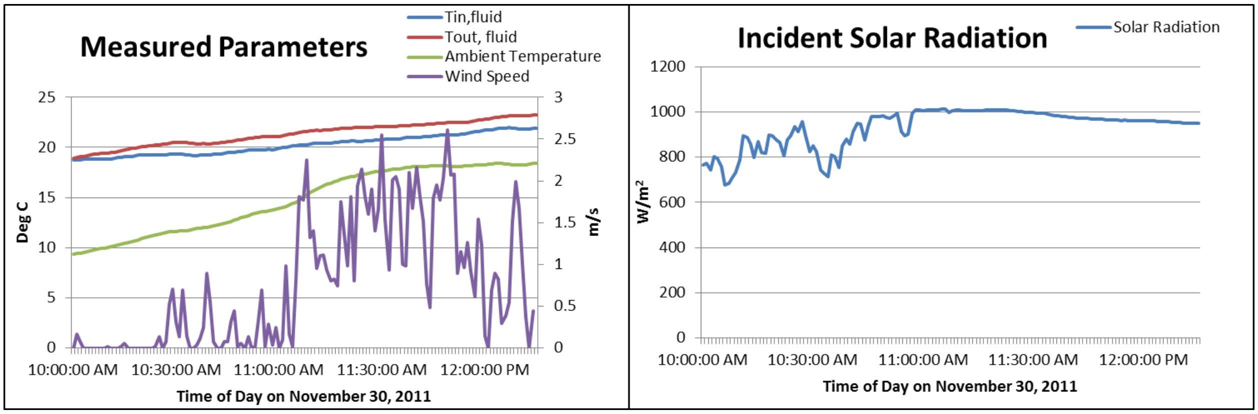

Figure 43. This figure is the remaining suite of measured data. The plot on the left shows all three temperatures (left axis) and the wind speed (right axis). The plot on the right is the measured solar radiation on the plane of the collector.

Figure 43 shows the remaining measured data. One can clearly see the correlation between PV power and the incident radiation. Another parameter correlation to notice is the effect of wind speed on the PV temperature and the useful energy gain. From 11am through the end of data collection, the wind speed picks up and the plots of PV temperature and useful energy gain become a bit more jagged.

ERROR ANALYSIS

When calculating the useful energy gain of the BIPV/T collectors, two measurement values are multiplied together in equation (3.7), $\dot{m}$ and ΔT. Uncertainty in a product is equal to the sum in quadrature of the original fractional uncertainties. So, for equation (3.7), the fractional uncertainty in Q_{useful} is equal to the sum in quadrature of the fractional uncertainty in the flow rate reading and the temperature difference (Taylor, 1997).

$$\frac{\delta Q_{useful}}{|Q_{useful,best}|} = \sqrt{\frac{\delta \dot{m}}{|\dot{m}_{best}|}^{2} + \frac{\delta \Delta T}{|\Delta T_{best}|}^{2}} \qquad (3.8)$$

The flow meter provided an accuracy curve with the product and, at 0.58 GPM, the fractional uncertainty is about 1%.

In order to assess the fractional uncertainty in the ΔT measurement a simple test was conducted on a cold December day, where a glass jar was filled with warm water (~33 °C), both thermocouple probes were inserted into the water and the temperatures were recorded every 10 seconds as the water cooled over the course of a couple of hours.

The results of the thermocouple test showed a 0.17°C error in the temperature measurements. Thus, the fractional uncertainty of the thermocouple measurements is

$$\frac{\delta \Delta T}{|\Delta T_{best}|} = \frac{0.17℃}{|\Delta T_{best}|} \tag{3.9}$$

For every data point, equation (3.8) was calculated and multiplied by the equation (3.7) to determine the absolute error in the Q_{useful} metric, and this value was used to set the error bars in Figure 42.

ISSUES AND COMMENTS ABOUT THE DATA

It pains the author to have to admit that after all of the effort that went into the physical experiment, the precious amount of data that was finally collected is probably flawed. The results are flawed for a couple of reasons. First of all, a week before the above data was collected; one of the prototypes suffered a catastrophic failure. The failure occurred during leak testing before all of the data acquisition instruments were fully installed. As water began to flow through the two modules creaking and cracking could be heard. When the modules were vented of air and pressurized to the closed-loop system, the failed module began to bulge, creak some more and eventually suffered the catastrophic failure and water burst out from underneath the module. The failed module was removed from the test frame and taken back to Colorado Plastics and the PV laminate was removed and the failure inspected. Believe it or not, there wasn't an obvious place of failure. However, when the module was pressure tested with compressed air, it was apparent that the construction of the absorber was compromised because the top sheet of the absorber bulged upward under pressure.

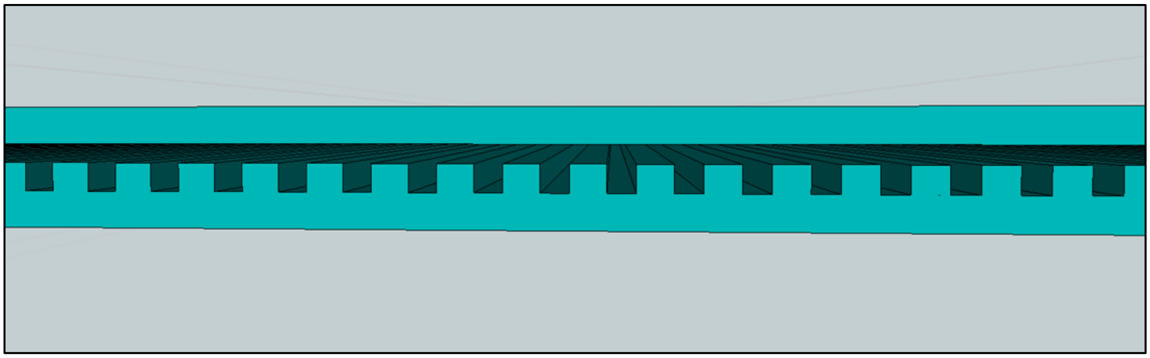

Figure 44. This image shows how the absorber was constructed, and, consequently, failed. The grooves were machined out and then a 3/32" thick piece of PVC was glued on top of the machined grooves, completing the channels.

Figure 44 shows the major design flaw that has plagued this project. The construction of the absorber was completed in two steps. First, a 5/32" thick piece of PVC (the bottom piece of Figure 44) had 1/16" square grooves machined out. Second, a piece of 3/32" thick PVC was glued on top of the machined PVC and the channels were enclosed. When the water pressure broke the glue bond between the machined grooves and the top sheet, flow was no longer confined to the channels. Figure 44 shows the top sheet lifted from the channels, creating a path of least resistance and changing the dynamic of intended heat transfer. The water will now flow above the channels in an open stream severely reducing the efficiency of the collector.

The gluing process was conducted by using clamps, a low viscosity solvent, a syringe and gravity. In other words, the two pieces of plastic were clamped together, angled down such that the solvent expelled into each flow channel, via syringe, would run down and wick itself into the cracks of the two surfaces. This process relies on the trust of the surface tension and wicking ability of the solvent. John at Colorado Plastics has had success with this technique before, but has never done it blind.

The author feels that there are two major problems that went wrong with the physical experiment, which made calibration of the computer model impossible.

1. **The tested module's absorber was compromised!** After the module was tested, it was taken down from the testing frame and sent back to Colorado Plastics, where the PV laminate was removed, and the compressed air test confirmed that the top sheet of the absorber was coming loose from the machined channels, as can be seen in Figure 44. In the opinion of the author, the failure was due to the lack of success of the gluing procedure described above. Since the gluing was performed without visual confirmation, there were probably sections along the length of the flow channel where the solvent did not make it into the cracks of the two PVC pieces. Once water is introduced into one of the unsealed cracks and becomes pressurized, the water will constantly try to exacerbate the problem and eventually break apart all bonds. This failure makes calibrating the model to match the collected data semi-irrelevant. Why would one want to calibrate to a prototype that is not working as designed?
2. **Only one module was tested and the electrical load was sized for two!** This creates a discrepancy between the computer model and the physical experiment because the model assumes that the PV is operating at the maximum power point (MPP). Unfortunately, there wasn't enough time before the Colorado winter set in to properly size the power resistors for one PV.

Ultimately, the failed absorber made calibration of the TRNSYS model somewhat irrelevant because the absorber no longer contained the flow of water inside specific channels. The PVT component of the model assumes confined flow, so basing a simulation on a model calibrated by data from a broken absorber doesn't make it very useful. See CALIBRATION RUNS for more information.

CHAPTER 4 COMPUTER SIMULATION

In order to properly account for the economic analysis of the performance and dollars saved by the new BIPV/T product, a detailed energy engineering analysis must be conducted and the target markets must be identified. Remembering that low cost manufacturing was a major requirement for the design, it is understood that the thermal efficiencies will not be comparable to glazed solar thermal collectors. That being said the target markets are new construction in non-freezing climates in the United States. TRNSYS was used to perform the transient hourly simulation for many different US locales.

The computer simulation portion of this project consisted of two models; 1) the calibration model and 2) the simulation model. The calibration model was used to input measured weather data into the TRNSYS model and then compare the simulation to the measured results and calibrate the mathematical model to match the actual performance of the prototype. The simulation model, modeled a typical US residential home consisting of a 5kW BIPV/T array plumbed into an electric water heater.

TRNSYS is a flexible graphically based software environment used to simulate the behavior of transient systems. The software is made up of two parts. The first is an engine that reads an input file, iteratively solves the system, determines convergence and plots system variables. The engine also provides utilities that determine thermophysical properties, invert matrices, perform linear regressions, and interpolate external data files. The second part of TRNSYS is an extensive library of components, each of which models the performance of one part of the system. These components range from physical equipment, like pumps and HVAC equipment, to multizone buildings, wind turbines to electrolyzers, weather data processors to economic routines. Inputs and outputs of components are graphically connected and parameters are entered to specify the system (TRNSYS Documentation, 2009).

THE CALIBRATION MODEL

The calibration model has to be capable of reading an input file, process the information and deliver the calculated outputs to various components and present the desired variables for interpretation. Figure 45 is the graphical representation of the TRNSYS calibration model.

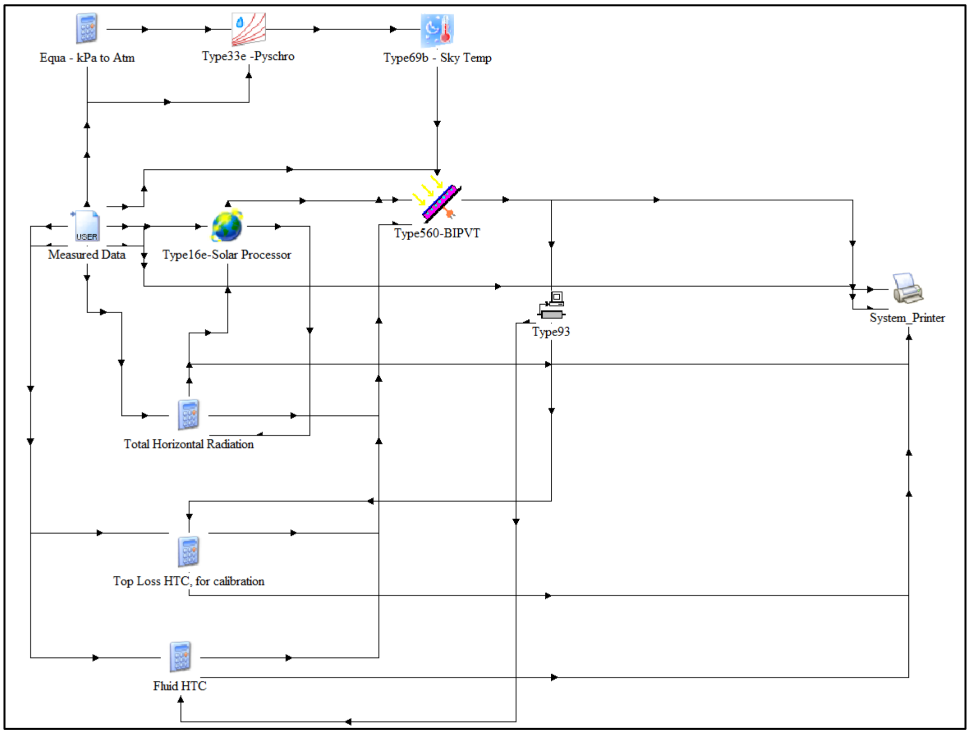

Figure 45. Graphical representation of the TRNSYS calibration model.

All components in the calibration model are a means to facilitate the inputs for the BIPV/T component. The following sections describe in detail the user-defined components and the BIPVT involved in the calibration model.

SKY TEMPERATURE CALCULATOR

In order to predict the performance of solar collectors it is necessary to evaluate the radiation exchange between the collector surface and the sky. The sky is considered a blackbody at some equivalent sky temperature. The sky temperature is required by the BIPVT component for radiation computations. The sky temperature is calculated using the relation (Duffie & Beckman, 2006):

$$T_{Sky} = T_{ambient}[0.711 + 0.0056T_{dp} + 0.000073T^2{}_{dp} + 0.013\cos(15t)]^{1/4} \qquad (4.1)$$

Where t = hour from midnight

T_{dp}= the dew point temperature

TOTAL HORIZONTAL RADIATION EQUATION BLOCK – USER DEFINED

The BIPV/T component requires the total horizontal radiation as an input for the mathematical model. The pyranometer was mounted on the same plane as the collectors themselves, thus measuring the incident solar radiation, or irradiance (W/m^2), G_T. In order to convert from incident radiation to total horizontal radiation, a system of equations must be solved. The following inputs, intermediates and outputs are used in the system of equations.

- INPUTS
  - G_T – the measured irradiance on the tilted plane of the collector
  - The incidence angle – the angle of incidence of the beam radiation on the tilted plane
  - The zenith angle – the angle between the vertical and line of sight of the sun
- INTERMEDIATES
  - B – the tilted angle from horizontal, 30°
  - R_b – the ratio of beam radiation on the tilted surface to that on a horizontal surface at any time, $= \frac{\cos(\theta)}{\cos(\theta_z)}$
  - ρ_g – the reflectivity of the ground, 0.2
- OUTPUTS
  - G_h – total horizontal radiation

- G_b – beam radiation on horizontal
- G_d – diffuse radiation on horizontal

In order to simplify the system of equations to be solved to find the total horizontal radiation from the measured incident radiation, the data collected should be during clear sky "bluebird" conditions. This allows for the simplification of the Erbs correlation (Duffie & Beckman, 2006),

$$\frac{G_d}{G_h} = \begin{cases} 1.0 - 0.09k_T & k_T \leq 0.22 \\ 0.9511 - 0.1604\, k_T + 4.388k_T{}^2 - 16.638k_T{}^3 + 12.336k_T{}^4 & 0.22 < k_T \leq 0.8 \\ 0.165 & k_T > 0.8 \end{cases} \tag{4.2}$$

where the clearness index, k_T, can be assumed to be greater the 0.8. The clearness index is defined as the ratio of instantaneous radiation on a horizontal surface to the instantaneous extraterrestrial radiation.

$$k_T = \frac{G_h}{G_o} > 0.8 \tag{4.3}$$

When this assumption is made then the Erbs correlation is reduced to the following

$$\frac{G_d}{G_h} = 0.165 \tag{4.4}$$

In other words, the ratio of diffuse radiation to total radiation is 16.5%. The equation that relates horizontal radiation to radiation on a sloped surface is called the isotropic diffuse model and is as follows:

$$G_T = G_b R_b + G_d \left(\frac{1 + \cos\beta}{2}\right) + G_h \rho_g \left(\frac{1 - \cos\beta}{2}\right) \tag{4.5}$$

The third equation is simply the sum of the radiation components as follows:

$$G_h = G_b + G_d \quad (4.6)$$

Equations 4.4 – 4.6 have three unknowns and can be solved simultaneously at every time-step for the total horizontal radiation (Duffie & Beckman, 2006).

TOP LOSS HTC, FOR CALIBRATION

This equation block is used to calculate the convective heat loss coefficient from the top of the collector to the ambient. TRNSYS did not have a component for calculating this value, thus, the following narrative describes the reasoning for the user-defined calculation.

Convective heat losses on the collector surface are dependent on the wind and natural convection. There have been many experimental wind tunnel studies on rectangular plates in an attempt to derive the Nusselt number. There is a slight difference between the calculation of the Nusselt number for the calibration model and the simulation model. The difference is due to the location of the wind measurement. For the simulation, wind speed data is taken at some regional site that is probably unobstructed. When simulating a solar array on a residential home the flow over the house is not well represented by wind tunnel tests of isolated plates. The collectors will sometimes be exposed directly to the wind and at other times will be in wake regions. However, for the experiment, the anemometer was located on the exact surface as the collectors and the wind speed is well represented by wind tunnel tests. Sparrow et al. (1979) found the following correlation for the Nusselt number:

$$Nu = 0.86 Re^{1/2} Pr^{1/3} \quad (4.7)$$

where the characteristic length (in calculating the Reynolds number) is four times the plate area divided by the plate perimeter.

However, at low wind speeds, natural convection conditions tend to dominate. Natural convection is driven by the buoyancy force. When the collector surface is hotter than the surrounding air the fluid in the vicinity of the collector surface will be heated and the density decreases, relative to the surrounding fluid, and will cause the heated fluid to rise. This is the buoyancy force. There are three forces acting on air in motion:

1. The force due to the pressure gradient
2. The body force
3. The frictional shearing forces due to the velocity gradient

Applying principles of conservation of momentum, using the simplification that the fluid far from the plate is in hydrostatic equilibrium, and finally the *Boussinesq approximation* (which assumes that the density depends only on the temperature (not pressure), the equation of motion for natural convection can be obtained. Furthermore, deriving the conservation of energy equation for the flow near the plate yields the temperature field for the natural-convection problem

Utilizing the Buckingham pi theorem, the dimensionless parameters can be determined. The three dimensionless groups are: Nu = Nu(Re,Pr,Gr). Since the flow velocity is determined by the temperature field, the Reynolds number is not an independent parameter. Experimental results for natural-convection heat transfer can therefore be correlated by an equation of the type:

$$Nu = \emptyset(Gr)\varphi(Pr) = \emptyset(Ra) \tag{4.8}$$

Where, Ra = the Rayleigh number, the product of the Grashof and Prandtl numbers

Gr = the Grashof number, the ratio of buoyant forces to viscous forces

Thus, the Nu number for natural convection is a function of the product of the ratio of buoyant forces to viscous forces (Grashof #) and the ratio of molecular momentum diffusivity to thermal diffusivity (Prandtl No.).

Using an equation of the type, $Nu = \emptyset(Ra)$, experimental data for natural convection can be plotted and the coefficients found. Lloyd and Moran (1974) and McAdams (1954) give relationships for the Nu number as a function of the Ra number for hot horizontal flat plates and vertical plates, respectively. For large Rayleigh numbers, as is typical for solar collectors (due to the large Grashof number), the heat transfer coefficient from the two relationships are nearly identical, because the Rayleigh coefficients differ slightly. Applying some temperature differences to the Nu number relationships for natural convection, it is determined that the minimum heat transfer coefficient for horizontal *or* vertical collectors is about 5W/m^{2}K for a 25°C temperature difference and 4W/m^{2}K for a 10°C temperature difference.

A solar collector is most likely to be experiencing natural convection and forced convection simultaneously. McAdams recommends calculating both heat transfer coefficients and using the larger of the two for design and modeling calculations**. Thus the top loss convective heat transfer coefficient (W/m^2 K) for flush mounted collectors can be expressed as**:

$$h_{wind} = max\left[5, \frac{Nu * \ k_{air}}{L_c}\right] \tag{4.9}$$

Where, Nu = the Nusselt number calculated from equation (4.7)

L_c = characteristic length, equal to 4 times the plate area divided by the perimeter

- Inputs
  - Measured wind speed
  - PV temperature
  - Ambient temperature
- Outputs
  - Top loss convective heat transfer coefficient.

FLUID HTC (HEAT TRANSFER COEFFICIENT)

This equation block is used to calculate the heat transfer coefficient between the wall of the fluid channels and the fluid flowing inside it. TRNSYS did not have a component for calculating this value, thus, the following narrative describes the reasoning for the user-defined calculation.

Flow ranges for the BIPV/T result in a Reynolds number well below the transitional and turbulent flow regime and will always be laminar. Knowing that the flow in the absorbers channels is fully developed laminar flow, a table developed by Shah and London (1978) (Kreith & Bohn, 2001), provide Nusselt numbers and friction factors for fully developed laminar flow of a Newtonian fluid through specific ducts. For a square channel, as is the case with the design BIPV/T, Shah and London provide an average Nusselt number for uniform heat flux in the flow direction and uniform wall temperature at any cross section, as well as a value for the average Nusselt number for uniform wall temperature. The Nusselt numbers for a square duct are 3.608 and 2.979, respectively. The theoretical performance for a solar collector will lie between the results for constant heat flux and constant wall temperature, thus it is recommended for design calculation to use the lesser of the two values, constant wall temperature, for a conservative design. This equation block also has the capability to calculate the fluid heat transfer coefficient in the turbulent regime; however, this will probably never be used. For this calculation, the Nu number is entered as 2.976, and the HTC is calculated as follows:

$$h_{fluid,laminar} = \frac{Nu_{water,laminar} * \ k_{water}}{D_h} \tag{4.15}$$

Where, $Nu_{water,laminar}$ = 2.976

k_{water} = conductivity of the water as a function of temperature

D_h = hydraulic diameter

- Inputs
    - Mass flow rate from the pump
    - Bulk temperature, or average fluid temperature for the conductivity calculation
- Outputs
    - $h_{fluid,laminar}$ to BIPV/T

THE BIPV/T COMPONENT

This component models an un-glazed solar collector which has the dual purpose of creating power from embedded photovoltaic (PV) cells and providing heat to a fluid stream passing through tubes bonded to an absorber plate located beneath the PV cells. The waste heat rejected to the fluid stream is useful in two ways. 1) The rejecting of heat from the PV cells reduces the PV cell temperature and improves the electrical power conversion efficiency and 2) the heated fluid stream can be used in many low grade temperature applications, namely domestic hot water (DHW) usage (TRNSYS Documentation, 2009).

- Parameters – this simulation is to model the prototype
    - Collector Length – Length of the absorber = 1.5144 m
    - Collector width – width of absorber = 0.6096m
    - Absorber plate thickness – the top layer of material of the absorber = 0.00238m (3/32")
    - Thermal conductivity of the absorber = 0.374 kJ/hr.m.K (from PVC spec sheet)
    - Number of tubes- 2*76 = 152
    - Tube diameter – the hydraulic diameter for a square channel is simply the length of its side = .0015875m (1/16")

The following three parameters apply to the bond material that connects the fluid tubes to the absorber plate. Equation 560.28 of **APPENDIX J TRNSYS PVT MATHEMATICAL MODEL**, implies that the temperature of the tube wall is uniform circumferentially, which is a reasonable assumption if the tube is made of a highly conductive material. Obviously, the prototype BIPV/T's absorber tubes are not highly conductive, and therefore a wall temperature profile will exist in the y-direction. In order to account for the temperature profile, a resistance should be imposed to drop the temperature to a more realistic average absorber temperature. This was done by using the C_B term in equation 560.28 of **APPENDIX J TRNSYS PVT MATHEMATICAL MODEL**.

- Bond width – 0.0015875m. The width of the fluid channel
- Bond thickness – 0.007938m. ½ the length of the side of the fluid channel. This length defines the resistance to a temperature node located in the middle of the absorber
- Bond thermal conductivity – 0.374 kJ/hr.m.K. The same conductivity as the PVC.
- Resistance of substrate (backsheet) material – This value combines the thermal network of several layers of material before reaching the surface of the absorber. SunPower was unable to supply a cross-sectional drawing with specific materials called out. Thus, a general search was performed to arrive at typical values**. This parameter was used as a calibration tuning knob.**

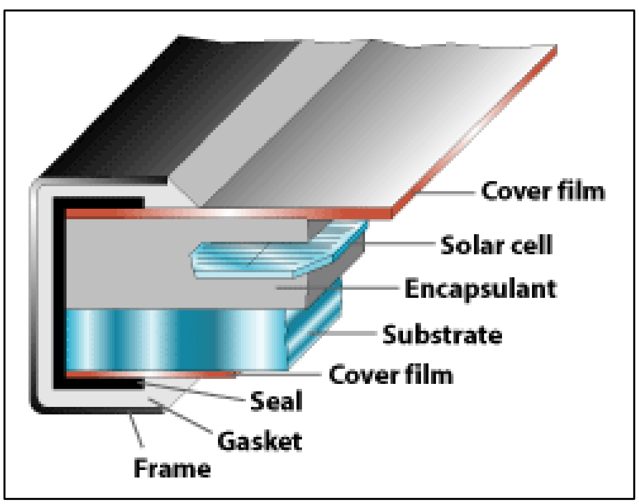

Figure 46. This image is a typical cross-section of a photovoltaic module. An understanding of the materials of the module is critical for determining the thermal resistance of the substrate material (Solar Energy Scene, 2010).

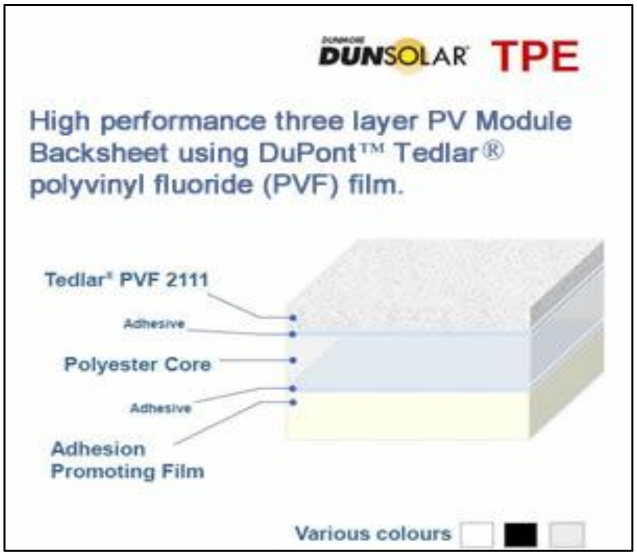

Figure 47. This image is a product made by DUNSOLAR that is sold to various PV module manufactures for use as a substrate/backsheet. This cross-sectional drawing helped provide an understanding of the materials used in the backsheet. Although SunPower's module cross-section was unavailable, technical support did say that they used a DuPont Tedlar (DUNSOLAR TPE BACKSHEETS, 2011).

DUNSOLAR was unable to provide me with the necessary thermal properties of their product and DuPont's available information for Tedlar PVF did not have thermal conductivity. A paper from *eXPRESS Polymer Letters* conducted a study on thermally conductive and electrically insulating EVA composite encapsulants for PV cells. In this paper the authors show a cross sectional drawing of a laminated and encapsulated Si solar cell, along with a table calling out the thickness and thermal conductivity, as seen in Figure 48.

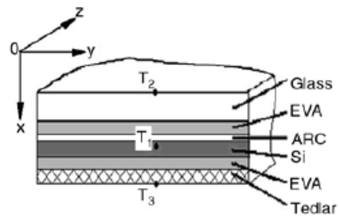

Figure 1. The configuration of laminated & encapsulated Si solar cells [11] (ARC: anti-reflecting coating, Tedlar: a kind of composite film of PET-PVF from DuPont)

Table 1. The sizes and properties of each layer in encapsulated Si solar cells

No.	Layer	Thickness δ [mm]	Thermal conductivity k [$W \cdot m^{-1} \cdot K^{-1}$]
1	Glass	3.0	0.98*
2	EVA	0.5	0.23*
3	ARC	$(0.06–0.1) \cdot 10^{-3}$	1.38
4	Si	0.25–0.4	148
5	EVA	0.5	0.23*
6	Tedlar	0.1	0.36*

*measured value

Figure 48: Abstracted from (Lee, Liu, Sun, Shen, & Dai, 2008)

Thicknesses and conductivities from Figure 48 were used for the calculation of the substrate resistance. Table 10 shows the calculations for the substrate resistance that was used in both the calibration and simulation models.

Table 10. This table shows the substrate resistance calculations for the BIPV/T. The EVA (ethylene-vinyl acetate) thickness was set at 1 mm instead of 0.5mm to conservatively accommodate the space between the Si cells.

No.	Layer	Thickness (mm)	Thermal Conductivity (W/m.K)	Resistance (m^2.K/W)	Resistance (hr.m^2.K/kJ)
1	EVA	1.000	0.23000	0.00435	0.00121
2	Tedlar	0.100	0.36000	0.00028	0.00008
3	PVC Spacer	3.175	0.10400	0.03053	0.00848
				total	**0.00977**

- Resistance of back material – (3) sheets of ½” thick R-3.0 board = 0.22 hr.m2.K/kJ (4.5hr.ft2.F/Btu)
- Fluid specific heat – Water = 4.190 kJ/kg.K

- Reflectance – the overall reflectance of the collector surface at normal incidence. The absorptance at normal incidence is found by subtracting this value from 1. The default value of 0.15 was used.
- Emissivity – the emissivity of the collector surface for long-wave radiation exchange with the sky. The default value of 0.9 was used.
- 1^{st} order IAM – coefficient (b_0) in the incidence angle modifier function. The default value of 0.1 was used.
- PV cell reference temperature – 25C, per spec sheet
- PV cell reference radiation – 3600 kJ/hr.m2, per spec sheet
- PV efficiency at reference conditions - .173, per spec sheet. This parameter needs to be modified. The PV area is calculated from the collector length and width parameters, which is not accurate. The collector width is 0.6096 m while the PV width is 0.798m. Thus, in order to achieve the same power generation from the PV with a reduced width, the efficiency must compensate.

$$PV_{power} = \eta_1 * G_T * A_1 \tag{4.7}$$

$$PV_{power} = \eta_2 * G_T * A_2 \tag{4.8}$$

Where, η_1 = 0.173, as per the spec sheet

A_1 = area of the PV

A_2 = area of the collector

G_T = total solar radiation striking the surface

In order to produce the same power out from a smaller area, set equations 4.7 and 4.8 equal to each other and solve for η_2. $\boldsymbol{\eta_2}$ **= 0.226 or 22.6%.**

  - Efficiency modifier – Temperature = -0.38%/C, per spec sheet
  - Efficiency modifier – radiation – the multiplier to correct the rated PV cell efficiency as a function of incident solar radiation. The default value of 0.000025 hr.m2/kJ was used.
- Inputs
  - Inlet fluid temperature, *from input file*
  - Inlet flow rate, *from the input file*
  - Ambient temperature, *from the input file.*
  - Back-surface temperature – the temperature of the air located behind the back surface of the collector. The BIPV/T is flush mounted (Building Integrated), thus I would say this back surface temperature is the same as the ambient, *from the input file.*
  - Incident solar radiation – the rate at which incident solar radiation (beam + diffuse) strikes the sloped collector surface, *from the input file.*
  - Total horizontal radiation – the rate at which total solar radiation (beam + diffuse) strikes a horizontal surface, *from the Total Horizontal Radiation Equation block.*
  - Horizontal diffuse radiation – the rate at which diffuse radiation strikes a horizontal surface, *from the Total Horizontal Radiation Equation block.*
  - Ground reflectance – the reflectance of the surface above which the solar collector is positioned. *Typical value is 0.2.*
  - Incidence angle – the angle of incidence between the beam solar radiation and the normal vector to the sloped collector surface, *from the Solar Processor.*
  - Collector slope – the slope of the collector surface. *The test setup was at 30 degrees, and will set at this slope for simulations.*
  - Top loss convection coefficient – the convective heat loss coefficient from the top of the collector to the ambient, *from the Top Loss convective HTC equation block*

- Back heat loss coefficient – the combined convective and radiative heat transfer coefficient from the back of the collector to the environment, tuning parameter that has little effect. *Default value is 15 kJ/hr.m2.K*
- Fluid heat transfer coefficient – the heat transfer coefficient from the fluid in the flow channels to the walls of the fluid channel enclosure, *from the Fluid HTC equation block.*

THE INPUT FILE

The data reader must be able to read the measured environmental conditions that occurred during the experiment and send the appropriate variables to be computed by the PVT component. The input file was a modified version of the datalogger record file where some of the parameters needed to be converted to the appropriate units. Table 11 shows the allocation of the input file parameters to the various components of the calibration model.

Table 11. This is a table representing the input file parameter allocation. The parameters on the left were read and allocated to the listed components.

Input File Parameter Allocation							
	Components						
Parameter	kPa to Atm	Wet-bulb calculator	BIPVT	Solar Processor	Total Horz. Rad.	Top Loss HTC	Fluid HTC
Atmoshperic Pressure	X						
T_ambient		X	X			X	
Fluid Temperature (In)			X				
Inlet flow rate			X				X
Incident Solar Radiation			X		X		
Wind Speed						X	
Time of last data read				X			
Time of next data read				X			

CALIBRATION RUNS

Unfortunately, the data collected is not a good representation of the design of the collector. As mentioned on page 58, the integrity of the absorber was compromised during the experiment. However, it is still important to have something to compare the computer model against.

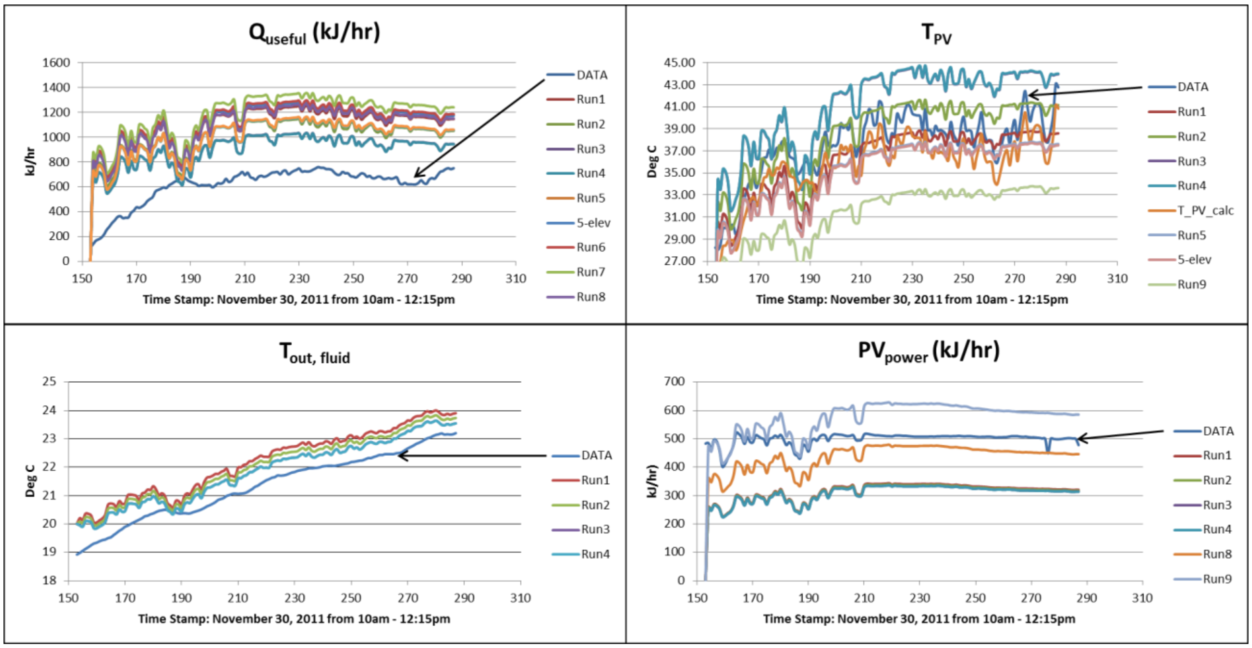

Figure 49. Various calibration runs to try to match the experimental data.

Figure 49 shows the various tuning runs of the computer model against the experimental data. The model was significantly over predicting the thermal performance of the collector (top left plot in Figure 49), most likely due to the fact that the flow was not confined to the square channel rather was more like a slower moving river. The leaving fluid temperature is similarly over predicted and the proportionalities are the same as Q_{useful}. The PV_{power} plot was not used for thermal calibration but was an interesting parameter to watch since the model assumes that the PV is operating at maximum power point (MPP), while the experimental data was operating pretty far off of the MPP due to the oversized load. Adjustments were made to the PV power by changing the reference temperature and reference efficiency. The T_{PV} plot is a good calibration check because it is the driving temperature for heat transfer, thus, a correctly calibrated model should match the measured PV temperature rather well.

Table 12. Various parameters and input changes for tuning the model

Run	Absorber Plate thickness (m)	Resistance of substrate material (h.m2.K/kJ)	Resistance of back material (h.m2.K/kJ)	Reflectance	Emissivity	PV cell Ref Temp	PV cell ref rad	Pv eff. @ ref cond	Back heat loss coeff (kJ/h.m2.K)	Nu# (fluid)
1	0.00238125	0.012019	0.220137	0.15	0.9	37.6	3600	0.12	10	3.608
2	0.00238125	0.0155446	0.220137	0.15	0.9	37.6	3600	0.12	10	3.608
3	0.00238125	0.020248	0.220137	0.15	0.9	37.6	3600	0.12	10	3.608
4	0.00238125	0.020248	0.220137	0.15	0.9	37.6	3600	0.12	10	3.091
	Plotted the calculated PV temperature. This temperature accounts for conduction through the glass cover.									
5	0.00238125	0.0108409	0.220137	0.15	0.9	37.6	3600	0.12	10	3.608
6	0.00238125	0.0108409	0.220137	0.15	0.9	37.6	3600	0.12	10	2.976
7	0.00238125	0.00917	0.220137	0.15	0.9	37.6	3600	0.12	10	2.976
8	0.00238125	0.00917	0.220137	0.15	0.9	25	3600	0.173	10	2.976
9	0.00238125	0.00917	0.220137	0.15	0.9	25	3600	0.226	10	2.976
10	0.00238125	0.00917	0.220137	0.15	0.9	25	3600	0.226	10	2.976
11	0.00238125	0.00917	0.220137	0.15	0.9	25	3600	0.226	10	2.976

Table 13. This table is the description of the adjustments made for the calibration runs of Table 13.

Run	Comments
1	Resistance of substrate (.25 W/mK) included 1/8" PET plus PVC spacer. T_PV is close but the measured PV temp is on top of the glass and EVA material.
2	Resistance of substrate (.25 W/mK) increased thickness due to assuming 1/4" PET
3	Resistance of substrate increased due to low end of conductivity spectrum (0.15 W/mK) @ 1/4"
4	Changing Nu # average value for uniform heat flux both axially and circumferentially
	Now that I think about this, I don't think that this is correct. Not accounting for radiation penetration. I think convection is negligible.
5	Same as run 1 except for the PET thickness 1/12" thick, which is probably more realistic
6	Changed Nu# to conservative constant wall temperature value. Also, needed to convert h_fluid from W/m2K to kJ/hr m2 K
7	Used measured thermal conductivities and thickness from eXPRESS Polymer Letters paper.
8	Going back to PV reference values
9	Changed PV efficiency to reflect the reduced PV area.
10	Realized that machined absorber was 3/16" vs 5/32". It is possible that this thicker side was placed against the PV vs. the 3/32" top sheet. This changes the substrate resistance.
11	Was using 156 flow channels, but its really 152

CALIBRATION 1 – TRNSYS BASE MODEL

This calibration run is set to all of the above listed parameters and inputs from section THE BIPV/T COMPONENT of this chapter. This is the most accurate and most justified model that the author was comfortable presenting. After all of the changes that were described in Table 12 and Table 13, it was apparent that the model just wasn't going to match the data properly, obviously due to the malfunctioning absorber. Thus, this calibration run is the closest mathematical match to the material and flow characteristics that make up the prototype. Changing parameters and inputs from here are not properly justified. Figure 50 shows the comparison of the TRNSYS BASE-CASE (Calibration 1) model to the collected data.

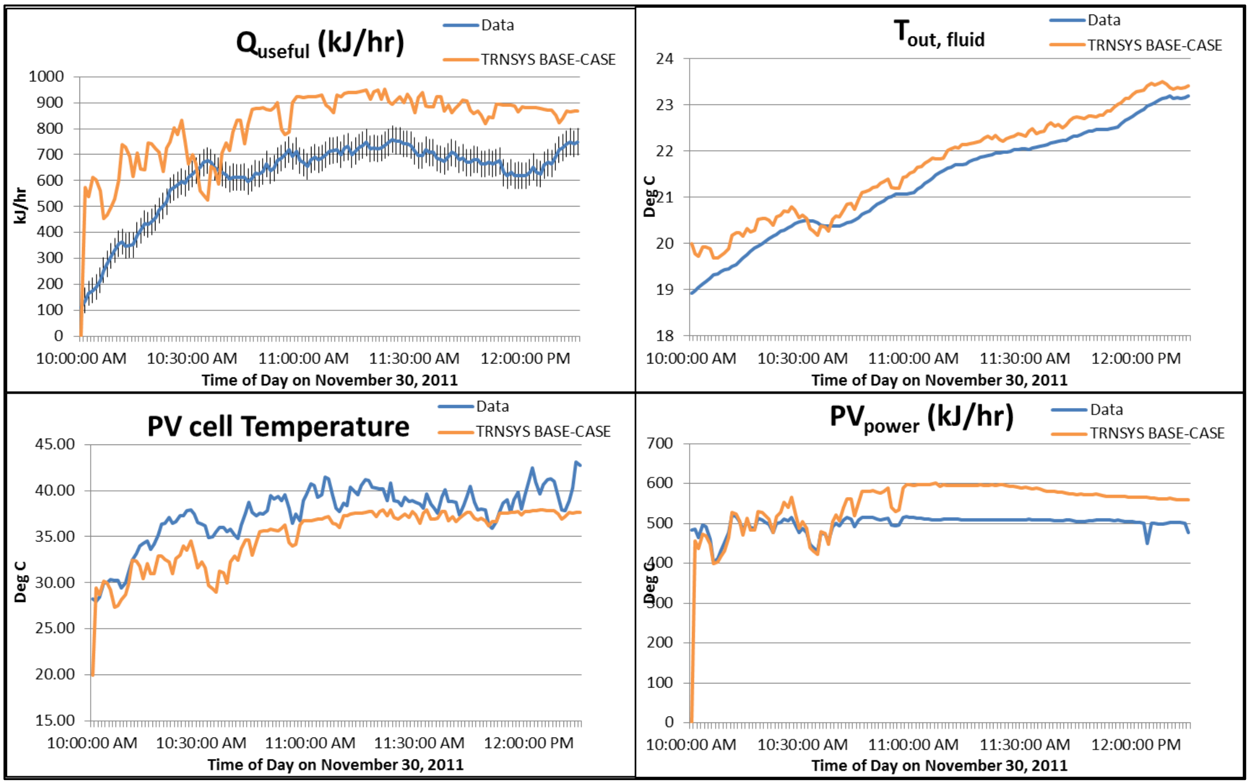

Figure 50. These plots show the comparison to the TRNSYS model base case versus the collected data.

JUSTIFICATION

Adjusting the thickness of the absorber to be the entire thickness versus just the top sheet had little effect on heat transfer. Initially, this seemed concerning, however, a closer inspection of the mathematical model for the BIPV/T (see APPENDIX J TRNSYS PVT MATHEMATICAL MODEL), indicates that the model assumes the absorber plate to be thin and made from a conductive material. In other words, the model assumes a constant temperature for the entire thickness of the absorber plate. Clearly the BIPV/T prototype's absorber is neither thin nor conductive and there will be a temperature profile across the thickness of the absorber. Future calibration (when the absorber construction remains intact), will achieve the actual temperature of the absorber flow channel walls by adjusting the substrate resistance parameter and the bond parameters to compensate for the temperature profile across the absorber thickness.

A qualitative investigation of Figure 51, leads one to assume that the TRNSYS model would be less efficient than the designed BIPV/T because the TRNSYS model has heat being transferred to the flow tubes in only one direction, from the top. As can be seen in Figure 51, the flow tubes are bonded to an absorber plate, and the temperature distribution in the x-direction is calculated by the classical fin problem where the absorber plate section between the midpoint of the two adjacent tubes and tube acts as the fin.

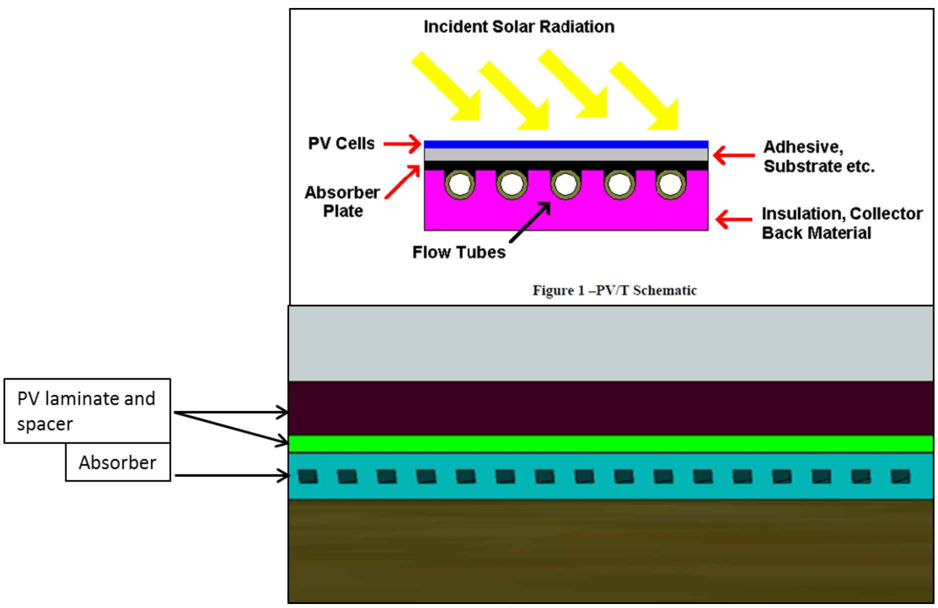

Figure 51. The top image shows a cross-section of the module that TRNSYS's mathematical model is based on. The bottom image is a cross-section of designed BPV/T.

Solving the fin problem for the temperature at the base of the fin results in a useful energy gain relation:

$$q'_{fluid} = \left(\frac{T_B - T_{fluid}}{\frac{1}{h_{fluid}\pi D_{tube}} + \frac{1}{C_B}} \right) \quad (4.9)$$

Where, T_B = base of the fin temperature

$C_B = \frac{k_b b}{\gamma}$ = the tube and absorber bond conductance, where k_b is the bond conductivity, b is the bond width, and γ is the bond thickness.

Equation 4.9 implies that the temperature of the tube wall is uniform circumferentially, which is a reasonable assumption if the tube is made of a highly conductive material. Obviously, the prototype BIPV/T's absorber tubes are not highly conductive, and therefore a wall temperature profile will exist in the y-direction. In order to account for the temperature profile, a resistance should be imposed to drop the temperature to a more realistic average absorber temperature. This was done by using the C_B term in equation 4.9. The conductivity of the bond is simply the same as the absorber material, the width is the width of the flow channel and the thickness was equal to half the length of the side wall.

CALIBRATION 2 – SUBSTRATE RESISTANCE TO MATCH Q_{USEFUL}

Of all the parameters and inputs that could be tweaked to calibrate the computer model, the substrate resistance was the most reasonable to adjust to account for failed construction techniques. The plots of Figure 52, show the calibration results from tuning the substrate resistance to match the useful energy gain. CAL2a and CAL2b represent an increase in substrate thermal resistance by 20% and 100% (relative to the TRNSYS BASE-CASE), respectively.

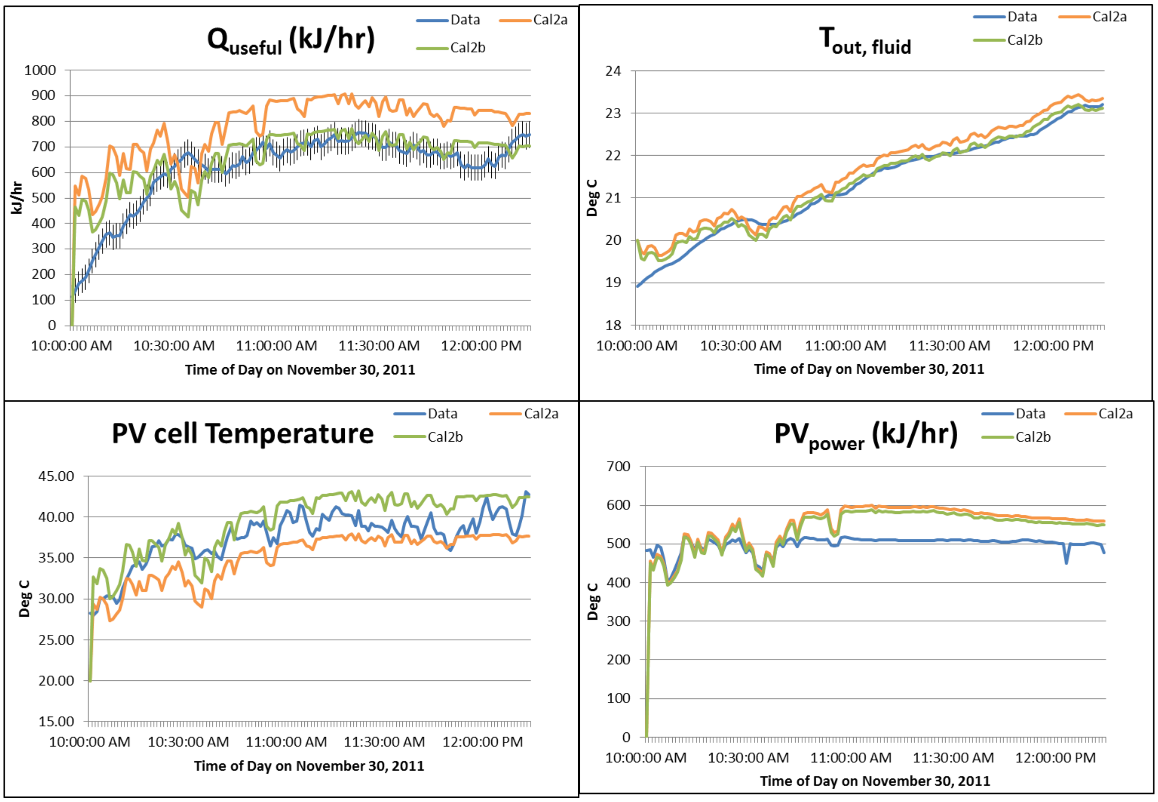

Figure 52. The above plots are the calibration results from tuning the substrate resistance to match the useful energy gain. CAL2a represents a 20% increase in substrate resistance and CAL2b represents a 100% increase in substrate resistance (relative to calibration 1).

Looking at Figure 52, it is evident that the increased substrate resistance (2 times more than Calibration 1) of Cal2b has brought the TRNSYS model useful energy gain within the range of measured uncertainty. Both Calibration components will be run in the simulation model and analyzed for annual energy savings and economic analysis.

THE SIMULATION MODEL

Figure 53 is the graphical representation of the simulation model. The simulation is to represent a typical 4-5person, American home, where the BIPV/T system is sized to produce 5kW of electrical power and the domestic hot water consumption is 100 gallons/day. Using the SunPower SPR-215 modules, this requires 25 modules on a roof space that can accommodate 31 m^2 of roof space. The house is assumed to be a two story home of about 2000 ft^2. These two assumptions affect the overall collector area and the top loss convective heat transfer coefficient, respectively.

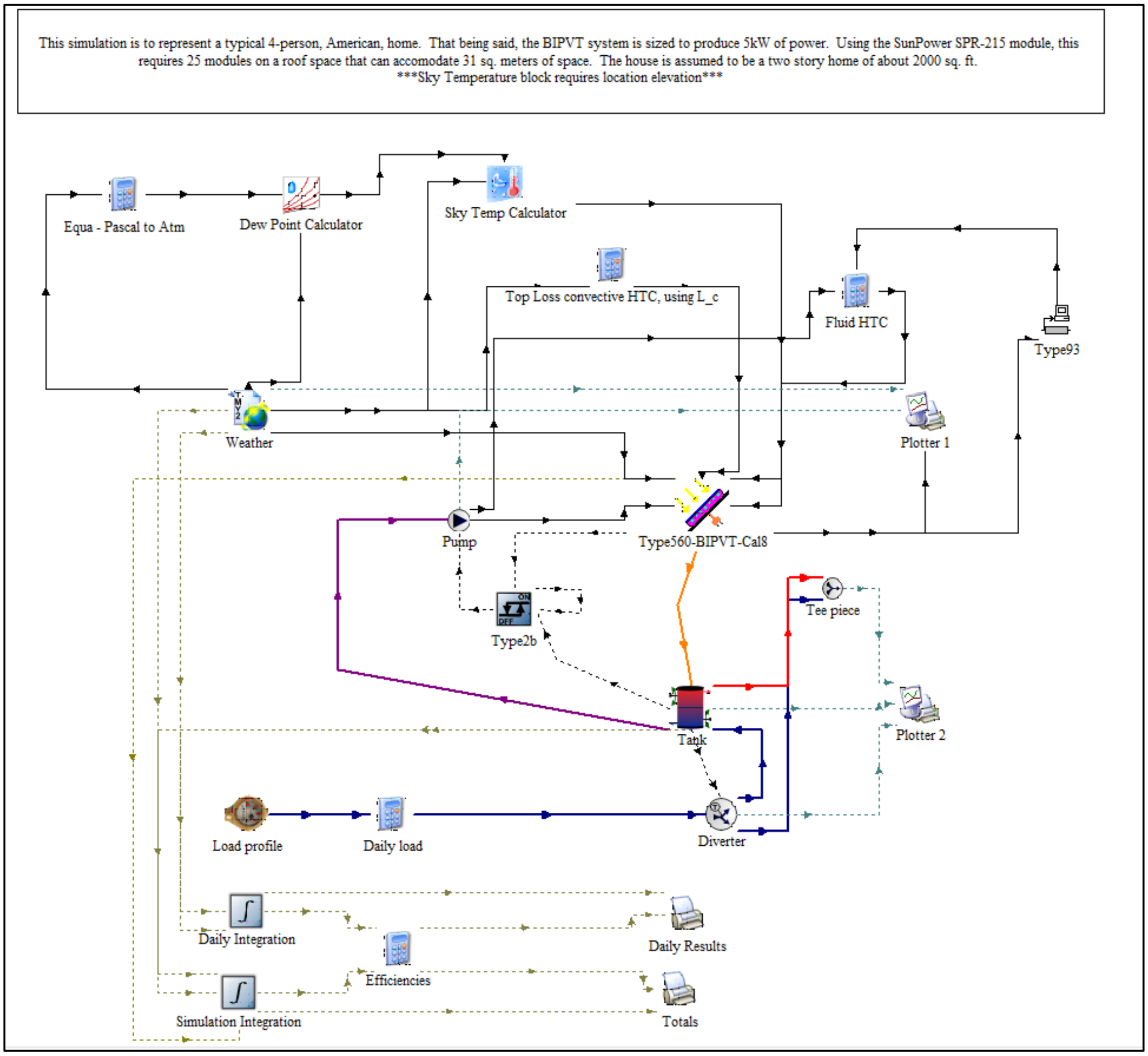

Figure 53. This is the graphical representation of the simulation model.

COMPONENT DESCRIPTIONS

Each component's function description and reasoning for the parameter, input and output values can be found in APPENDIX K DETAILED SIMULATION COMPONENT DESCRIPTION. However, some comments about particular components warrant a discussion in the main body.

TOP LOSS HTC, USING L_C

The top loss coefficient for simulation purposes differs from the calculation used in the calibration model because flow over a collector mounted on a house is not necessarily well represented by wind tunnel tests of isolated plates. Mitchell (1976) (Duffie & Beckman, 2006)found that many shapes were well represented by a sphere when the equivalent sphere diameter (L_c) is the cube root of the volume. Mitchell suggests that the wind tunnel results of the various animal shapes be increased by approximately 15% for outdoor conditions. Thus, assuming a house to be a sphere, the Nusselt number can be expressed as:

$$Nu = 0.42Re^{0.6} \tag{4.10}$$

Or,

$$h_{wind} = \frac{8.6V^{0.6}}{L^{0.4}} \tag{4.11}$$

Thus the top loss convective heat transfer coefficient (W/m^2 K) for flush mounted collectors on a house can be expressed as:

$$h_{wind} = max\left[5, \frac{8.6V^{0.6}}{L^{0.4}}\right] \tag{4.12}$$

STORAGE TANK

This storage tank model has variable inlets and uniform losses. The thermal performance of a fluid-filled sensible energy storage tank, subject to thermal stratification, can be modeled by assuming that the tank consists of N (N<= 100) fully-mixed equal volume segments. The degree of stratification is determined by the value of N. If N is equal to 1, the storage tank is fully mixed. This instance of Type 4 models a stratified tank having variable inlet positions such that entering fluid may be added to the tank at a temperature as nearly equal to its own temperature as possible. The tank modeled in simulation has four nodes of equal depth where stratification can occur. This tank has one 4500 W electric heater located in the second node from the top, and its thermostat is located in the top node of the tank. The thermostat set point is at 60 °C with a 5°C deadband.

THE LOAD PROFILE

The load profile is abstracted from ASHRAE 90.2, table 8-4, *Daily Domestic Water Load Profile.* The values in the right column of Table 14 simply are multiplied by daily consumption of the household, assumed to be 100 gallons/day.

Table 14. ASHRAE daily domestic water load profile.

TABLE 8-4
Daily Domestic Hot Water Load Profile

Time of Day	
MID - 1 a.m.	0.0085
1 - 2 a.m.	0.0085
2 - 3 a.m.	0.0085
3 - 4 a.m.	0.0085
4 - 5 a.m.	0.0085
5 - 6 a.m.	0.0100
6 - 7 a.m.	0.0750
7 - 8 a.m.	0.0750
8 - 9 a.m.	0.0650
9 - 10 a.m.	0.0650
10 - 11 a.m.	0.0650
11 - NOON	0.0460
12 - 13 p.m.	0.0460
13 - 14 p.h	0.0370
14 - 15 p.m.	0.0370
15 - 16 p.m.	0.0370
16 - 17 p.m.	0.0370
17 - 18 p.m.	0.0630
18 - 19 p.m.	0.0630
19 - 20 p.m.	0.0630
20 - 21 p.m.	0.0630
21 - 22 p.m.	0.0510
22 - 23 p.m.	0.0510
23 - MID	0.0085

Note: These hourly values include a large diversity factor and should not be used to calculate peak loads for equipment sizing.

ON/OFF DIFFERENTIAL CONTROLLER

This differential controller sends either a 0 or 1 control signal to the pump. The upper temperature deadband is set at 5°C and the lower temperature deadband at 0°C, where the deadband temperature is the difference between the collectors leaving fluid temperature and the temperature at the bottom node of the tank. Thus, the pump cycles until the leaving fluid temperature is 5°C above the bottom tank node temperature, then stays on until the leaving fluid temperature is the same temperature as the bottom node temperature.

THE PUMP

The pump is a 1/6 HP pump with a flow rate set at 0.06 GPM/ft^2, which works out to about 0.6 GPM/module, or 3385 kg/hr for all 25 modules.

CHAPTER 5 SIMULATION RESULTS AND ECONOMIC ANALYSIS

Table 15 is a summary of all the locations that were simulated in TRNSYS. The cities in the table were selected in order to represent the State's climate diversity without entering a freezing climate zone.

Table 15. This table represents the locations that will be simulated. The selected cities are nonfreezing climates, in large urban areas.

STATES	CITIES				
CALIFORNIA	San Diego	Los Angeles	Sacramento	Fresno	
NEVADA	Las Vegas				
ARIZONA	Phoenix	Tucson			
TEXAS	El Paso	Dallas	Austin	San Antonio	Houston
LOUISIANA	New Orleans				
GEORGIA	Atlanta				
FLORIDA	Miami	Tampa	Jacksonville	Tallahassee	
HAWAII	Honolulu				

For each location in Table 15, both calibration BIPV/T components will be used, and the range of results presented. Calibration 1 was also simulated for each city using a highly thermally conductive polymer. The flow rate for the simulation was set a 0.06 GPM/ft^2, which is in between typical flat-plate collectors and unglazed pool heating flows. It was desirable to lower the flow from that of pool heating applications, in order to increase the leaving fluid temperature and increase the useful energy gains into the storage tank. The simulation time step was set to 6 minutes because this prevented convergence problems, which were related to the pump controller.

All cities were run in the TRNSYS simulation model under heat collection and stagnation conditions. The stagnation condition was tested to investigate the potential electrical energy efficiency improvement due to cooling of the PV cells.   The electricity rates were gathered from the US Energy Information Administration, Form EIA-861, as seen in Figure 54.

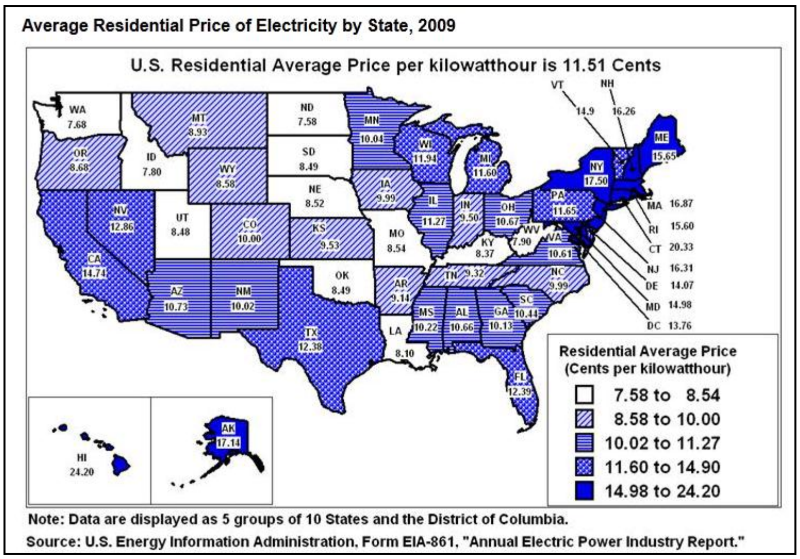

Figure 54. Average Residential Price of Electricity by State

Table 16 and Table 17 present the results for all the key performance characteristics for all simulated cities. The dollars saved per year was calculated as the difference between the DHW load and the electrical demand, as follows

$$\$_{saved}/_{year} = DHW\ Load - (Auxilliary\ Energy + Pump\ Energy) \tag{5.1}$$

The last column, Lifetime Thermal Savings, in Table 16, Table 17, and Table 18 is calculated by the following

$$PV = A * USPW(d, N) \tag{5.2}$$

Where PV = Present Value, or lifetime thermal savings

A = Annual Energy Savings per module due to the thermal component of the BIPVT

$USPW(d, N)$ = the Uniform Series Present Worth factor; N = 30 years, d = 5%

The present value indicates the maximum amount of additional cost over a PV array that can be passed onto the consumer to justify the investment on a per module basis. The lifetime thermal savings parameter was calculated on a per module basis because this is where the additional costs for the BIPVT array versus traditional PV array show themselves. Each PV module will have to be shipped to a warehouse/machine shop, stripped of the existing frame, fabricated up by hand, and then shipped to the installation site. Installation costs should be less than traditional PV array because of the direct building integrated mounting, and the fact that it will be on new construction and will not have roofing materials cost where the array is installed might be able to further increase the competitive margin for profits.

Table 16. Annual simulation results for Calibration 1, using PVC. The last column indicates the maximum amount of additional cost over a PV array that can be passed onto the consumer to justify the investment on a per module basis.

Annual Results sorted by the Solar Fraction - Calibration 1 - PVC														
	Incident Solar Radiation (kJ/m^2)	Collector Useful Energy (kJ)	DHW Load (kJ)	Auxiliary Energy (kJ)	Collector Efficiency	Solar Fraction	PV Efficiency (collection)	PV Efficiency (stagnation)	PV Efficiency % improvement	Elec Rate $/kWh	$\$_{saved}$/yr	$\$_{saved}/ft^2/yr$	$\$_{saved}$/module/yr	Lifetime Thermal Savings
Phoenix	8.62E+06	1.58E+07	1.85E+07	4.89E+06	7.70%	73.50%	15.30%	15.00%	1.96%	0.11	$405.65	$1.63	$16.23	$249.44
Tuscon	8.67E+06	1.41E+07	1.85E+07	6.36E+06	6.86%	65.60%	15.60%	15.32%	1.79%	0.11	$361.84	$1.46	$14.47	$222.49
Las Vegas	8.67E+06	1.39E+07	1.85E+07	6.57E+06	6.73%	64.40%	15.60%	15.31%	1.86%	0.13	$426.17	$1.72	$17.05	$262.05
El Paso	8.59E+06	1.36E+07	1.85E+07	6.87E+06	6.65%	62.80%	15.70%	15.43%	1.75%	0.12	$399.94	$1.61	$16.00	$245.92
Fresno	7.64E+06	1.31E+07	1.85E+07	7.32E+06	7.20%	60.40%	15.50%	15.25%	1.65%	0.15	$457.76	$1.84	$18.31	$281.48
Tampa	7.05E+06	1.31E+07	1.85E+07	7.31E+06	7.82%	60.40%	15.50%	15.28%	1.42%	0.12	$385.12	$1.55	$15.40	$236.81
Honolulu	7.43E+06	1.31E+07	1.85E+07	7.33E+06	7.40%	60.30%	15.40%	15.24%	1.04%	0.24	$750.87	$3.02	$30.03	$461.71
Miami	6.93E+06	1.29E+07	1.85E+07	7.48E+06	7.84%	59.50%	15.50%	15.27%	1.48%	0.12	$379.27	$1.53	$15.17	$233.21
San Antonio	7.11E+06	1.23E+07	1.85E+07	8.04E+06	7.27%	56.40%	15.60%	15.37%	1.47%	0.12	$359.71	$1.45	$14.39	$221.18
Tallahassee	6.78E+06	1.22E+07	1.85E+07	8.09E+06	7.59%	56.20%	15.60%	15.35%	1.60%	0.12	$358.28	$1.44	$14.33	$220.30
Austin	7.03E+06	1.21E+07	1.85E+07	8.19E+06	7.26%	55.70%	15.60%	15.37%	1.47%	0.12	$354.55	$1.43	$14.18	$218.01
Jacksonville	6.63E+06	1.20E+07	1.85E+07	8.27E+06	7.63%	55.20%	15.60%	15.33%	1.73%	0.12	$352.08	$1.42	$14.08	$216.49
New Orleans	6.59E+06	1.18E+07	1.85E+07	8.49E+06	7.53%	54.00%	15.60%	15.38%	1.41%	0.08	$225.23	$0.91	$9.01	$138.49
San Diego	7.58E+06	1.17E+07	1.85E+07	8.56E+06	6.50%	53.70%	15.90%	15.64%	1.64%	0.15	$406.99	$1.64	$16.28	$250.26
Dallas	7.19E+06	1.15E+07	1.85E+07	8.72E+06	6.75%	52.80%	15.70%	15.48%	1.40%	0.12	$336.32	$1.35	$13.45	$206.80
Houston	6.30E+06	1.15E+07	1.85E+07	8.72E+06	7.69%	52.80%	15.60%	15.35%	1.60%	0.12	$336.32	$1.35	$13.45	$206.80
Sacramento	7.24E+06	1.14E+07	1.85E+07	8.83E+06	6.63%	52.20%	15.70%	15.46%	1.53%	0.15	$395.93	$1.59	$15.84	$243.46
Los Angeles	7.40E+06	1.13E+07	1.85E+07	8.95E+06	6.41%	51.50%	15.90%	15.71%	1.19%	0.15	$391.02	$1.57	$15.64	$240.44
Atlanta	6.83E+06	1.07E+07	1.85E+07	9.45E+06	6.61%	48.80%	15.80%	15.58%	1.39%	0.10	$254.66	$1.03	$10.19	$156.59

Table 17. Annual Results sorted by the Solar Fraction for Calibration 2. Calibration 2 differed from Calibration 1 by an increased PV substrate resistance to better match the experimental data.

Annual Results sorted by the Solar Fraction - Calibration 2 - PVC														
	Incident Solar Radiation (kJ/m^2)	Collector Useful Energy (kJ)	DHW Load (kJ)	Auxiliary Energy (kJ)	Collector Efficiency	Solar Fraction	PV Efficiency (collection)	PV Efficiency (stagnation)	PV Efficiency % improvement	Elec Rate $/kWh	$\$_{saved}$/yr	$\$_{saved}$/ft^2/yr	$\$_{saved}$/module/yr	Lifetime Thermal Savings
Phoenix	8.62E+06	1.47E+07	1.85E+07	5.86E+06	7.17%	68.30%	15.30%	15.00%	2.00%	0.11	$376.74	$1.52	$15.07	$231.66
Tucson	8.67E+06	1.31E+07	1.85E+07	7.24E+06	6.38%	60.80%	15.60%	15.32%	1.83%	0.11	$335.61	$1.35	$13.42	$206.37
Las Vegas	8.67E+06	1.29E+07	1.85E+07	7.49E+06	6.25%	59.50%	15.50%	15.31%	1.24%	0.13	$393.30	$1.58	$15.73	$241.84
El Paso	8.59E+06	1.26E+07	1.85E+07	7.76E+06	6.16%	58.00%	15.70%	15.43%	1.78%	0.12	$369.34	$1.49	$14.77	$227.10
Honolulu	7.43E+06	1.22E+07	1.85E+07	8.07E+06	6.93%	56.30%	15.40%	15.24%	1.05%	0.24	$701.13	$2.82	$28.05	$431.12
Tampa	7.05E+06	1.22E+07	1.85E+07	8.14E+06	7.28%	55.90%	15.50%	15.28%	1.44%	0.12	$356.56	$1.44	$14.26	$219.25
Fresno	7.64E+06	1.21E+07	1.85E+07	8.24E+06	6.64%	55.40%	15.50%	15.25%	1.67%	0.15	$420.09	$1.69	$16.80	$258.31
Miami	6.93E+06	1.21E+07	1.85E+07	8.23E+06	7.33%	55.40%	15.50%	15.27%	1.51%	0.12	$353.46	$1.42	$14.14	$217.34
San Antonio	7.11E+06	1.14E+07	1.85E+07	8.85E+06	6.77%	52.10%	15.60%	15.37%	1.50%	0.12	$331.85	$1.34	$13.27	$204.06
Tallahassee	6.78E+06	1.13E+07	1.85E+07	8.87E+06	7.05%	52.00%	15.60%	15.35%	1.63%	0.12	$331.43	$1.33	$13.26	$203.80
Austin	7.03E+06	1.13E+07	1.85E+07	8.94E+06	6.77%	51.60%	15.60%	15.37%	1.50%	0.12	$328.76	$1.32	$13.15	$202.15
Jacksonville	6.63E+06	1.12E+07	1.85E+07	9.01E+06	7.12%	51.20%	15.50%	15.33%	1.11%	0.12	$326.61	$1.32	$13.06	$200.83
New Orleans	6.59E+06	1.10E+07	1.85E+07	9.23E+06	7.02%	50.00%	15.60%	15.38%	1.43%	0.08	$208.58	$0.84	$8.34	$128.25
San Diego	7.58E+06	1.09E+07	1.85E+07	9.31E+06	6.04%	49.60%	15.80%	15.64%	1.02%	0.15	$376.28	$1.52	$15.05	$231.37
Dallas	7.19E+06	1.07E+07	1.85E+07	9.44E+06	6.28%	48.90%	15.70%	15.48%	1.42%	0.12	$311.56	$1.25	$12.46	$191.58
Houston	6.30E+06	1.07E+07	1.85E+07	9.45E+06	7.18%	48.80%	15.50%	15.35%	0.98%	0.12	$311.22	$1.25	$12.45	$191.37
Sacramento	7.24E+06	1.06E+07	1.85E+07	9.57E+06	6.15%	48.20%	15.70%	15.46%	1.55%	0.15	$365.63	$1.47	$14.63	$224.83
Los Angeles	7.40E+06	1.05E+07	1.85E+07	9.69E+06	5.95%	47.50%	15.90%	15.71%	1.21%	0.15	$360.72	$1.45	$14.43	$221.81
Atlanta	6.83E+06	9.95E+06	1.85E+07	1.02E+07	6.13%	44.90%	15.80%	15.58%	1.41%	0.10	$233.55	$0.94	$9.34	$143.61

Figure 55 and Figure 56 are a graphical representation of the solar fraction and the lifetime thermal savings per module. Figure 55 goes to show that the prototype can handle a solid annual percentage of the domestic hot water load. The highest solar fraction is found to be located in Phoenix, Az where over 70% of the annual DHW load can be met by the BIPVT and the lowest solar fraction being in Atlanta, Ga where nearly 47% of the annual DHW load can be met.

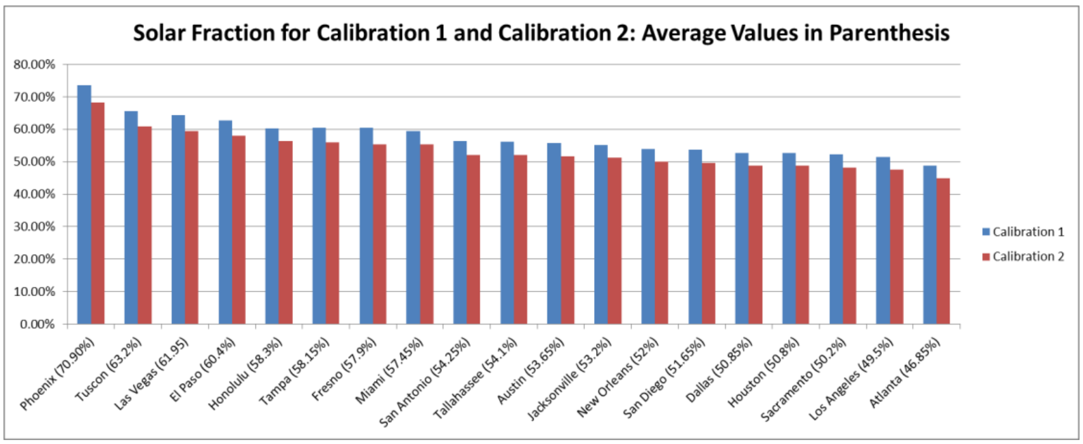

Figure 55. Solar Fraction by city for both calibrations.

Figure 56 takes into account the cost of electricity and calculates lifetime thermal savings. In Honolulu, Hi where electricity rates are more than double the rest of the simulated cities, the incremental savings over a traditional PV panel are over $500 per module over the lifetime of the system. This metric allows the BIPVT supplier a large margin for profits and savings to be passed onto the consumer.

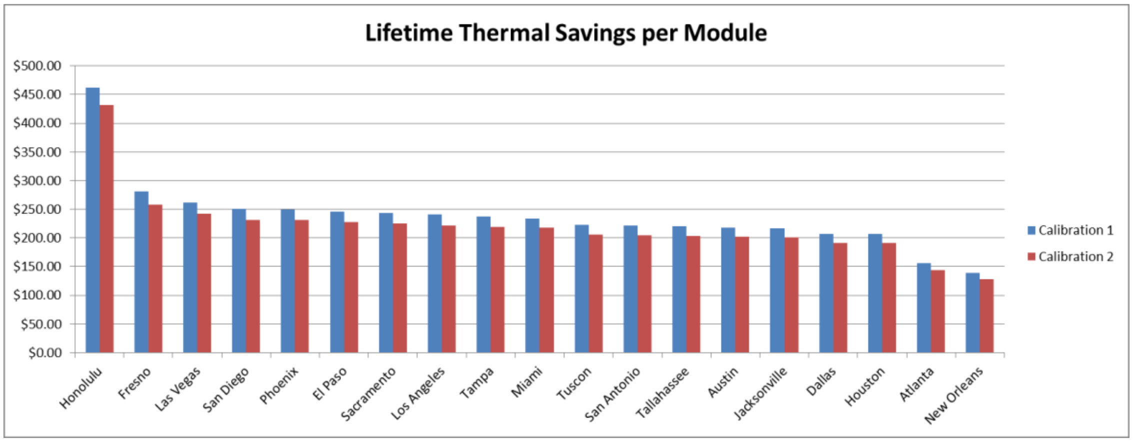

Figure 56. This parameter is the incremental savings over the lifetime of the BIPVT when compared to a PV only module.

Table 18 is the annual simulation results for Calibration 1 but instead of using a PVC absorber, a special highly thermally conductive material was used. It is important to understand that these types of materials are out on the market, but the only way to know if the additional cost of the material is worth the improved performance is to run a simulation to make the right economic decision. The results presented in Figure 57 clearly show a point of diminishing returns with improved absorber thermal conductivity and increasing solar fraction. The manufacturer of the thermally conductive plastic is a company based out of Rhode Island called Cool Polymers. Their family of thermally conductive plastics range from conductivities of 2 W/mk to 100 W/mk. The polymer selected for simulation had a conductivity of 20 W/mk and its specification sheet can be viewed in APPENDIX JTRNSYS PVT MATHEMATICAL MODEL.

Table 18. Annual simulation results for Calibration 1 using the CoolPoly thermally conductive absorber material.

Annual Results sorted by the Solar Fraction - Calibration 1 - CoolPoly														
	Incident Solar Radiation (kJ/m^2)	Collector Useful Energy (kJ)	DHW Load (kJ)	Auxiliary Energy (kJ)	Collector Efficiency	Solar Fraction	PV Efficiency (collection)	PV Efficiency (stagnation)	PV Efficiency % improvement	Elec Rate $/kWh	$\$_{saved}/yr$	$\$_{saved}/ft^2/yr$	$\$_{saved}/module/yr$	Lifetime Thermal Savings
Phoenix	8.62E+06	1.73E+07	1.85E+07	3.52E+06	8.46%	81.00%	15.40%	15.00%	2.60%	0.11	$446.49	$1.80	$17.86	$274.54
Tucson	8.67E+06	1.58E+07	1.85E+07	4.81E+06	7.69%	73.90%	15.60%	15.32%	1.79%	0.11	$408.04	$1.64	$16.32	$250.90
Las Vegas	8.67E+06	1.54E+07	1.85E+07	5.17E+06	7.50%	72.00%	15.60%	15.31%	1.86%	0.13	$476.18	$1.92	$19.05	$292.80
El Paso	8.59E+06	1.52E+07	1.85E+07	5.35E+06	7.46%	71.00%	15.70%	15.43%	1.75%	0.12	$452.21	$1.82	$18.09	$278.07
Tampa	7.05E+06	1.47E+07	1.85E+07	5.86E+06	8.77%	68.20%	15.50%	15.28%	1.42%	0.12	$435.03	$1.75	$17.40	$267.50
Honolulu	7.43E+06	1.45E+07	1.85E+07	5.98E+06	8.23%	67.60%	15.50%	15.24%	1.68%	0.24	$841.62	$3.39	$33.66	$517.51
Fresno	7.64E+06	1.45E+07	1.85E+07	6.04E+06	7.99%	67.30%	15.60%	15.25%	2.28%	0.15	$510.17	$2.05	$20.41	$313.70
Miami	6.93E+06	1.44E+07	1.85E+07	6.10E+06	8.75%	67.00%	15.50%	15.27%	1.48%	0.12	$426.77	$1.72	$17.07	$262.42
San Antonio	7.11E+06	1.37E+07	1.85E+07	6.74E+06	8.12%	63.50%	15.60%	15.37%	1.47%	0.12	$404.41	$1.63	$16.18	$248.67
Tallahassee	6.78E+06	1.37E+07	1.85E+07	6.73E+06	8.52%	63.50%	15.60%	15.35%	1.60%	0.12	$405.08	$1.63	$16.20	$249.09
Austin	7.03E+06	1.36E+07	1.85E+07	6.84E+06	8.13%	62.90%	15.60%	15.37%	1.47%	0.12	$400.97	$1.61	$16.04	$246.56
Jacksonville	6.63E+06	1.34E+07	1.85E+07	6.96E+06	8.54%	62.30%	15.60%	15.33%	1.73%	0.12	$397.17	$1.60	$15.89	$244.22
New Orleans	6.59E+06	1.32E+07	1.85E+07	7.22E+06	8.43%	60.90%	15.60%	15.38%	1.41%	0.08	$253.80	$1.02	$10.15	$156.06
San Diego	7.58E+06	1.31E+07	1.85E+07	7.24E+06	7.29%	60.80%	15.90%	15.64%	1.64%	0.15	$461.03	$1.86	$18.44	$283.49
Houston	6.30E+06	1.29E+07	1.85E+07	7.45E+06	8.62%	59.70%	15.60%	15.35%	1.60%	0.12	$380.00	$1.53	$15.20	$233.66
Dallas	7.19E+06	1.29E+07	1.85E+07	7.49E+06	7.53%	59.40%	15.70%	15.48%	1.40%	0.12	$378.62	$1.52	$15.14	$232.81
Sacramento	7.24E+06	1.28E+07	1.85E+07	7.56E+06	7.43%	59.00%	15.70%	15.46%	1.53%	0.15	$447.93	$1.80	$17.92	$275.43
Los Angeles	7.40E+06	1.27E+07	1.85E+07	7.66E+06	7.21%	58.50%	16.00%	15.71%	1.81%	0.15	$443.84	$1.79	$17.75	$272.91
Atlanta	6.83E+06	1.21E+07	1.85E+07	8.20E+06	7.45%	55.60%	15.80%	15.58%	1.39%	0.10	$289.83	$1.17	$11.59	$178.22

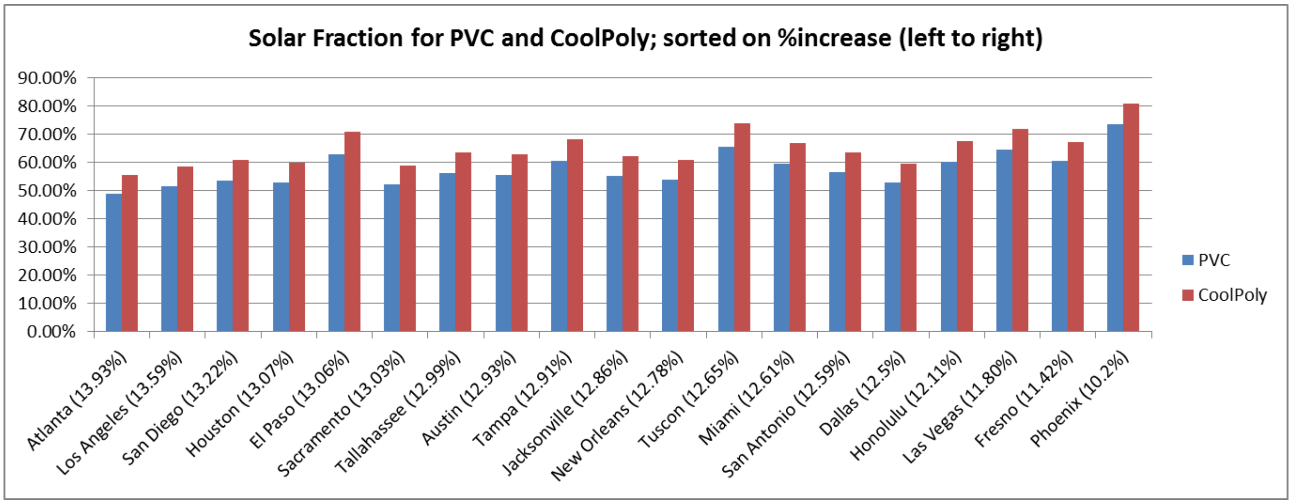

Figure 57. Solar Fraction Comparison among cities and absorber material.

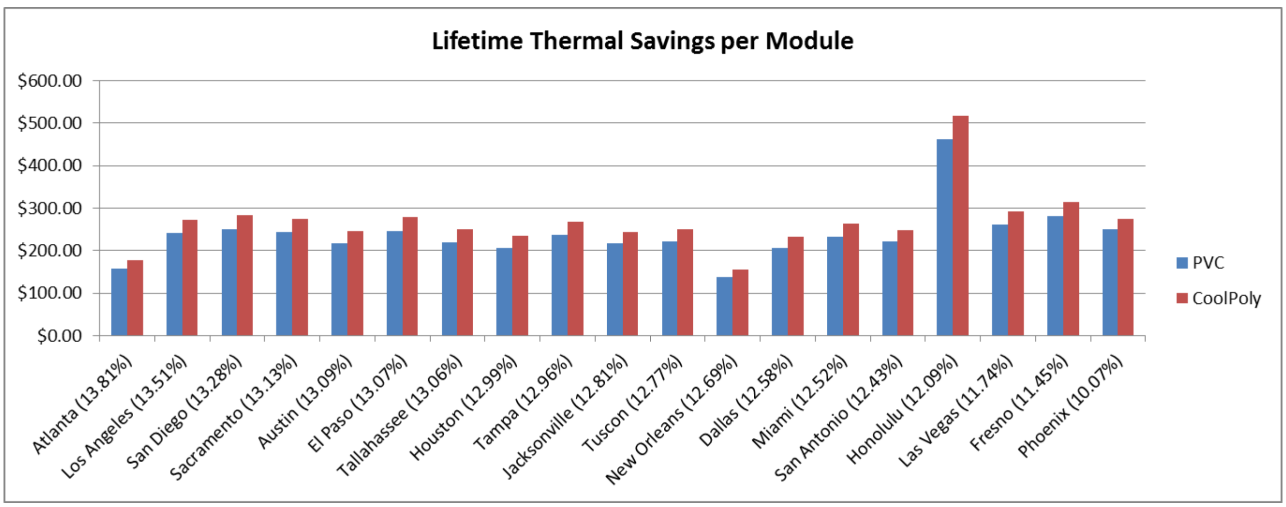

Figure 58. BIPVT maximum price margin comparison among cities and absorber material, sorted by percent increase.

Figure 57 and Figure 58 reveal an important manufacturing optimization problem. Notice that there is a significant improvement in thermal performance with the improved thermal conductivity of the CoolPoly material. However, the thermal improvements are far from linearly related to the conductivities.

The optimization problem is to maximize the NPW by varying the material, and consequentially the material conductivity, as shown in equation 5.2.

$$Max[NPW] = -Material\ Cost\ per\ module + A * USPW(d, N) \tag{5.3}$$

Where, $A = \emptyset\ (material\ conductivity)$

Table 19 provides a summary of the range of solar fraction and lifetime thermal savings results.

Table 19. Summary of the range of results for the Solar Fraction and the Lifetime Thermal Savings per module

Annual Solar Fraction Ranges			
Calibration	**Max**	**Min**	**Avg**
Cal 1 - PVC	73.5% (Phoenix)	48.8% (Atlanta)	57.69%
Cal 2 - PVC	68.3% (Phoenix)	44.9% (Atlanta)	53.39%
Cal 1 - CoolPoly	81% (Phoenix)	55.6% (Atlanta)	64.95%
Lifetime Thermal Savings (per module)			
Calibration	**Max**	**Min**	**Avg**
Cal 1 - PVC	\$461.71 (Honolulu)	\$138.49 (New Orleans)	\$237.47
Cal 2 - PVC	\$431.12 (Honolulu)	\$128.25 (New Orleans)	\$219.82
Cal 1 - CoolPoly	\$517.51 (Honolulu)	\$156.06 (New Orleans)	\$267.29

The above analysis has laid the foundation for a future manufacturing business model. There is a cost per module that the manufacturer can compete against for an increased profit margin. The simulations demonstrate an improved electrical performance due to the heat collection component and all costs can be rolled into a 30-year mortgage plan on a new residence. For example, if the manufacturer charges \$130 more per module than a traditional PV then, the consumer will realize savings in about 15 years, and the manufacturer will be able to make a 30% profit. It is possible that the additional cost per BIPVT module over a traditional PV module may be closer to zero, making the BIPVT even more attractive to customers and more lucrative for the supplier.

SPOTLIGHT ON PHOENIX

Typical Seasonal Day Analysis

In order to gain a better understanding of the system on a daily basis, the simulation was run in Phoenix, AZ on typical winter, spring and summer days. Figure 59 is the graphical representation of the typical seasonal days. The top plots show the incident radiation and the pump control signal, while the bottom plots show the pump signal, temperature in and out of the tank, and average tank temperature. At first glance, it seems a bit concerning that the temperature rise across the collector is very small. This occurrence is because the pump is most likely circulating water from the same node. The collector is pulling from the bottom of the tank, and if the return temperature rise across the collector is only slightly warmer than the supply temperature, the tank will dump the heat back into the same node. This causes a gradual heating of the tank from the bottom up breaking down stratification, but increasing thermal capacity. I believe the increase in thermal capacity is where significant energy savings can be found, by coasting longer into the night using less auxiliary power as stratification sets back up.

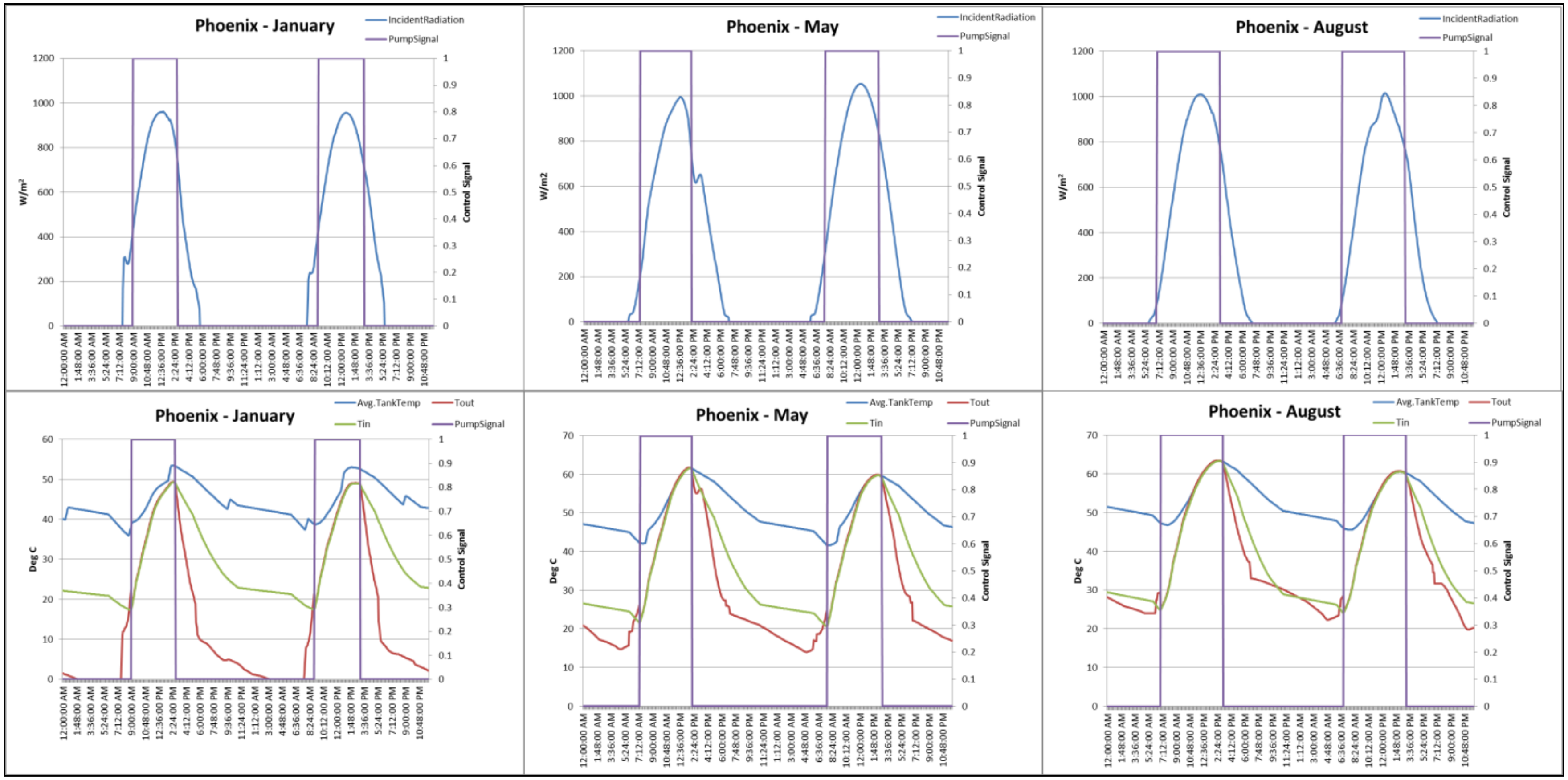

Figure 59. This figure demonstrates the behavior of the system for a couple of days during the winter, spring and summer in Phoenix, Az. The upper plots show the incident radiation striking the surface and the pump control signal (On/Off). The bottom plots consist of the average tank temperature, the entering and leaving fluid temperature of the collector and the pump control signal. Note that Tin is also the temperature at the bottom of the tank and all values where Tout is not under the pump control curve are calculated values.

Effect of Flow Rate and Pumping Power on Annual Performance

Figure 59 is showing very little temperature rise across the collector. Slowing the flow rate across the collector will undoubtedly improve the temperature rise. A parametric flow rate analysis was conducted to see the impact on annual performance. Pumping power was also taken into account. The simulation was run for a couple of days during the summer. Specifically, July 15 – 17 was chosen and the TMY2 data for those hours of the year were the forcing functions. Figure 60 shows the collector temperature rise over the course of two days. The first and third peaks correspond to values when the pump was signaled on during the day. The second and fourth peaks are calculated values by TRNSYS during the course of the night. When the pump is off, stratification in the tank starts to setup. The residual heat of the collectors from the day would still create a temperature rise from water at the bottom of the tank, but not significant enough for the pump control sequence to turn on the pump at night.

Based on Figure 60, it is obvious that the slow flow rate is indeed improving temperature rise across the collector. Improved temperature rise is also improving tank stratification because the water entering the tank from the collector is being introduced to the tank at a higher level versus the bottom. Better stratification lowers the average tank temperature (lower heat loss from the tank) and lowers the entering fluid temperature to the collector (improves collector efficiency). Table 20 represents the results of the parametric flow rate analysis. 0.06 GPM/ft^2 was the typical flow rate used for the regional annual comparisons of the previous section. The flow rate was parametrically reduced down to a very slow rate. The collector efficiency and solar fraction improved slightly with slower flows.

The pump HP was assumed to be reduced from 1/6 to 1/8 HP based on pump selections from Taco pumps for flow rates less than .02 GPM/ft^2. The reduction in pump HP was the driving factor for dollars saved improvement. The improved temperature rise with flow rate had negligible impact on the number of hours the pump ran per year. The kWh improved by 1 kWh when flow was reduced from 0.06 to 0.04 and 2 kWh when reduced from 0.02 to 0.01 GPM/ft^2.

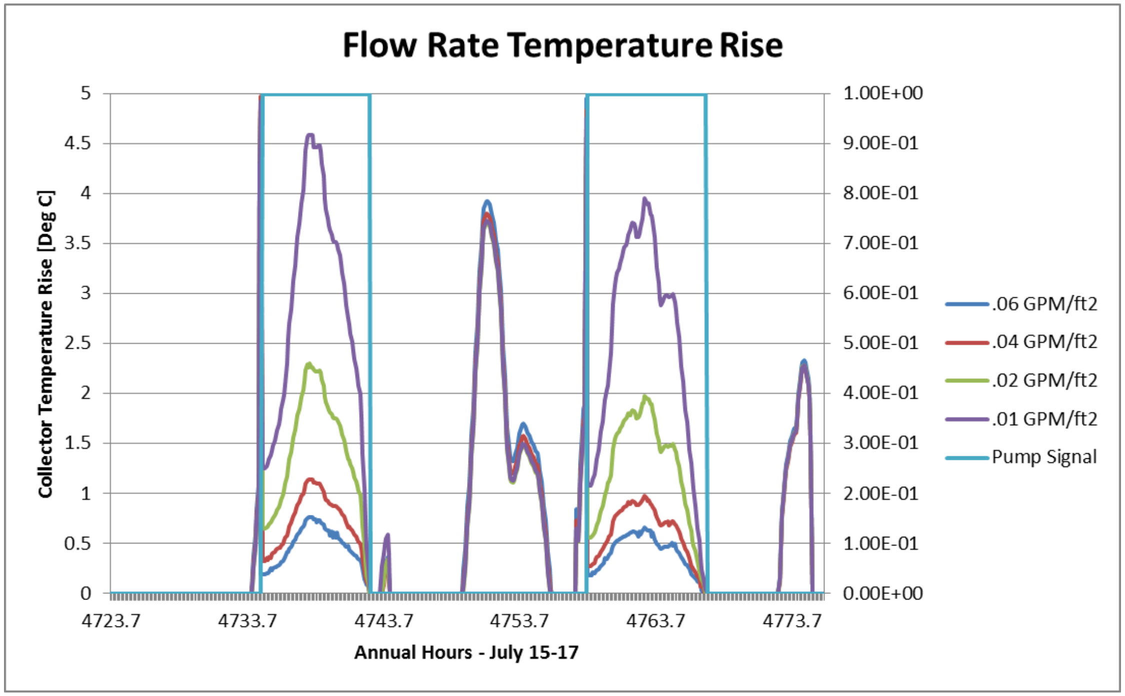

Figure 60. The above figure shows the calculated values of collector temperature rise as a function of time. The first and third peaks represent times when the pump is on. The second and fourth peaks represent calculated values. The pump control sequence doesn't signal the pump on until a 5 degree temperature difference is achieved.

Table 20 Parametric analysis of flow rate on annual performance.

Flow Rate Parametric Analysis for Phoenix																	
Flow Rate (0.06 GPM/ft2)	Incident Solar Radiation (kJ/m^2)	Collector Useful Energy (kJ)	DHW Load (kJ)	Auxiliary Energy (kJ)	Collector Efficiency	Solar Fraction	PV Efficiency (collection)	PV Efficiency (stagnation)	PV Efficiency % improvement	Pump HP	PumpEnergy/yr (kWh)	Elec Rate $/kWh	$\$_{saved}$/yr	$\$_{saved}$/yr % Increase	$\$_{saved}/ft^2$/yr	$\$_{saved}$ /module /yr	Lifetime Thermal Savings per module
0.06	8.62E+06	1.577E+07	1.85E+07	4.89E+06	7.70%	73.50%	15.3%	15.00%	1.96%	1/6	301	0.11	$373.45	0.00%	$1.50	$14.94	$229.63
0.04	8.62E+06	1.580E+07	1.85E+07	4.78E+06	7.71%	74.11%	15.3%	15.00%	2.22%	1/6	302	0.11	$376.50	0.82%	$1.52	$15.06	$231.51
0.02	8.62E+06	1.586E+07	1.85E+07	4.72E+06	7.74%	74.46%	15.3%	15.00%	2.15%	1/8	228	0.11	$386.35	3.45%	$1.56	$15.45	$237.56
0.01	8.62E+06	1.590E+07	1.85E+07	4.68E+06	7.76%	74.66%	15.3%	15.00%	2.15%	1/8	230	0.11	$387.23	3.69%	$1.56	$15.49	$238.11

Additional System Sensitivities

Thus far, all annual results have been based on a single system size and economic assumptions. Clearly, not all residential systems will be identical. The primary assumption of this thesis is that the BIPVT will be part of the new construction. Systems will differ in numerous ways: the slope of the collector will vary based on varying roof angles, the number of modules will vary based on available roof space, DHW use will change with differing family size, size of the storage tank. The following sub sections will look into additional system sensitivities on annual performance. The lifetime of the modules is set at 30 years for the determining the USPW multiplier.

Slope of Collector

All previous simulations have been based on a roof angle of 30 degrees. The parameter will be varied from 20 degrees to 40 degrees to analyze the impact on annual performance. All other system parameters will remain the same (flow rate set back to 0.06 GPM/ft2). Table 21 shows the results of the parametric analysis. Notice the change in incident solar radiation which peaks around Phoenix's latitude of 33 degrees. Performance results propagate as a function of the incident solar radiation. One reason for tilting solar thermal collectors beyond local latitude angles is to take advantage of lower winter sun angles. This simulation did not see improvement with higher roof angles.

Size of the Storage Tank

All previous simulations have been based on a storage tank of approximately 120 gallons. The size of the storage tank will be varied from 100 gallons to 200 gallons. By varying the size of the tank, one must decide whether the height or diameter or both will vary. Stratification is of the most interest here, so the diameter remained constant while the height of the tank and of each node increases with capacity. The slope of the collector was set back to 30 degrees. Table 22 shows the results of the storage tank parametric analysis. As the tank capacity increased, the ability for stratification to set up increased as well. Improved performance results propagated as a function of tank size. Notice the improving trend of collector efficiency, solar fraction and savings with increased tank size. Improved stratification lowers the average tank temperature (lowering heat losses) and allows cooler water to be supplied to the collector from the bottom of the tank, thus improving performance.

Number of BIPVT modules

All previous simulations have been based upon a 5kW system, which translated into a total of 25 modules. Previous investigation about residential energy use has suggested that a 5kW PV system is an appropriate starting place for typical domestic energy needs. However, differing architecture may not provide the roof space to accommodate a 5 kW array. The size of the BIPVT system will be varied to test the impact on annual performance. The size of the tank was set back to a typical 120 gallon tank at a height of 1.75 m (~5.5 ft) for all runs.

Table 23 shows the results of the system size parametric analysis. A couple of metrics to notice are the collector efficiency and the solar fraction. While the solar fraction improves with system size (expected), the collector efficiency degrades significantly. The BIPVT system tank is sized for typical DHW use and not necessarily for integration with a solar thermal system. Tank stratification is again responsible for improved collector efficiency at smaller system sizes.

There are a few other metrics to notice in Table 23 that make small BIPVT systems attractive. Moving from left to right across the table, the PV efficiency % improvement is significantly better at the 1 kW size. Also, dollars saved per square foot and per module improve with decreasing system size. The last column in Table 23 is the lifetime thermal savings ($) per module is the annual energy savings per module multiplied by the uniform series present worth (USPW) assuming a discount rate of 5% and a lifetime of 30 years.

Table 21. Parametric Analysis of roof angle on performance.

Roof Angle Parametric Analysis for Phoenix																
Roof Angle (deg)	Incident Solar Radiation (kJ/m^2)	Collector Useful Energy (kJ)	DHW Load (kJ)	Auxiliary Energy (kJ)	Collector Efficiency	Solar Fraction	PV Efficiency (collection)	PV Efficiency (stagnation)	PV Efficiency % improvement	Flow Rate (GPM/ ft2)	PumpEnergy/yr (kWh)	Elec Rate $/kWh	$\$_{saved}$/yr	$\$_{saved}/ft^2$/ yr	$\$_{saved}$ /module /yr	Lifetime Thermal Savings per module
20	8.50E+06	1.54E+07	1.85E+07	5.20E+06	7.63%	71.85%	15.31%	15.00%	2.03%	0.06	300.06	0.11	$427.01	$1.72	$17.08	$262.57
25	8.59E+06	1.56E+07	1.85E+07	5.01E+06	7.66%	72.88%	15.33%	15.00%	2.17%	0.06	300.97	0.11	$433.55	$1.75	$17.34	$266.59
30	8.62E+06	1.58E+07	1.85E+07	4.89E+06	7.70%	73.54%	15.34%	15.00%	2.23%	0.06	301.70	0.11	$437.62	$1.76	$17.50	$269.09
35	8.61E+06	1.58E+07	1.85E+07	4.86E+06	7.71%	73.70%	15.34%	15.00%	2.21%	0.06	301.91	0.11	$437.46	$1.76	$17.50	$268.99
40	8.53E+06	1.57E+07	1.85E+07	4.98E+06	7.72%	73.04%	15.33%	15.00%	2.13%	0.06	302.21	0.11	$434.30	$1.75	$17.37	$267.05

Table 22. Parametric Analysis of tank size on performance.

Tank Size Parametric Analysis for Phoenix																
Tank Size (gallons)	Incident Solar Radiation (kJ/m^2)	Collector Useful Energy (kJ)	DHW Load (kJ)	Auxiliary Energy (kJ)	Collector Efficiency	Solar Fraction	PV Efficiency (collection)	PV Efficiency (stagnation)	PV Efficiency % improvement	Flow Rate (GPM/ ft2)	PumpEnergy/yr (kWh)	Elec Rate $/kWh	$\$_{saved}$/yr (Including pump losses)	$\$_{saved}/ft^2$/ yr	$\$_{saved}$ /module /yr	Lifetime Thermal Savings per module
100	8.62E+06	1.59E+07	1.85E+07	5.45E+06	7.76%	70.48%	15.34%	15.00%	2.23%	0.06	314.41	0.11	$440.49	$1.77	$17.62	$270.85
120	8.62E+06	1.64E+07	1.85E+07	5.08E+06	8.00%	72.47%	15.35%	15.00%	2.31%	0.06	305.65	0.11	$455.92	$1.84	$18.24	$280.34
140	8.62E+06	1.66E+07	1.85E+07	4.85E+06	8.12%	73.75%	15.36%	15.00%	2.36%	0.06	300.68	0.11	$463.82	$1.87	$18.55	$285.20
160	8.62E+06	1.69E+07	1.85E+07	4.76E+06	8.23%	74.24%	15.37%	15.00%	2.40%	0.06	297.38	0.11	$470.70	$1.90	$18.83	$289.43
180	8.62E+06	1.70E+07	1.85E+07	4.71E+06	8.29%	74.47%	15.37%	15.00%	2.42%	0.06	293.49	0.11	$474.51	$1.91	$18.98	$291.77
200	8.62E+06	1.73E+07	1.85E+07	4.75E+06	8.43%	74.28%	15.38%	15.00%	2.47%	0.06	291.35	0.11	$483.56	$1.95	$19.34	$297.34

Table 23. Parametric analysis of system size on performance.

System Size (kW)	No. of Modules	Module Roof Area (ft2)	Incident Solar Radiation (kJ/m^2)	Collector Useful Energy (kJ)	DHW Load (kJ)	Auxiliary Energy (kJ)	Collector Efficiency	Solar Fraction	PV Efficiency (collection)	PV Efficiency (stagnation)	PV Efficiency % improvement	Flow Rate (GPM/ft2)	PumpEnergy /yr (kWh)	Elec Rate $/kWh	$\$_{saved}$/yr	$\$_{saved}/ft^2$ /yr	$\$_{saved}$ /module /yr	Lifetime Thermal Savings per module
System Size Parametric Analysis for Phoenix																		
1	5	49.67	8.62E+06	9.02E+06	1.85E+07	1.10E+07	22.00%	40.40%	15.90%	15.00%	6.00%	0.06	83.20	0.11	$220.01	$4.43	$44.00	$676.43
2	10	99.34	8.62E+06	1.22E+07	1.85E+07	8.13E+06	14.80%	56.00%	15.60%	15.00%	4.00%	0.06	166.40	0.11	$298.56	$3.01	$29.86	$458.96
3	15	149.02	8.62E+06	1.39E+07	1.85E+07	6.50E+06	11.30%	64.80%	15.50%	15.00%	3.33%	0.06	249.60	0.11	$339.21	$2.28	$22.61	$347.63
4	20	198.69	8.62E+06	1.53E+07	1.85E+07	5.63E+06	9.31%	69.50%	15.40%	15.00%	2.67%	0.06	332.80	0.11	$356.64	$1.79	$17.83	$274.12
5	25	248.36	8.62E+06	1.63E+07	1.85E+07	5.06E+06	7.96%	72.60%	15.40%	15.00%	2.67%	0.06	416.00	0.11	$364.91	$1.47	$14.60	$224.38
6	30	298.03	8.62E+06	1.70E+07	1.85E+07	4.60E+06	6.90%	75.10%	15.30%	15.00%	2.00%	0.06	499.20	0.11	$369.81	$1.24	$12.33	$189.50

CHAPTER 6 CONCLUSIONS AND RECOMMENDATIONS

The purpose of this research was to design and build a patentable, modular BIPV/T prototype to assess the following:

- Performance
- Economics
- Constructability
- Operation and Maintenance

Three of the four topics were addressed in this research with favorable results. The Operation and Maintenance of a full scale BIPVT array cannot be commented on at this time. However, with repairs to the two existing prototypes, and an improved absorber design, long term observations of the material integrity, the operation and maintenance of the system could be commented on by another researcher.

The performance of the BIPVT module was best assessed by the TRNSYS simulations. Cities in the southwest desert performed quite well, with solar fractions reaching over 70% for an all PVC BIPV/T module. Using the special CoolPoly thermally conductive polymer properties for the absorber in the TRNSYS model, on average, increased the solar fraction by about 10%. Looking at the typical winter, spring and summer daily system behavior for Phoenix, Az, showed that the collector was circulating water from the same node that it was drawing water from. Thus T_{in} and T_{out} increased in tandem and essentially heated the tank from the bottom up, discouraging tank stratification. This discovery encouraged the need for more simulations using a two-tank system.

The economics were assessed by assuming that the BIPVT modules would be plumbed into an electric water tank with variable inlet positioning. Average statewide electric rates were used to get a ball park figure for annual dollars saved. A more extensive analysis of summer demand and tier rates might reveal further savings and incentives. This research didn't looking into the possibility of state rebates for a BIPVT system, but there may be additional opportunities for savings there.

The constructability of a low-cost building-integrated photovoltaic module was completed. The prototype design is by no means ready to go to mass production, but does provide a nice place to start. Just like with any product development, prototypes go through design changes as the research realize what does and doesn't work. Spending money on an extrudable absorber would be well worth it to guarantee a more robust prototype that can be subjected to higher water pressures and better flow control.

RECOMMENDATIONS

All of the simulation results were verified by an extremely small and unreliable amount of data. The author is keenly aware of the need for more testing and a better calibrated model, including a detailed error analysis. Unfortunately, weather and timing prevented this study from achieving better results. The experience has a left the author with a feeling of unfinished business and would like to make some suggestions for future work.

FUTURE WORK

First and foremost, confidence must be restored in the integrity of the prototypes. Throughout the entire experiment, a feeling of paranoia and fear of breaking the costly prototypes lingered in the air. It is my recommendation that a PVC absorber be extruded and sent to Colorado Plastics to be installed in the prototypes. If money is available for extrusion, consider using circular channels versus square channels, and perform a cost-benefit analysis on tooling expense versus improved convective heat transfer coefficient. There is still much room for improvement on the module to module connection. This study chose to use a union because of the reliability and ease of use. The pending patent is most concerned that the PV module frame serve as the fluid conduit, but perhaps the module to module integration concept is also patentable.

As mentioned above, this study is clearly unfinished. The first thing that needs to be address before more testing is performed is to fix the leaks that currently exist in the plumbing system. There are a couple joint leaks where water got caught and froze, and is causing a leak. With confidence restored in the prototypes and the plumbing system back in action, more testing can begin. The best time of year for testing is going to be in the summer where the temperature rise across the modules is well outside the range of error of the thermocouples. With non-freezing temperatures, the system can simply run 24 hours a day, and will be able to track a wide range of entering and leaving fluid temperatures and environmental conditions. More data will provide better insight in calibration techniques, and may inspire the rewriting of the TRNSYS source code to better match the BIPVT absorber physical character.

PV efficiency during heat collection and stagnation needs to be compared to verify the TRNSYS model, along with a parametric analysis of changing flow rates for optimized performance. This is easily doable when the system is back up and running.

Finally, simulations should be run for all above cities using a two tank system. The diverter should send the city water into the buffer tank, which is plumbed into the collectors, as well as to the tee piece for load use. The circulator pump should pull from the bottom of the buffer tank and return to the top, promoting tank stratification. The second tank (the hot water tank) will have an auxiliary heating element to meet the thermostat set point, along with variable inlet positions from the buffer tank. This setup will most likely improve the thermal and electrical efficiencies of the BIPVT due to the larger temperature gradient and lower PV cell temperatures. However, a two-tank system certainly increases the startup cost and takes up valuable living space.

Works Cited

TRNSYS Documentation. (2009). Retrieved from TRNSYS Documentation.

Solar Energy Scene. (2010). Retrieved from Solar Energy Scene: http://www.solar-energy-scene.com/how-do-solar-panels-work.html

DUN-SOLAR TPE BACKSHEETS. (2011). Retrieved from DUN-SOLAR: http://www.dunmore.com/products/tedlar-pv-backsheet.html

Echo Solar Systems. (2011). Retrieved from Echo Solar Systems: http://echofirst.com/datasheets.php

Google SketchUp Match Photo. (2011). Retrieved from Google: http://support.google.com/sketchup/bin/answer.py?hl=en&answer=94919

MillenniumSolar. (2011). Retrieved from MillenniumSolar: http://www.millenniumsolar.com/default.asp?catid={FF7A51A4-4AF9-410D-A2B0-860E9D4F6D2F}

PVTWINS. (2011). Retrieved from PVTWINS: http://www.pvtwins.nl/main01.html

RA-cell. (2011). Retrieved from RA-cell: http://racell.com/

SolarDuct Modular Rooftop Solar Air Heating. (2011). Retrieved from SolarWall: http://solarwall.com/en/products/solarwall-air-heating/solarduct.php

Butler, J. (2011, May). Master Fabricator. (G. Estep, Interviewer)

Charalambous, P., G.G., M., Kalogirou, S., & Yiakoumetti, K. (2007). Photovoltaic thermal (PV/T) collectors: A review. *Applied Thermal Engineering*, 276-285.

Corbin, C., Voboril, D., & Wilson, B. (2008). Presentation (Power Point file). *Building Integrated Solar PV/Thermal Market Assessment*. Boulder, CO, USA.

Duffie, J. A., & Beckman, W. A. (2006). *Solar Engineering of Thermal Processes 3rd edition.* Hoboken, New Jersey: John Wiley & Sons.

Kreith, F., & Bohn, M. S. (2001). *Principles in Heat Transfer, 6th edition.* Pacific Grove, CA: Brooks/Cole.

Lee, B., Liu, L., Sun, B., Shen, C., & Dai, G. (2008). Thermally conductive and electrically insulating EVA composite encapsulants for solar photovoltaic (PV). *eXPRESS Polymer Letters*, 357-363.

Lilliestierna, N., & Zdrowski, J. (2010). *Building-Integrated Photovoltaic/Thermal Collector Panel Design.* Boulder, Co: n/a.

McQuiston, F. C., Parker, J. D., & Spitler, J. D. (2005). *Heating, Ventilating, and Air Conditioning: Analysis and Design, 6th edition.* Hoboken, NJ: Wiley & Sons.

SolarWall. (2012, January). *Solarwall.com*. Retrieved from solarwall.com: http://solarwall.com/en/products/solarwall-pvt/solarduct-pvt.php

Taylor, J. R. (1997). *An Introduction to Error Analysis: The study of Uncertainties in physical measurements.* Sausalito, CA: University Science Books.

APPENDIX A PROVISIONAL PATENT

DORSEY™
DORSEY & WHITNEY LLP

BRAD J. HATTENBACH
Direct: (303) 628-1512
hattenbach.brad@dorsey.com

21 May 2010

VIA ELECTRONIC MAIL

Tara Dressler
Patent Administrator
University of Colorado
4740 Walnut Street, Suite 100
Campus Box 588
Boulder, CO 80309

FOR YOUR INFORMATION

Re: U.S. Provisional Patent Application No. 61/330,941
Title: LOW-COST, MODULAR MOUNTING SYSTEM FOR BUILDING-INTEGRATED PHOTOVOLTAIC-THERMAL COLLECTOR
Filing Date: 5 May 2010
Your Ref.: CU2225B
Our Ref.: 487031-19; P216206.US.01

Dear Tara:

Enclosed please find a copy of the above-referenced provisional patent application as filed with the United States Patent and Trademark Office (USPTO). We will let you know as soon as we receive the official filing receipt, confirming the filing date and the application number assigned to this application by the USPTO.

Any devices manufactured or sold under the patent application may now be marked with the legend "Patent Applied For" or "Patent Pending" or an abbreviation thereof. If possible, you should not disclose the filing date of your patent application.

A provisional patent application is not examined except for formal requirements. Thus, no patent ever issues based solely upon the filing of a provisional application. The application is considered an interim filing procedure that establishes a priority filing date. The provisional application becomes abandoned after one year and is not renewable.

Further Filing Required

If you desire an issued patent, we must file a formal, nonprovisional application, and any desired foreign applications, by **4 MAY 2011**. A nonprovisional application filed within one year of the provisional filing date may claim the provisional filing date as a priority date. When making your decision about pursuing an issued patent, please keep in mind the statutory bars to obtaining patent protection in the United States and other countries. Under 35 U.S.C. § 102(b),

DORSEY & WHITNEY LLP • WWW.DORSEY.COM • T 303.629.3400 • F 303.629.3450
REPUBLIC PLAZA BUILDING • SUITE 4700 • 370 SEVENTEENTH STREET • DENVER, CO 80202-5647
USA CANADA EUROPE ASIA-PACIFIC

4810-5731-9942\1

inventors in the United States have a one-year grace period from the first public disclosure, public use, offer for sale, or sale of their invention to file an application for patent protection. If more than one year passes after the occurrence of any of these triggering events and before an application is filed, an inventor is barred from obtaining patent protection for the invention in the United States. In most other countries there is no grace period and thus any public disclosure, public use, offer for sale, or sale of the invention before the filing of a priority patent application will bar the grant of a patent in those countries. Thus, if you have either publicly disclosed your invention or offered it for sale or intend to within the next year, we strongly recommend that you preserve your right to claim the benefit of the provisional filing date.

Duty of Disclosure

Please keep in mind that applicants and their representatives have a duty of disclosure to the USPTO. Thus, if you are or become aware of any references (e.g., patents, books, and other publicly available information), prior public disclosures, or prior sales or offers for sale of the invention that a patent examiner may consider material to patentability, we must disclose that information to the USPTO within three months of filing a nonprovisional patent application (if previously known). Please let us know as soon as possible if you are aware of any references at this time that should be disclosed to the USPTO when a nonprovisional application is ultimately filed. We will place the references in our files now to ensure that they are appropriately disclosed. Please note that this duty is continuing. Thus, if you become aware of any relevant prior art reference during the pendency of this application or a subsequent nonprovisional application, please advise us immediately and provide a copy of the reference. In general, once a nonprovisional application is filed, we have three months within which to make the required disclosures after a material reference becomes known to us.

Conclusion

If you have any questions on any of the foregoing, please let us know.

Sincerely,

Brad J. Hattenbach

BJH/MJ/pge
Enclosure (Application)

cc: Kate Tallman

Electronic Acknowledgement Receipt

EFS ID:	7543806
Application Number:	61330941
International Application Number:	
Confirmation Number:	5185
Title of Invention:	Low-Cost, Modular Mounting System for Building-Integrated Photovoltaic-Thermal Collector
First Named Inventor/Applicant Name:	Charles Corbin
Customer Number:	20686
Filer:	Brad Hattenbach/Marilyn Johnson
Filer Authorized By:	Brad Hattenbach
Attorney Docket Number:	P216206.US.01
Receipt Date:	04-MAY-2010
Filing Date:	
Time Stamp:	10:55:41
Application Type:	Provisional

Payment information:

Submitted with Payment	yes
Payment Type	Deposit Account
Payment was successfully received in RAM	$110
RAM confirmation Number	14035
Deposit Account	041415
Authorized User	

The Director of the USPTO is hereby authorized to charge indicated fees and credit any overpayment as follows:

Charge any Additional Fees required under 37 C.F.R. Section 1.16 (National application filing, search, and examination fees)

Charge any Additional Fees required under 37 C.F.R. Section 1.17 (Patent application and reexamination processing fees)

Charge any Additional Fees required under 37 C.F.R. Section 1.21 (Miscellaneous fees and charges)

File Listing:

Document Number	Document Description	File Name	File Size(Bytes)/ Message Digest	Multi Part /.zip	Pages (if appl.)
1	Provisional Cover Sheet (SB16)	Cover_Sheet_pp2.pdf	97182 [illegible]	no	2
Warnings:					
This is not a USPTO supplied Provisional Cover Sheet SB16 form.					
Information:					
2	Application Data Sheet	ADS_pp4.pdf	198407 [illegible]	no	4
Warnings:					
Information:					
This is not an USPTO supplied ADS fillable form					
3	Specification	Specification_pp4.pdf	153628 [illegible]	no	4
Warnings:					
Information:					
4	Drawings-only black and white line drawings	Drawings_pp2.pdf	56591 [illegible]	no	2
Warnings:					
Information:					
5	Fee Worksheet (PTO-875)	fee-info.pdf	29298 [illegible]	no	2
Warnings:					
Information:					
		Total Files Size (in bytes):	535106		

This Acknowledgement Receipt evidences receipt on the noted date by the USPTO of the indicated documents, characterized by the applicant, and including page counts, where applicable. It serves as evidence of receipt similar to a Post Card, as described in MPEP 503.

New Applications Under 35 U.S.C. 111
If a new application is being filed and the application includes the necessary components for a filing date (see 37 CFR 1.53(b)-(d) and MPEP 506), a Filing Receipt (37 CFR 1.54) will be issued in due course and the date shown on this Acknowledgement Receipt will establish the filing date of the application.

National Stage of an International Application under 35 U.S.C. 371
If a timely submission to enter the national stage of an international application is compliant with the conditions of 35 U.S.C. 371 and other applicable requirements a Form PCT/DO/EO/903 indicating acceptance of the application as a national stage submission under 35 U.S.C. 371 will be issued in addition to the Filing Receipt, in due course.

New International Application Filed with the USPTO as a Receiving Office
If a new international application is being filed and the international application includes the necessary components for an international filing date (see PCT Article 11 and MPEP 1810), a Notification of the International Application Number and of the International Filing Date (Form PCT/RO/105) will be issued in due course, subject to prescriptions concerning national security, and the date shown on this Acknowledgement Receipt will establish the international filing date of the application.

Document Description: Provisional Cover Sheet (SB16)

PTO/SB/16 (11-08)
Approved for use through 06/30/2010 OMB 0651-0032
U.S. Patent and Trademark Office: U.S. DEPARTMENT OF COMMERCE
Under the Paperwork Reduction Act of 1995, no persons are required to respond to a collection of information unless it displays a valid OMB control number

Provisional Application for Patent Cover Sheet

This is a request for filing a PROVISIONAL APPLICATION FOR PATENT under 37 CFR 1.53(c)

Inventor(s)

Inventor 1 Remove

Given Name	Middle Name	Family Name	City	State	Country i
Charles		Corbin	Boulder	CO	US

Inventor 2 Remove

Given Name	Middle Name	Family Name	City	State	Country i
Michael		Brandemuehl	Niwot	CO	US

Inventor 3 Remove

Given Name	Middle Name	Family Name	City	State	Country i
Zhiqiang		Zhai	Longmont	CO	US

All Inventors Must Be Listed – Additional Inventor Information blocks may be generated within this form by selecting the **Add** button. Add

Title of Invention	Low-Cost, Modular Mounting System for Building-Integrated Photovoltaic-Thermal Collector
Attorney Docket Number (if applicable)	P216206.US.01

Correspondence Address

Direct all correspondence to (select one):

⦿ The address corresponding to Customer Number	○ Firm or Individual Name
Customer Number	20686

The invention was made by an agency of the United States Government or under a contract with an agency of the United States Government.

⦿ No.

○ Yes, the name of the U.S. Government agency and the Government contract number are:

Document Description: Provisional Cover Sheet (SB16)

PTO/SB/16 (11-08)
Approved for use through 06/30/2010 OMB 0651-0032
U.S. Patent and Trademark Office: U.S. DEPARTMENT OF COMMERCE
Under the Paperwork Reduction Act of 1995, no persons are required to respond to a collection of information unless it displays a valid OMB control number

Entity Status

Applicant claims small entity status under 37 CFR 1.27

◉ Yes, applicant qualifies for small entity status under 37 CFR 1.27

○ No

Warning

Petitioner/applicant is cautioned to avoid submitting personal information in documents filed in a patent application that may contribute to identity theft. Personal information such as social security numbers, bank account numbers, or credit card numbers (other than a check or credit card authorization form PTO-2038 submitted for payment purposes) is never required by the USPTO to support a petition or an application. If this type of personal information is included in documents submitted to the USPTO, petitioners/applicants should consider redacting such personal information from the documents before submitting them to USPTO. Petitioner/applicant is advised that the record of a patent application is available to the public after publication of the application (unless a non-publication request in compliance with 37 CFR 1.213(a) is made in the application) or issuance of a patent. Furthermore, the record from an abandoned application may also be available to the public if the application is referenced in a published application or an issued patent (see 37 CFR1.14). Checks and credit card authorization forms PTO-2038 submitted for payment purposes are not retained in the application file and therefore are not publicly available.

Signature

Please see 37 CFR 1.4(d) for the form of the signature.

Signature	Brad J Hattenbach			Date (YYYY-MM-DD)	2010-05-04
First Name	Brad J.	Last Name	Hattenbach	Registration Number (If appropriate)	42642

This collection of information is required by 37 CFR 1.51. The information is required to obtain or retain a benefit by the public which is to file (and by the USPTO to process) an application. Confidentiality is governed by 35 U.S.C. 122 and 37 CFR 1.11 and 1.14. This collection is estimated to take 8 hours to complete, including gathering, preparing, and submitting the completed application form to the USPTO. Time will vary depending upon the individual case. Any comments on the amount of time you require to complete this form and/or suggestions for reducing this burden, should be sent to the Chief Information Officer, U.S. Patent and Trademark Office, U.S. Department of Commerce, P.O. Box 1450, Alexandria, VA 22313-1450. DO NOT SEND FEES OR COMPLETED FORMS TO THIS ADDRESS. **This form can only be used when in conjunction with EFS-Web. If this form is mailed to the USPTO, it may cause delays in handling the provisional application.**

PTO/SB/14 (11-08)
Approved for use through 06/30/2010. OMB 0651-0032
U.S. Patent and Trademark Office; U.S. DEPARTMENT OF COMMERCE
Under the Paperwork Reduction Act of 1995, no persons are required to respond to a collection of information unless it contains a valid OMB control number.

Application Data Sheet 37 CFR 1.76	Attorney Docket Number	P216206.US.01
	Application Number	
Title of Invention	Low-Cost, Modular Mounting System for Building-Integrated Photovoltaic-Thermal Collector	

The application data sheet is part of the provisional or nonprovisional application for which it is being submitted. The following form contains the bibliographic data arranged in a format specified by the United States Patent and Trademark Office as outlined in 37 CFR 1.76.
This document may be completed electronically and submitted to the Office in electronic format using the Electronic Filing System (EFS) or the document may be printed and included in a paper filed application.

Secrecy Order 37 CFR 5.2

☐ Portions or all of the application associated with this Application Data Sheet may fall under a Secrecy Order pursuant to 37 CFR 5.2 (Paper filers only. Applications that fall under Secrecy Order may not be filed electronically.)

Applicant Information:

Applicant 1

Applicant Authority	⦿ Inventor	◯ Legal Representative under 35 U.S.C. 117	◯ Party of Interest under 35 U.S.C. 118	
Prefix	**Given Name**	**Middle Name**	**Family Name**	**Suffix**
	Charles		Corbin	
Residence Information (Select One)	⦿ US Residency	◯ Non US Residency	◯ Active US Military Service	
City	Boulder	**State/Province** CO	**Country of Residence**	US
Citizenship under 37 CFR 1.41(b)	US			
Mailing Address of Applicant:				
Address 1	623 Hartford Drive			
Address 2				
City	Boulder	**State/Province**	CO	
Postal Code	80305	**Country**	US	

Applicant 2

Applicant Authority	⦿ Inventor	◯ Legal Representative under 35 U.S.C. 117	◯ Party of Interest under 35 U.S.C. 118	
Prefix	**Given Name**	**Middle Name**	**Family Name**	**Suffix**
	Michael		Brandemuehl	
Residence Information (Select One)	⦿ US Residency	◯ Non US Residency	◯ Active US Military Service	
City	Niwot	**State/Province** CO	**Country of Residence**	US
Citizenship under 37 CFR 1.41(b)	US			
Mailing Address of Applicant:				
Address 1	6664 Bird Cliff Way			
Address 2				
City	Niwot	**State/Province**	CO	
Postal Code	80503	**Country**	US	

Applicant 3

Applicant Authority	⦿ Inventor	◯ Legal Representative under 35 U.S.C. 117	◯ Party of Interest under 35 U.S.C. 118	
Prefix	**Given Name**	**Middle Name**	**Family Name**	**Suffix**
	Zhiqiang		Zhai	
Residence Information (Select One)	⦿ US Residency	◯ Non US Residency	◯ Active US Military Service	
City	Longmont	**State/Province** CO	**Country of Residence**	US

Application Data Sheet 37 CFR 1.76	Attorney Docket Number	P216206.US.01
	Application Number	
Title of Invention	Low-Cost, Modular Mounting System for Building-Integrated Photovoltaic-Thermal Collector	

Citizenship under 37 CFR 1.41(b)	CN		
Mailing Address of Applicant:			
Address 1	1554 Turin Drive		
Address 2			
City	Longmont	**State/Province**	CO
Postal Code	80503	**Country**	US

All Inventors Must Be Listed - Additional Inventor Information blocks may be generated within this form by selecting the **Add** button.

Correspondence Information:

Enter either Customer Number or complete the Correspondence Information section below. For further information see 37 CFR 1.33(a).

☐ **An Address is being provided for the correspondence Information of this application.**

Customer Number	20686
Email Address	docketing-dv@dorsey.com

Application Information:

Title of the Invention	Low-Cost, Modular Mounting System for Building-Integrated Photovoltaic-Thermal Collector		
Attorney Docket Number	P216206.US.01	**Small Entity Status Claimed**	☒
Application Type	Provisional		
Subject Matter	Utility		
Suggested Class (if any)		**Sub Class (if any)**	
Suggested Technology Center (if any)			
Total Number of Drawing Sheets (if any)	2	**Suggested Figure for Publication (if any)**	

Publication Information:

☐ Request Early Publication (Fee required at time of Request 37 CFR 1.219)

☐ **Request Not to Publish.** I hereby request that the attached application not be published under 35 U.S. C. 122(b) and certify that the invention disclosed in the attached application **has not and will not** be the subject of an application filed in another country, or under a multilateral international agreement, that requires publication at eighteen months after filing.

Representative Information:

Representative information should be provided for all practitioners having a power of attorney in the application. Providing this information in the Application Data Sheet does not constitute a power of attorney in the application (see 37 CFR 1.32).
Enter either Customer Number or complete the Representative Name section below. If both sections are completed the Customer Number will be used for the Representative Information during processing.

Please Select One:	◉ Customer Number	○ US Patent Practitioner	○ Limited Recognition (37 CFR 11.9)

Application Data Sheet 37 CFR 1.76	Attorney Docket Number	P216206.US.01
	Application Number	

Title of Invention	Low-Cost, Modular Mounting System for Building-Integrated Photovoltaic-Thermal Collector

Customer Number	20686

Domestic Benefit/National Stage Information:

This section allows for the applicant to either claim benefit under 35 U.S.C. 119(e), 120, 121, or 365(c) or indicate National Stage entry from a PCT application. Providing this information in the application data sheet constitutes the specific reference required by 35 U.S.C. 119(e) or 120, and 37 CFR 1.78(a)(2) or CFR 1.78(a)(4), and need not otherwise be made part of the specification.

Prior Application Status		Remove	
Application Number	Continuity Type	Prior Application Number	Filing Date (YYYY-MM-DD)

Additional Domestic Benefit/National Stage Data may be generated within this form by selecting the **Add** button.

Foreign Priority Information:

This section allows for the applicant to claim benefit of foreign priority and to identify any prior foreign application for which priority is not claimed. Providing this information in the application data sheet constitutes the claim for priority as required by 35 U.S.C. 119(b) and 37 CFR 1.55(a).

Remove

Application Number	Country i	Parent Filing Date (YYYY-MM-DD)	Priority Claimed
			⦿ Yes ◯ No

Additional Foreign Priority Data may be generated within this form by selecting the **Add** button.

Assignee Information:

Providing this information in the application data sheet does not substitute for compliance with any requirement of part 3 of Title 37 of the CFR to have an assignment recorded in the Office.

Assignee 1

If the Assignee is an Organization check here. ☐

Prefix	**Given Name**	Middle Name	**Family Name**	Suffix

Mailing Address Information:

Address 1			
Address 2			
City		**State/Province**	
Country i		Postal Code	
Phone Number		Fax Number	
Email Address			

Additional Assignee Data may be generated within this form by selecting the **Add** button.

Signature:

A signature of the applicant or representative is required in accordance with 37 CFR 1.33 and 10.18. Please see 37

Application Data Sheet 37 CFR 1.76	Attorney Docket Number	P216206.US.01
	Application Number	
Title of Invention	Low-Cost, Modular Mounting System for Building-Integrated Photovoltaic-Thermal Collector	

Signature	Brad J. Hattenbach			Date (YYYY-MM-DD)	2010-05-04
First Name	Brad J.	Last Name	Hattenbach	Registration Number	42642

CU2225B – Low-cost, Modular Mounting System for Building-integrated Photovoltaic-Thermal Collector

Abstract

Abstract

The invention is a solar module frame that serves as a low-profile façade mounting system and conduit through which a heat conducting fluid can be passed. The novel aspect of this invention is the use of the module frame as a pipe and integrated mounting system. The frame allows standard photovoltaic laminates to be converted into photovoltaic-thermal collectors. Photovoltaic-thermal collectors are capable of producing both electricity and heated fluid using sunlight. The frame consists of a thermal absorber bonded to a photovoltaic laminate and two extrusions, which can be cut to accommodate any new or existing laminate. Two inter-module fittings installed in the extrusions allow the modules to self-plumb when installed on a building surface without the need for plumbing tools. The interlocking design of the extrusions simplifies installation and results in a uniform collector surface. No additional mounting system is required. Weather resistant gaskets in the frame allow an array of collectors to serve as façade elements, replacing traditional shingles or siding. Alternatively, the frame can be used with clear glass instead of photovoltaic laminates, yielding a low-profile façade integrated solar thermal collector.

Description of the Drawings

Figure 1 shows a section cut through a single collector. The section cut is perpendicular to fluid flow through the supply and return headers.

Figure 2 shows a section cut through two adjacent collectors. The section cut is perpendicular to fluid flow through the supply and return headers.

Figure 3 shows a section cut through two adjacent collectors. The section cut is parallel to fluid flow through the supply and return headers. Both male and female self-plumbing fittings are shown.

Figure 4 shows an isometric view of a single collector. The male version of the self-plumbing fitting is shown.

Figure 5 shows an isometric view of a single collector. The female version of the self-plumbing fitting is shown.

Background

Building integrated photovoltaic-thermal systems (BIPV/T) currently require a high level of skill to install. There is a need for modular mounting systems that can be installed on roofs without specialized training. A challenge in designing such a modular mounting system is to accommodate separate channels for the hot fluid used in the solar thermal component. The fluid channels must be separate from the channels for electricity in the photovoltaic component. Another challenge is to design a building integrated mounting system, meaning that the panels lie flat on the roof, attached directly to the roof, and replace existing roofing or siding materials. This invention overcomes these challenges with a design composed of structural elements that also serve as fluid channels. Modularity is another goal of the design. These structural fluid channels on two adjacent mounting systems are designed to join, which allow for straightforward installation of building integrated photovoltaic-solar thermal systems.

Description of the Invention

The invention is a solar collector frame capable of carrying hot fluid, either water or air, that serves as a structural element and as a façade mounting system. The novel aspect of this invention is the use of the module frame as a pipe and mounting system through which the hot fluid is conveyed. The frame will allow low-cost solar arrays to be manufactured and installed on buildings that are capable of producing electricity, hot water, or hot air. Cost savings are realized through the use of polymers, the elimination of separate mounting systems, the elimination of separate framing and fluid conveying elements, and the elimination of roofing or siding materials beneath the collector surface.

The invention consists of two frame extrusions, an absorber plate, and two plumbing fittings. Extrusion profiles are shown in Figure 1, parts #1 and #2. Both parts consist of upper flanges and lower tabs connected to a rectangular tube. The upper flange of part #1 is offset to allow it to slide beneath the upper flange of part #2. A gasket, part #5, creates a weather resistant barrier when two collectors are installed adjacent to one another. Part #4 is a fluid-conducting absorber plate bonded to parts #1 and #2. This absorber allows a fluid, either water or air, to pass between parts #1 and #2 and be heated by sunlight striking and/or passing through part #3. Note that an assembled collector has two each of #1 and #2 parts. Only one each carries the heated fluid.

When installed, fluid would be forced into part #1 in a direction perpendicular to the page, through part #4 into part #2 in a direction parallel to the page, and exit part #2 to the next collector in the array installed in series. Part #3 is an off-the-shelf photovoltaic laminate or clear low-iron glass, bonded to the assembled frame and absorber. Part #6 is a roofing fastener used to attach the collector to the building façade.

Figure 2 illustrates how the flanges of parts #1 and #2 on two adjacent collectors overlap when installed in parallel on a building façade. Parallel installation means that no fluid is transferred between the collectors. Note that the bottom tabs do not overlap in the same way. Instead, the tabs are offset to prevent them from interfering with the adjacent panel. When viewed from an isometric angle, as illustrated in Figure 4 and Figure 5, the tabs geometry can be clearly seen. Tabs would be cut from the profiles following their extrusion, prior to being assembled into a finished collector.

Figure 3 illustrates the self-pluming connection between two adjacent collectors installed in series. The section plane is perpendicular to that of Figure 1 and Figure 2. Parts #7 and #8 are molded from a heat-tolerant semi-rigid rubber such as EPDM and bonded to the ends of parts #1 and #2 during collector assembly. During installation, part #7 of one collector is inserted into part #8 of another collector in series, forming a watertight seal. Part #8 is slightly smaller, tapered, and more flexible than part #7, allowing it to better conform to part #7. Note that an assembled collector has two each of #7 and #8 parts.

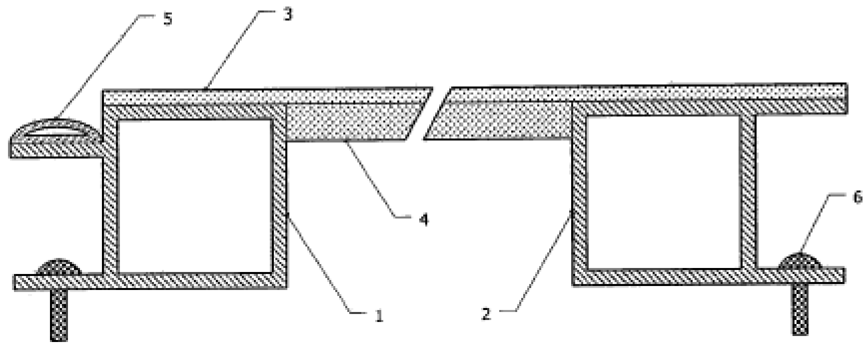

FIGURE 1

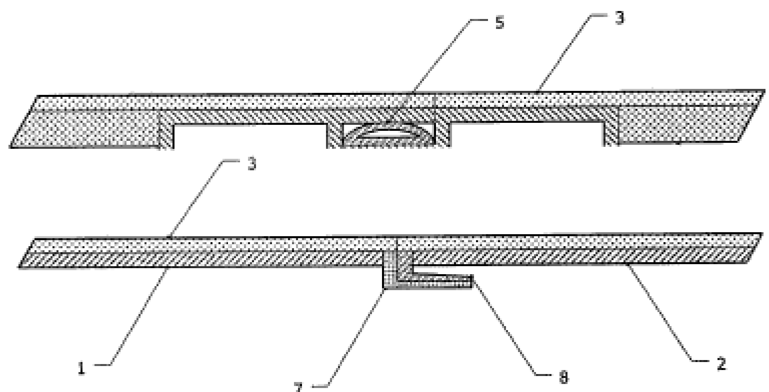

FIGURE 2

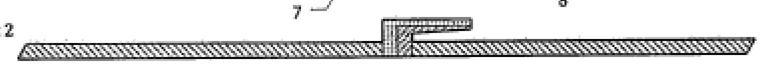

FIGURE 3

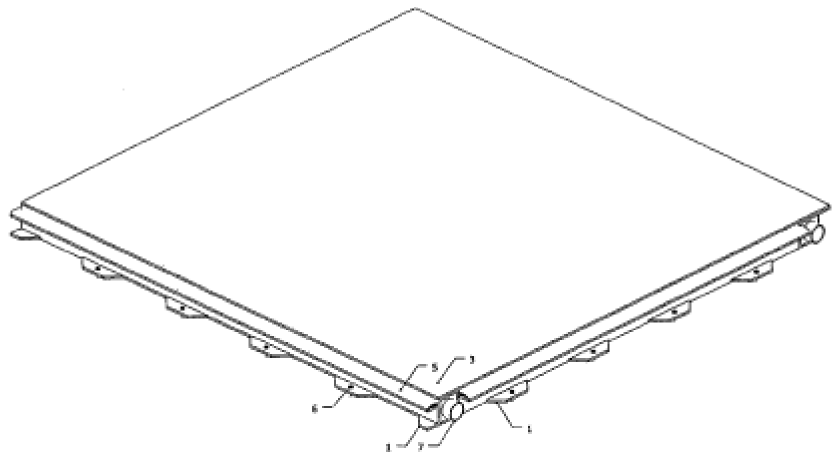

FIGURE 5

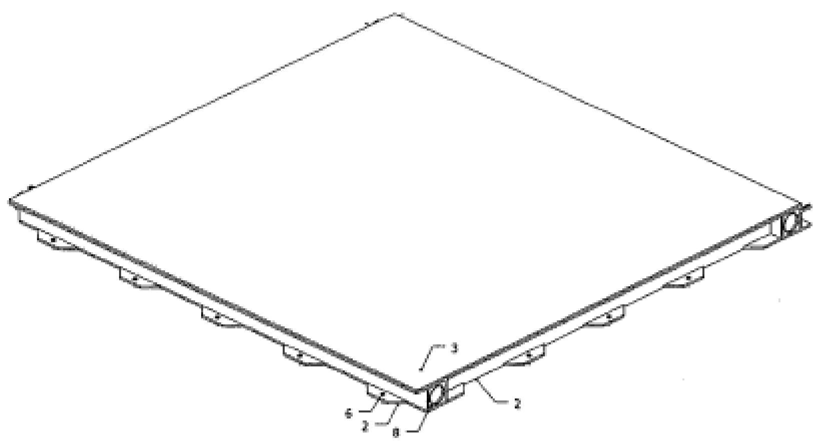

FIGURE 4

APPENDIX B PROTOTYPE FABRICATION DRAWINGS

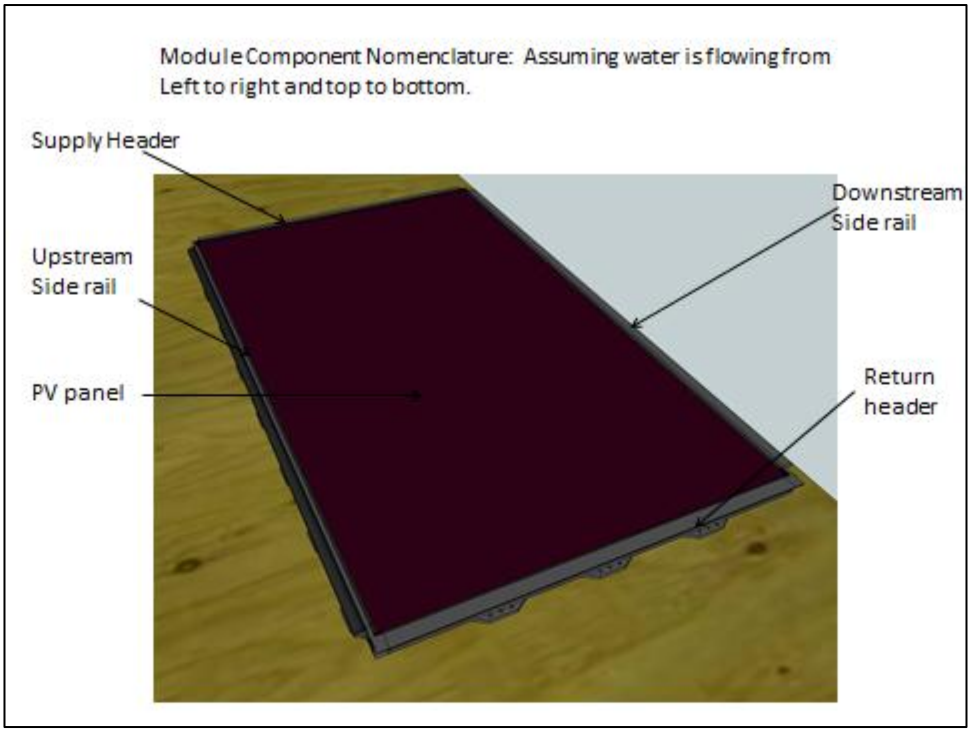

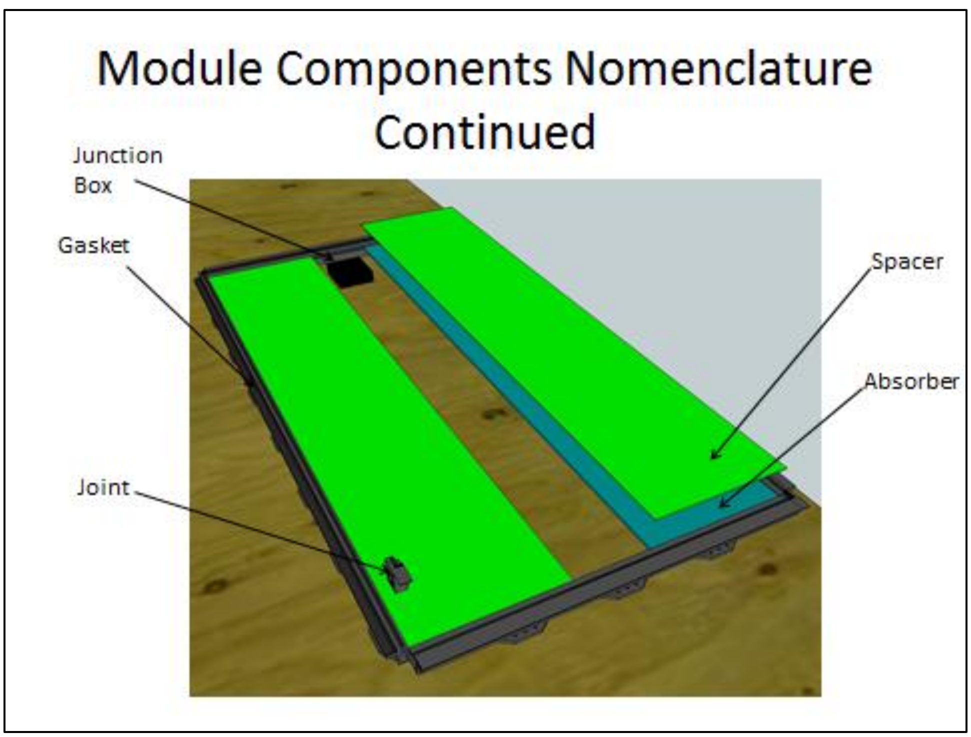

Supply Header Dimensions: Profile

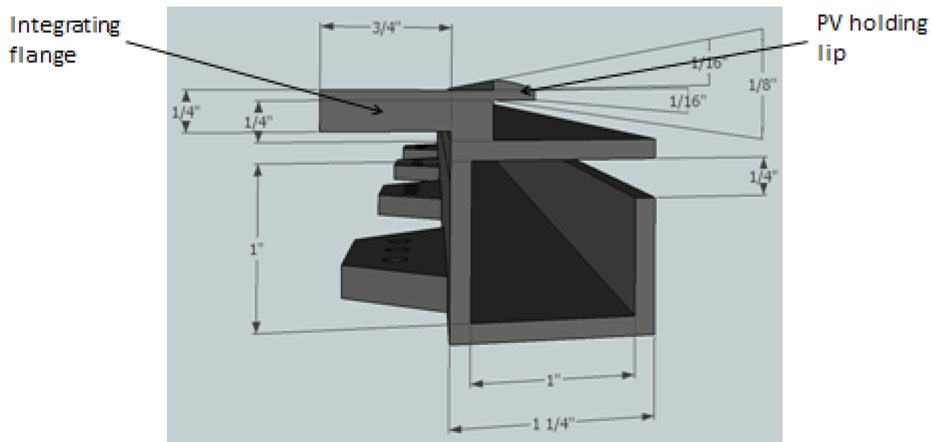

All PVC thickness to be 1/8” unless specified otherwise. Thickness of integrating flange neck Is ¼”. PV holding lip to be rounded (beveled?) from 1/16” to 1/8”.

Supply Header Dimensions: Elevation view.

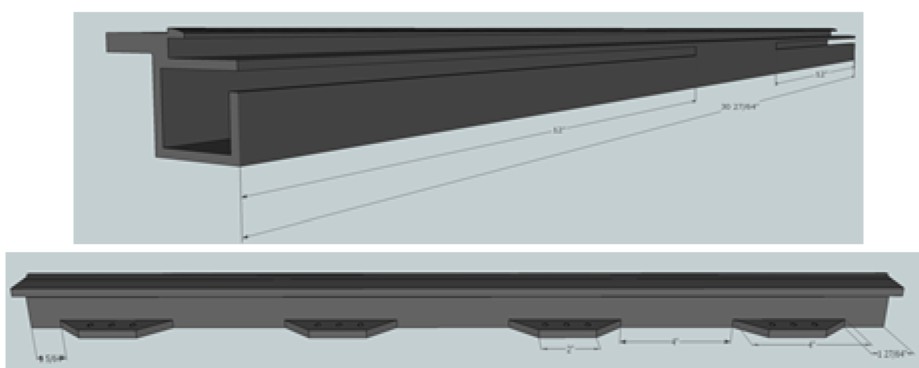

The mounting flanges are to be centered along the header, 4” apart. Each mounting flange is ¼” thick. The return header has three mounting flanges that will consume the space Between these flanges. The length of each header is 30.5”, not sure why it got dimensioned Slightly off!

Mounting Flange Detail

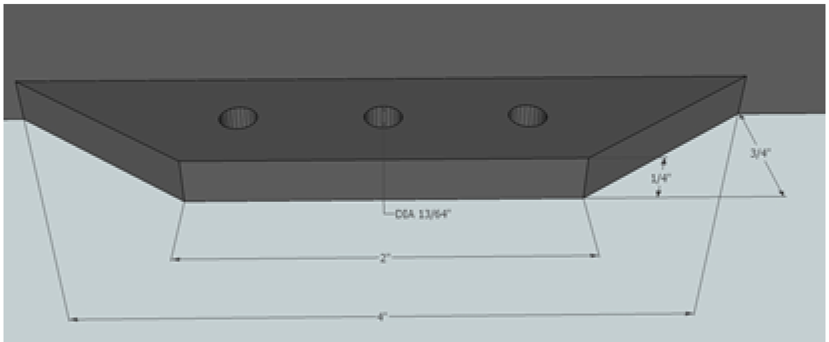

All mounting flanges on headers and side rails are the same. The center screw hole is Centered, and the flanking screw holes are ¾" on center from center hole. Diameter Is about 0.2", to accommodate a #10 wood screw at a 72 degree angle.

Return Header

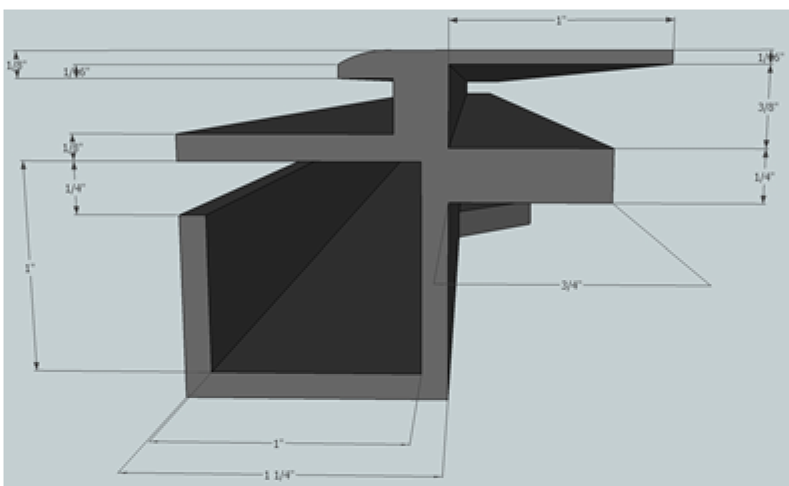

PV holding lip is beveled from 1/16" to 1/8". Upper integrating flange is 1/16" thick.

Return Header: Elevation view

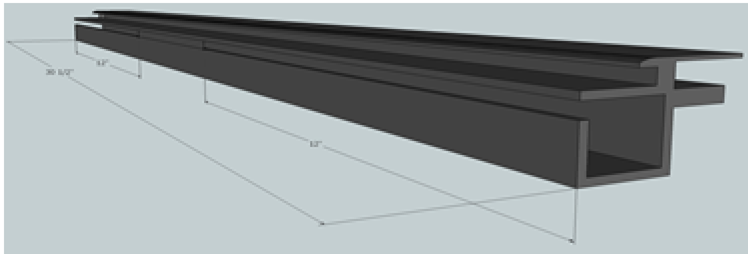

Mounting flangesspaced so as not to interfere with supply header mounting flanges when Placed next to each other.

Upstream Side Rail (left-hand side): Profile view

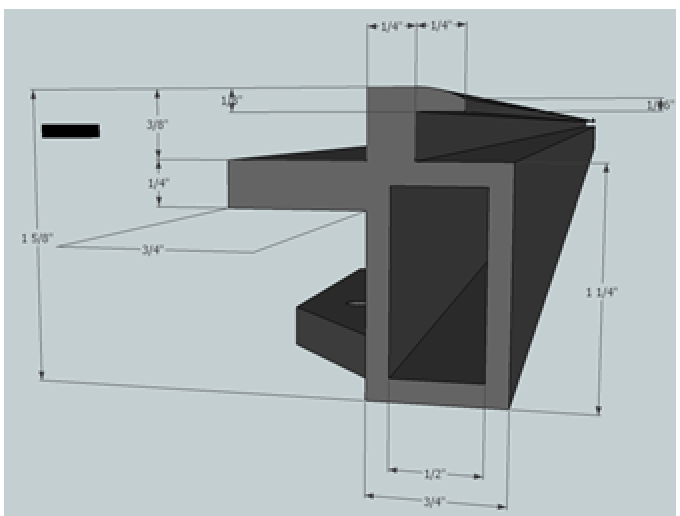

Upstream Side Rail: Elevation view.

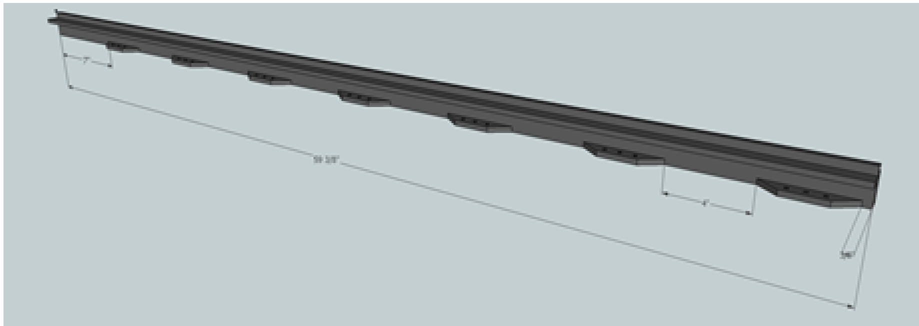

Downstream Side Rail (right-hand side): Profile view

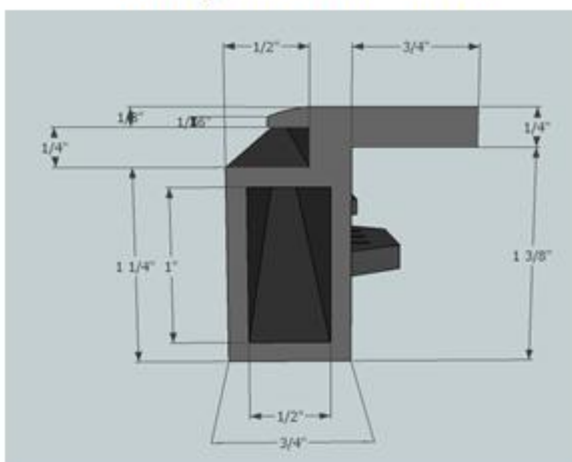

Downstream Side Rail: Elevation view

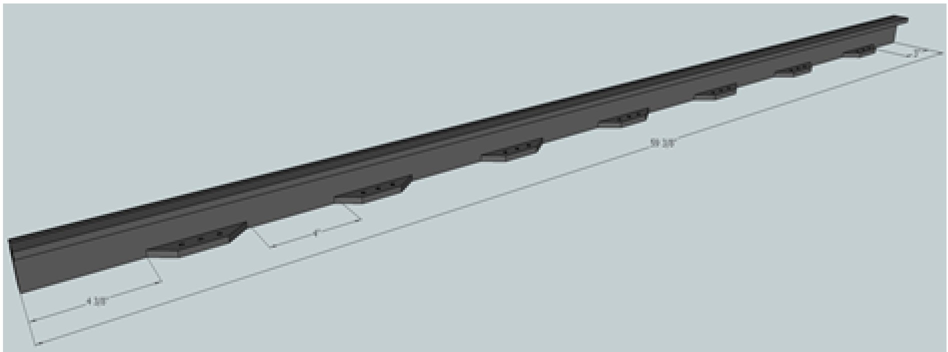

The Absorber

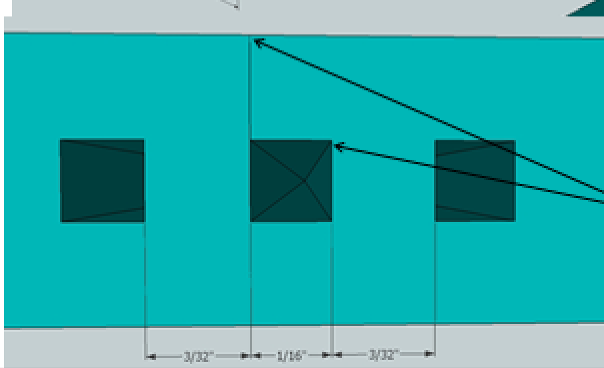

Channels are square: all sides 1/16". The distance from the Edge of channel to edge of Absorber is 3/32".
Each of absorber is to be Pushed against the inside Corners of the headers and Side rails.

The Spacers

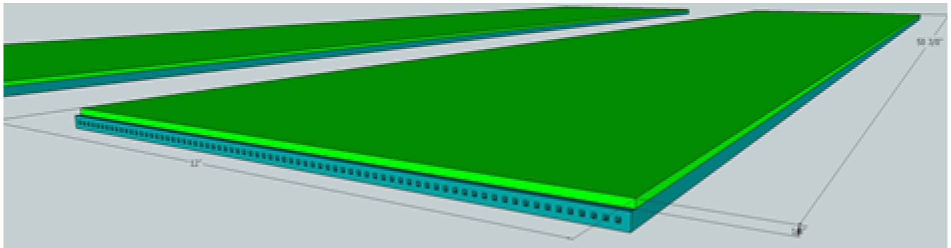

These are the spacer dimensions. The thickness is 1/8". The function of the spacer is to Provide a thermal bridge between the back of the PV panel and the absorber.

Joints: Upstream/Return header

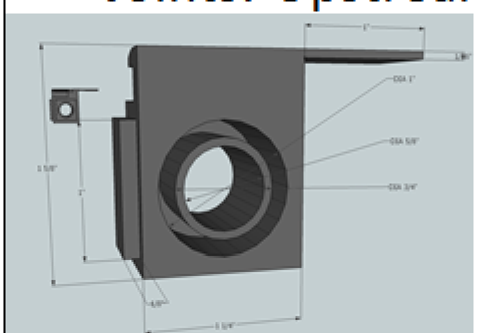

Left image: Looking downstream. We are to use a union to connect each module to each Other. Each half of a union is to be counter-sunk and solved into the joint. For this, and all upstream joints, the union half with the free nut is to be Solved in. Dimensions of the counter sink to Be able to accommodate a ½" union.

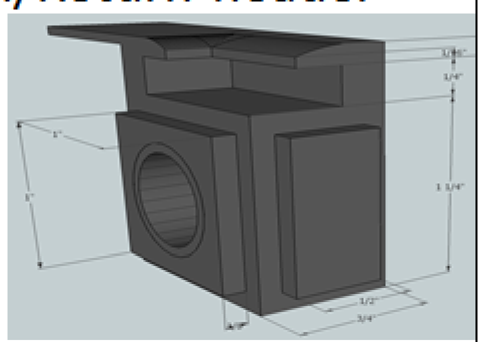

Right image: rotated about 180 degrees of left image. The squared out bevels are to be slipped and solved into the corresponding header and side rail.

The opposite cornered joint are the same with the exception of the top integrating details! The next slide will be of the Downstream/Supply header joint which is the same orientation As this one, just will different integrating details on the top.

Joints: Downstream/Supply Header

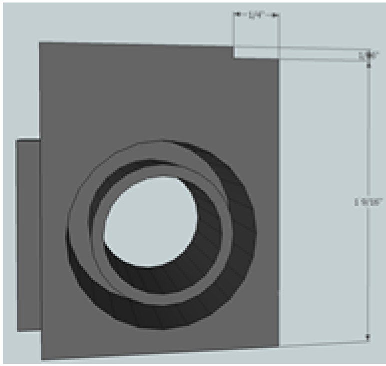

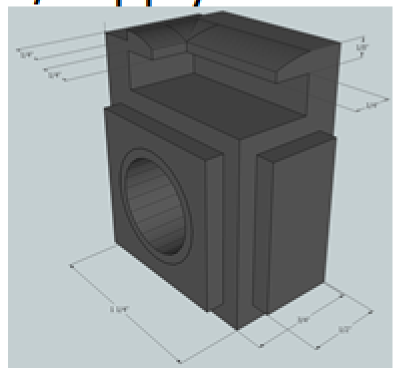

The integrating notch at the top of this Joint if 1/16". The threaded half of the Union is to be solved into this joint.

Joints: Upstream/Supply header

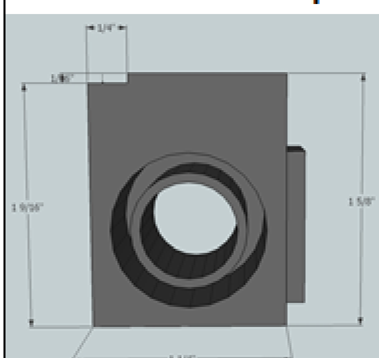

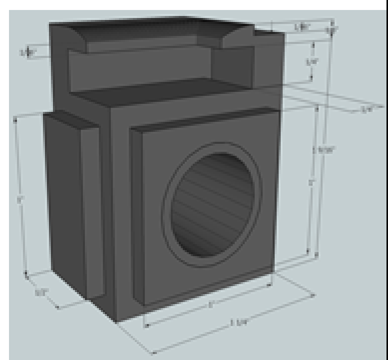

Upstream joint to be solved with a Counter-sunk union half with the free Nut.

Joints: Downstream/Return Header

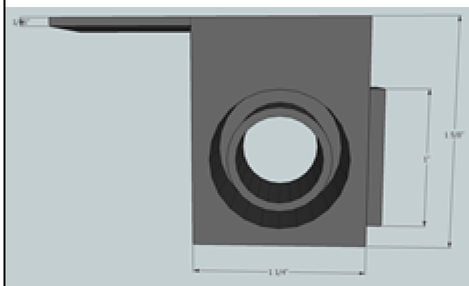

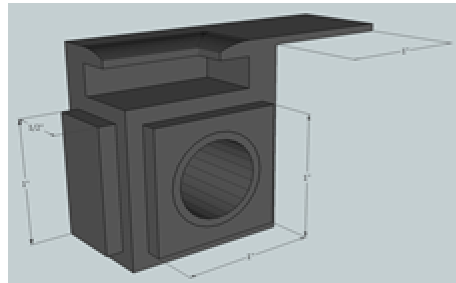

The threaded half of the union to be counter-
Sunk on this joint and all downstream joints.

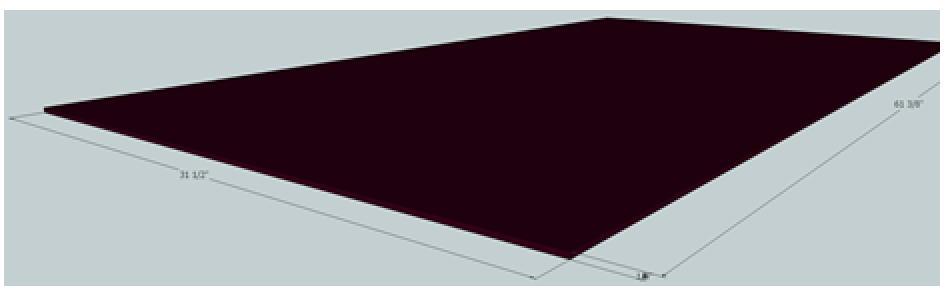

Dimensions for the PV panel. The thickness is about 1/4". Once all of the pieces have
Been fabricated, the module will need to be assembled around the PV.

Suggested Sequence of Assembly

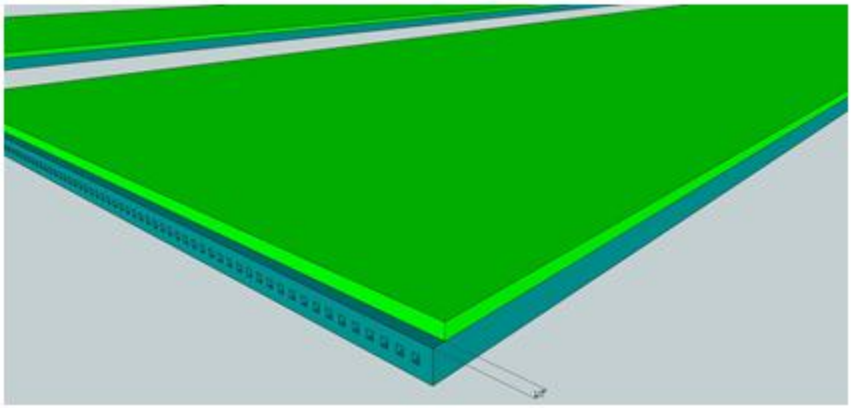

Step 1: Bond Spacer to absorber. Thermally conductive solvent?

Suggested Sequence of Assembly

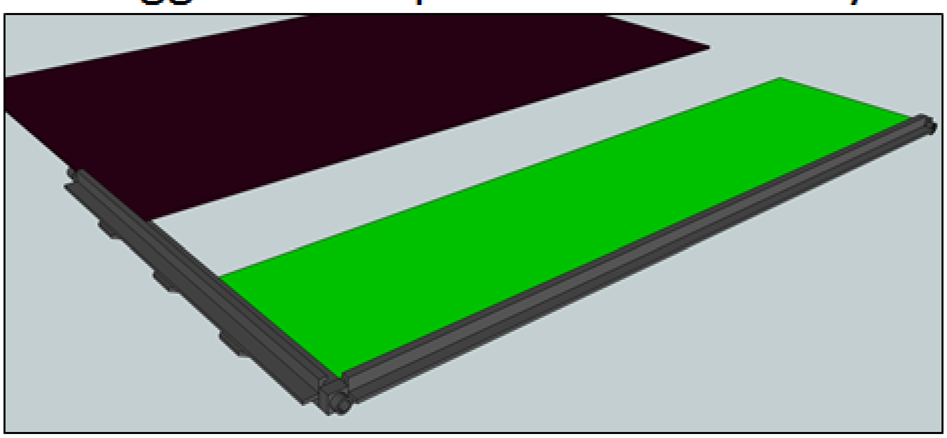

Step 2: Attach the **upstream** spacer and absorber assembly (so the PV J-box can slide into place) to the supply header.
Step 3: Attach the supply header and upstream side rail by using the joint and solvent.
Step 4: Slide the PV into the holding rails, ensuring contact with the back of the PV.
Step 5: Attach the downstream spacer and absorber assembly to the supply header and ensure contact with PV.

Suggested Sequence of Assembly

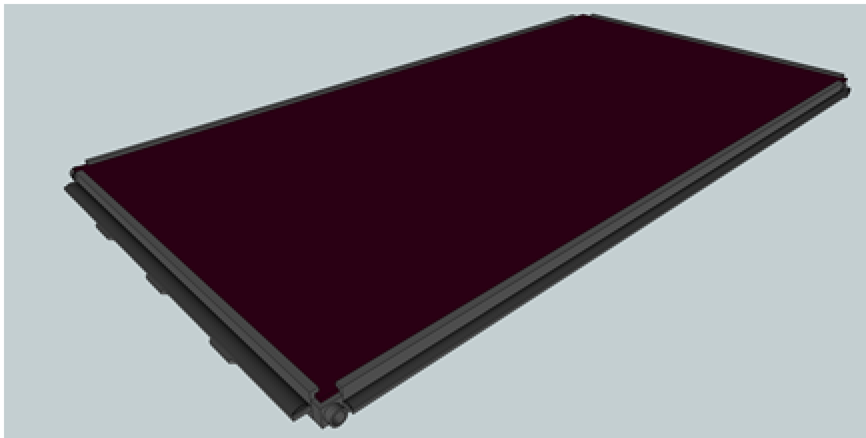

Step 6: Attach return header and downstream side rail by combing with the joints and solvent.
Notes: Obviously the water ways need to be water tight. The headers are drawn with an open channel (where the absorber sits) the entire length of the header. This will be ideal for extrusion, but not for the prototype. For the prototype the absorber channel opening in the headers can be cut out!!
Thanks!

Overall Concept for a Rooftop

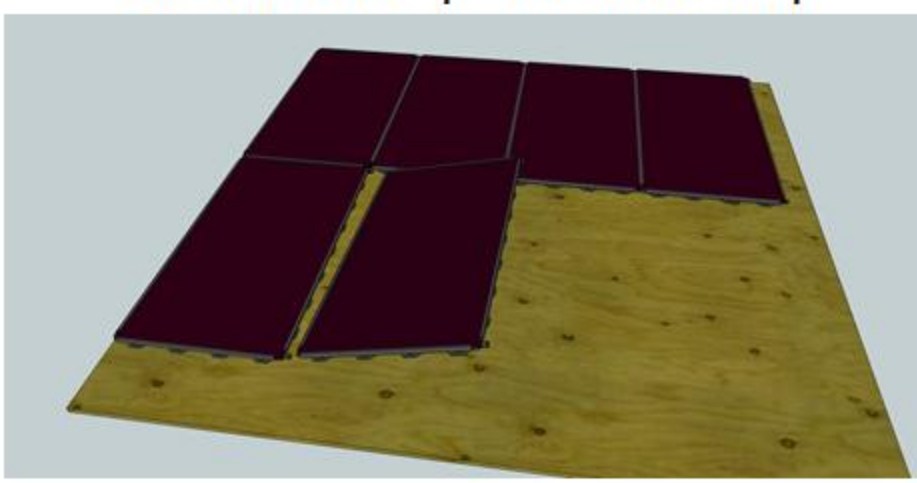

APPENDIX C PV PANEL DIMENSION RANGES AND THE SUNPOWER SPEC SHEET

The following table is a compilation of the most popular PV manufacturers and all of their PV models. The table was used to get an idea of typical dimensions for sizing the absorber so that it would fit in any PV laminate.

Manufacturer	Model	Length (in.)	Length (ft.)	Width (in)	Width (ft)	Depth (in.)(includes cover and/or frame)	Weight (lb)	Watt	VOC	Isc
First Solar (Thin Film, no residential specific)	FS Series 3 (Thin Film)	47.24	3.94	23.62	1.97	0.52	26.40			
	FS Series 2 (Thin Film)	47.24	3.94	23.62	1.97	0.52				
Suntech (monocrystalline silicon)	STP190S-24/Ad	62.20	5.18	31.80	2.65	1.40	34.10	190	45.20	5.62
	STP185S-24/Adb+	62.20	5.18	31.80	2.65	1.40		185	45.00	5.43
Sharp (monocrystalline)	NU-U235F4	64.60	5.38	39.10	3.26	1.80	41.90	235	37.00	8.50
Q-cells	Q.PRO (monocrystalline)	65.75	5.48	39.37	3.28	1.97	44.00	210-245	35.83-37.48	8.09-8.52
	Q.SMART (CIGS[Cu(In, Ga)])	47.09	3.92	25.04	2.09	1.42	31.90			
	Q.SMART UF (CIGS[Cu(In, Ga)Se2])	46.85	3.90	24.80	2.07	0.87	29.04			
	Q.SMART UF L (CIGS[Cu(In, Ga) Se2])	46.85	3.90	31.10	2.59	0.87	36.30			
	Q.BASE (Multicrystalline)	65.75	5.48	39.37	3.28	1.97	46.20			
Yingli	YGE 185 (multicrystalline)	51.57	4.30	38.98	3.25	1.97	34.80	175-185	29.0-29.5	8.2-8.45
	YL 210 (polycrystalline)	58.86	4.90	38.98	3.25	1.97	39.60	190-210	32.8-33.6	8.03-8.45
	YGE 235 (mulitcrystalline)	64.96	5.41	38.98	3.25	1.97	43.70	225-235	36.5-37	8.28-8.54
	YGE 280 (multicrystalline)	77.56	6.46	38.98	3.25	1.97	57.30	270-280	44.8-45	8.2-8.35
JA Solar	JAM5 72(Mono)	62.20	5.18	31.81	2.65	1.57	34.10	155-195	44.45-45.81	4.86-5.54
	JAM6 60(Mono)	64.96	5.41	39.02	3.25	1.57	42.90	200-250	36.12-37.8	7.83-8.68
	JAM6 72(Mono)	77.56	6.46	39.02	3.25	1.97	60.50	280-320	45.02-46.76	8.52-8.76
	JAM5L (Mono)	62.20	5.18	31.81	2.65	1.57	34.10	155-195	43.68-45.04	4.94-5.62
	JAM5 (Mono)	62.20	5.18	31.81	2.65	1.57	34.10			
	JAM6 (Mono)	64.96	5.41	39.02	3.25	1.57	42.90			
	JAP6 (Multi)	64.96	5.41	39.02	3.25	1.57	42.90	200-260	36.15-37.85	7.8-8.65
	JAP6 72 (Multi)	77.56	6.46	39.02	3.25	1.97	60.50	270-300	45.16-45.67	8.47-8.73

Trina Solar	TSM-DC01 (Mono)	62.24	5.19	31.85	2.65	1.57	34.40	175-185	43.9-44.5	5.3-5.4
	TSM-DC01A (Mono)	62.24	5.19	31.85	2.65	1.57	34.40	180-195	44.2-45.6	5.44-5.56
	Mono	62.24	5.19	31.85	2.65	1.57	34.40	195-210	45.4-46.6	5.56-5.78
	TSM-PC05 (multi)	64.95	5.41	39.05	3.25	1.81	43.00	220-240	36.8-37.2	8.15-8.37
	TSM-PC14 (multi)	77.00	6.42	39.05	3.25	1.81	61.70	265-285	44.2-44.5	8.2-8.5
Kyocera	KD Modules (ranges)	65.40	5.45	39.00	3.25	1.80	46.30			
		59.10	4.93	26.30	2.19		39.70			
		52.70	4.39				35.30			
							27.60			
							27.50			
SunPower	E19	61.39	5.12	31.42	2.62	1.81	33.1	238	48.5	6.25
	E19 318	61.39	5.12	41.18	3.43	1.81	41	318	64.7	6.2
	E18	61.39	5.12	31.42	2.62	1.81	33.1	230	48.2	6.05
	E18 225	61.39	5.12	31.42	2.62	1.81	33.1			
For all included panels										
		Length (in.)	Length (ft.)	Width (in)	Width (ft)	Depth (in.)(includes cover and/or frame)	Weight (lb)			
Max		77.56	6.46	41.18	3.43	1.97	61.70			
Min		46.85	3.90	23.62	1.97	0.52	26.40			
Average		61.67	5.14	34.26	2.85	1.60	39.47			
StDev		8.47	0.71	5.42	0.45	0.40	9.32			
Without CIGS and thin film										
		Length (in.)	Length (ft.)	Width (in)	Width (ft)	Depth (in.)(includes cover and/or frame)	Weight (lb)	area		
Max		77.56	6.46	41.18	3.43	1.97	61.70	22.18		
Min		51.57	4.30	26.30	2.19	1.40	27.50	9.4187		
Average		64.19	5.35	35.79	2.98	1.75	40.61	15.956		
StDev		6.32	0.53	4.14	0.35	0.19	9.25			

SUNPOWER

SPR-215-BLK
RESIDENTIAL PV MODULE

The SunPower SPR-215-BLK is designed specifically for on-grid residential systems where a combination of high module efficiency and outstanding appearance is desirable. Utilizing 72 series-connected A-300 solar cells, the SPR-215-BLK delivers industry-leading power density in a unique all-black module package with exceptionally uniform appearance.

SunPower modules—innovative design, proven materials, outstanding performance.

FEATURES & BENEFITS

- All-black module package eliminates harsh reflections and other noticeable cosmetic module features to provide optimum array appearance
- Unique all-back-contact solar cells with conversion efficiency up to 21.5%
- Low voltage-temperature coefficient, exceptional low-light performance, and high sensitivity to light across the entire solar spectrum maximize yearly energy delivery
- Highest quality, high-transmission tempered glass provides enhanced stiffness and impact resistance
- Aerospace style cell interconnects with in-plane strain relief provide extremely high reliability
- Advanced EVA encapsulation system with multi-layer backsheet meets the most stringent safety requirements for high-voltage operation
- A sturdy, black anodized aluminium frame allows modules to be easily roof-mounted with a wide variety of standard mounting systems

SPR-215-BLK RESIDENTIAL PV MODULE
An unequaled combination of power and grace.

UL LISTED UL 1703, Class C Fire Rating

IEC 61215, Safety Class II Certified

Document# 001-06638 Rev **

SunPower Corporation®
1.877.786.0123 Email: sales@sunpowercorp.com www.sunpowercorp.com
Engineered in California

SUNPOWER

ELECTRICAL CHARACTERISTICS AT STANDARD TEST CONDITIONS (STC)

STC is defined as: irradiance of 1000W/m^2, spectrum AM 1.5g and cell temperature of 25°C

Peak Power[1,2]	P_{max}	215W
Rated Voltage	V_{mp}	40.0V
Rated Current	I_{mp}	5.4A
Open Circuit Voltage	V_{oc}	47.7V
Short Circuit Current	I_{sc}	5.9A
Series Fuse Rating		15A
Maximum System Voltage		600V (UL)
		1000V (IEC)
Temperature Co-efficients	Power	-0.38%/°C
	Voltage	-136.8mV/°C
	Current	2.3mA/°C
Module Efficiency		17.3%
PTC Rating		197.6W

IV CURVE

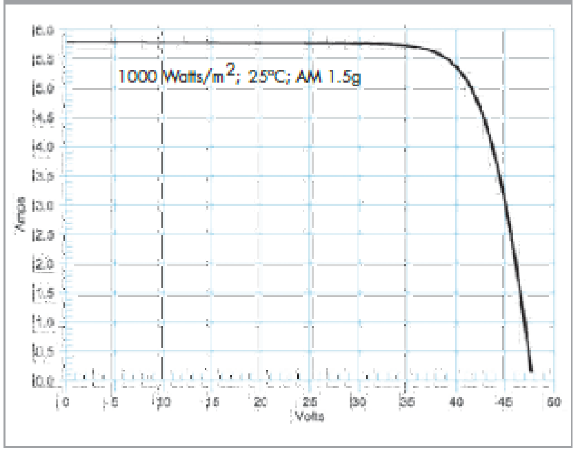

[1]Peak Power Tolerance: +/- 5%

[2]Power guaranteed for 25 years. See SunPower Limited Warranty for details.

MECHANICAL SPECIFICATIONS

Length (mm) x Width (mm)	1559 x 798
Thickness, including junction box (mm)	46
Weight (kg)	15

DIMENSIONS

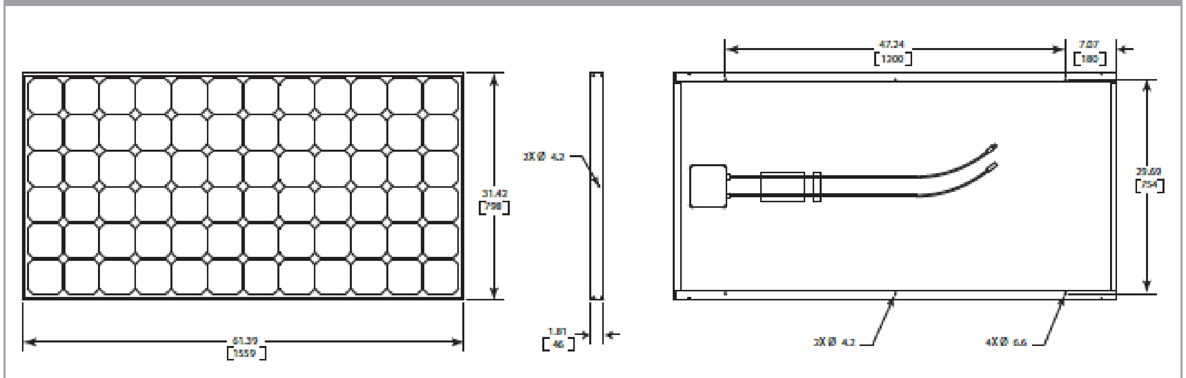

Document# 001-06638 Rev **

SunPower Corporation®

1.877.786.0123 Email: sales@sunpowercorp.com www.sunpowercorp.com

Engineered in California

APPENDIX D PLUMBING COMPONENTS

The pump.

ARMSTRONG

FILE NO:	10.591
DATE:	June 14, 2011
SUPERSEDES:	10.591
DATE:	May 14, 2010

ARM*flo* E Series Circulators - Models E8/E8B

SUBMITTAL

JOB/PROJECT: ______________________

REPRESENTATIVE: ______________________

ENGINEER: ______________________

CONTRACTOR: ______________________

ORDER NO: ______________ DATE: ________

SUBMITTED BY: ______________ DATE: ________

APPROVED BY: ______________ DATE: ________

Quantity	TAG No.	Part No.	Flow (USgpm)	Head (feet)	Voltage	Phase	Comments

TECHNICAL DATA

Flow Range	0 to 38.0 USgpm (0 to 2.4 L/s)
Head Range	0 to 34.0 feet (0 to 10.4 m)
Max. Fluid Temperature	230°F (110°C)
Max. Working Pressure	150 psi (1034 kPa)

MATERIALS OF CONSTRUCTION

Pump Body	Cast Iron (closed systems)	Bronze (open systems)	Lead Free Bronze*
Face Plate	Stainless Steel		
Impeller	30% Glass-filled Noryl		
Shaft	Stainless Steel		
Bearings	Permanently lubricated Stainless Steel		
Volute Gasket	EPDM		
Seal	Silicon Carbide *EnviroSeal* c/w viton elastomer		

PERFORMANCE CURVE

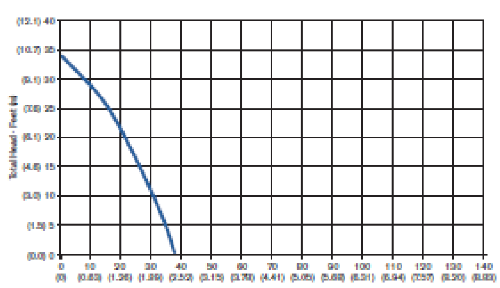

MOTOR DATA

Nominal Power	1/6 hp (125 W)		
Voltage	120 V	208 V	240 V
Full Load Amp Draw	2.0 A	1.0 A	1.0 A
Frequency	60 Hz		
Motor Type	2 pole, Single Phase		
Speed	3400 rpm		

MOUNTING ORIENTATION

FOR INDOOR USE ONLY

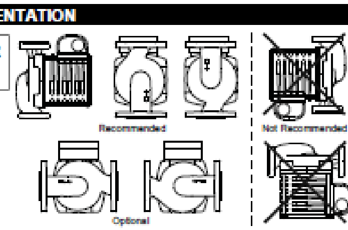

PART NUMBER

	120 V	240 V
E8	180200-657	180200-645
E8B	180200-658	180200-646
E8B	180200LF-658	180200LF-646

E8/E8B ACCESSORIES

¾" Flange kits	Timer
1" Flange kits	Aquastat
1¼" Flange kits	Spool Pieces
1½" Flange kits	

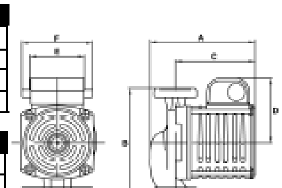

DIMENSIONS AND WEIGHTS

Model	Body	A	B	C	D	E	F	Connection Type & Size	Shipping Weight
ARM*flo* E8	Cast Iron	6.4 (164)	6.4 (164)	4.8 (122)	3.8 (97)	3.2 (81)	4.2 (107)	1.25" diameter 2-bolt flanges	11.5 (5.2)
ARM*flo* E8B	Bronze /LF Bronze*	6.4 (164)	6.4 (164)	4.8 (122)	3.8 (97)	3.2 (81)	4.2 (107)	1.25" diameter 2-bolt flanges	12.8 (5.8)

Note: All dimensions are in inches (mm) and weights in lbs (kg)

*Contains less than 0.25% lead, weighted average.

Page 1 of 2

The water filter housing.

HIGH TEMPERATURE FILTER HOUSINGS

- **Ideal for a wide range of industrial applications**
- **Excellent alternative to stainless and carbon steel vessels**
- **Durable glass-reinforced nylon construction**

Constructed of glass-reinforced nylon. High Temperature filter housings are an economical alternative to stainless and carbon steel housings.

These 1/2" and 3/4" NPT housings can withstand temperatures up to a maximum of 160°F (71.1°C). Excellent chemical compatibility makes High Temperature housings an ideal choice for a wide variety of industrial applications including those involving organic solvents, sea water, alcohol, petroleum and vegetable oils. They should not be used with ketones.

A #241 Viton® o-ring provides dependable sealing. Both 10" and 20" lengths are available to accommodate flow rates up to 20 gpm (76 L/min.).

PENTEK FILTRATION

Pure Quality.

HIGH TEMPERATURE

Filter Housings

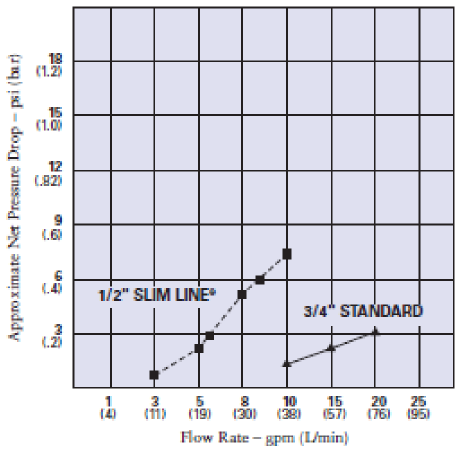

Housing Specifications and Performance Data

Model	Maximum Dimensions	Initial ΔP (psi) @ Flow Rate (gpm)
#10, 3/4"	12-1/8" x 5-1/8" (308 mm x 130 mm)	<1 psi @ 8 gpm (< 0.1 bar @ 30 L/min)
#20, 3/4"	22-1/4" x 5-1/8" (565 mm x 130 mm)	<1 psi @ 8 gpm (< 0.1 bar @ 30 L/min)
#10 SL, 1/2"	11-3/4" x 4-3/8" (298 mm x 111 mm)	5 psi @ 8 gpm (< 0.4 bar @ 30 L/min)
#20 SL, 1/2"	21-7/8" x 4-3/8" (556 mm x 111 mm)	5 psi @ 8 gpm (< 0.4 bar @ 30 L/min)

Materials of Construction

- **Housing** Glass-Reinforced Nylon
- **Cap** Glass-Reinforced Nylon
- **O-Ring** Viton®

- **Maximum Temperature** 160°F (71.1°C) (High Temperature)
- **Maximum Pressure** 125 psi (8.62 bar)

CAUTION: Protect against freezing to prevent cracking of the filter and water leakage.

PENTEK FILTRATION
502 Indiana Avenue • P.O. Box 1047 • Sheboygan, Wisconsin 53082-1047
Customer Service: 800-645-0267 • Fax: 888-203-7361 • supportspecialist@pentekfiltration.com
International: 920-457-9435 • Fax: 920-457-2417 • international@pentekfiltration.com
www.pentekfiltration.com

ISO 9001

Pentair Water Treatment

Printed in U.S.A. 01/04 310054

The filter cartridge.

CW/WP SERIES POLYPROPYLENE WOUND CARTRIDGES

- **String-wound design reduces fine sediment from a variety of fluids**
- **Withstands temperatures up to 165° F (73.9° C)**
- **Economically priced**
- **Nominal 10, 30, 50-micron rating (CW) and nominal 5, 30-micron rating (WP)**

CW and WP Series cartridges are manufactured from a durable polypropylene cord that is wound around a rigid polypropylene core. They are an economical solution to reduce fine sediment, including sand, silt, rust and scale particles.

CW cartridges are very economical and wound in a standard pattern around the core. They are available in 10, 30 and 50-micron ratings.

WP Series cartridges are wound in a precise pattern around the core providing greater surface area. The result is higher dirt-loading capacity and greater efficiency than standard wound cartridges like the CW.

Both of these string-wound cartridge styles are capable of withstanding temperatures up to 165° F (73.9° C), and will accommodate flow rates between 7 and 10 GPM with minimal pressure drop.

CW and WP Series cartridges are suitable for a wide variety of sediment filtration applications, including municipal and well water as well as many industrial fluids.

PENTEK FILTRATION

Pure Quality.™

CW/WP SERIES

Polypropylene Wound Cartridges

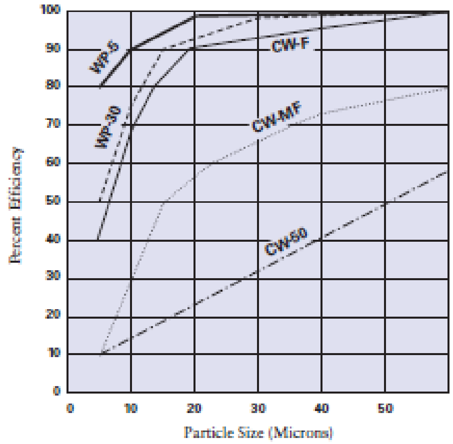

Cartridge Specifications and Performance Data

Model	Maximum Dimensions	Micron Rating (Nominal)	Initial ΔP (psi) @ Flow Rate (gpm)
CW-F	2-1/4" x 9-7/8" (60 mm x 251 mm)	10	<1 psi @ 10 gpm (<0.07 bar @ 27 L/min)
CW-MF	2-1/4" x 9-7/8" (60 mm x 251 mm)	30	<1 psi @ 10 gpm (<0.07 bar @ 38 L/min)
CW-50	2-1/4" x 9-7/8" (60 mm x 251 mm)	50	<1 psi @ 10 gpm (<0.07 bar @ 38 L/min)
WP-5	2-1/4" x 9-7/8" (60 mm x 251 mm)	5	<2.5 psi @ 10 gpm (<0.17 bar @ 38 L/min)
WP-30	2-1/4" x 9-7/8" (60 mm x 251 mm)	30	<1.4 psi @ 10 gpm (<0.10 bar @ 38 L/min)

Materials of Construction

- Filter Media — Polypropylene Fiber Cord
- Core — Polypropylene
- Temperature Rating — 40°F to 165°F (4.4°C to 73.9°C)

WARNING: Do not use with water that is microbiologically unsafe or of unknown quality without adequate disinfection before or after the system.

PENTEK FILTRATION

502 Indiana Avenue • P.O. Box 1047 • Sheboygan, Wisconsin 53082-1047
Customer Service: 800-645-0267 • Fax: 888-203-7361 • supportspecialist@pentekfiltration.com
International: 920-457-9435 • Fax: 920-457-2417 • international@pentekfiltration.com
www.pentekfiltration.com

ISO 9001

Pentair Water Treatment

Printed in U.S.A. 01/04 310062

APPENDIX E ABSORBER SIZING CALCULATIONS

File:C:\Users\estep\Documents\Master's Project\WeeklyMeeting\BIPVTCalcs.EES 12/16/2011 3:32:21 PM Page 1
EES Ver. 8.908: #0317: For use only by students and faculty in Civil & Environmental Engineering Univ. of Colorado

BIPV/T absorber sizing calculations

Constants

$\dot{V}_{ASHRAE} = 0.1$ [gpm/ft2] *ASHRAE Test flow rate metric*

$T_{ch} = \dfrac{3}{32 \ [in]}$

$T_{abs} = 0.25$

Absorber specifications with square channels

$W_{abs} = 12$ [in] *width of the absorber*

$h = T_{abs} - 2 \cdot T_{ch}$ *height of the channel*

$w = h$

$A_{ch} = h \cdot w$ *channel cross-sectional area*

$V_{ch} = A_{ch} \cdot L_{PV}$ *channel volume*

Typical PV dimensions

$L_{PV} = 61.5$ [in] *average length of PV*

$W_{PV} = 31.5$ [in] *average width of PV*

$A_{PV} = L_{PV} \cdot W_{PV}$

$A_{collector} = L_{PV} \cdot W_{abs} \cdot 2$

Properites of water

$P_{atm} = 14.7$ [psi] *atmospheric pressure*

$P_{ch} = 2 \cdot \dfrac{12}{CF_2}$ *fluid pressure in channel*

$P = P_{atm} + P_{ch}$ *absolute pressure*

$T = 95$ [F] *bulk water temperature*

$\rho_w = \rho[\text{'Water'}, T=T, P=P] \cdot \left| 0.000578704 \cdot \dfrac{\text{lbm/in3}}{\text{lbm/ft3}} \right|$ *density of water*

Mechanics of Materials
Beam deflection formula - special case
Using typical values of HDPE for modulus of elasticity and tensile yeild strength

$Load = \dfrac{\rho_w \cdot V_{ch} + P_{ch} \cdot A}{w}$ *distributed load: lbf/in*

$A = w \cdot L_{PV}$ *area over which the pressure is acting*

$E = 130000$ *average HDPE modulus of elasticity*

$I = w \cdot \frac{T_{ch}^3}{12}$ *centroidal moment of inertia*

$\sigma_{yeild} = \delta_{max} \cdot \frac{E}{L_{PV}}$ *yeild stress of the material = approx. 4000 psi*

$\delta_{max} = Load \cdot \frac{w^4}{384 \cdot E \cdot I}$ *maximum deflection of material*

Fluid and pipe parameters of interest

$D_H = 4 \cdot \frac{A_{ch}}{2 \cdot [h + w]}$ *hydraulic diameter*

$CF_2 = 27.73$ [in-WG/psi] *psi to inches of water conversion factor*

$g_c = 32.17 \cdot \left| 43200 \cdot \frac{\text{in/min2}}{\text{ft/s2}} \right|$ *gravitational proportionality constant*

Entrance effect neglected when greater than zero

$Entrance = \frac{L_{PV}}{D_H} - 0.05 \cdot Re_D$

$N = \textbf{Trunc}\left[\frac{W_{abs} - T_{ch}}{w + T_{ch}}\right]$ *Maximum number of channels*

$T_{ch,act} = \frac{W_{abs} - N \cdot w}{N}$ *actual channel wall thickness*

$N_{abs} = 2$ *number of absorbers per module*

$A_{c,fluid} = A_{ch} \cdot N \cdot N_{abs}$ *Total fluid cross-sectional area per module*

$\dot{V}_{module} = \dot{V}_{ASHRAE} \cdot A_{collector} \cdot \left| 0.006944444 \cdot \frac{\text{ft2}}{\text{in2}} \right|$ *Flow rate per module*

$v_{fluid} = \dot{V}_{module} \cdot \frac{\left| 231 \cdot \frac{\text{in3/min}}{\text{gpm}} \right|}{A_{c,fluid}}$ *fluid velocity across module*

$Re_D = \frac{v_{fluid} \cdot D_H \cdot \rho_w}{\textbf{Visc}[\text{'Water'}, T = T, P = P] \cdot \left| 0.001388889 \cdot \frac{\text{lbm/in*min}}{\text{lbm/ft*hr}} \right|}$ *Reynolds number*

$f = \frac{56.91}{Re_D}$ *friction factor for laminar flow in a square channel*

$\Delta P = f \cdot \frac{L_{PV}}{D_H} \cdot \frac{\rho_w \cdot v_{fluid}^2}{2 \cdot g_c} \cdot CF_2$ *head loss across absorber*

$$\text{MaxHeaderVelocity} = \dot{V}_{module} \cdot \left| 0.002228009 \cdot \frac{\text{ft3/s}}{\text{gpm}} \right| \cdot \frac{10}{\frac{1^2}{144}}$$

SOLUTION

Unit Settings: Eng F psia mass deg

A = 3.844 [in²]
A_{ch} = 0.003906 [in²]
$A_{collector}$ = 1476
$A_{c,fluid}$ = 0.5938 [in²]
A_{PV} = 1937 [in²]
CF_2 = 27.73 [in·WG/psi]
ΔP = 8.619 [in * WC]
δ_{max} = 0.000003801 [in]
D_H = 0.0625 [in]
E = 130000 [psi]
Entrance = 965.5
f = 0.1537
g_c = 1.390E+06
h = 0.0625 [in]
I = 0.000004292
Load = 53.37 [lbf/in]
L_{PV} = 61.5 [in]
MaxHeaderVelocity = 3.289
N = 76
N_{abs} = 2
P = 15.57 [psi]
P_{atm} = 14.7 [psi]
P_{ch} = 0.8655 [psi]
Re_D = 370.2
ρ_w = 0.03591 [lbm/in³]
σ_{yeild} = 0.008035 [psi]
T = 95 [F]
T_{abs} = 0.25 [in]
T_{ch} = 0.09375 [in]
$T_{ch,act}$ = 0.09539 [in]
V_{ch} = 0.2402 [in³]
$\dot{V}_{ASHRAE}$ = 0.1 [gpm/ft²]
$\dot{V}_{module}$ = 1.025 [gpm]
v_{fluid} = 398.8 [in/min]
w = 0.0625 [in]
W_{abs} = 12 [in]
W_{PV} = 31.5 [in]

10 potential unit problems were detected.

Parametric Table: Table 1

	T_{abs} [in]	T_{ch} [in]	$T_{ch,act}$ [in]	D_H [in]	N	Re_D	Load [lbf/in]	v_{fluid} [in/min]	ΔP [in * WC]
Run 1	0.3	0.09375	0.09803	0.1125	57	274.2	53.48	164.1	1.095
Run 2	0.29	0.09375	0.0975	0.1025	60	285.9	53.45	187.8	1.509
Run 3	0.28	0.09375	0.09798	0.0925	63	301.7	53.43	219.6	2.167
Run 4	0.27	0.09375	0.0966	0.0825	67	318.1	53.41	259.6	3.22
Run 5	0.26	0.09375	0.09651	0.0725	71	341.6	53.39	317.2	5.095
Run 6	0.25	0.09375	0.09539	0.0625	76	370.2	53.37	398.8	8.619
Run 7	0.24	0.09375	0.09565	0.0525	81	413.5	53.34	530.3	16.24
Run 8	0.23	0.09375	0.09543	0.0425	87	475.5	53.32	753.4	35.21
Run 9	0.22	0.09375	0.09516	0.0325	94	575.6	53.3	1192	95.31
Run 10	0.21	0.09375	0.09515	0.0225	102	766.2	53.28	2293	382.4
Run 11	0.2	0.09375	0.09464	0.0125	112	1256	53.26	6765	3655
Run 12	0.19	0.09375	0.09506	0.0025	123	5718	53.23	154000	2.080E+06

APPENDIX F MODULE PVC SPECIFICATION SHEET

1050 BOLTARON

1050 Type I PVC

GENERAL INFORMATION

Boltaron 1050 is a normal impact ,high corrosion resistant Type I PVC sheet with an industrial smooth finish on both sides. Boltaron 1050 conforms to ASTM D-1784.

AVAILABILITY

Standard Colors: Dark Gray (2079) (stock)
White (1150) & Black (2803)
(min. order required)
Custom Colors: Upon Request (min. order required)
Gauges: .032 to 3.00"
Width: 48"
Length: 96"
Custom Sizes: Upon request
Standard Texture: Industrial Smooth (Both Sides)
Custom Textures: Upon Request
Poly Masking: (Upon Request)

SUGGESTED APPLICATIONS

Fume Hoods and Ducts
Machined Parts
Fume Scrubbers
Acid Etching Machines
Acid Tanks and Linings

Typical Physical Properties

Property	Test Method	Typical Values
Mechanical		
Specific gravity	ASTM D-792	1.37
Tensile strength (PSI)	ASTM D-638	7,400
Elongation □		
Ultimate (%)	ASTM D-638	132
Yield (%)	ASTM D-638	3.5
Modulus of Elasticity (PSI)	ASTM D-638	4.0×10^5
Flexural strength (PSI)	ASTM D-790	12,000
Flexural modulus (PSI)	ASTM D-790	4.2×10^5
Izod impact		
(Ft. lbs./in. of notch)	ASTM D-256	1-3
Hardness Rockwell R	ASTM D-785	116
Hardness Shore D	ASTM D-2240	82
Compression Strength (PSI)	ASTM D-695	10,830
Shear Strength (PSI)	ASTM D-732	9,240
Water Absorption 24 hrs. (%)	ASTM D-570	0.032
Thermal		
Vicat Softening Point (°C)	ASTM D-1525	85
Thermal Expansion		
(in/in°C)	ASTM D-696	2.95×10^{-5}
Heat Deflection (°F)		
264 PSI (annealed)	ASTM D-648	165
Thermal Conductivity		
(BTU/HR/FT/F/in.)	ASTM C-177	0.72
Specific Heat		
(CAL/GM/°C)	ASTM C-351	0.20
Electrical		
Dielectric Strength (Volts/Mil.)	ASTM D-149	552
Volume Resistivity		
(Ohms/cm)$\times10^{14}$	ASTM D-257	1.48
Dielectric Constant (60Hz)	ASTM D-150	2.910
Dissipation Factor (60Hz)	ASTM D-150	0.018
Loss Index□ □	ASTM D-150	0.051
Flammability		
UL	UL-94	V-0[1]

[1] Values based on minimum thickness of .032", UL File # E54688

LIMITATION OF WARRANTY

The application suggestions, specifications and other data described here are based upon experience and information that is believed, by BPF to be reliable. However, BPF makes no express or implied warranty that BOLTARON 1050 will perform in accordance with such specifications in any particular circumstance. Therefore, ALL EXPRESS OR IMPLIED WARRANTIES IN CONNECTION WITH BOLTARON 1050, INCLUDING THE WARRANTIES OF MERCHANTABILITY AND FITNESS FOR A PARTICULAR PURPOSE, ARE EXPRESSLY DISCLAIMED. The prospective user should determine the suitability of BOLTARON 1050 and the application suggestions before actual application.

One General Street, Newcomerstown, OH 43832
P 800.342.7444 **F** 740.498.5448 **E** info@boltaron.com
www.boltaron.com

APPENDIX G CONSTRUCTION MATERIAL SPECIFICATIONS

UNISTRUT — 1⅝" Framing System – Channel

P1000 H3

Wt/100 Ft: 175 Lbs (260 kg/100 m)

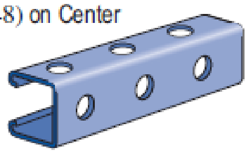

Notes:
* Load limited by spot weld shear.
** KL/r > 200
NR = Not Recommended.

1. Above loads include the weight of the member. This weight must be deducted to arrive at the net allowable load the beam will support.
2. Long span beams should be supported in such a manner as to prevent rotation and twist.
3. Allowable uniformly distributed loads are listed for various simple spans, that is, a beam on two supports. If load is concentrated at the center of the span, multiply load from the table by 0.5 and corresponding deflection by 0.8.
4. For Pierced Channel, Beam Load Values in the tables are multiplied by the following factor:

"H3" Series 90%

MATERIAL

Unistrut channels are accurately and carefully cold formed to size from low-carbon strip steel. All spot-welded combination members, except P1001T, are welded 3" (76 mm) maximum on center.

STEEL: PLAIN
12 Ga. (2.7 mm), 14 Ga.(1.9 mm) and
16 Ga. (1.5 mm) ASTM A1011 SS GR 33.

STEEL: PRE-GALVANIZED
12 Ga. (2.7 mm), 14 Ga. (1.9 mm) and
16 Ga. (1.5mm) ASTM A653 GR 33.

For other materials, see Special Metals or Fiberglass sections.

FINISHES

All channels are available in:

- Perma Green III (GR).
- Pre-galvanized (PG), conforming to ASTM A653 G90.
- Hot-dipped galvanized (HG), conforming to ASTM A123.
- Plain (PL).

Project: Solar testing frame
Architect / Engineer: Greg Estep
Date: 06/24/2011 **Phone:** 303.579.2403
Contractor: Greg Estep
Address: 1952 Oxford lane, Superior, CO
Notes 1:
Notes 2:

Approval Stamp:

9/12/08

P2101 THRU P2104

Wt/100 pcs: 58 Lbs (26.3 kg)

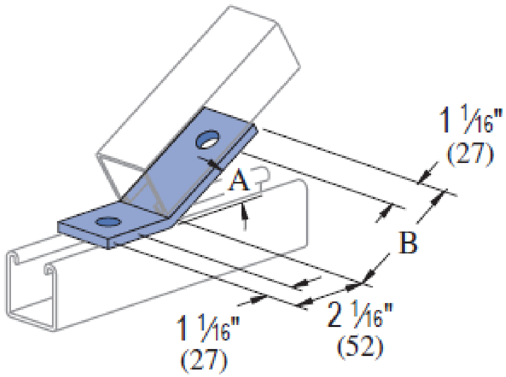

Part No.	"A" Degree *(rad)*	"B" In *(mm)*
P2101	30° *0.52*	3¼ *83*
P2102	22½° *0.39*	3⁵⁄₁₆ *84*
P2103	15° *0.26*	3⁵⁄₁₆ *84*
P2104	7½° *0.13*	3⁵⁄₁₆ *84*

Standard Dimensions for 1⅝" (41mm) width series channel fittings *(Unless Otherwise Shown on Drawing)*
Hole Diameter: ⁹⁄₁₆" (14mm); Hole Spacing - From End: ¹³⁄₁₆" (21mm); Hole Spacing - On Center: 1⅞" (48mm); Width: 1⅝"(41mm); Thickness: ¼" (6mm)

MATERIAL

Fittings, unless noted, are made from hot-rolled, pickled and oiled steel plates, strip or coil, and conform to ASTM specifications A575, A576, A635, or A36. The fitting steel also meets the physical requirements of ASTM A1011 SS GR 33. The pickling of the steel produces a smooth surface free from scale.

Many fittings are also available in stainless steel, aluminum and fiberglass. Consult factory for ordering information.

FINISHES

Fittings are available in:

- Perma-Green III (GR),
- Electro-galvanized (EG), conforming to ASTM B633 Type III SC1;
- Hot-dipped galvanized (HG), conforming to ASTM A123 or A153 and
- Plain (PL).

Project: ______________________________

Architect / Engineer: ______________________________

Date: ______________ **Phone:** ______________

Contractor: ______________________________

Address: ______________________________

____

Notes 1: ______________________________

____

Notes 2: ______________________________

____

Approval Stamp:

9/12/08

P1186, P2105 THRU P2110

Wt/100 pcs: 58 Lbs (26.3 kg)

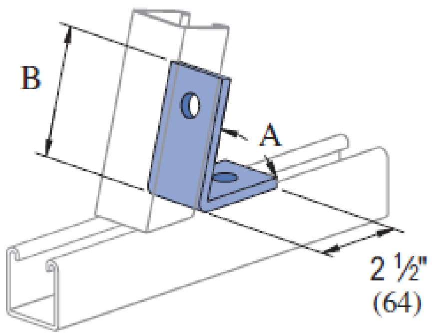

Part Number	"A" Degree *(rad)*	"B" In *(mm)*
P2105	82½° *1.44*	3³⁄₁₆ *81*
P2106	75° *1.31*	3³⁄₁₆ *81*
P2107	67½° *1.18*	3⅛ *79*
P2108	60° *1.05*	3⅛ *79*
P2109	52½° *0.92*	3¹⁄₁₆ *78*
P1186	45° *0.79*	3⅛ *79*
P2110	37½° *0.65*	3 *76*

Standard Dimensions for 1⅝" (41mm) width series channel fittings *(Unless Otherwise Shown on Drawing)*
Hole Diameter: ⁹⁄₁₆" (14mm); Hole Spacing - From End: ¹³⁄₁₆" (21mm); Hole Spacing - On Center: 1⅞" (48mm); Width: 1⅝"(41mm); Thickness: ¼" (6mm)

MATERIAL

Fittings, unless noted, are made from hot-rolled, pickled and oiled steel plates, strip or coil, and conform to ASTM specifications A575, A576, A635, or A36. The fitting steel also meets the physical requirements of ASTM A1011 SS GR 33. The pickling of the steel produces a smooth surface free from scale.

Many fittings are also available in stainless steel, aluminum and fiberglass. Consult factory for ordering information.

FINISHES

Fittings are available in:

- Perma-Green III (GR),
- Electro-galvanized (EG), conforming to ASTM B633 Type III SC1;
- Hot-dipped galvanized (HG), conforming to ASTM A123 or A153 and
- Plain (PL).

Project: ______________________________

Architect / Engineer: ______________________________

Date: ______________ **Phone:** ______________

Contractor: ______________________________

Address: ______________________________

____

Notes 1: ______________________________

____

Notes 2: ______________________________

____

Approval Stamp:

9/12/08

P2459-36 THRU P2459-96 — TUBULAR BACK BRACES

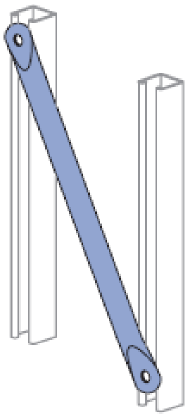

1. The vertical lines of the graph correspond to the center to center line dimension of the uprights.
2. Along this vertical line locate the (maximum usable) horizontal bracing height line.
3. The arc line that intersects the point formed by the intersection of the two lines, indicates the brace required.
4. 60° - 30° maximum, minimum brace angles are indicated for maximum effect.

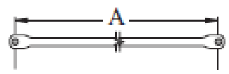

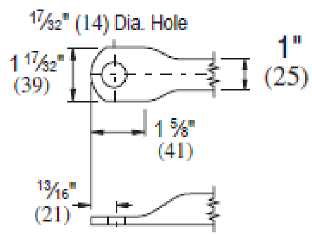

Part Number	"A" In *(mm)*	Wt/100 pcs Lbs *(kg)*
P2459-36	36 *914*	255 *115.7*
P2459-42	42 *1,067*	296 *134.3*
P2459-48	48 *1,219*	336 *152.4*
P2459-54	54 *1,372*	377 *171.0*
P2459-60	60 *1,524*	418 *189.6*
P2459-72	72 *1,829*	499 *226.3*
P2459-84	84 *2,134*	580 *263.1*
P2459-96	96 *2,438*	661 *299.8*

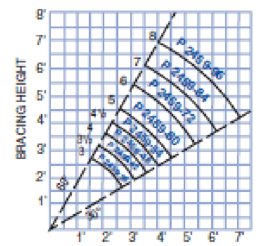

Standard Dimensions for 1⅝" (41mm) width series channel fittings *(Unless Otherwise Shown on Drawing)*
Hole Diameter: 9/16" (14mm); Hole Spacing - From End: 13/16" (21mm); Hole Spacing - On Center: 1⅞" (48mm); Width: 1⅝"(41mm); Thickness: ¼" (6mm)
Note : When used for mechanical supports, load capacities of brackets and fittings should be in compliance with the American Standard Code for Pressure Piping.

MATERIAL

Fittings, unless noted, are made from hot-rolled, pickled and oiled steel plates, strip or coil, and conform to ASTM specifications A575, A576, A635, or A36. The fitting steel also meets the physical requirements of ASTM A1011 SS GR 33. The pickling of the steel produces a smooth surface free from scale.

Many fittings are also available in stainless steel, aluminum and fiberglass. Consult factory for ordering information.

FINISHES

Fittings are available in:

- Perma-Green III (GR),
- Electro-galvanized (EG), conforming to ASTM B633 Type III SC1;
- Hot-dipped galvanized (HG), conforming to ASTM A123 or A153 and
- Plain (PL).

Project: ______________________

Architect / Engineer: ______________________

Date: __________ **Phone:** __________

Contractor: ______________________

Address: ______________________

Notes 1: ______________________

Notes 2: ______________________

Approval Stamp:

9/12/08

P1075

Wt/100 pcs: 229 Lbs (103.9 kg)

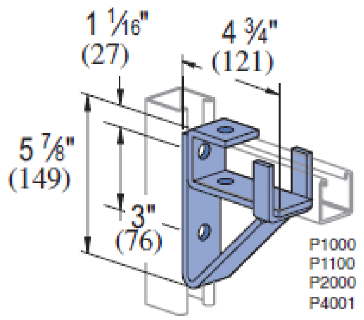

Material: ¼" (6.4) thick steel.

Vertical Channel Part No.	Gauge	Allowable Moment* In-Lbs (N•M)
P1000	12	5,100 (576)
P1100	14	4,400 (497)
P2000	16	3,200 (362)

Safety Factor 2½

* Allowable moment for fitting only. Channel may determine overall capacity.

Standard Dimensions for 1⅝" (41mm) width series channel fittings *(Unless Otherwise Shown on Drawing)*
Hole Diameter: 9⁄16" (14mm); Hole Spacing - From End: 13⁄16" (21mm); Hole Spacing - On Center: 1⅞" (48mm); Width: 1⅝"(41mm); Thickness: ¼" (6mm)
Note: When used for mechanical supports, load capacities of brackets and fittings should be in compliance with the American Standard Code for Pressure Piping.

MATERIAL

Fittings, unless noted, are made from hot-rolled, pickled and oiled steel plates, strip or coil, and conform to ASTM specifications A575, A576, A635, or A36. The fitting steel also meets the physical requirements of ASTM A1011 SS GR 33. The pickling of the steel produces a smooth surface free from scale.

Many fittings are also available in stainless steel, aluminum and fiberglass. Consult factory for ordering information.

FINISHES

Fittings are available in:

- Perma-Green III (GR),
- Electro-galvanized (EG), conforming to ASTM B633 Type III SC1;
- Hot-dipped galvanized (HG), conforming to ASTM A123 or A153 and
- Plain (PL).

Project: ______________________

Architect / Engineer: ______________________

Date: ____________ **Phone:** ____________

Contractor: ______________________

Address: ______________________

____

Notes 1: ______________________

____

Notes 2: ______________________

____

Approval Stamp:

9/12/08

P2458-18 THRU P2458-36 — TUBULAR KNEE BRACES

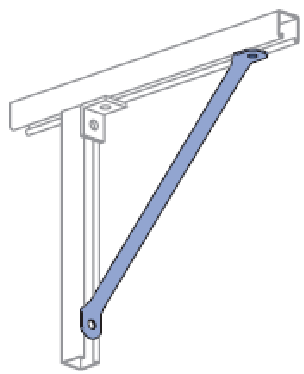

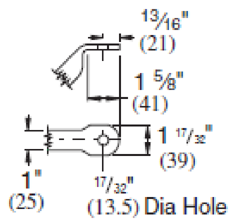

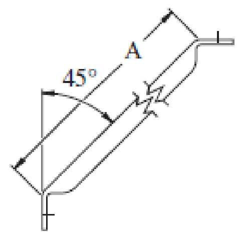

Part Number	"A" In (mm)	Wt/100 pcs Lbs (kg)
P2458-18	18 *457*	146 *66.2*
P2458-24	24 *610*	186 *84.4*
P2458-30	30 *762*	227 *103.0*
P2458-36	36 *914*	267 *121.1*

Design Loads
Compression = 1500 Lbs (6.67 kN)
Tension = 300 Lbs (1.33 kN)

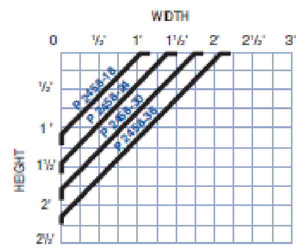

Standard Dimensions for 1⅝" (41mm) width series channel fittings *(Unless Otherwise Shown on Drawing)*
Hole Diameter: 9/16" (14mm); Hole Spacing - From End: 13/16" (21mm); Hole Spacing - On Center: 1⅞" (48mm); Width: 1⅝" (41mm); Thickness: ¼" (6mm)
Note : When used for mechanical supports, load capacities of brackets and fittings should be in compliance with the American Standard Code for Pressure Piping.

MATERIAL

Fittings, unless noted, are made from hot-rolled, pickled and oiled steel plates, strip or coil, and conform to ASTM specifications A575, A576, A635, or A36. The fitting steel also meets the physical requirements of ASTM A1011 SS GR 33. The pickling of the steel produces a smooth surface free from scale.

Many fittings are also available in stainless steel, aluminum and fiberglass. Consult factory for ordering information.

FINISHES

Fittings are available in:

Perma-Green III (GR),

Electro-galvanized (EG), conforming to ASTM B633 Type III SC1;

Hot-dipped galvanized (HG), conforming to ASTM A123 or A153 and

Plain (PL).

Project: ______________________________

Architect / Engineer: ______________________________

Date: ______________ **Phone:** ______________

Contractor: ______________________________

Address: ______________________________

____

Notes 1: ______________________________

____

Notes 2: ______________________________

____

Approval Stamp:

9/12/08

Channel Nuts With Spring

P1006 - P1010 Pg 67 | P1012S - P1024S Pg 67 | P4006 - P4010 Pg 67 | P4012S - P4023S Pg 67 | P5506 - P5510 Pg 67 | P2378 - P2382 Pg 68

Channel Nuts Without Spring

P3016 Pg 67 | P3006 - P3013 Pg 67 | P1012 - P1024 Pg 67 | P4012 - P4023 Pg 67 | P1006T - P1010T, P4010T Pg 67 | P4908 Pg 67 | P1016 Pg 67

Hardware

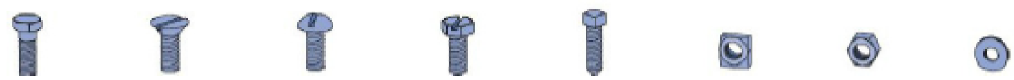

HHCS Pg 68 | HFMS Pg 68 | HRMS Pg 68 | HSHS Pg 68 | HCSS Pg 68 | HSQN Pg 69 | HHXN Pg 69 | HFLW Pg 69

HLKW Pg 69 | HOCW Pg 70 | HTHR Pg 69 | HRCN Pg 69 | P2486 Pg 70 | P2485 Pg 70 | P2485K Pg 70 | K1062 - K1064 Pg 70

Maximum Allowable Pull-out And Slip Loads

Channel	Channel Nut Size-Thread	Gauge	Allowable Pull-Out Strength Lbs *(kN)*	Resistance to Slip Lbs *(kN)*	Torque Ft-Lbs *(N•m)*
P1000 P3000 P5000 P5500	7/8" - 9	12	2,500 *11.12*	1,700 *7.56*	*125 *170*
	3/4" - 10	12	2,500 *11.12*	1,700 *7.56*	*125 *170*
	5/8" - 11	12	2,500 *11.12*	1,500 *6.67*	*100 *135*
	1/2" - 13	12	2,000 *8.90*	1,500 *6.67*	50 *70*
	7/16" - 14	12	1,400 *6.23*	1,000 *4.45*	35 *50*
	3/8" - 16	12	1,000 *4.45*	800 *3.56*	19 *25*
	5/16" - 18	12	800 *3.56*	500 *2.22*	11 *15*
	1/4" - 20	12	600 *2.67*	300 *1.33*	6 *8*
P3300	1/2" - 13	12	1,500 *6.67*	1,500 *6.67*	50 *70*
	3/8" - 16	12	1,000 *4.45*	800 *3.56*	19 *25*
	5/16" - 18	12	800 *3.56*	500 *2.22*	11 *15*
	1/4" - 20	12	600 *2.67*	300 *1.33*	6 *8*

Channel	Channel Nut Size-Thread	Gauge	Allowable Pull-Out Strength Lbs *(kN)*	Resistance to Slip Lbs *(kN)*	Torque Ft-Lbs *(N•m)*
P1100 & P4100	1/2" - 13	14	1,400 *6.23*	1,000 *4.45*	50 *70*
	3/8" - 16	14	1,000 *4.45*	750 *3.34*	19 *25*
	5/16" - 18	14	800 *3.56*	400 *1.78*	11 *15*
	1/4" - 20	14	600 *2.67*	300 *1.33*	6 *8*
P2000 & P4000	1/2" - 13	16	1,000 *4.45*	1,000 *4.54*	50 *70*
	3/8" - 16	16	1,000 *4.45*	750 *3.34*	19 *25*
	5/16" - 18	16	800 *3.56*	400 *1.78*	11 *15*
	1/4" - 20	16	600 *2.67*	300 *1.33*	6 *8*

* May require 3/8" or 1/2" thick fitting.

Nut design loads include a minimum safety factor of 3.

Note: Refer to the Channel Nut Selection Chart on the following two pages for the part number.

Trubolt Wedge

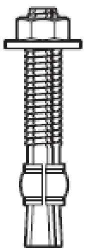

SPECIFIED FOR ANCHORAGE INTO CONCRETE

Trubolt Wedge anchors feature a stainless steel expansion clip, threaded stud body, nut and washer. Anchor bodies are made of plated carbon steel, hot-dipped galvanized carbon steel, type 304 stainless steel or type 316 stainless steel as identified in the drawings or other notations.

The exposed end of the anchor is stamped to identify anchor length. Stampings should be preserved during installation for any subsequent embedment verification.

Use carbide tipped hammer drill bits made in accordance with ANSI B212.15-1994 to install anchors.

Anchors are tested to ACI 355.2 and ICC-ES AC193. Anchors are listed by the following agencies as required by the local building code: ICC-ES, UL, FM, City of Los Angeles, California State Fire Marshal and Caltrans.

See pages 42-43 for performance values in accordance to 2006 IBC.

INSTALLATION STEPS

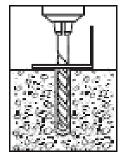

1. Select a carbide drill bit with a diameter equal to the anchor diameter. Drill hole to any depth exceeding the desired embedment. See chart for minimum recommended embedment.

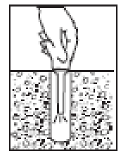

2. Clean hole or continue drilling additional depth to accommodate drill fines.

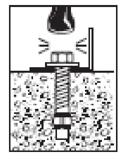

3. Assemble washer and nut, leaving nut flush with end of anchor to protect threads. Drive anchor through material to be fastened until washer is flush to surface of material.

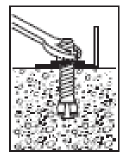

4. Expand anchor by tightening nut 3-5 turns past the hand tight position, or to the specified torque requirement.

APPROVALS/LISTINGS

Trubolt®
Wedge Anchors

ICC Evaluation Service, Inc. # ESR-2251
- Category 1 performance rating
- 2006 IBC compliant
- Meets ACI 318 ductility requirements
- Tested in accordance with ACI 355.2 and ICC-ES AC193
- For use in seismic zones A & B
- 1/4", 3/8" & 1/2" diameter anchors listed in ESR-2251

Underwriters Laboratories
Factory Mutual
City of Los Angeles - #RR2748
California State Fire Marshall
Caltrans
Meets or exceeds U.S. Government G.S.A. Specification A-A-1923A Type 4
(formerlyGSA: FF-S-325 Group II, Type 4, Class 1)

LENGTH INDICATION CODE *

CODE	LENGTH OF ANCHOR		CODE	LENGTH OF ANCHOR	
A	1-1/2 < 2	(38.1 < 50.8)	K	6-1/2 < 7	(165.1 < 177.8)
B	2 < 2-1/2	(50.8 < 63.5)	L	7 < 7-1/2	(177.8 < 190.5)
C	2-1/2 < 3	(63.5 < 76.2)	M	7-1/2 < 8	(190.5 < 203.2)
D	3 < 3-1/2	(76.2 < 88.9)	N	8 < 8-1/2	(203.2 < 215.9)
E	3-1/2 < 4	(88.9 < 101.6)	O	8-1/2 < 9	(215.9 < 228.6)
F	4 < 4-1/2	(101.6 < 114.3)	P	9 < 9-1/2	(228.6 < 241.3)
G	4-1/2 < 5	(114.3 < 127.0)	Q	9-1/2 < 10	(241.3 < 254.0)
H	5 < 5-1/2	(127.0 < 139.7)	R	10 < 11	(254.0 < 279.4)
I	5-1/2 < 6	(139.7 < 152.4)	S	11 < 12	(279.4 < 304.8)
J	6 < 6-1/2	(152.4 < 165.1)	T	12 < 13	(304.8 < 330.2)

*Located on top of anchor for easy inspection.

PERFORMANCE TABLE

Trubolt Wedge Anchors

Ultimate Tension and Shear Values (Lbs/kN) in Concrete*

ANCHOR DIA. In. (mm)	INSTALLATION TORQUE Ft. Lbs. (Nm)	EMBEDMENT DEPTH In. (mm)	ANCHOR TYPE	f'c = 2000 PSI (13.8 MPa) TENSION Lbs. (kN)	f'c = 2000 PSI (13.8 MPa) SHEAR Lbs. (kN)	f'c = 4000 PSI (27.6 MPa) TENSION Lbs. (kN)	f'c = 4000 PSI (27.6 MPa) SHEAR Lbs. (kN)	f'c = 6000 PSI (41.4 MPa) TENSION Lbs. (kN)	f'c = 6000 PSI (41.4 MPa) SHEAR Lbs. (kN)
1/4 (6.4)	4 (5.4)	1-1/8 (28.6)	WS-Carbon or WS-G Hot-Dipped Galvanized or WW-304 S.S. or SWW-316 S.S.	1,180 (5.2)	1,400 (6.2)	1,780 (7.9)	1,400 (6.2)	1,900 (8.5)	1,400 (6.2)
		1-15/16 (49.2)		2,100 (9.3)	1,680 (7.5)	3,300 (14.7)	1,680 (7.5)	3,300 (14.7)	1,680 (7.5)
		2-1/8 (54.0)		2,260 (10.1)	1,680 (7.5)	3,300 (14.7)	1,680 (7.5)	3,300 (14.7)	1,680 (7.5)
3/8 (9.5)	25 (33.9)	1-1/2 (38.1)		1,680 (7.5)	2,320 (10.3)	2,240 (10.0)	2,620 (11.7)	2,840 (12.6)	3,160 (14.1)
		3 (76.2)		3,480 (15.5)	4,000 (17.8)	5,940 (26.4)	4,140 (18.4)	6,120 (27.2)	4,500 (20.0)
		4 (101.6)		4,800 (21.4)	4,000 (17.8)	5,940 (26.4)	4,140 (18.4)	6,120 (27.2)	4,500 (20.0)
1/2 (12.7)	55 (74.6)	2-1/4 (57.2)		4,660 (20.7)	4,760 (21.2)	5,100 (22.7)	4,760 (21.2)	7,040 (31.3)	7,040 (31.3)
		4-1/8 (104.8)		4,660 (20.7)	7,240 (32.2)	9,640 (42.9)	7,240 (32.2)	10,820 (48.1)	8,160 (36.3)
		6 (152.4)		5,340 (23.8)	7,240 (32.2)	9,640 (42.9)	7,240 (32.2)	10,820 (48.1)	8,160 (36.3)
5/8 (15.9)	90 (122.0)	2-3/4 (69.9)		6,580 (29.3)	7,120 (31.7)	7,180 (31.9)	7,120 (31.7)	9,720 (43.2)	9,616 (42.8
		5-1/8 (130.2)		6,580 (29.3)	9,600 (42.7)	14,920 (66.4)	11,900 (52.9)	16,380 (72.9)	12,520 (55.7)
		7-1/2 (190.5)		7,060 (31.4)	9,600 (42.7)	15,020 (66.8)	11,900 (52.9)	16,380 (72.9)	12,520 (55.7)
3/4 (19.1)	110 (149.2)	3-1/4 (82.6)		7,120 (31.7)	10,120 (45.0)	10,840 (48.2)	13,720 (61.0)	13,300 (59.2)	15,980 (71.1)
		6-5/8 (168.3)		10,980 (48.8)	20,320 (90.4)	17,700 (78.7)	23,740 (105.6)	20,260 (90.1)	23,740 (105.6)
		10 (254.0)		10,980 (48.8)	20,320 (90.4)	17,880 (79.5)	23,740 (105.6)	23,580 (104.9)	23,740 (105.6)
7/8 (22.2)	250 (339.0)	3-3/4 (95.3)		9,520 (42.3)	13,160 (58.5)	14,740 (65.6)	16,580 (73.8)	17,420 (77.5)	19,160 (85.2)
		6-1/4 (158.8)		14,660 (65.2)	20,880 (92.9)	20,940 (93.1)	28,800 (128.1)	24,360 (108.4)	28,800 (128.1)
		8 (203.2)		14,660 (65.2)	20,880 (92.9)	20,940 (93.1)	28,800 (128.1)	24,360 (108.4)	28,800 (128.1)
1 (25.4)	300 (406.7)	4-1/2 (114.3)		13,940 (62.0)	16,080 (71.5)	20,180 (89.8)	22,820 (101.5)	21,180 (94.2)	24,480 (108.9)
		7-3/8 (187.3)		14,600 (64.9)	28,680 (127.6)	23,980 (106.7)	37,940 (168.8)	33,260 (148.0)	38,080 (169.4)
		9-1/2 (241.3)		18,700 (83.2)	28,680 (127.6)	26,540 (118.1)	37,940 (168.8)	33,260 (148.0)	38,080 (169.4)

*Allowable values are based upon a 4 to 1 safety factor. Divide by 4 for allowable load values.
* For Tie-Wire Wedge Anchor, TW-1400, use tension data from 1/4" diameter with 1-1/8" embedment.
*For continuous extreme low temperature applications, use stainless steel.

PERFORMANCE TABLE

Trubolt Wedge Anchors

Ultimate Tension and Shear Values (Lbs/kN) in Lightweight Concrete*

ANCHOR DIA. In. (mm)	INSTALLATION TORQUE Ft. Lbs. (Nm)	EMBEDMENT DEPTH In. (mm)	ANCHOR TYPE	LIGHTWEIGHT CONCRETE f'c = 3000 PSI (20.7 MPa) TENSION Lbs. (kN)	LIGHTWEIGHT CONCRETE f'c = 3000 PSI (20.7 MPa) SHEAR Lbs. (kN)	LOWER FLUTE OF STEEL DECK WITH LIGHTWEIGHT CONCRETE FILL f'c = 3000 PSI (20.7 MPa) TENSION Lbs. (kN)	LOWER FLUTE OF STEEL DECK WITH LIGHTWEIGHT CONCRETE FILL f'c = 3000 PSI (20.7 MPa) SHEAR Lbs. (kN)
3/8 (9.5)	25 (33.9)	1-1/2 (38.1)	WS-Carbon or WS-G Hot-Dipped Galvanized or WW-304 S.S. or SWW-316 S.S.	1,175 (5.2)	1,480 (6.6)	1,900 (8.5)	3,160 (14.1)
		3 (76.2)		2,825 (12.6)	2,440 (10.9)	2,840 (12.6)	4,000 (17.8)
1/2 (12.7)	55 (74.6)	2-1/4 (57.2)		2,925 (13.0)	2,855 (12.7)	3,400 (15.1)	5,380 (23.9)
		3 (76.2)		3,470 (15.4)	3,450 (15.3)	4,480 (19.9)	6,620 (29.4)
		4 (101.6)		4,290 (19.1)	3,450 (15.3)	4,800 (21.4)	6,440 (28.6)
5/8 (15.9)	90 (122.0)	3 (76.2)		4,375 (19.5)	4,360 (19.4)	4,720 (21.0)	5,500 (24.5)
		5 (127.0)		6,350 (28.2)	6,335 (28.2)	6,580 (29.3)	9,140 (40.7)
3/4 (19.1)	110 (149.2)	3-1/4 (82.6)		5,390 (24.0)	7,150 (31.8)	5,840 (26.0)	8,880 (39.5)
		5-1/4 (133.4)		7,295 (32.5)	10,750 (47.8)	7,040 (31.3)	N/A

*Allowable values are based upon a 4 to 1 safety factor. Divide by 4 for allowable load values.

PERFORMANCE TABLE

Trubolt Wedge Anchors — Recommended Edge and Spacing Distance Requirements for Shear Loads*

ANCHOR DIA. In. (mm)	EMBEDMENT DEPTH In. (mm)	ANCHOR TYPE	EDGE DISTANCE REQUIRED TO OBTAIN MAX. WORKING LOAD In. (mm)	MIN. EDGE DISTANCE AT WHICH THE LOAD FACTOR APPLIED = .60 In. (mm)	MIN. EDGE DISTANCE AT WHICH THE LOAD FACTOR APPLIED = .20 In. (mm)	SPACING REQUIRED TO OBTAIN MAX. WORKING LOAD In. (mm)	MIN. ALLOWABLE SPACING BETWEEN ANCHORS In. (mm) LOAD FACTOR APPLIED = .40
1/4 (6.4)	1-1/8 (28.6) 1-15/16 (49.2)	WS-Carbon or WS-G Hot-Dipped Galvanized or WW-304 S.S. or SWW-316 S.S.	2 (50.8) 1-15/16 (49.2)	1-5/16 (33.3) 1 (25.4)	N/A N/A	3-15/16 (100.0) 3-7/8 (98.4)	2 (50.8) 1-15/16 (49.2)
3/8 (9.5)	1-1/2 (38.1) 3 (76.2)		2-5/8 (66.7) 3-3/4 (95.3)	1-3/4 (44.5) 3 (76.2)	N/A 1-1/2 (38.1)	5-1/4 (133.4) 6 (152.4)	2-5/8 (66.7) 3 (76.2)
1/2 (12.7)	2-1/4 (57.2) 4-1/8 (104.8)		3-15/16 (100.0) 5-3/16 (131.8)	2-9/16 (65.1) 3-1/8 (79.4)	N/A 1-9/16 (39.7)	7-7/8 (200.0) 6-3/16 (157.2)	3-15/16 (100.0) 3-1/8 (79.4)
5/8 (15.9)	2-3/4 (69.9) 5-1/8 (130.2)		4-13/16 (122.2) 6-7/16 (163.5)	3-1/8 (79.4) 3-7/8 (98.4)	N/A 1-15/16 (49.2)	9-5/8 (244.5) 7-11/16 (195.3)	4-13/16 (122.2) 3-7/8 (98.4)
3/4 (19.1)	3-1/4 (82.6) 6-5/8 (168.3)		5-11/16 (144.5) 6-5/16 (160.3)	3-3/4 (95.3) 5 (127.0)	N/A 2-1/2 (63.5)	11-3/8 (288.9) 9-15/16 (252.4)	5-11/16 (144.5) 5 (127.0)
7/8 (22.2)	3-3/4 (95.3) 6-1/4 (158.8)		6-9/16 (166.7) 8-1/2 (215.9)	4-5/16 (109.5) 6-1/4 (158.8)	N/A 3-1/8 (79.4)	13-1/8 (333.4) 12-1/2 (317.5)	6-9/16 (166.7) 6-1/4 (158.8)
1 (25.4)	4-1/4 (108.0) 7-3/8 (187.3)		7-7/8 (200.0) 10-1/16 (255.6)	5-1/8 (130.2) 7-3/8 (187.3)	N/A 3-11/16 (93.7)	15-3/4 (400.1) 14-3/4 (374.7)	7-7/8 (200.0) 7-3/8 (187.3)

*Spacing and edge distances shall be divided by 0.75 when anchors are placed in structural lightweight concrete. Linear interpolation may be used for intermediate spacing and edge distances.

PERFORMANCE TABLE

Trubolt Wedge Anchors — Recommended Edge and Spacing Distance Requirements for Tension Loads*

ANCHOR DIA. In. (mm)	EMBEDMENT DEPTH In. (mm)	ANCHOR TYPE	EDGE DISTANCE REQUIRED TO OBTAIN MAX. WORKING LOAD In. (mm)	MIN. ALLOWABLE EDGE DISTANCE AT WHICH THE LOAD FACTOR APPLIED = .65 In. (mm)	SPACING REQUIRED TO OBTAIN MAX. WORKING LOAD In. (mm)	MIN. ALLOWABLE SPACING AT WHICH THE LOAD FACTOR APPLIED = .70 In. (mm)
1/4 (6.4)	1-1/8 (28.6) 1-15/16 (49.2) 2-1/8 (54.0)	WS-Carbon or WS-G Hot-Dipped Galvanized or WW-304 S.S. or SWW-316 S.S.	2 (50.8) 1-15/16 (49.2) 1-5/8 (41.3)	1 (25.4) 1 (25.4) 13/16 (20.6)	3-15/16 (100.0) 3-7/8 (98.4) 3-3/16 (81.0)	2 (50.8) 1-15/16 (49.2) 1-5/8 (41.3)
3/8 (9.5)	1-1/2 (38.1) 3 (76.2) 4 (101.6)		2-5/8 (66.7) 3 (76.2) 3 (76.2)	1-5/16 (33.3) 1-1/2 (38.1) 1-1/2 (38.1)	5-1/4 (133.4) 6 (152.4) 6 (152.4)	2-5/8 (66.7) 3 (76.2) 3 (76.2)
1/2 (12.7)	2-1/4 (57.2) 4-1/8 (104.8) 6 (152.4)		3-15/16 (100.0) 3-1/8 (79.4) 4-1/2 (114.3)	2 (50.8) 1-9/16 (39.7) 2-1/4 (57.2)	7-7/8 (200.0) 6-3/16 (157.2) 9 (228.6)	3-15/16 (100.0) 3-1/8 (79.4) 4-1/2 (114.3)
5/8 (15.9)	2-3/4 (69.9) 5-1/8 (130.2) 7-1/2 (190.5)		4-13/16 (122.2) 3-7/8 (98.4) 5-5/8 (142.9)	2-7/16 (61.9) 1-15/16 (49.2) 2-13/16 (71.4)	9-5/8 (244.5) 7-1/16 (195.3) 11-1/4 (285.8)	4-13/16 (122.2) 3-7/8 (98.4) 5-5/8 (142.9)
3/4 (19.1)	3-1/4 (82.6) 6-5/8 (168.3) 10 (254.0)		5-11/16 (144.5) 5 (127.0) 7-1/2 (190.5)	2-7/8 (73.0) 2-1/2 (63.5) 3-3/4 (95.3)	11-3/8 (288.9) 9-15/16 (252.4) 15 (381.0)	5-11/16 (144.5) 5 (127.0) 7-1/2 (190.5)
7/8 (22.2)	3-3/4 (95.3) 6-1/4 (158.8) 8 (203.2)		6-9/16 (166.7) 6-1/4 (158.8) 6 (152.4)	3-5/16 (84.1) 3-1/8 (79.4) 3 (76.2)	13-1/8 (333.4) 12-1/2 (317.5) 12 (304.8)	6-9/16 (166.7) 6-1/4 (158.8) 6 (152.4)
1 (25.4)	4-1/2 (114.3) 7-3/8 (187.3) 9-1/2 (241.3)		7-7/8 (200.0) 7-3/8 (187.3) 7-1/8 (181.0)	3-15/16 (100.0) 3-11/16 (93.7) 3-9/16 (90.5)	15-3/4 (400.1) 14-3/4 (374.7) 14-1/4 (362.0)	7-7/8 (200.0) 7-3/8 (187.3) 7-1/8 (181.0)

*Spacing and edge distances shall be divided by 0.75 when anchors are placed in structural lightweight concrete. Linear interpolation may be used for intermediate spacing and edge distances.

Combined Tension and Shear Loading—for Trubolt Anchors

Allowable loads for anchors subjected to combined shear and tension forces are determined by the following equation:

$$(Ps/Pt)^{5/3} + (Vs/Vt)^{5/3} \leq 1$$

Ps = Applied tension load Vs = Applied shear load Pt = Allowable tension load Vt = Allowable shear load

Trubolt Strength Design Performance values in accordance to 2006 IBC

ITW RED HEAD TRUBOLT WEDGE ANCHOR

DESIGN INFORMATION TESTED TO ICC-ES AC193 AND ACI 355.2, IN ACCORDANCE WITH 2006 IBC

Trubolt® Wedge Anchors

TRUBOLT WEDGE ANCHOR DESIGN INFORMATION[1,2,3]

DESIGN INFORMATION	Symbol	Units	Nominal Anchor Diameter									
			1/4		3/8		1/2		5/8		3/4	
Anchor O.D.	d_o	in	0.250		0.375		0.500		0.625		0.750	
Effective embedment	h_{ef}	in	1-1/2	2	1-3/4	2-5/8	1-7/8	3-3/8	2-1/2	4	3-1/2	4-3/4
Minimum member thickness	h_{min}	in	4	4	4	5	5	6	5	8	6	8
Critical edge distance	c_{ac}	in	2-5/8	3	2-5/8	5-1/4	3-3/4	6-3/4	5	8	7	9
Minimum edge distance	c_{min}	in	1-3/4	1-1/2	2-1/4	2	3-3/4	3-3/4	4-1/4	3-1/4	3-3/4	3-1/2
Minimum anchor spacing	s_{min}	in	1-3/4	1-1/2	2-1/4	2	3-3/4	3-3/4	4-1/4	3-1/4	3-3/4	3-1/2
Min. Specified Yield Strength	f_y	lb/in²	55,000									
Min. Specified Ultimate Strength	f_{uta}	lb/in²	75,000									
Effective tensile stress area	A_{se}	in²	0.032		0.078		0.142		0.226		0.334	
Steel strength in tension	N_s	lb	2,385		5,815		10,645		16,950		25,050	
Steel strength in shear	V_s	lb	1,430		2,975	3,490	4,450	6,385	6,045	10,170	10,990	15,030
Pullout strength, uncracked concrete	$N_{p,uncr}$	lb	1,392	1,706	2,198	3,469	2,400	4,168	4,155	6,638	8,031	10,561
Anchor Category (All anchors are ductile)			1									
Effectiveness factor k_{uncr}, uncracked concrete			24									
Axial stiffness in service load range	β	lb/in	14,651	9,385	17,515	26,424	32,483	26,136	42,899	21,749	43,576	28,697
Coefficient for variation for axial stiffness in service load range			34	47	28	45	17	33	55	22	63	28
Strength reduction factor ϕ for tension, steel failure modes			0.75									
Strength reduction factor ϕ for shear, steel failure modes			0.65									
Strength reduction factor ϕ for tension, concrete failure modes, Condition B			0.65									
Strength reduction factor ϕ for shear, concrete failure modes, Condition B			0.70									

[1] Trubolt+ Anchor Design Strengths must be determined in accordance with ACI 318-05 Appendix D and this table
[2] The Trubolt+ Wedge Anchor is a ductile steel element as defined by ACI 318 D.1
[3] 1/4", 3/8", & 1/2" diameter data is listed in ICC-ES ESR-2251.

Trubolt® Wedge Anchors

TRUBOLT WEDGE ANCHOR (INSTALLED)

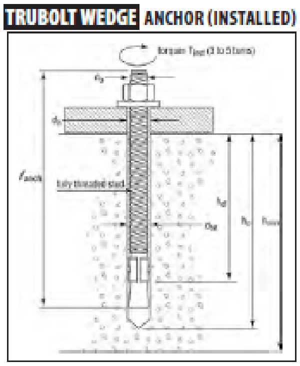

TRUBOLT WEDGE INSTALLATION INFORMATION

	Symbol	Units	Nominal Anchor Diameter (in.)									
			1/4		3/8		1/2		5/8		3/4	
Anchor outer diameter	d_o	in	0.25		0.375		0.5		0.625		0.750	
Nominal carbide bit diameter	d_{bit}	in	1/4		3/8		1/2		5/8		3/4	
Effective embedment depth	h_{ef}	in	1-1/2	2	1-3/4	2-5/8	1-7/8	3-3/8	2-1/2	4	3-1/2	4-3/4
Min hole depth	h_o	in	2	2-1/2	2-1/2	3-3/8	2-3/4	4-1/4	3-3/4	5-1/4	4-3/4	6
Min slab thickness	h_{min}	in	4		4	5	5	6	5	8	6	8
Installation torque	T_{inst}	ft-lb	4		25		55		90		110	
Min hole diameter in fixture	d_h	in	5/16		7/16		9/16		11/16		13/16	

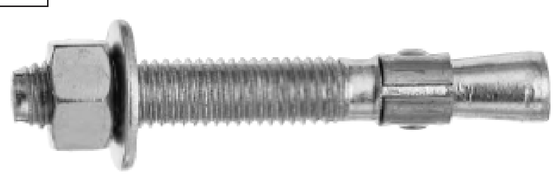

Trubolt Strength Design Performance values in accordance to 2006 IBC

Trubolt®
Wedge Anchors

TRUBOLT WEDGE PULLOUT STRENGTH ($N_{p,\,unc}$) (POUNDS) [1]

Nominal Anchor Diameter (in.)	Effective Embedment Depth (in.)	Concrete Compressive Strength			
		f'c = 2,500 psi	f'c = 3,000 psi	f'c = 4,000 psi	f'c = 6,500 psi
1/4	1-1/2	1,392	1,525	1,610	1,822
	2	1,706	1,869	1,947	2,151
3/8	1-3/4	2,198	2,408	2,621	3,153
	2-5/8	3,469	3,800	3,936	4,275
1/2	1-7/8	2,400	2,629	3,172	4,520
	3-3/8	4,168	4,520	4,520	4,520
5/8	2-1/2	4,155	4,155	4,376	5,578
	4	6,638	6,900	7,968	10,157
3/4	3-1/2	8,031	8,322	9,610	12,251
	4-3/4	10,561	10,561	10,561	12,251

For SI: 1 Inch = 25.4 mm, 1 lbf = 4.45 N, 1 psi = 0.006895 Mpa
1 Values are for single anchors with no edge distance or spacing reduction.

TRUBOLT WEDGE ANCHOR ALLOWABLE STATIC TENSION (ASD), NORMAL-WEIGHT UNCRACKED CONCRETE [1-6]

Nominal Anchor Diameter (in.)	Effective Embedment Depth (in.)	Concrete Compressive Strength			
		f'c = 2,500 psi	f'c = 3,000 psi	f'c = 4,000 psi	f'c = 6,500 psi
1/4	1-1/2	611	670	707	800
	2	749	821	855	945
3/8	1-3/4	965	1,058	1,151	1,385
	2-5/8	1,524	1,669	1,729	1,878
1/2	1-7/8	1,054	1,155	1,393	1,985
	3-3/8	1,831	1,985	1,985	1,985
5/8	2-1/2	1,825	1,825	1,922	2,450
	4	2,915	3,030	3,499	4,461
3/4	3-1/2	3,527	3,655	4,221	5,381
	4-3/4	4,638	4,638	4,638	5,381

For SI: 1 Inch = 25.4 mm, 1 lbf = 4.45 N, 1 psi = 0.006895 Mpa
Design Assumptions:
1 Single anchor with static tension load only.
2 Concrete determined to remain uncracked for the life of the anchorage.
3 Load combinations from 2006 IBC, Sections 1605.2.1 and 1605.3.1 (no seismic loading).
4 Thirty percent dead load and 70 percent live load, controlling load combination 1.2D + 1.6L
5 Calculation of weighted average: 1.2D + 1.6L = 1.2 (0.3) + 1.6 (0.7) = 1.48
6 Values do not include edge distance or spacing reductions.

2006 IBC Compliant

TRUBOLT WEDGE ANCHOR ALLOWABLE STATIC SHEAR (ASD), STEEL (POUNDS) [1-5]

Nominal Anchor Diameter (in.)	Effective Embedment Depth (in.)	Allowable Steel Capacity, Static Shear
1/4	1-1/2	628
	2	
3/8	1-3/4	1,307
	2-5/8	1,533
1/2	1-7/8	1,954
	3-3/8	2,804
5/8	2-1/2	2,655
	4	4,467
3/4	3-1/2	4,827
	4-3/4	6,601

For SI: 1 Inch = 25.4 mm, 1 lbf = 4.45 N, 1 psi = 0.006895 Mpa
Design Assumptions:
1 Single anchor with static shear load only.
2 Load combinations from 2006 IBC, Sections 1605.2.1 and 1605.3.1 (no seismic loading).
3 Thirty percent dead load and 70 percent live load, controlling load combination 1.2D + 1.6L
4 Calculation of weighted average: 1.2D + 1.6L = 1.2 (0.3) + 1.6 (0.7) = 1.48
5 Values do not include edge distance or spacing reductions.

APPENDIX H DATA ACQUISTION INSTRUMENTION

Omega Type T thermocouples were used for the fluid temperature measurements.

Quick Disconnect Thermocouples

with Miniature Connectors
Standard and Metric Dimensions

Starts at **$24**

MADE IN USA — See Section W

Available as SUPER OMEGACLAD XL — See page A-43 to A-48.

- Glass Filled Nylon Connector Body Rated to 220°C (425°F)
- 304, 310, 316, 321 SS, Inconel, or Super OMEGACLAD® XL Sheath
- Standard 6 and 12" Lengths Available†
- Sheath Diameters from 0.010 to 0.125"
- Grounded, Ungrounded, or Exposed Junction
- Mating Connector, Cable Clamp, and Locking Clip Included FREE!
- Color-Coded SMP Miniature Connector Termination
- Custom Lengths Available

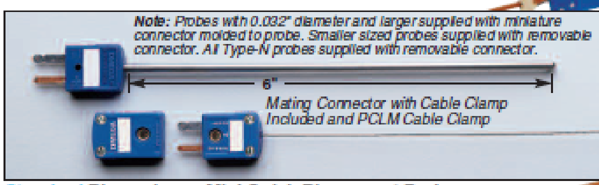

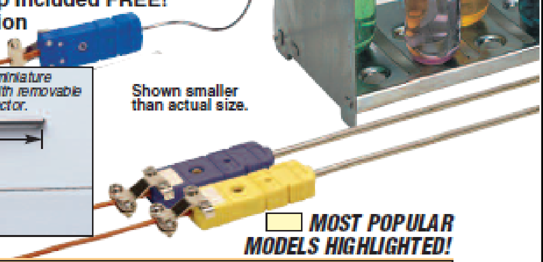

MOST POPULAR MODELS HIGHLIGHTED!

Standard Dimensions - Mini Quick Disconnect Probes

To Order *(Specify Model Number)*

Alloy/ANSI Color Code	Sheath Dia. inches	Model No. 6" Length	Price G*/E*	Price U*	Model No. 12" Length	Price G*/E*	Price U*	Price/Add'l 6"
Iron-Constantan 304 SS Sheath J	0.010	JMQSS-010(*)-6	$48.00	$68.00	JMQSS-010(*)-12	$49.25	$69.25	$1.25
	0.020	JMQSS-020(*)-6	28.00	30.00	JMQSS-020(*)-12	28.65	30.65	0.65
	0.032	JMQSS-032(*)-6	28.00	30.00	JMQSS-032(*)-12	28.65	30.65	0.65
	0.040	JMQSS-040(*)-6	28.00	30.00	JMQSS-040(*)-12	28.65	30.65	0.65
	0.062	JMQSS-062(*)-6	24.00	26.00	JMQSS-062(*)-12	24.80	26.80	0.80
	0.125	JMQSS-125(*)-6	24.00	26.00	JMQSS-125(*)-12	24.95	26.95	0.95
CHROMEGA®-ALOMEGA® 304 SS Sheath K	0.010	KMQSS-010(*)-6	$48.00	$68.00	KMQSS-010(*)-12	$49.25	$69.25	$1.25
	0.020	KMQSS-020(*)-6	28.00	30.00	KMQSS-020(*)-12	28.65	30.65	0.65
	0.032	KMQSS-032(*)-6	28.00	30.00	KMQSS-032(*)-12	28.65	30.65	0.65
	0.040	KMQSS-040(*)-6	28.00	30.00	KMQSS-040(*)-12	28.65	30.65	0.65
	0.062	KMQSS-062(*)-6	24.00	26.00	KMQSS-062(*)-12	24.80	26.80	0.80
	0.125	KMQSS-125(*)-6	24.00	26.00	KMQSS-125(*)-12	24.95	26.95	0.95
CHROMEGA®-ALOMEGA® Super OMEGACLAD® XL Sheath K	0.010	KMQXL-010(*)-6	$51.00	$71.00	KMQXL-010(*)-12	$52.20	$72.35	$2.50
	0.020	KMQXL-020(*)-6	31.00	33.00	KMQXL-020(*)-12	31.65	33.65	2.50
	0.032	KMQXL-032(*)-6	31.00	33.00	KMQXL-032(*)-12	31.65	33.65	2.50
	0.040	KMQXL-040(*)-6	31.00	33.00	KMQXL-040(*)-12	31.65	33.65	0.85
	0.062	KMQXL-062(*)-6	27.00	29.00	KMQXL-062(*)-12	27.80	29.80	1.05
	0.125	KMQXL-125(*)-6	27.00	29.00	KMQXL-125(*)-12	27.95	29.80	2.10
OMEGA-P®-OMEGA-N® Super OMEGACLAD® XL Sheath N	0.020	NMQXL-020(*)-6	$31.00	$33.00	NMQXL-020(*)-12	$31.65	$33.65	$2.50
	0.032	NMQXL-032(*)-6	31.00	33.00	NMQXL-032(*)-12	31.65	33.65	2.50
	0.040	NMQXL-040(*)-6	31.00	33.00	NMQXL-040(*)-12	31.65	33.65	0.85
	0.062	NMQXL-062(*)-6	27.00	29.00	NMQXL-062(*)-12	27.80	29.80	1.05
	0.125	NMQXL-125(*)-6	27.00	29.00	NMQXL-125(*)-12	27.95	29.80	2.10
CHROMEGA®-Constantan 304 SS Sheath E	0.010	EMQSS-010(*)-6	$48.00	$68.00	EMQSS-010(*)-12	$49.25	$69.80	$1.25
	0.020	EMQSS-020(*)-6	28.00	30.00	EMQSS-020(*)-12	28.65	30.65	0.65
	0.032	EMQSS-032(*)-6	28.00	30.00	EMQSS-032(*)-12	28.65	30.65	0.65
	0.040	EMQSS-040(*)-6	28.00	30.00	EMQSS-040(*)-12	28.65	30.65	0.65
	0.062	EMQSS-062(*)-6	24.00	26.00	EMQSS-062(*)-12	24.80	26.80	0.80
	0.125	EMQSS-125(*)-6	24.00	26.00	EMQSS-125(*)-12	24.95	26.95	0.95
Copper-Constantan 304 SS Sheath T	0.020	TMQSS-020(*)-6	$28.00	$30.00	TMQSS-020(*)-12	$28.65	$30.65	$0.65
	0.032	TMQSS-032(*)-6	28.00	30.00	TMQSS-032(*)-12	28.65	30.65	0.65
	0.040	TMQSS-040(*)-6	28.00	30.00	TMQSS-040(*)-12	28.65	30.65	0.65
	0.062	TMQSS-062(*)-6	24.00	26.00	TMQSS-062(*)-12	24.80	26.95	0.80
	0.125	TMQSS-125(*)-6	24.00	26.00	TMQSS-125(*)-12	24.95	26.95	0.95
OMEGALLOY® Inconel 600 Sheath N	0.010	NMQIN-010(*)-6	$48.00	$68.00	NMQIN-010(*)-12	$49.25	$69.25	$1.25
	0.020	NMQIN-020(*)-6	28.00	30.00	NMQIN-020(*)-12	29.00	30.80	0.65
	0.032	NMQIN-032(*)-6	28.00	30.00	NMQIN-032(*)-12	29.00	30.80	0.65
	0.040	NMQIN-040(*)-6	28.00	30.00	NMQIN-040(*)-12	29.00	30.80	0.65
	0.062	NMQIN-062(*)-6	24.00	26.00	NMQIN-062(*)-12	24.80	26.95	0.80
	0.125	NMQIN-125(*)-6	24.00	26.00	NMQIN-125(*)-12	24.95	26.95	0.95

** Specify junction type: E (exposed), G (grounded), or U (ungrounded). † Other lengths available, consult Sales Department.* ***To order with Inconel Sheath,*** *Change "SS" in model no. to "IN". No additional charge. Type J is not available in Inconel 0.010 diameter. Example:* ***KMQIN-125G-6, $24.***

For metric probe configurations with glass filled nylon connector body refer to page A-54 and remove the "H" from the model number, and $3 from price.

To Order with 310, 316, or 321 SS Sheath, *change "SS" in model no. to "310SS", "316SS", or "321SS", respectively. No add'l charge. Example:* ***TMQ321SS-125G-6, $24.***

Ordering Example: KMQSS-125G-6, *subminiature quick-disconnect probe, Type K, 0.125" OD stainless steel sheath, 6" length, grounded junction,* ***$24.***

KMQSS-M300U-300, *subminiature quick-disconnect probe, Type K, stainless steel sheath, 3 mm OD, 300 mm length, ungrounded junction,* ***$26.95.***

A-53

PreCon/Kele thermistor.

TEMPERATURE

OUTDOOR AIR THERMISTOR AND RTD SENSORS

ST-O* SERIES

DESCRIPTION

The Precon **ST-O* Series Outdoor Air Sensors** provide remote temperature sensing for building automation systems and mechanical equipment room instrumentation. The temperature-sensitive element is sheathed in a stainless steel tube and mounted inside a ventilated, to minimize radiant energy and weather related effects.

FEATURES

- ***Lifetime warranty***
- ***Vented weather shield for quick response***
- ***Moistureproof with 8' (2.4m) lead***

Precon A Division of Kele, Inc.

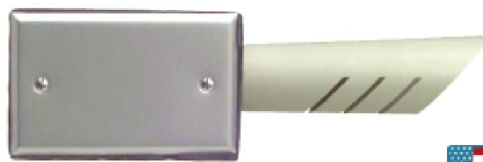

ST-O

MADE IN USA

MOUNTING/WIRING

Mounting
Toggle bolts or other direct wall mount screws can be used for outside mounting. For conduit connections, 3/4" NPT threads are available in the back and side.

Wiring
Terminate using the full 8' (2.44m) lead length provided to avoid moisture migration from the field connection. Solder the leads where possible or use crimp-type butt splice. Wire nuts are not recommended.

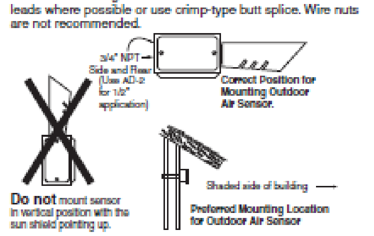

For best results do not mount above doors, windows, air intakes, or exhausts.

DIMENSIONS

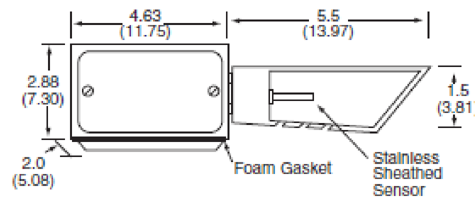

SPECIFICATIONS

Accuracy	
Thermistor	±0.36°F (0.2°C)
RTD (.385)	±0.27°F (±0.15°C)
RTD (.375)	±0.54°F (±0.30°C)
Sensor types available	
Thermistor	2.252 kΩ, 3 kΩ, 10 kΩ, 20 kΩ, 100 kΩ
RTD	Platinum 100Ω, 1000Ω, 385 curve Platinum 1000Ω, 375 curve
Temperature range	
Thermistor	-30° to 140°F (-34° to 60°C)
RTD	-67° to 140°F (-55° to 60°C)
Temperature response	
Thermistor	Negative temperature coefficient
RTD	Positive temperature coefficient
Stability	
Thermistor	0.24°F (0.13°C) over five years
RTD	<0.09°F (0.05°C) over five years
Connections	8' (2.44m) of 24 AWG pigtails prestripped
Mounting	Directly to wall with screws or toggle bolts
Weight	1 lb (0.45 kg)
Warranty	Lifetime

ORDERING INFORMATION

MODEL	DESCRIPTION
ST-O3	OSA temperature sensor, 10 kΩ thermistor Type III
ST-O21	OSA temperature sensor, 2250Ω thermistor Type II
ST-O22	OSA temperature sensor, 3 kΩ thermistor Type II
ST-O24	OSA temperature sensor, 10 kΩ thermistor Type II
ST-O27	OSA temperature sensor, 100 kΩ thermistor Type II
ST-O42	OSA temperature sensor, 20 kΩ thermistor Type IV
ST-O81	OSA temperature sensor, 100Ω RTD .385 curve
ST-O85	OSA temperature sensor, 1 kΩ RTD .385 curve
ST-O91	OSA temperature sensor, 1 kΩ RTD .375 curve

Kele thermistor resistance chart.

The **PreCon** sensor has a dissipation constant in still air at 25°C of 2.7 mW/°C. The heat dissipation constant is an expression in milliwatts of the power required to raise the temperature of a thermistor 1°C above the ambient.

	PreCon TYPE II				PreCon TYPE III	PreCon TYPE IV
	Model 21 2,252 ohm at 77°F ±0.36°F from 32°F to 158°F	**Model 22** 3,000 ohm at 77°F ±0.36°F from 32°F to 158°F	**Model 24** 10,000 ohm at 77°F ±0.36°F from 32°F to 158°F	**Model 27** 100,000 ohm at 77°F ±0.36°F at 77°F ±1.3°F from 32° to 158°F	**Model 3** 10,000 ohm at 77°F ±0.36°F from 32°F to 158°F	**Model 42** 20,000 ohm at 77°F ±0.36°F from 32°F to 158°F
TEMP°F	RESISTANCE	RESISTANCE	RESISTANCE	RESISTANCE	RESISTANCE	RESISTANCE
-35	63.08K	84.09K	280.1K	2801K	203.6K	
-30	52.72K	70.27K	234.1K	2341K	173.6K	
-25	44.20K	58.92K	196.3K	1963K	148.3K	
-20	37.19K	49.56K	165.1K	1651K	127.1K	
-15	31.38K	41.83K	139.3K	1393K	109.2K	
-10	26.57K	35.41K	118.0K	1180K	94.07K	270.6K
-5	22.57K	30.07K	100.2K	1002K	81.23K	228.0K
0	19.22K	25.61K	85.35K	853.5K	70.32K	192.6K
5	16.42K	21.88K	72.91K	729.1K	61.02K	163.1K
10	14.07K	18.74K	62.48K	624.8K	53.07K	138.7K
15	12.08K	16.10K	53.64K	536.4K	46.27K	118.3K
20	10.41K	13.87K	46.23K	462.3K	40.42K	101.0K
25	8988	11.98K	39.91K	399.1K	35.39K	86.60K
30	7782	10.37K	34.56K	345.6K	31.06K	74.40K
35	6755	8999	30.00K	300.0K	27.31K	64.10K
40	5877	7830	26.10K	261.0K	24.06K	55.30K
45	5126	6830	22.76K	227.6K	21.24K	47.89K
50	4482	5971	19.90K	199.0K	18.79K	41.40K
55	3927	5231	17.44K	174.4K	16.65K	36.10K
60	3448	4594	15.31K	153.1K	14.78K	31.44K
65	3035	4043	13.48K	134.8K	13.15K	27.46K
70	2676	3565	11.88K	118.8K	11.72K	24.02K
75	2365	3150	10.50K	105.0K	10.46K	21.06K
80	2094	2789	9298	92.98K	9354	18.50K
85	1858	2475	8250	82.50K	8378	16.29K
90	1651	2200	7331	73.31K	7516	14.37K
95	1471	1959	6532	65.32K	6754	12.69K
100	1312	1748	5826	58.26K	6078	11.24K
105	1173	1562	5209	52.09K	5479	9.97K
110	1050	1399	4663	46.63K	4947	8.86K
115	941.8	1254	4182	41.82K	4472	7.88K
120	846.0	1127	3757	37.57K	4049	7.03K
125	761.3	1014	3381	33.81K	3671	6.27K
130	686.1	913.9	3047	30.47K	3333	5.61K
135	619.4	825.0	2750	27.50K	3031	5.03K
140	559.9	745.9	2486	24.86K	2759	4.51K
145	507.0	675.4	2251	22.51K	2515	4.06K
150	459.7	612.4	2041	20.41K	2296	3.65K
155	417.5	556.2	1854	18.54K	2098	3.29K
160	379.6	505.8	1686	16.86K	1920	2.97K
165	345.7	460.7	1535	15.35K	1759	2.69K
170	315.2	420.1	1400	14.00K	1614	2.43K
175	287.8	383.7	1278	12.78K	1482	2.20K
180	263.1	350.8	1168	11.68K	1362	2.00K
185	240.9	321.2	1070	10.70K	1254	1.82K
190	220.8	294.5	980.5	9805	1156	1.65K
195	202.6	270.3	899.6	8996	1066	1.51K
200	186.2	248.4	826.8	8268	984.0	1.38K
205	171.3	228.5	760.7	7607	909.8	1.26K
210	157.8	210.5	700.7	7007	841.9	1.15K
215	145.5	194.1	646.1	6461	779.8	1.05K
220	134.3	179.2	596.4	5964	723.0	967.5
225	124.2	165.6	551.5	5515	671.0	888.4
230	114.9	153.2	510.2	5102	623.3	816.6
235	106.4	141.9	472.5	4725	579.5	
240	98.7	131.5	438.3	4383	539.4	

Example Solution of the thermistor Steinhart-Hart equation

File:G:\Master's Project\Campbell Scientific\thermistor.EES 12/22/2011 9:53:15 AM Page 1

EES Ver. 8.908: #0317: For use only by students and faculty in Civil & Environmental Engineering Univ. of Colorado

"PreCon Resistance chart"

T_1 = (-10+459.67) * (5/9) *"Farenheit to Kelvin"*
R_1 = 118000 *"Sensor Resistance"*

T_2 = (40+459.67) * (5/9) *"Farenheit to Kelvin"*
R_2 = 26100 *"Sensor Resistance"*

T_3 = (90+459.67) * (5/9) *"Farenheit to Kelvin"*
R_3 = 7331 *"Sensor Resistance"*

1/T_1 = A + B*ln(R_1) + C * (ln(R_1))^3 *"Solving for the three coefficients"*

1/T_2 = A + B*ln(R_2) + C * (ln(R_2))^3

1/T_3 = A + B*ln(R_3) + C * (ln(R_3))^3

"Checking the measurements"

E_th = 3.065 *"Diff. voltage measured"*
E_ex = 4.94 *"Excitation voltage"*

R_r = 10000 *"Reference Resistance"*

R = (R_r*E_th)/(E_ex -E_th) *"Resistance of thermistor"*
1/T = A + B*ln(R) + C * (ln(R))^3 *"The Steinhart-Hart Equation"*

DissipationConstant = 0.0027 [W/C] *"Dissipation Constant"*

T_corrected = T - ((E_ex^2/R)/DissipationConstant)
T_F = ((T_corrected * (9/5)) - 459.67) *"Farenheit"*
T_C = T_corrected- 273.15 *"Celcius"*

SOLUTION

Unit Settings: SI C kPa kJ mass deg

A = 0.001128	B = 0.0002343
C = 8.701E-08	DissipationConstant = 0.0027 [W/C]
E_{ex} = 4.94 [volts]	E_{th} = 3.065 [volts]
R = 16347 [Ωs]	R_1 = 118000
R_2 = 26100	R_3 = 7331
R_r = 10000 [Ωs]	T = 287.3
T_1 = 249.8	T_2 = 277.6
T_3 = 305.4	T_C = 13.6
$T_{corrected}$ = 286.7 [kelvin]	T_F = 56.47

5 potential unit problems were detected.

KEY VARIABLES

A = 0.001128
B = 0.0002343
C = 8.701E-08
E_{th} = 3.065 [volts] *Measured Differential voltage*
E_{ex} = 4.94 [volts] *Excitation voltage*
R = 16347 [Ωs] *Calculated Thermistor resistance*

File:G:\Master's Project\Campbell Scientific\thermistor.EES 12/22/2011 9:53:15 AM Page 2
EES Ver. 8.908: #0317: For use only by students and faculty in Civil & Environmental Engineering Univ. of Colorado

R_r = 10000 [Ωs] *Reference resistance*
$T_{corrected}$ = 286.7 [kelvin] *Corrected temperature after applying the dissipation constant*

The omega flow meter.

LONG-LIFE PULSE OUTPUT WATER METERS

For Remote Rate Indication and Totalization

FTB4600 Series
Starts at
$180

1 YEAR WARRANTY

- For Water Flows from 0.15 to 20 GPM
- Economical
- High Turndown Ratio
- Up to ±1.5% Rdg Accuracy

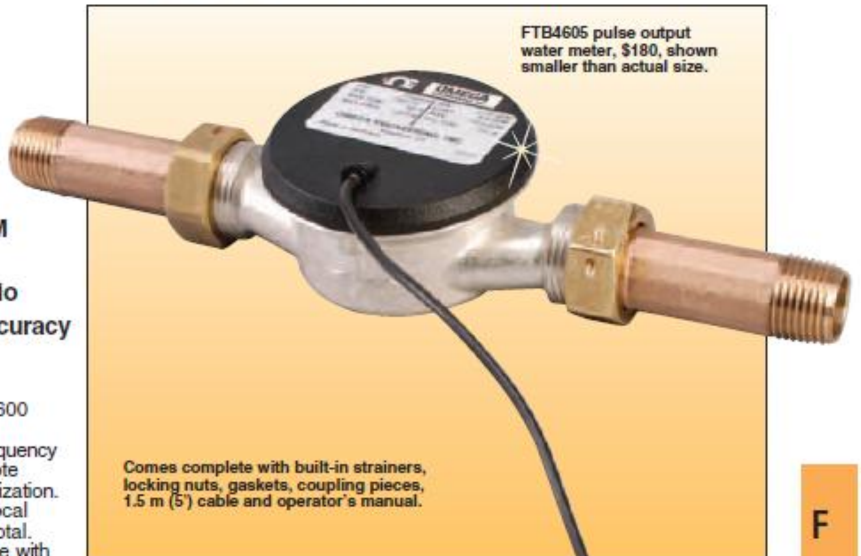

FTB4605 pulse output water meter, $180, shown smaller than actual size.

Comes complete with built-in strainers, locking nuts, gaskets, coupling pieces, 1.5 m (5') cable and operator's manual.

Designed for long-term water billing applications, the FTB4600 Series flowmeters are highly accurate and feature a high-frequency pulse output suitable for remote flow-rate indication or flow totalization. For economy, they have no local indication of the flow rate or total. The pulse output is compatible with OMEGA's DPF400 and DPF700 Series ratemeter/totalizers. All meters come with built-in strainers, locking nuts, gaskets, coupling pieces, and 1.5 m (5') of 3-conductor copper wire.

SPECIFICATIONS

Accuracy: From 10% of continuous to max flow: ±1.5% of rate; below 10% of continuous flow: 2% of rate
Fluid Temperature Range: 0 to 88°C (32 to 190°F)
Wetted Parts: Brass body, stainless steel, polyimide (fiberglass), polypropylene, EPDM O-ring
Pressure Drop (at Continuous Flow Rate): 2.9 psid
Max Pressure: 150 psig
Pulse Output: Requires 6 to 16 Vdc @ 10 mA max power; output requires pull-up to positive DC voltage; includes 1.5 m (5') of cable
Duty Cycle: 50-50

DPF700 Series ratemeter/totalizer/ batch controller, $260. See page M-5.

F

AVAILABLE FOR FAST DELIVERY!

To Order *(Specify Model Number)*

Bronze Body

Model No.	Price	Port Size	Flow Rate (GPM) Min	Flow Rate (GPM) Cont	Flow Rate (GPM) Max	Dimensions: mm (in) Length	Dimensions: mm (in) Height	Dimensions: mm (in) Width	Weight kg (lb)	Pulses per Gallon
FTB4605	$180	½"	0.15	6.6	13.0	110 (4.3)	70 (2.75)	70 (2.75)	0.5 (1.1)	151.4
FTB4607	200	¾"	0.22	11.0	20.0	130 (5.13)	73 (2.9)	70 (2.75)	0.6 (1.4)	75.7
FW-0119	160	Reference Book: Flow Measurement								

Comes complete with built-in strainers, locking nuts, gaskets, coupling pieces, 1.5 m (5') cable and operator's manual.
***Ordering Examples:** **FTB4605**, bronze body water meter, ½" port size, **$180**.*

LI-200SA Pyranometer Sensor

LI-COR, Inc. Toll Free: 1-800-447-3576 (U.S. & Canada) • Phone: 402-467-3576 • FAX: 402-467-2819 • E-mail: envsales@env.licor.com • Internet: http://www.licor.com

Total Solar Radiation

The LI-200SA Pyranometer is designed for field measurement of global solar radiation in agricultural, meteorological, and solar energy studies. In clear unobstructed daylight conditions, the LI-COR pyranometer compares favorably with first class thermopile type pyranometers (1, 2), but is priced at a fraction of the cost.

Patterned after the work of Kerr, Thurtell and Tanner (3), the LI-200SA features a silicon photovoltaic detector mounted in a fully cosine-corrected miniature head. Current output, which is directly proportional to solar radiation, is calibrated against an Eppley Precision Spectral Pyranometer (PSP) under natural daylight conditions in units of watts per square meter (w m^{-2}). Under most conditions of natural daylight, the error is <5%.

The spectral response of the LI-200SA does not include the entire solar spectrum (Figure 1), so it must be used in the same lighting conditions as those under which it was calibrated. Therefore, the LI-200SA should only be used to measure unobstructed daylight. It should NOT be used under vegetation, artificial lights, in a greenhouse, or for reflected solar radiation.

LI-200SA Pyranometer Sensor

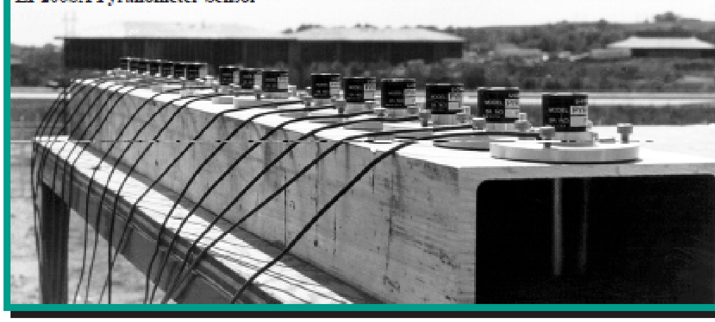

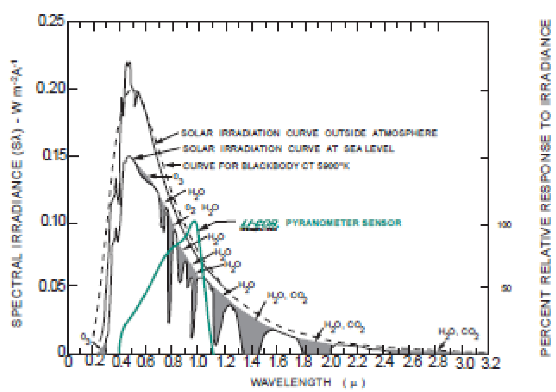

Figure 1. The LI-200SA Pyranometer spectral response is illustrated along with the energy distribution in the solar spectrum (3).

LI-200SA Specifications

Calibration: Calibrated against an Eppley Precision Spectral Pyranometer (PSP) under natural daylight conditions. Typical error under these conditions is ± 5%.

Sensitivity: Typically 90 μA per 1000 W m^{-2}.

Linearity: Maximum deviation of 1% up to 3000 W m^{-2}.

Stability: < ± 2% change over a 1 year period.

Response Time: 10 μs.

Temperature Dependence: 0.15% per °C maximum.

Cosine Correction: Cosine corrected up to 80° angle of incidence.

Azimuth: < ± 1% error over 360° at 45° elevation.

Tilt: No error induced from orientation.

Operating Temperature: -40 to 65°C.

Relative Humidity: 0 to 100%.

Detector: High stability silicon photovoltaic detector (blue enhanced).

Sensor Housing: Weatherproof anodized aluminum case with acrylic diffuser and stainless steel hardware.

Size: 2.38 Dia. × 2.54 cm H (0.94" × 1.0").

Weight: 28 g (1 oz).

Cable Length: 3.0 m (10 ft).

Ordering Information

The LI-200SA Pyranometer Sensor cable terminates with a BNC connector that connects directly to the LI-250 Light Meter or LI-1400 DataLogger. The 2220 Millivolt Adapter should be ordered if the LI-200SA will be used with a strip chart recorder or datalogger that measures millivolts. The 2220 uses a 147 ohm precision resistor to convert the LI-200SA output from microamps to millivolts. The sensor can also be ordered with bare leads (without the connector) designated LI-200SZ. Both are available with 50 foot cables, LI-200SA-50 or LI-200SZ-50. The 2003S Mounting and Leveling Fixture is recommended for each sensor unless other provisions for mounting are made. Other accessories are described on the Accessory Sheet.

LI-200SA Pyranometer
LI-200SZ Pyranometer
LI-200SA-50 Pyranometer
LI-200SZ-50 Pyranometer
2220 Millivolt Adapter
2003S Mounting and Leveling Fixture
2222SB-50 Extension Cable
2222SB-100 Extension Cable

HOME | ABOUT US | CONTACT US

HOW TO ORDER

Home » Anemometers » Vortex Wind Sensor

INSPEED VORTEX WIND SENSOR

Rugged wind sensor handles speeds from 5 to over 125 mph. Reed switch/magnet provides one pulse per rotation. Comes with exterior grade wire (click add to cart to see standard wire lengths), custom lengths available on request. The VORTEX wind sensor is great for do-it-yourself projects, replacement, or additional parts. Mounting pole not included.

NEW (as of April 2008): Now with a Sapphire Bearing to minimize wear!

Select Add To Cart for wire length and other options.

Price: from $55.00

ADD TO CART

Click for larger view of image

FULL PRODUCT DESCRIPTION | SPECIFICATIONS | ADDITIONAL PHOTOS | OWNERS MANUAL | WARRANTY / SUPPORT

SENSOR TYPE	3-Cup rotor Reed switch/magnet provide 1 pulse per rotation.
OUTPUT for D2 Rotor (Shown in photo)	1 pulse per rotation 2.5 mph per Hz
OUTPUT for Maximum Rotor (Sold on products prior to ~May 2005)	1 pulse per rotation 3.4 mph per Hz
ROTOR DIAMETER	approx. 5 in (~125 mm)
SPEED RANGE	approx. 3 mph to 125+ mph (~5 kph to over 200 kph)
MOUNTING BRACKET	Supplied with an aluminum mounting bracket with 2 holes for screws. Designed to be mounted on top of a pole or bracket. Custom brackets available up request (offset, for example)
WIRE	Standard length is 25 feet (8m) custom lengths available upon request - tested OK to over 1,500 feet The wire is provided stripped and unterminated 2 small wire nuts provided to connect to the display once installed
DISPLAY	None provided with the sensor only Formula for converting pulses to speed: 2.5 mph per Hz (2.5 mph per pulse/second)
POWER	No power required

Related Keywords: anemometer, hand held wind meter, stormchaser, weather instruments, wind,windmeter, wind sensor, windsensor

INSPEED.COM

Anemometers | Wind Energy | Wind Speed & Direction | About Us | How to Order | Contact Us
10 Hudson Road Sudbury, MA 01776 Phone: (978) 397-6813 Email: see "Contact Us"

APPENDIX I STRUCTURAL CALCULATIONS

File:C:\Users\estep\Documents\Master's Project\Unistrut\Anchor Calcs.EES 10/27/2011 1:06:16 PM Page 1
EES Ver. 8.908: #0317: For use only by students and faculty in Civil & Environmental Engineering Univ. of Colorado

A simplified approach for determining the pull-out strength of wind on the solar framing and the static loading on the structure and concrete anchors.

Design wind calculations

Given Information

$P_{atm,5000} = 84.3$ *atmospheric pressure at 5000'*

$T_{winter,typical} = 40 \cdot \left| 0.55555556 \cdot \frac{C}{F} \right|$ *typical winter temperature, for air properites*

$RH_{winter,typical} = 0.2$ *typical relative humidity, for air properties*

$v_{wind,design} = 110 \cdot \left| 0.44704 \cdot \frac{m/s}{mph} \right|$ *design wind speed*

$h_{ply} = 7$

$l_{ply} = 8$

$A_{plywood} = h_{ply} \cdot l_{ply} \cdot \left| 0.09290304 \cdot \frac{m2}{ft2} \right|$ *area of plywood*

$\theta_{plywood,horiz} = 30$ *angle of plywood from horizontal*

$\rho_{air} = \rho\left[\text{'AirH2O'}, T = T_{winter,typical}, R = RH_{winter,typical}, P = P_{atm,5000} \right]$ *air density*

$C_d = 1.17$ *drag coefficient for square flat plate at 90 deg, from reference table*

$F_{wind} = \frac{\rho_{air} \cdot v_{wind,design}^{\ 2} \cdot A_{plywood} \cdot C_d}{2}$ *force of the wind on the the plywood at 90 deg*

$F_{wind,lbf} = F_{wind} \cdot \left| 0.2248 \cdot \frac{lbf}{N} \right|$

$Reaction_{anchors,pullout} = F_{wind} \cdot \mathbf{cos}\left[\theta_{plywood,horiz} \right]$

$Reaction_{anchors,pullout,IP} = Reaction_{anchors,pullout} \cdot \left| 0.2248 \cdot \frac{lbf}{N} \right|$

$Reaction_{anchors,shear,IP} = F_{wind} \cdot \mathbf{sin}\left[\theta_{plywood,horiz} \right] \cdot \left| 0.2248 \cdot \frac{lbf}{N} \right|$

Trubolt wedge anchor by Redhead for nominal diamter of 1/2in. and effective enbedment depth of4-1/8in. have an ultimate Tension and shear values of 4660 and 7,240 pounds, respectively, in 2000 psi concrete compressive strength

$Anchor_{pullout,performance} = 4660$ [pounds]

$Anchor_{shear,performance} = 7240$ [pounds]

Static loading

The frame that I have drawn in Sketch-up is statically indeterminate. However, if I simplify the frame, and change all bolted fixed supports to a simple triangle with a frictionless hinge at the top, frictionless hinge connecting the two members and a rough surface as the bottom support, then the problem can be statically determined

The reactions to be determined are at the hinges, which will define the required strength of the anchors to hold the plate of the hinge. The problem that I drew and solved is simply two-dimensional problem where the distrubuted load is simplified into a point load on one triangular frame with only one bolt providing the reaction. This was chosen because if one bolt can be proven to hold the load then the additional two frames with 5 bolts each will certainly be sufficient

The load will consist of the weight of the plywood, the water filled solar modules, and the angled channel of unistrut

$\rho_{plywood} = 700$ [kg/m3]

$Vol_{plywood} = A_{plywood} \cdot 0.5 \cdot \left| 0.0254 \cdot \frac{m}{in} \right|$

$W_{plywood} = \rho_{plywood} \cdot Vol_{plywood}$ *weight of the plywood*

$W_{pv} = 15$ [kg] *weight of the PV composite*

$SG_{pvc} = 1.37$ *specific gravity of PVC*

$\rho_{water} = \rho\left[\text{'Water'}, T=20, P=P_{atm,5000}\right]$

$\rho_{pvc} = SG_{pvc} \cdot \rho_{water}$ *density of pvc*

Volume of pvc based on material order form and assuming that 60% of the material was cut and actually used (a conservative guess).

$$Vol_{pvc} = \left[0.093 \cdot \left| 0.083333333 \cdot \frac{ft}{in} \right| \cdot 4 \cdot 8 \cdot \left| 0.028316847 \cdot \frac{m3}{ft3} \right| + \frac{3}{16} \cdot \left| 0.083333333 \cdot \frac{ft}{in} \right| \cdot 4 \cdot 8 \cdot \left| 0.028316847 \cdot \frac{m3}{ft3} \right| + 1 / 4 \cdot \left| 0.083333333 \cdot \frac{ft}{in} \right| \cdot 4 \cdot 8 \cdot \left| 0.028316847 \cdot \frac{m3}{ft3} \right| + 1 / 8 \cdot 2 \cdot \left| 0.083333333 \cdot \frac{ft}{in} \right| \cdot 4 \cdot 8 \cdot \left| 0.028316847 \cdot \frac{m3}{ft3} \right| \right] \cdot 0.6$$

$W_{pvc} = \rho_{pvc} \cdot Vol_{pvc}$ *weight of the pvc*

Weight of water in module

$Vol_{headers} = 2 \cdot 1 \cdot 1 \cdot 31 \cdot \left| 0.0000163871 \cdot \frac{m3}{in3} \right|$

$Vol_{absorber} = 2 \cdot 78 \cdot 0.0625^2 \cdot 60 \cdot \left| 0.0000163871 \cdot \frac{m3}{in3} \right|$

$Vol_{water,module} = Vol_{headers} + Vol_{absorber}$

$W_{water} = \rho_{water} \cdot Vol_{water,module}$ *weight of water*

Weight of the unistrut

$Length_{uni} = 7$ [ft]

$W_{uni} = \frac{175}{100} \cdot Length_{uni} \cdot \left| 0.4536 \cdot \frac{kg}{lbm} \right|$ *weight of unistrut*

Total load distributed across 3 frames

$g = 9.81$

$Load = 2 \cdot [W_{pvc} + W_{water} + W_{pv}] + W_{plywood} + W_{uni} \cdot g$

For a conservative approach, I will assume the distributed load to be a point load centered in the plywood area, and only consider one frame instead of three.

the sum of the moments at point A (top hinge) is = 0, thus...

$Reaction_{Bx} = \dfrac{Load \cdot \dfrac{6.06}{2}}{3.5}$ *compressing the rough surface*

the sum of the forces in the x-dir = 0, thus...

$Tension_{static} = Reaction_{Bx} \cdot \left| 0.2248 \cdot \dfrac{lbf}{N} \right|$ *tension on the anchor supporting the top hinge*

the frame must now be broken up into its members, member AC is the hypotenuse, and will be looked at first. Summing the moment at point C, I can solve for Ay.

$Shear_{static} = \dfrac{Load \cdot \dfrac{6.06}{2}}{6.06} \cdot \left| 0.2248 \cdot \dfrac{lbf}{N} \right|$

Now back to the entire frame and sum the forces in the y-dir to find the By.

$B_y = Load \cdot \left| 0.2248 \cdot \dfrac{lbf}{N} \right| - Shear_{static}$

Anchor allowable static tension

$Tension_{allowable,static} = 1831$

$Shear_{allowable,static} = 2804$

Final Comments: Based on what I have calculated here, from a very conservative standpoint the anchors that I have chosen should be well suited to accomodate the static load, and a 110 mph wind blast normal to the plywood.

Response to Will Johnson's Comments

1. Show that the combined tension and shear loading (from both weight and wind) will not exceed allowable for the choesn Trubolt anchors (see formula for this on the bottom of the Trubolt cutsheet).
2. How are the Unistrut frames braced horizontally?
3. Show that the plywood-to-frame connection doesn't exceed allowable stress (from wind) for the chosen hardware.
4. Ensure (and show) that edge and spacing distance requirements for the Trubolt anchors for shear and tension loads are met.

1.

$CombinedTensionShearLoading = \left[\dfrac{P_s}{P_t} \right]^{[5/3]} + \left[\dfrac{V_s}{V_t} \right]^{[5/3]}$

$P_s = Tension_{static}$ *Applied tension load*

$V_s = Shear_{static}$ *Applied shear load*

P_t = $Tension_{allowable,static}$ *Allowable tension load*

V_t = $Shear_{allowable,static}$ *Allowable shear load*

See calculated value in the key variables section. value is passing, at a value less than 1.

*3. See attached *.pdf ChannelNutPulloutLoad*

As per Unistrut general engineering catalog: for channel P1000 with 5/8 inches channel nut size-thread
Allowable Pull-out Strength (Lbf) = 2500
Resistance to slip (Lbf) = 1700

I calculated the force of the wind on the plywood (acting normal to the plywood at 110 mph) to be, $F_{wind,lbf}$=1635 lbf. This is under the channel nut rating.

4. I'm not sure if I understand what the edge and spacing requirements mean. Is the Edge distance the distance from the anchor position to the edge of the concrete? If so, I ensure that the frame closest to the edge of the concrete is no closer than 6inches, as per the Trubolt performance table for 1/2in diameter anchors.

Is the spacing distance the spacing from one anchor to another anchor, (radially)? If so, then I will ensure that no anchor is placed closer than 7 inches from another anchor, as per the Trubolt performance table for 1/2in diameter anchors. Note edge and spacing requirements are larger for shear loads, thus if shear requirements are met, then tension requirements are also met.

SOLUTION
Unit Settings: SI C kPa kJ mass deg
$Anchor_{pullout,performance}$ = 4660 [pounds]
$Anchor_{shear,performance}$ = 7240 [pounds]
$A_{plywood}$ = 5.203
B_y = 25.93
CombinedTensionShearLoading = 0.002477 [dimensionless]
C_d = 1.17
F_{wind} = 7271
$F_{wind,lbf}$ = 1635 [pounds]
g = 9.81
h_{ply} = 7
$Length_{uni}$ = 7 [ft]
Load = 230.7 [N]
l_{ply} = 8
$P_{atm,5000}$ = 84.3
P_s = 44.9
P_t = 1831
$Reaction_{anchors,pullout}$ = 6297
$Reaction_{anchors,pullout,IP}$ = 1416 [pounds]
$Reaction_{anchors,shear,IP}$ = 817.3 [pounds]
$Reaction_{Bx}$ = 199.7
ρ_{air} = 0.988
$\rho_{plywood}$ = 700 [kg/m^3]
ρ_{pvc} = 1368
ρ_{water} = 998.2
$RH_{winter,typical}$ = 0.2
SG_{pvc} = 1.37
$Shear_{allowable,static}$ = 2804 [pounds]
$Shear_{static}$ = 25.93 [pounds]
$Tension_{allowable,static}$ = 1831 [pounds]

$Tension_{static}$ = 44.9 [pounds]
$\theta_{plywood,horiz}$ = 30
$T_{winter,typical}$ = 22.22
$Vol_{absorber}$ = 0.0005992
$Vol_{headers}$ = 0.001016
$Vol_{plywood}$ = 0.06607
Vol_{pvc} = 0.03536
$Vol_{water,module}$ = 0.001615
V_s = 25.93
V_t = 2804
$V_{wind,design}$ = 49.17
$W_{plywood}$ = 46.25
W_{pv} = 15 [kg]
W_{pvc} = 48.36
W_{uni} = 5.557
W_{water} = 1.612

22 potential unit problems were detected.

KEY VARIABLES

$Shear_{allowable,static}$ = 2804 [pounds]	*Anchor allowable static shear*
$Shear_{static}$ = 25.93 [pounds]	*calculated static shear on anchor. well below rating*
$Tension_{allowable,static}$ = 1831 [pounds]	*Anchor allowable static tension*
$Tension_{static}$ = 44.9 [pounds]	*calculated static tension on anchor. well below rating*
$Anchor_{pullout,performance}$ = 4660 [pounds]	*Ultimate tension on anchor, for wind load comparison*
$Reaction_{anchors,pullout,IP}$ = 1416 [pounds]	*Calculated wind force of tension on anchor. Well below the rating.*
$Anchor_{shear,performance}$ = 7240 [pounds]	*Ultimate shear an anchor, for wind load comparison*
$Reaction_{anchors,shear,IP}$ = 817.3 [pounds]	*Calculated wind force of shear on anchor. Well below rating.*
Load = 230.7 [N]	*Load on frame*
CombinedTensionShearLoading = 0.002477 [dimensionless]	*Combined Tension and Shear Loading - for Trubolt Anchors. Value is passing if it is less than or equal to 1.*
$F_{wind,lbf}$ = 1635 [pounds]	*Force the wind places on the channel nut holding the plywood*

APPENDIX J TRNSYS PVT MATHEMATICAL MODEL

TYPE 560: COMBINED PHOTOVOLTAIC / THERMAL SOLAR COLLECTOR (INTERACTS WITH ZONE AIR TEMPERATURE)

This component is intended to model an un-glazed solar collector which has the dual purpose of creating power from embedded photovoltaic (PV) cells and providing heat to a fluid stream passing through tubes bonded to an absorber plate located beneath the PV cells. The waste heat rejected to the fluid stream is useful for two reasons; 1) it cools the PV cells allowing higher power conversion efficiencies and 2) it provides a source of heat for many possible low-grade temperature applications.

This model relies on linear factors relating the efficiency of the PV cells to the cell temperature and also the incident solar radiation. The cells are assumed to be operating at their maximum power point condition.

The thermal model of this collector relies on algorithms presented in Chapter 6 of the classic "Solar Engineering of Thermal Processes" textbook by Duffie and Beckman.

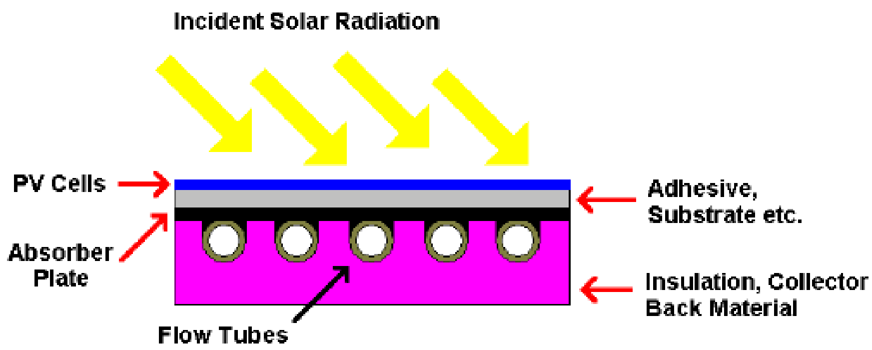

Figure 1 –PV/T Schematic

Nomenclature

β	- slope of the collector surface
η	- efficiency
θ	- angle of incidence
ρ	- ground reflectance
$\tau\alpha$	- transmittance-absorptance product for the solar collector
ε	- emissivity of the top surface of the collector (PV surface)
σ	- Stefan-Boltzmann constant
λ	- thickness of the absorber plate

Area	- area (top) of the solar collector; this can be either gross area or net area but should be consistent with the provided loss coefficients and PV power conversion coefficients.
b_0	- incidence angle modifier multiplier
C_p	- specific heat of the fluid flowing through the PV/T collector
C_B	- the conductance between the absorber plate and the bonded tube
D_{tube}	- the diameter of the tubes
F_R	- collector heat removal factor
G_t	- total solar radiation (beam + diffuse) incident upon the collector surface
h_{fluid}	- internal fluid heat transfer coefficient
h_{inner}	- heat transfer coefficient from the back of the collector to the air
h_{outer}	- heat transfer coefficient from the top of the collector (PV surface) to the ambient air
h_{rad}	- radiative heat transfer coefficient from the top of the collector (PV surface) to the sky
IAM	- incidence angle modifier
k	- thermal conductivity of the plate material
L	- the length of the collector along the flow direction
$\dot{m}$	- flow rate of fluid through the solar collector
N_{tubes}	- number of identical tubes carrying fluid through the collector
Power	- rate at which electrical energy is produced by the PV cells
$Q_{loss,top,conv}$	- rate at which energy is lost to the ambient through convection off the top of the collector
$Q_{loss,top,rad}$	- rate at which energy is lost to the sky through radiation off the top of the collector
$Q_{loss,back}$	- rate at which energy is lost to the ambient through the back of the collector
Q_{fluid}	- rate at which energy is added to the flow stream by the collector, this term includes the energy that is also lost from the fluid stream through the back of the collector
$Q_{absorbed}$	- net rate at which energy is absorbed by the collector plate (does not include PV power production)
Q_u	- rate at which energy is added to the flow stream by the collector
q'_{fin}	- heat transfer to the fin base per unit length of collector
q'_{fluid}	- heat transfer to the fluid stream per unit length of collector
q'_u	- heat transfer to the fluid stream per unit length of collector
R_t	- resistance to heat transfer from the PV cells to the absorber plate
R_b	- resistance to heat transfer from the absorber through the back of the collector
R_1	- resistance to heat transfer provided by the material between the PV cells and the absorber
R_2	- resistance to heat transfer provided by the material between the absorber plate and the back surface of the collector
S	- net absorbed solar radiation (total absorbed – PV power production)
T_{abs}	- absorber plate temperature
T_{amb}	- ambient temperature for convective losses from the top surface
T_{back}	- environment temperature for convective losses from the bottom surface
T_{fluid}	- bulk temperature of the fluid flowing through the solar collector
$T_{fluid,in}$	- temperature of the fluid flowing into the solar collector
$T_{fluid,out}$	- temperature of the fluid flowing out of the solar collector
T_{fluid}	- local fluid temperature
T_{PV}	- PV cell temperature

TYPE 560: COMBINED PHOTOVOLTAIC / THERMAL SOLAR COLLECTOR (INTERACTS WITH ZONE AIR TEMPERATURE)

T_{sky}	- sky temperature for long-wave radiation calculations
$\overline{T}$	- mean temperature
W	- the width (x-direction) between adjacent fluid tubes in the collector
Width	- the width of the collector
$X_{Cell\ Temp}$	- multiplier for the PV cell efficiency as a function of the cell temperature
X_{NS}	- multiplier to account for collectors connected in series (thermally)
$X_{Radiation}$	- multiplier for the PV cell efficiency as a function of the incident radiation
y	- a variable indicating the direction of flow through the collector (y=L is the collector outlet)

Subscripts

b	- beam radiation
d	- diffuse radiation
g	- ground
G	- radiation
h	- total horizontal
n	- normal incidence
nominal	- refers to the reference conditions
PV	- photovoltaic
s	- sky diffuse
t	- total (beam + diffuse)

Mathematical Description:

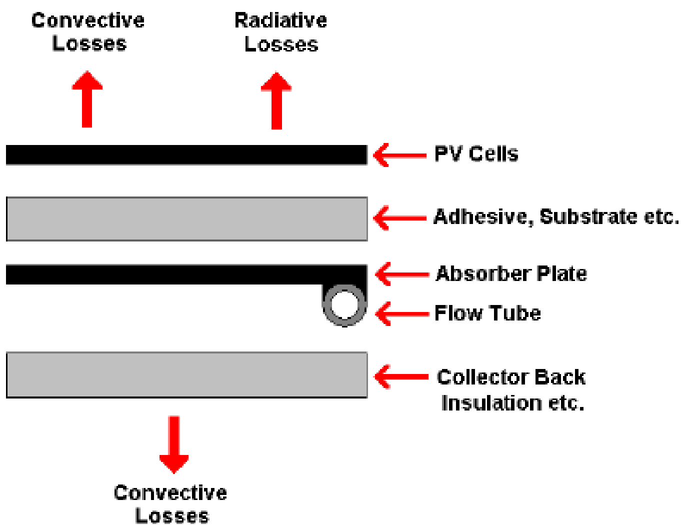

Figure 2 - PV/T Definitions

An energy balance on the collector surface (PV cells) at any point along the surface, (neglecting conduction along the surface) shows the following relationship:

$$0 = S - h_{outer}(T_{PV} - T_{amb}) - h_{rad}(T_{PV} - T_{sky}) - \frac{(T_{PV} - T_{abs})}{R_T} \qquad \text{(Eq. 560.1)}$$

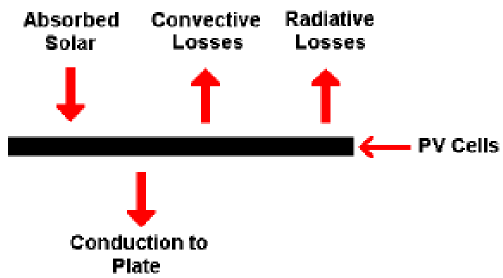

Figure 3: Surface Energy Balance

where:

$$R_T = R_1 \qquad \text{(Eq. 560.2)}$$

$$h_{rad} = \varepsilon\sigma(T_{PV} + T_{sky})(T_{PV}^2 + T_{sky}^2) \qquad \text{(Eq. 560.3)}$$

S is the net absorbed solar radiation and accounts for the absorbed solar radiation minus the PV power production. To account for off-normal solar radiation effects, the transmittance-absorptance product at normal incidence is multiplied by the following term in order to get the transmittance-absorptance at other incidence angles. This term is referred to as the incidence angle modifier (IAM).

$$IAM = \frac{(\tau\alpha)}{(\tau\alpha)_n} = \frac{G_{bT}\frac{(\tau\alpha)_b}{(\tau\alpha)_n} + G_d\frac{(1+\cos\beta)}{2}\frac{(\tau\alpha)_s}{(\tau\alpha)_n} + G_h\,\rho_g\frac{(1-\cos\beta)}{2}\frac{(\tau\alpha)_g}{(\tau\alpha)_n}}{G_T} \qquad \text{(Eq. 560.4)}$$

where:

$$\frac{(\tau\alpha)_b}{(\tau\alpha)_n} = 1 - b_0\left(\frac{1}{\cos\theta} - 1\right) \qquad \text{(Eq. 560.5)}$$

The incidence angle modifiers for both sky and diffuse radiation are determined by defining equivalent incidence angles for beam radiation that give the same transmittance as for diffuse radiation (Duffie and Beckman). The effective angles for sky diffuse and ground reflected radiation are:

$$\theta_{sky} = 59.68 - 0.1388\,\beta + 0.001497\,\beta^2 \qquad \text{(Eq. 560.6)}$$

$$\theta_{ground} = 90.0 \quad - \quad 0.5788\ \beta \quad + \quad 0.002693\ \beta^2 \qquad \text{(Eq. 560.7)}$$

With these definitions S, the net absorbed solar radiation, from equation 560.1 can be determined as:

$$S = (\tau\alpha)_n\ IAM\ G_T\ (1-\eta_{PV}) \qquad \text{(Eq. 560.8)}$$

The efficiency of the PV cells is a function of the cell temperature and the incident solar radiation:

$$\eta_{PV} = \eta_{nominal}\ X_{CellTemp}\ X_{Radiation} \qquad \text{(Eq. 560.9)}$$

where:

$$X_{CellTemp} = 1 + Eff_T\ (T_{PV} - T_{ref}) \qquad \text{(Eq. 560.10)}$$

$$X_{Radiation} = 1 + Eff_G\ (G_T - G_{ref}) \qquad \text{(Eq. 560.11)}$$

An energy balance taken for a differential sized section along the absorber plate, at any point along the plate away from the tube section, shows the following relationship (assuming the plate is thin and made from a conductive material):

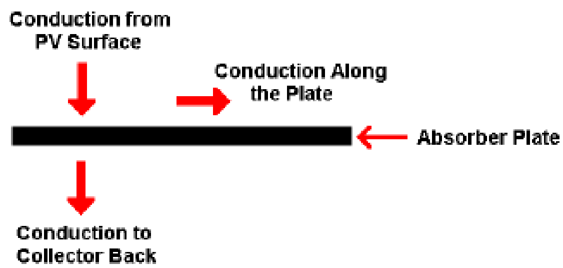

Figure 4: Absorber Fin Heat Flows

$$k\,\lambda \frac{d^2 T_{abs}}{dx^2} = \frac{(T_{abs} - T_{back})}{R_B} - \frac{(T_{PV} - T_{abs})}{R_T} \qquad \text{(Eq. 560.12)}$$

where:

$$R_B = R_2 + \frac{1}{h_{inner}} \qquad \text{(Eq. 560.13)}$$

This is a classical fin problem where the absorber plate section between the midpoint of two adjacent tubes and the tube acts as the fin. Solving equation 560.1 for T_{PV} and substituting into equation 560.12, we derive the following differential equation for the temperature distribution (x-direction) along the absorber plate:

$$\frac{d^2T_{abs}}{dx^2} = \frac{F'}{k\lambda}\left(T_{abs}\left(\frac{1}{R_T F'}+\frac{1}{R_B F'}-\frac{1}{R_T}\right)-\left(S+h_{rad}T_{sky}+h_{outer}T_{amb}+\frac{T_{back}}{R_B F'}\right)\right) \quad \text{(Eq. 560.14)}$$

where:

$$F' = \frac{1}{h_{rad}R_T + h_{outer}R_T + 1} \quad \text{(Eq. 560.15)}$$

We can recast equation 560.14 as:

$$\frac{d^2\Psi}{dx^2} - m^2\Psi = 0 \quad \text{(Eq. 560.16)}$$

where:

$$\Psi = T_{abs} - \frac{S+h_{rad}T_{sky}+h_{outer}T_{amb}+\dfrac{T_{back}}{R_B F'}}{\dfrac{1}{R_T F'}+\dfrac{1}{R_B F'}-\dfrac{1}{R_T}} \quad \text{(Eq. 560.17)}$$

$$m = \sqrt{\frac{F'\left(\dfrac{1}{R_T F'}+\dfrac{1}{R_B F'}-\dfrac{1}{R_T}\right)}{k\lambda}} \quad \text{(Eq. 560.18}$$

Solving equation 560.16 we find:

$$\Psi = C_1 \sinh(mx) + C_2 \cosh(mx) \quad \text{(Eq. 560.19)}$$

Equation 560.19 defines the temperature distribution along the plate in the x-direction, where x=0 is the mid-point between two adjacent tubes and $x=(W-D_{tube})/2$ is the base of the fin. To find the constants C_1 and C_2, we need to apply our boundary conditions. For this problem we have the boundary conditions from symmetry at the midpoint between adjacent tubes (x=0) and from the known base temperature (T_b) at $x=(W-D_{tube})/2$:

$$\frac{d\Psi}{dx} = 0 \quad at\ x = 0 \quad \text{(Eq. 560.20)}$$

$$\Psi = T_b - \frac{S + h_{rad}T_{sky} + h_{outer}T_{amb} + \frac{T_{back}}{R_B F'}}{\frac{1}{R_T F'} + \frac{1}{R_B F'} - \frac{1}{R_T}} \qquad \text{at } x = (W - D_{tube})/2 \qquad \text{(Eq. 560.21)}$$

Applying our boundary conditions and solving for C_1 and C_2 we find:

$$C_1 = 0 \qquad \text{(Eq. 560.22)}$$

$$C_2 = \frac{T_b - \left(\frac{S + h_{rad}T_{sky} + h_{outer}T_{amb} + \frac{T_{back}}{R_B F'}}{\frac{1}{R_T F'} + \frac{1}{R_B F'} - \frac{1}{R_T}} \right)}{\cosh\left(m \frac{(W - D_{tube})}{2} \right)} \qquad \text{(Eq. 560.23)}$$

Substituting C1 and C2 into equation 560.19, and then applying equation 560.17, we derive the expression for the temperature distribution along the plate as a function of the base temperature:

$$T_{abs}(x) = \frac{b}{j} + \left(T_b - \frac{b}{j} \right) \frac{\cosh(m\,x)}{\cosh\left(m \frac{(W - D_{tube})}{2} \right)} \qquad \text{(Eq. 560.24)}$$

where:

$$\frac{b}{j} = \left(\frac{S + h_{rad}T_{sky} + h_{outer}T_{amb} + \frac{T_{back}}{R_B F'}}{\frac{1}{R_T F'} + \frac{1}{R_B F'} - \frac{1}{R_T}} \right) \qquad \text{(Eq. 560.25)}$$

With the temperature distribution known along the fin (equation 560.24), we can calculate the energy conducted to the base from the fin:

$$q'_{fin} = -k\,\lambda \frac{dT_{abs}(x)}{dx} = k\,\lambda\,m\,(\frac{b}{j} - T_b)\tanh\left(m\left(\frac{W - D_{tube}}{2} \right) \right) \qquad \text{(Eq. 560.26)}$$

An energy balance on the base (non-fin) area of the absorber plate shows:

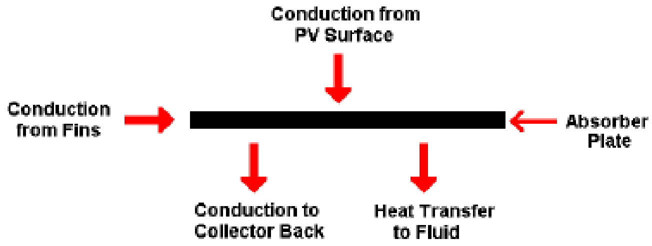

Figure 5: Heat Flows for Fin Base

$$q'_{fluid} = D_{tube}\left(\frac{T_{PV} - T_B}{R_T}\right) - D_{tube}\left(\frac{T_B - T_{Back}}{R_B}\right) + 2\,q'_{fin} \quad \text{(Eq. 560.27)}$$

The useful energy gain to the fluid may also be expressed as a function of the base temperature:

$$q'_{fluid} = \left(\frac{T_B - T_{fluid}}{\dfrac{1}{h_{fluid}\,\pi\,D_{tube}} + \dfrac{1}{C_B}}\right) \quad \text{(Eq. 560.28)}$$

An expression for the collector useful energy gain as a function of the fluid temperature may be derived by substituting terms from equations 560.1, 560.26 and 560.28 into equation 560.27 and re-arranging:

$$q'_{fluid} = \frac{\kappa}{\theta} T_{fluid} + \frac{\varepsilon}{\theta} \quad \text{(Eq. 560.29)}$$

where:

$$\kappa = -D_{tube}F'\left(h_{rad} + h_{outer} + \frac{1}{R_B\,F'}\right) - 2\,k\,\lambda\,m\tanh\left(m\left(\frac{W - D_{tube}}{2}\right)\right) \quad \text{(Eq. 560.30)}$$

$$\begin{aligned}\theta = 1 + D_{tube}F'\left(\frac{1}{h_{fluid}\,\pi\,D_{tube}} + \frac{1}{C_B}\right)\left(h_{rad} + h_{outer} + \frac{1}{R_B\,F'}\right) \\ + 2\,k\,\lambda\,m\tanh\left(m\left(\frac{W - D_{tube}}{2}\right)\right)\left(\frac{1}{h_{fluid}\,\pi\,D_{tube}} + \frac{1}{C_B}\right)\end{aligned} \quad \text{(Eq. 560.31)}$$

$$\varepsilon = D_{tube} F' \left(S + h_{rad} T_{sky} + h_{outer} T_{amb} + \frac{T_{back}}{R_B F'} \right) + 2k\lambda m \tanh\left(m \left(\frac{W - D_{tube}}{2} \right) \right) \left(\frac{S + h_{rad} T_{sky} + h_{outer} T_{amb} + \frac{T_{back}}{R_B F'}}{\frac{1}{R_T F'} + \frac{1}{R_B F'} - \frac{1}{R_T}} \right) \quad \text{(Eq. 560.32)}$$

An energy balance taken around a differential section of fluid moving through the collector (in the y-direction) can be written as:

$$\dot{m} C_p \frac{dT_{fluid}}{dy} - N_{tubes}\, q'_{fluid} = 0 \quad \text{(Eq. 560.33)}$$

Subbing equation 560.29 into equation 560.33 we find:

$$\frac{dT_{fluid}}{dy} = \frac{N_{tubes}}{\dot{m} C_p} \frac{\kappa}{\theta} T_{fluid} + \frac{N_{tubes}}{\dot{m} C_p} \frac{\varepsilon}{\theta} \quad \text{(Eq. 560.34)}$$

Integrating this equation from zero to y we find:

$$T_{fluid}(y) = \left(T_{fluid,in} + \frac{\varepsilon}{\kappa} \right) \exp\left(\frac{N_{tubes}}{\dot{m} C_p} \frac{\kappa}{\theta} y \right) - \frac{\varepsilon}{\kappa} \quad \text{(Eq. 560.35)}$$

If we let y=L, we can solve for the fluid outlet temperature:

$$T_{fluid,out} = \left(T_{fluid,in} + \frac{\varepsilon}{\kappa} \right) \exp\left(\frac{N_{tubes}}{\dot{m} C_p} \frac{\kappa}{\theta} L \right) - \frac{\varepsilon}{\kappa} \quad \text{(Eq. 560.36)}$$

The collector useful energy gain can now be calculated:

$$Q_u = \dot{m} C_p \left(T_{fluid,out} - T_{fluid,in} \right) \quad \text{(Eq. 560.37)}$$

And the collector useful energy gain per unit length can be calculated as:

$$q'_u = q'_{fluid} = \frac{\dot{m} C_p \left(T_{fluid,out} - T_{fluid,in} \right)}{L\, N_{tubes}} \quad \text{(Eq. 560.38)}$$

The mean fluid temperature can be found by integrating the fluid temperature with respect to y and dividing by the flow length:

$$\overline{T}_{fluid} = \frac{1}{L} \int_0^L T_{fluid}(y)\, dy \quad \text{(Eq. 560.39)}$$

Using equation 560.35 and 560.39 and solving the differential equation we find:

$$\overline{T}_{fluid} = \left(\frac{T_{fluid,in} + \frac{\varepsilon}{\kappa}}{\frac{N_{tubes}}{\dot{m} C_p} \frac{\kappa}{\theta} L} \right) \exp\left(\frac{N_{tubes}}{\dot{m} C_p} \frac{\kappa}{\theta} L \right) - \left(\frac{T_{fluid,in} + \frac{\varepsilon}{\kappa}}{\frac{N_{tubes}}{\dot{m} C_p} \frac{\kappa}{\theta} L} \right) - \frac{\varepsilon}{\kappa} \qquad \text{(Eq. 560.40)}$$

With mean fluid temperature found from equation 560.40, and the collector useful energy gain per unit length found from equation 560.38, the mean base temperature can be solved from equation 560.28. With the mean base temperature solved, the temperature distribution across the absorber (fin section) can be found from applying equation 560.24.

The mean fin temperature can then be found by integrating the fin temperature function over the width of the fin, and dividing by the fin width:

$$\overline{T}_{fin} = \int_0^{\left(\frac{W-D_{tube}}{2}\right)} T(x)dx \qquad \text{(Eq. 560.41)}$$

$$\overline{T}_{fin} = \frac{S + h_{rad}T_{sky} + h_{outer}T_{amb} + \frac{T_{back}}{R_B F'}}{\frac{1}{R_T F'} + \frac{1}{R_B F'} - \frac{1}{R_T}} + \frac{\left(\overline{T}_B - \frac{S + h_{rad}T_{sky} + h_{outer}T_{amb} + \frac{T_{back}}{R_B F'}}{\frac{1}{R_T F'} + \frac{1}{R_B F'} - \frac{1}{R_T}} \right) \tanh\left(m\left(\frac{W - D_{tube}}{2} \right) \right)}{m\left(\frac{W - D_{tube}}{2} \right)} \qquad \text{(Eq. 560.42)}$$

The mean absorber temperature can then be found by area weighting the mean base temperature and the mean fin temperature:

$$\overline{T}_{abs} = \frac{\left(D_{tube}\overline{T}_B + (W - D_{tube})\overline{T}_{fin} \right)}{W} \qquad \text{(Eq. 560.43)}$$

The mean PV surface temperature ($\overline{T}_{PV}$) can then be found from equation 560.1. The solution of this set of equations requires an iterative approach as S is a function of the mean PV surface temperature:

1. Guess a value for the PV surface temperature.
2. Calculate the radiation heat transfer coefficient using equation 560.3.
3. Calculate the PV efficiency using equations 560.9 and 560.10.
4. Calculate the net absorbed solar radiation using equation 560.8.

5. Calculate the fluid outlet temperature using equation 560.36 and the mean fluid temperature using equation 560.40.
6. Calculate the collector useful energy gain per unit length using equation 560.38.
7. Calculate the mean base temperature from Equation 560.28.
8. Calculate the mean fin temperature from Equation 560.42.
9. Calculate the mean absorber temperature from Equation 560.43.
10. Calculate the mean PV surface temperature using Equation 560.1 and repeat steps 2 to 9 until convergence is reached

With convergence attained, equation 6.9.3 from Duffie and Beckman can be used to find the overall loss coefficient from the collector (U_L):

$$Q_u = Area\left[S - U_L\left(\overline{T}_{abs} - T_{amb}\right)\right] \quad \text{(Eq. 560.44)}$$

Finally, with the collector overall loss coefficient calculated, the collector heat removal factor can be calculated from equation 6.7.6 of Duffie and Beckman:

$$Q_u = Area\ F_R\left[S - U_L\left(T_{fluid,in} - T_{amb}\right)\right] \quad \text{(Eq. 560.45)}$$

With the PV cell temperature converged the PV power can be calculated:

$$Power = (\tau\alpha)_n\ IAM\ G_T\ Area\ \ \eta_{PV} \quad \text{(Eq. 560.46)}$$

The remaining relevant heat transfers for the collector are then calculated as:

$$Q_{loss,top,conv} = h_{outer}\ Area\left(\overline{T}_{PV} - T_{amb}\right) \quad \text{(Eq. 560.47)}$$

$$Q_{loss,top,rad} = h_{rad}\ Area\left(\overline{T}_{PV} - T_{sky}\right) \quad \text{(Eq. 560.48)}$$

$$Q_{loss,back} = Area\frac{\left(\overline{T}_{abs} - T_{back}\right)}{R_B} \quad \text{(Eq. 560.49)}$$

$$Q_{PV\rightarrow Plate} = Area\left(\frac{\overline{T}_{PV} - \overline{T}_{ABS}}{R_T}\right) \quad \text{(Eq. 560.50)}$$

$$Q_{absorbed} = A\left(\tau\alpha\right)_n\ IAM\ G_T\ \left(1 - \eta_{PV}\right) \quad \text{(Eq. 560.51)}$$

An energy balance on the collector surface is then:

$$Q_{absorbed} = Q_{loss,top,conv} + Q_{loss,top,rad} + Q_{PV\rightarrow plate} \quad \text{(Eq. 560.52)}$$

An energy balance on the entire collector can also be written:

$$Q_{absorbed} = Q_{loss,top,conv} + Q_{loss,top,rad} + Q_u + Q_{loss,back} \quad \text{(Eq. 560.53)}$$

CoolPoly Thermally Conductive Plastic Spec Sheet

Cool Polymers®

Product Data
Rev. 8/8/2007

CoolPoly® E2 Thermally Conductive Liquid Crystalline Polymer (LCP)

CoolPoly E series of thermally conductive plastics transfers heat, a characteristic previously unavailable in injection molding grade polymers. CoolPoly is lightweight, netshape moldable and allows design freedom in applications previously restricted to metals. The E series is electrically conductive and provides inherent EMI/RFI shielding characteristics.

Thermal	SI/Metric	Testing Standard
Thermal Conductivity	20 W/mK	ASTM E1461
Thermal Diffusivity	0.1 cm^2/sec	ASTM E1461
Specific Heat	0.9 J/g°C	ASTM E1461
Coefficient of Linear Thermal Expansion		
Parallel	8.2 ppm/°C	ISO 11359-2
Normal	9.1 ppm/°C	ISO 11359-2
Temperature of Deflection		
@ 0.45MPa	>300 °C	ISO 75-1,2
@ 1.80MPa	268 °C	ISO 75-1,2
Flammability	V-0 @ 1.5mm	UL 94

Mechanical	SI/Metric	English	Testing Standard
Tensile Modulus	24300 MPa	3524 ksi	ISO 527-1
Tensile Strength	80 MPa	11600 psi	ISO 527-1
Nominal Strain @ Break	0.25 %	0.25 %	ISO 527-1
Flexural Modulus	32300 MPa	4640 ksi	ISO 178
Flexural Strength	139 MPa	20155 psi	ISO 178
Impact Strength			
Charpy Unnotched	4.74 kJ/m^2	2.26 ft-lb/in^2	ISO 179-1
Charpy Notched	1.96 kJ/m^2	0.933 ft-lb/in^2	ISO 179-1

Electrical	SI/Metric	Testing Standard
Surface Resistivity	1 ohm/square	ASTM D257
Volume Resistivity	70 ohm - cm	ASTM D257

Physical	SI/Metric	English	Testing Standard
Density	1.84 g/cc	0.066 lb/in^3	ISO 1183
Mold Shrinkage			
Flow	0.1 %	0.001 in/in	ASTM D551
Cross-Flow	0.3 %	0.003 in/in	ASTM D551

Cool Polymers, Inc. • (888)-811-3787 • www.coolpolymers.com • ISO 9001:2000

APPENDIX K DETAILED SIMULATION COMPONENT DESCRIPTION

DETAILED COMPONENT DESCRIPTIONS

The following sections describe each of the simulations components and the logic behind the parameter and input values.

THE WEATHER FILE

This component serves the main purpose of reading weather data at regular time intervals from a data file, converting it to desired system of units and processing the solar radiation data to obtain tilted surface radiation and angle of incidence for an arbitrary number of surfaces. In this mode, this component reads a weather data file in the standard TMY2 format. See Table 15 for a list of all simulated cities.

EQUATION BLOCK – PASCAL TO ATM

This block converts Pa to Atmosphere for the Dew Point calculator

- Inputs
  - Pressure (Pa) via weather file
- Outputs
  - Pressure (atm) to Dew Point Calculator

DEW POINT CALCULATOR

This block calculates the Dew Point at each time step for Sky Temperature Calculator.

- Inputs
  - Pressure (atm) via equation block
  - Ambient temperature (C) via weather file
  - Relative humidity via weather file
- Outputs
  - Dew point temperature to Sky Temp calculator

SKY TEMP CALCULATOR

In order to predict the performance of solar collectors it is necessary to evaluate the radiation exchange between the collector surface and the sky. The sky is considered a blackbody at some equivalent sky temperature. The sky temperature is required by the BIPVT component for radiation computations. The sky temperature is calculated using the relation (Duffie & Beckman, 2006):

$$T_{Sky} = T_{ambient}[0.711 + 0.0056T_{dp} + 0.000073T^2{}_{dp} + 0.013\cos(15t)]^{1/4} \qquad (4.10)$$

Where t = hour from midnight

T_{dp}= the dew point temperature

- Inputs
  - Dew Point Temperature via Dew point calculator
  - Ambient temperature via weather file
  - Beam radiation on the horizontal via weather file
  - Diffuse radiation on the horizontal via weather file
- Outputs
  - The effective sky temperature to BIPV/T

****For the next two equation blocks, air and water properties were calculated using EES, plotting the properties as a function of temperature, and fitting a curve to the plots. The equations for the curves were copied into TRNSYS.****

TOP LOSS HTC, USING L_C

This equation block is used to calculate the convective heat loss coefficient from the top of the collector to the ambient. TRNSYS did not have a component for calculating this value, thus, the following narrative describes the reasoning for the user-defined calculation.

Convective heat losses on the collector surface are dependent on the wind and natural convection. There have been many experimental wind tunnel studies on rectangular plates in an attempt to derive the Nusselt number. Flow over a collector mounted on a house is not necessarily well represented by wind tunnel tests of isolated plates. Mitchell (1976) (Duffie & Beckman, 2006)found that many shapes were well represented by a sphere when the equivalent sphere diameter (L_c) is the cube root of the volume. Mitchell suggests that the wind tunnel results of the various animal shapes be increased by approximately 15% for outdoor conditions. Thus, assuming a house to be a sphere, the Nusselt number can be expressed as:

$$Nu = 0.42Re^{0.6} \tag{4.11}$$

Or,

$$h_{wind} = \frac{8.6V^{0.6}}{L^{0.4}} \tag{4.12}$$

However, at low wind speeds, natural convection conditions tend to dominate. Natural convection is driven by the buoyancy force. When the collector surface is hotter than the surrounding air the fluid in the vicinity of the collector surface will be heated and the density decreases, relative to the surrounding fluid, and will cause the heated fluid to rise. This is the buoyancy force. There are three forces acting on air in motion:

4. The force due to the pressure gradient
5. The body force
6. The frictional shearing forces due to the velocity gradient

Applying principles of conservation of momentum, using the simplification that the fluid far from the plate is in hydrostatic equilibrium, and finally the *Boussinesq approximation* (which assumes that the density depends only on the temperature (not pressure), the equation of motion for natural convection can be obtained. Furthermore, deriving the conservation of energy equation for the flow near the plate yields the temperature field for the natural-convection problem

Utilizing the Buckingham pi theorem, the dimensionless parameters can be determined. The three dimensionless groups are: Nu = Nu(Re,Pr,Gr). Since the flow velocity is determined by the temperature field, the Reynolds number is not an independent parameter. Experimental results for natural-convection heat transfer can therefore be correlated by an equation of the type:

$$Nu = \emptyset(Gr)\varphi(Pr) = \emptyset(Ra) \qquad (4.13)$$

Where, Ra = the Rayleigh number, the product of the Grashof and Prandtl numbers

Gr = the Grashof number, the ratio of buoyant forces to viscous forces

Thus, the Nu number for natural convection is a function of the product of the ratio of buoyant forces to viscous forces (Grashof #) and the ratio of molecular momentum diffusivity to thermal diffusivity (Prandtl No.).

Using an equation of the type, $Nu = \emptyset(Ra)$, experimental data for natural convection can be plotted and the coefficients found. Lloyd and Moran (1974) and McAdams (1954) give relationships for the Nu number as a function of the Ra number for hot horizontal flat plates and vertical plates, respectively. For large Rayleigh numbers, as is typical for solar collectors (due to the large Grashof number), the heat transfer coefficient from the two relationships are nearly identical, because the Rayleigh coefficients differ slightly. Applying some temperature differences to the Nu number relationships for natural convection, it is determined that the minimum heat transfer coefficient for horizontal *or* vertical collectors is about 5W/m^{2}K for a 25°C temperature difference and 4W/m^{2}K for a 10°C temperature difference.

A solar collector is most likely to be experiencing natural convection and forced convection simultaneously. McAdams recommends calculating both heat transfer coefficients and using the larger of the two for design and modeling calculations**. Thus the top loss convective heat transfer coefficient (W/m^2 K) for flush mounted collectors can be expressed as**:

$$h_{wind} = max\left[5, \frac{8.6V^{0.6}}{L^{0.4}}\right] \tag{4.14}$$

Where, V = wind speed in meter per second

L = the cube root of the house volume, in meters

- Inputs
  - Wind velocity from the weather file
- Outputs
  - Top loss convective heat transfer coefficient.

FLUID HTC (HEAT TRANSFER COEFFICIENT)

This equation block is used to calculate the heat transfer coefficient between the wall of the fluid channels and the fluid flowing inside it. TRNSYS did not have a component for calculating this value, thus, the following narrative describes the reasoning for the user-defined calculation.

Flow ranges for the BIPV/T result in a Reynolds number well below the transitional and turbulent flow regime and will always be laminar. Knowing that the flow in the absorbers channels is fully developed laminar flow, a table developed by Shah and London (1978) (Kreith & Bohn, 2001), provide Nusselt numbers and friction factors for fully developed laminar flow of a Newtonian fluid through specific ducts. For a square channel, as is the case with the design BIPV/T, Shah and London provide an average Nusselt number for uniform heat flux in the flow direction and uniform wall temperature at any cross section, as well as a value for the average Nusselt number for uniform wall temperature. The Nusselt numbers for a square duct are 3.608 and 2.979, respectively. The theoretical performance for a solar collector will lie between the results for constant heat flux and constant wall temperature, thus it is recommended for design calculation to use the lesser of the two values, constant wall temperature, for a conservative design. This equation block also has the capability to calculate the fluid heat transfer coefficient in the turbulent regime; however, this will probably never be used. For this calculation, the Nu number is entered as 2.976, and the HTC is calculated as follows:

$$h_{fluid,laminar} = \frac{Nu_{water,laminar} * k_{water}}{D_h} \tag{4.15}$$

Where, $Nu_{water,laminar}$ = 2.976

k_{water} = conductivity of the water as a function of temperature

D_h = hydraulic diameter

- Inputs
  - Mass flow rate from the pump
  - Bulk temperature, or average fluid temperature for the conductivity calculation
- Outputs
  - $h_{fluid,laminar}$ to BIPV/T

BIPV/T

For a complete description of the component please see THE BIPV/T COMPONENT in THE CALIBRATION MODEL section. All listed parameters, inputs and outputs are listed because they are different from the calibration.

- Parameters – the simulation is to model a 5kW array (25 modules)
  - Collector Length – Length of the absorber = 1.5144 m

- Collector width – width of absorber = 0.6096m *25 = 15.24 m
  - This width assumes an array of 25 modules plumbed in parallel
- Inputs
  - Inlet fluid temperature, *from the pump via the tank*
  - Inlet flow rate, from the pump. *0.6 GPM*
  - Ambient temperature, *from the weather file.*
  - Back-surface temperature – the temperature of the air located behind the back surface of the collector. The BIPV/T is flush mounted (Building Integrated), thus I would say this back surface temperature is the same as the ambient, *from the weather file.*
  - Incident solar radiation – the rate at which incident solar radiation (beam + diffuse) strikes the sloped collector surface, *from the weather file.*
  - Total horizontal radiation – the rate at which total solar radiation (beam + diffuse) strikes a horizontal surface, *from the weather file.*
  - Horizontal diffuse radiation – the rate at which diffuse radiation strikes a horizontal surface, *from the weather file.*
  - Ground reflectance – the reflectance of the surface above which the solar collector is positioned. *Typical value is 0.2.*
  - Incidence angle – the angle of incidence between the beam solar radiation and the normal vector to the sloped collector surface, *from the weather file.*
  - Collector slope – the slope of the collector surface. *The test setup was at 30 degrees, and will set at this slope for simulations.*
  - Top loss convection coefficient – the convective heat loss coefficient from the top of the collector to the ambient, *from the Top Loss convective HTC equation block*

- Back heat loss coefficient – the combined convective and radiative heat transfer coefficient from the back of the collector to the environment, tuning parameter that has little effect. *Default value is 15 kJ/hr.m2.K*
- Fluid heat transfer coefficient – the heat transfer coefficient from the fluid in the flow channels to the walls of the fluid channel enclosure, *from the Fluid HTC equation block.*

- Outputs
  - Temperature at outlet – the temperature of the fluid exiting the collector. *Sent to plotter 1.*
  - Flow rate at outlet – the flow rate of fluid exiting the collector. *Sent to plotter 1.*
  - Useful energy gain – the net rate at which energy is transferred to the fluid flowing through the solar collector. *Currently not using this parameter.*
  - PV power –the rate at which the photovoltaic cells are producing electrical power. *Sent Simulation Integration.*
  - PV efficiency – the efficiency of the PV cells in converting incident solar radiation to electrical energy; expressed as a fraction. *Currently not using this parameter.*
  - Thermal efficiency – the efficiency of the solar collector in converting incident solar radiation to delivered fluid energy. *Currently not using this parameter.*
  - Collector FR – the calculated value of the collector heat removal factor (FR). The heat removal factor is the quantity that relates the actual useful energy gain of the collector to the useful gain if the whole collector surface were at the fluid inlet temperature. FR is equivalent to the effectiveness of a conventional heat exchanger, which is defined as the ratio of the actual heat transfer to the maximum possible heat transfer. The maximum possible useful energy gain (heat transfer) in a solar collector occurs when the

whole collector is at the inlet fluid temperature; heat losses to the surroundings are then at a minimum. *Currently not using parameter on its own.*

- Mean PV temperature – the average temperature of the PV cells. *Currently not using this parameter.*
- Mean fluid temperature – the mean temperature of the fluid in the solar collector. *Currently not using this parameter.*
- Incidence angle modifier – the overall (beam plus diffuse) incidence angle modifier for the collector. IAM is defined for each solar radiation stream as the ratio of the transmittance-absorptance product at some angle to the transmittance absorptance product at normal incidence.
- Collector top losses – convective. The rate at which energy is lost to the environment through convection from the top surface of the collector
- Collector top losses – radiative. The rate at which energy is lost to the environment through radiation losses from the top surface of the collector.
- Collector back losses. The rate at which energy is lost to the environment through the back surface of the collector.
- Absorbed solar radiation. The net rate at which solar radiation is absorbed by the collector. This value does not include the radiation that was absorbed by the PV cells and converted to electrical energy.
- Overall heat loss coefficient. The calculated overall loss coefficient for this collector.
- FRTAN ($F_R(\tau\alpha)_n$). The intercept term for the collector efficiency equation.
- FRUL ($F_R U_L$). The linear term for the collector efficiency equation.

PLOTTER 1

Plotter 1 shows results immediately after the simulation.

- Inputs
    - Left axis variable 1 – TiColl. Temperature into the collector
    - Left axis variable 2 – ToColl. Temperature exiting the collector
    - Right axis variable 1 – GColl. Hourly irradiance (total radiation) striking the collector
    - Right axis variable2 – mdColl. Mass flow rate through the collector
- Output is hourly plots

Plotter 2

Plotter 2 shows graphically shows results immediately after the simulation

- Inputs
    - Left axis variable-1. TTop. Temperature at Top of the tank. Temperature to the load
    - Left axis variable-2. T2. Temperature of node 1+-1
    - Left axis variable-3. T3. Temperature of node 1+-2
    - Left axis variable-4. T4. Temperature of node 1+-3
    - Left axis variable-5. T5. Temperature of node 1+-4
    - Left axis variable-6. TBottom. Temperature at bottom of tank.
    - Left axis variable-7. TDHW. Outlet temperature of the tee piece to the load.
    - Right axis variable – 1. QAux. Auxiliary heating rate
    - Right axis variable – 2. mdDHW. Mass flow rate leaving the Tee piece
    - Right axis variable – 3. mdTank. Mass flow rate of the city water entering the tank from the diverter.
    - Right axis variable – 4. mdByPass. Mass flow to the tee piece from the diverter.
- Output is hourly plots

Tee Piece

This parameter indicates to the general model that a simple tee piece is to be modeled.

- Inputs
    - Temperature at inlet 1. From the tank
    - Flow rate at inlet 1. From the tank
    - Temperature at inlet 2. From diverter.
    - Flow rate at inlet 2. From diverter.
- Outputs
    - Outlet temperature. The temperature of the mixed fluid leaving the tee piece. If the tee piece is under no flow conditions, the outlet temperature will be set to the minimum of the two inlet temperatures. For this reason, control decisions should not be based on this outlet temperature. Tout to load
    - Outlet flow rate. The flow rate of mixed fluid leaving the tee piece. Flow rate to load.

Diverter

This parameter indicates to the general model that a tempering valve is to be modeled. If the parameter is set to 4, the entire flow stream will be sent through the first outlet if the inlet temperature is less than the heat source temperature. If set to 5, the entire flow stream will instead be sent through the second outlet if the inlet temperature is less than the heat source. Currently set to 4, where the entire flow stream will be sent to the tank if the city water temperature is less than the heat source temperature.

- Inputs
    - mdDHW – mass flow rate of Domestic hot water use, from Daily Load equation block, via Load profile block
        - *value changes every hour*
    - TCold – inlet temperature, from Daily Load equation block.
        - *Temperature set at 12.8C*

- Heat source temperature. Temperature of water exiting the top of the tank to the tee piece, via tank setting
- Set point temperature. The temperature below which the heat source flow stream is to be kept at all times. The heat source flow stream temperature will be kept at or below the set point temperature (if possible) by the diversion of the cooler fluid from the inlet of the heat source to a mixing component at the exit of the heat source. *Set by user in the Diverter input tab.*

- Outputs
  - Temperature at outlet 1. The temperature of the fluid exiting through the first outlet of the tempering valve. The first outlet temperature is set to the inlet temperature for all cases. This output is typically hooked up to the temperature of the inlet flow stream to the heat source. *This output goes to the heat source.*
  - Flowrate at outlet 1. The flow rate of fluid leaving the first outlet of the tempering valve. This flow rate is typically hooked up to the inlet flow rate of the heat source. The first outlet flow rate is: mdot,1 = mdot,in*Y
    - Where: mdot,1 = this output
    - Mdot,in = inlet flow rate
    - Y = calculated control signal
  - Temperature at outlet 2. The temperature of the fluid exiting through the second outlet of the flow diverter. The temperature at the second outlet is set to the inlet temperature for all cases. In most cases, this temperature is hooked up to a mixing valve component mixing the flow from the 2nd outlet of this component and the heat source exiting flow stream.

- Flowrate at outlet 2. The flow rate of fluid exiting the tempering valve through the second outlet. This flow rate is typically hooked up to an inlet flow rate of a mixing valve component mixing this flow stream the flow stream of exiting heat source fluid. The flow rate from the second outlet is calculated by: Mdot,2 = (1-Y) * mdot,in
    - Where: mdot,2 = flow rate from the second outlet (this output)
    - Mdot,in = inlet flow rate
    - Y = calculated control signal
- Control function. The calculated fraction of fluid exiting through the first outlet of the tempering valve. The fraction is defined as:
    - Y = mdot,1 / mdot,in
    - Where:
    - Mdot,1 = flow rate through outlet 1
    - Mdot,in = inlet flow rate
    - Y = calculated control signal (this output)

Storage tank

This storage tank model has variable inlets and uniform losses. The thermal performance of a fluid-filled sensible energy storage tank, subject to thermal stratification, can be modeled by assuming that the tank consists of N (N<= 100) fully-mixed equal volume segments. The degree of stratification is determined by the value of N. If N is equal to 1, the storage tank is fully mixed. This instance of Type 4 models a stratified tank having variable inlet positions such that entering fluid may be added to the tank at a temperature as nearly equal to its own temperature as possible. The node sizes in this instance need not be equal. Temperature deadband on heater thermostats are available. This instance further assumes that losses from each tank node are equal and does not compute losses to the gas flue of the auxiliary heater.

- Parameters
    - Variable inlet positions – the auxiliary storage tank may operate in one of three modes in determining the inlet positions of the flow streams. Mode 2 (this mode) indicates that the heat source flow and the cold-side flow enter the tank in the nodes closest in temperature to the temperature of the respective flows. With a sufficient number of nodes, this permits a maximum degree of stratification.
    - Tank volume – the actual volume of the storage tank (not the nominal value) = 450 liters ~ 120 gallons
    - Fluid specific heat – the specific heat of the fluid contained in the storage tank. Using pure water, where the fluid in the tank is circulated to the solar collector = 4.190 kJ/kg.K
    - Fluid density – the density of the fluid contained in the storage tank. Using pure water, the density = 1000 kg/m3
    - Tank loss coefficient per unit area. The default value of 2.5 kJ/hr.m2.K is used
    - Height of node-1-4 – the height of the storage tank node in question. The total tank height will be determined by summing the heights of the nodes.
        - Depth of each node to be 335mm
        - Thus, total height of tank to be 1677mm
    - Auxiliary heater mode – the auxiliary heater may be operated in one of two modes:
        - Master/Slave relation: the lower heating element is only enabled when the upper heating element is satisfied. In this mode, only one heater may be on at any instant of time. This is a common design in residential electric hot water tanks, which is exactly what I'm trying to mode. *Using mode 1 for all simulations.*

- Node containing heating element 1. The node containing the specified auxiliary heating element. Make sure that the specified node for the heater is between 1 and the total number of nodes specified. Node 1 is the topmost node in the tank. *The auxiliary heating element is located in node 2.*
- Node containing the thermostat – 1. The node containing the thermostat for the specified auxiliary heater. The thermostat is typically either located in the same node as the heating element or in a node located above the element. Node 1 is the topmost node in the tank. *The thermostat is to be located at node 1.*
- Set point temperature for element 1. The set point temperature for the specified heating element. The thermostat will enable the heating element when the temperature of the fluid in the node containing the thermostat falls below: Tset –Tdb, and continue to heat the fluid until it reaches the set point temperature. Tset = this parameter; Tdb = the deadband temperature (next parameter)
    - *Setpoint temperature is set to 60C. At this temperature Legionella die within 32 minutes.*
- Deadband for heating element 1. The dead band temperature difference for the specified heating element.
    - *Deadband delta C is 5 °C. The thermostat will enable heating when the temperature of the water in the thermostat node falls below 55 Deg. C. At this temperature Legionella die within 5-6 hours.*
- Maximum heating rate of element 1.
    - *Set to 16200 kJ/hr (4500W)*
- Node containing heating element 2 – node 4
- Node containing thermostat 2 – node 3

- Deadband for heating element 2 - 5°C
- Maximum heating rate of element 2 – 16200 kJ/hr (4500W)

- Inputs
  - Hot-side temperature. This is the temperature of the fluid flowing into the tank from the heat source. The inlet location for this hot-side fluid is the node closest in temperature to the temperature of the hot-side flow (variable inlet setting).
    - *This temperature is from the leaving temperature of the BIPVT.*
  - Hot-side flowrate. This is the flowrate of the fluid into the storage tank from the heat source. An equal flowrate of fluid leaves the bottom of the storage tank for return to the heat source.
    - *Flowrate from the BIPVT*
  - Cold-side temperature. This is the temperature of the replacement fluid flowing into the storage tank. This temperature also enters the tank at the node closest in temperature to the cold-side flow.
    - *This temperature is from the leaving fluid temperature of the diverter which is set to the entering temperature of the diverter, which is set to typical city water temperature of 12.8 °C.*
  - Cold-side flowrate. This is the flowrate of city water entering the tank. An equal amount of fluid is assumed to flow from the top of the tank to meet the load.
    - *This flowrate is set at the diverter and is 100 kg/hr (.44 gpm)*
  - Environment temperature. The temperature of the environment in which the storage tank is located. This temperature is s*et at 21C (69.8F)*
  - The control signal for heating elements 1 and 2. The available power for the heating element will be this input multiplied by the maximum power for the element. *The*

control signal for the heating element will be set at 1, because this is a simple on/off control.

- Outputs
  - Temperature to heat source. The temperature of the fluid flowing from the bottom of the storage tank, and returning to the heat source (the bottom node temperature).
    - *This temperature is connected to the pump, then to the BIPVT*
  - Flow rate to heat source. The flow rate of fluid entering the storage tank in the node closest in temperature and exiting at the bottom of the storage tank to return to the heat source.
    - *This flowrate is connected to the pump, then to the BIPVT*
  - Temperature to load. The temperature of the fluid flowing from the top of the storage tank to the load (the top node temperature).
    - *This temperature is connected to the tee piece.*
  - Flowrate to load. Flowrate of fluid entering the tank at the node closet in temperature and leaving the tank at the top to meet the load.
    - *This flow rate is connected to the tee piece.*
  - Thermal losses. The rate of thermal energy loss to the environment. Includes the vented energy if a boiling condition is reached.
    - *Currently not being used*
  - Energy rate to load. The rate at which energy is removed from the tank to supply the load. The energy rate to the load is calculated by:

$$Q_{load} = \dot{m}_{load} * C_p * (T_{top} - T_{replace}) \tag{4.16}$$

Where, Q_{load} = this output

$\dot{m}_{load}$ = the DHW load profile

T_{top} = the temperature of the fluid flowing from the top of the storage tank to the load

$T_{replace}$ = temperature of the city water, set at 15 Deg C

    - *This output is sent to the Daily Integrator and is integrated over 24hrs, and to the simulation integrator, which integrates over the entire length of the simulation.*

- Internal energy change. The internal energy change of the tank relative to its initial condition. This output should not be integrated as it is an energy quantity and not an energy rate.
    - *Currently no being used.*
- Auxiliary heating rate. The average rate at which power was added to the tank by both auxiliary heaters. This value will be constant because the control signal is 1 at all times.
    - *Connected to Plotter 2, the daily integrator, and the simulation integrator.*
- Element 1 power. The average power supplied to the storage tank over the timestep by the first heating element specified in the parameter list.
    - *Currently not being used*
- Element 2 power.
    - *Currently not being used*
- Energy rate from heat source. The rate of energy transfer from the heat source to the storage tank. The rate is calculated from:

$$Q_{in} = \dot{m}_{source} * C_p * (T_{hot} - T_{to\ source}) \tag{4.17}$$

$\dot{m}_{source}$ = to the pump flowrate

T_{hot} = temperature of the fluid leaving the BIPVT and entering the tank

$T_{to\ source}$ = the bottom tank node temperature

    - *Connected to the daily integrator and the simulation integrator.*

    - Average tank temperature. The average temperature of the fluid in the storage tank over the timestep.
        - *Currently not being used.*
    - Temperature of nodes 2-4.
        - *Connected to Plotter 2*
- Derivative Tab. The initial temperatures of all nodes are set here. The tank is assumed to be stratified at the beginning of the simulation
    - Initial temperature of node-1 = 60C
    - Node-2 = 50C
    - Node-3 = 40C
    - Node-4 = 30C
    - Node-5 = 20C

ON/OFF Differential Controller

This controller is for control of the pump. The on/off differential controller generates a control function which can have a value of 1 or 0. The value of the control signal is chosen as a function of the difference between upper and lower temperatures Th and Tl, compared with two deadband temperature differences DTh and DTl. The new value of the control function depends on the value of the input control function at the previous timestep. The controller is normally used with an input control signal connected to the output control signal, providing a hysteresis effect. However, control signals from different components may be used as the input control signal for this component if a more detailed form of hysteresis is desired.

For safety considerations, a high limit cut-out is included with this controller. Regardless of the deadband conditions, the control function will be set to zero if the high limit condition is exceeded. This controller is not restricted to sensing temperature, even though temperature notation is used. This controller instance uses unit descriptions of °C so that it is readily usable as a thermostatic differential controller.

- Inputs
    - Upper input temperature Th. The temperature difference that will be compared to the dead bands is Th minus Tl.
        - *This temperature is the BIPVT outlet temperature*
    - Lower input temperature Tl.
        - *This temperature is the tank bottom node temperature*
    - Monitoring temperature Tin. Temperature to monitor for hi-limit cut-out checking. The controller signal will be set to OFF if this Input exceeds the high limit cut-out temperature. The controller will remain OFF until this input falls below the high limit cut-out
        - *This is tank top node temperature (the temperature of the fluid leaving the tank to the load).*
    - Input control function. The input control function is used to promote controller stability by the use of hysteresis. The control decision will be based on the deadband conditions and controller state at the previous time step (this input)
        - *This is connected to the controllers output control function*
    - Upper dead band dT
        - *Setting this delta T to 5°C. At a 5 degree difference between Inputs 1 and 2 the pump will start*
    - Lower dead band dT

        - *Setting this delta T to 0°C. The pump will stop running when the collectors no longer produce any useful gain.*
- Outputs
    - Output control function. The output control function may be ON (=1) or OFF (=0).

The Pump

This pump model computes a flow rate using a variable control function, which must have a value between 1 and 0, and a fixed maximum flow capacity. For this simulation, the control signal is either 1 or 0, as determined by the ON/OFF differential controller. Pump power may be calculated, either as a linear function of mass flow rate or by a user defined relationship between mass flow rate and power consumption. A user-specified portion of the pump power is converted to fluid thermal energy.

- Parameters
    - Maximum flow rate. The outlet flow rate is simply the maximum flow rate multiplied by the inlet control signal.
        - *All modules will be plumbed in parallel. Thus maxflow rate will be the desired flow per module, times the number of modules.*
    - Fluid specific heat = 4.19 kJ/kg K
    - Maximum power.
        - *Assuming a 1/6 Horsepower (447 kJ/hr)*
    - Conversion coefficient. The fraction of pump power that is converted to fluid thermal energy.
        - *Leaving as default value of 0.05.*
    - Power coefficient.

        - *This parameter is set to 1, such that the power consumed is always the maximum power (constant speed pump).*
- Inputs
    - Inlet fluid temperature
        - *Equal to the tank bottom node temperature.*
    - Inlet mass flow rate. Simply for visualization purposes
    - Control signal.
        - *Either a 1 or 0 from the Differential controller.*
- Outputs
    - Outlet fluid temperature. This value is slightly greater than the inlet fluid temperature due to the fraction of pump power that is converted to fluid thermal energy.
        - *This temperature is connected to the BIPVT fluid inlet temperature*
    - Outlet flow rate. This flow rate always the maximum flow rate specified in the parameters. This is a constant speed pump with a control signal of either 0 or 1.
    - Power consumption. This is the calculated value as specified in the parameter tab's power coefficient options.

The Load Profile

In a transient simulation, it is sometimes convenient to employ a time dependent forcing function which has a behavior characterized by a repeating pattern. The pattern of the forcing function is established by a set of discrete data points indicating the value of the function at various times throughout one cycle. Linear interpolation is provided in order to generate a continuous forcing function from the discrete data. The cycle will repeat every N hours where N is the last value of time specified. While the code of Type 14 is entirely general, this version of the component uses units of kg/hr so as to be more useful for creating water draw forcing functions.

- Parameters. The following table is abstracted from ASHRAE 90.2, Table 8-4, *Daily Domestic Hot Water Load Profile.*

Table 24. This table is abstracted from ASHRAE 90.2, and is the Daily Domestic Hot Water Load Profile.

TABLE 8-4 Daily Domestic Hot Water Load Profile	
Time of Day	
MID - 1 a.m.	0.0085
1 - 2 a.m.	0.0085
2 - 3 a.m.	0.0085
3 - 4 a.m.	0.0085
4 - 5 a.m.	0.0085
5 - 6 a.m.	0.0100
6 - 7 a.m.	0.0750
7 - 8 a.m.	0.0750
8 - 9 a.m.	0.0650
9 - 10 a.m.	0.0650
10 - 11 a.m.	0.0650
11 - NOON	0.0460
12 - 13 p.m.	0.0460
13 - 14 p.h	0.0370
14 - 15 p.m.	0.0370
15 - 16 p.m.	0.0370
16 - 17 p.m.	0.0370
17 - 18 p.m.	0.0630
18 - 19 p.m.	0.0630
19 - 20 p.m.	0.0630
20 - 21 p.m.	0.0630
21 - 22 p.m.	0.0510
22 - 23 p.m.	0.0510
23 - MID	0.0085
Note: These hourly values include a large diversity factor and should not be used to calculate peak loads for equipment sizing.	

Table 25. This table is the parameter inputs for the TRNSYS forcing function load profile component.

Time (hr)	Water Draw (kg/hr)
0	0.0085
5	0.0085
6	0.01
6	.075
8	0.075
8	0.065
11	.065
11	.046
13	0.046
13	0.037

17	0.037
17	.063
21	0.063
21	0.051
23	0.051
23	0.0085
24	0.0085

- No inputs
- Outputs
    - Average water draw. The average values of the water draw function over the timestep.
        - *This flow rate is sent to the Daily Load equation.*
    - Instantaneous water draw. The instantaneous values of the water draw function occurring at the end of the timestep.
        - *Currently not being used*

Daily Load equation block

This block is used to convert the DHW profile into a kg/hr rate.

- The DHW profile is multiplied by an average 4-person household daily hot water consumption of 375 kg/day.
- The temperature of the city water entering the tank is set at 12.8 Deg C (55F)

Daily Integration

This component integrates a series of quantities over a period of time. Each quantity integrator can have up to, but no more than 500 inputs. Type 24 is able to reset periodically throughout the simulation either after a specified number of hours or after each month of the year.

- Parameters
    - Integration period. The time interval over which the inputs are to be investigated. The outputs are reset to zero after each reset time interval.
        - For the daily integration, this value is set to 24 hrs
    - Absolute start time.

        - *Setting of 0: integrate at time intervals relative to the simulation start time.*

- Inputs/outputs
    - Total radiation on tilted surface, out to Daily Results file and efficiency calculator.
    - Energy rate from heat source, out to Daily Results file and efficiency calculator.
    - Energy rate to load, out to Daily Results file and efficiency calculator.
    - Auxiliary heating rate, out to daily Results file and efficiency calculator.

Simulation integration

Same as Daily integration, except that the integration period is for the entire simulation period ("STOP").

Efficiencies calculation Block

This equation block does exactly what it says; it calculates various efficiencies.

- Inputs
    - IColl_d - Total radiation on the tilted surface (daily)
    - QuColl_d - Energy from the BIPVT (daily)
    - QDHW_d - DHW energy used (daily)
    - QAux_d - Auxiliary energy used (daily)
    - IColl – Total radiation on the tilted surface (annually)
    - QuColl – Energy from the BIPVT (annually)
    - QDHW – DHW energy used (annually)
    - QAux – auxiliary energy used (annually)
- Outputs
    - EtaColl_d. efficiency of the collector (daily)

$$\eta_{collector,daily} = \frac{Q_{useful,collector,daily}}{A_{collector} * I_{collector,daily}} \tag{4.18}$$

    - FSol_d. The fraction of useful solar energy used to meet the DHW load (daily)

$$F_{solar,daily} = 1 - \left(\frac{Q_{auxiliary,daily}}{Q_{DHW,daily}}\right) \tag{4.19}$$

- EtaColl. The efficiency of the collector (annually)

$$\eta_{collector,yearly} = \frac{Q_{useful,collector,yearly}}{A_{collector} * I_{collector,yearly}} \tag{4.20}$$

- FSol_d. The fraction of useful solar energy used to meet the DHW load (annually)

$$F_{solar,yearly} = 1 - \left(\frac{Q_{auxiliary,yearly}}{Q_{DHW,yearly}}\right) \tag{4.21}$$